# EFFECTS OF AGRICULTURE LAND-USE ON SUBSURFACE RECHARGE AND CONTAMINANT TRANSPORT IN SHALLOW KARSTIC AQUIFERS IN THE CUMBERLAND ESCARPMENT, UPPER-OHIO RIVER BASIN.

A DISSERTATION

SUBMITTED TO THE GRADUATE SCHOOL

IN PARTIAL FULFILLMENT OF THE REQUIREMENTS

FOR THE DEGREE

DOCTOR OF PHILOSOPHY.

BY

GILLES VALDEZ TAGNE

DISSERTATION ADVISOR: DR. CAROLYN B. DOWLING

BALL STATE UNIVERSITY

MUNCIE, INDIANA

MAY 2019

## ABSTRACT

This project aims to characterize contaminants' fate and transport in karstic aquifers in the Cumberland Plateau of Southeastern Kentucky, a region mainly covered by forests (~70%) and agricultural lands (~30%) and strongly influenced by changes in water quality driven by the effects of varying land use (Dale et al., 2009). The scope of this research is the critical zone, which examines flow paths from surface recharge through the vadose zone and saturated parts of the aquifers. More specifically, the impact of recent and past changes in land-use on the quality of the groundwater resource at various scales is investigated. Primary research methods include the use of multivariate statistical analyses and geochemical modeling tools to better quantify fluxes and understand spatial and temporal changes in the quantity of surface contaminants and nutrients transported from surface to groundwater.

Within the physiographic range of the Cumberland Plateau of Southeastern Kentucky, the focus of this research on the surface-groundwater interactions in two karstic aquifers (recharge basins < 100 $km^2$) primarily discharging into the Cumberland River: 1) the Grayson-Gunnar Cave (GGC) system located in the upper Cumberland, a region that has been affected by a rapid proliferation of concentrated-animal feeding operations (CAFOs), and 2) the Mill Springs (MS) system located in the lower part of the Cumberland range, a region relatively unaffected by CAFOs development. The GGC watershed, a small agricultural watershed in the Cumberland ensemble, has a heterogenetic surface land-use distribution that makes it an ideal monitoring site for comparative studies on long-term controls of human interactions on groundwater quality by contrasting it to pristine aquatic systems (e.g., Mill Springs) in the same physiographic region.

The understanding of contaminant transport and fate in conduit-dominated karstic aquifers requires the knowledge of groundwater flow routes and recharge patterns, which are highly

dependent on the history of diagenetic and erosional processes that have affected the formation and evolution of carbonates (Davis, 1930; White, 1988; Sasowky and White, 1994; Vacher and Mylroie, 2002). Despite the panoply of hydrogeological data that are available for major carbonate platforms such as the Floridan aquifer (Budd and Vacher, 2004; Renken et al. 2005; Florea and Vacher, 2006) and the contiguous South-Central Kentucky platform (Mammoth Cave Region; Ryan and Meiman 1996; Anthony 1998; Groves et al. 2003; Groves et al. 2005; Groves and Meiman, 2005), there has been a very limited understanding of karstification processes that control subsurface preferential flow and thus contaminant migration from surface to groundwater in the Southeastern Kentucky carbonate platform. Through time-series analyses of high-frequency (10 minute-interval) physico-chemical data (specific conductivity, temperature, fluorescent dissolved organic matter, chlorophyll, and turbidity) from continuous monitoring at three targeted sites within the GGC system, this work attempts to provide preliminary insights regarding groundwater flow and recharge patterns at the scale of an epigenic karst aquifer. Data and results presented in the third chapter suggest the existence of two hydrologically separated conduit branches responding 2 to 3 hours apart.

Among other surface land-use changes that have been observed in Midwestern karstic terranes, the recent proliferation of CAFOs has been extensively discussed (Hodne, 2005; Burkholder et al., 2007; Brahana et al., 2014). The sporadic development of CAFOs in the upper parts of the Cumberland Plateau region (GGC) provides a unique site to examine the fractional mixing of end-member sources of nutrients and organic carbon in comparison to unaffected systems regarding CAFO's development (MS). Thus, further consideration is given to the impact of those facilities on nutrient loads in epigenic karst aquifers in the study area. In order to identify primary surface land-use control on total inorganic nitrogen loads and answer the

question concerning which end-members (wastes deriving from crop lands, residential areas, CAFOs, etc) account for the loads of nutrients in SE Kentucky aquifers, correlation analyses and analyses of covariance on low-frequency data (4 months record of weekly water quality sample) obtained at targeted located within the GGC system were performed. Data include major ions chemistry, nutrients ($NO_3^-$, $NH_4^+$, $PO_4^{3-}$), dissolved organic carbon (DOC), stable isotopes ($^{13}C$-DOC) and trace metals (Cu, Pb, and Zn). Presented in the fourth chapter, the results suggest that manure from poultry CAFOs exert a higher control on Total Inorganic Nitrogen (TIN) loads when compared to other non-point agricultural sources and discharge, and it strongly emphasize the needs to focus on site-specific (farm level) nutrient management plans to achieve targeted nitrate reduction goals at the scale of the Ohio River Basin.

Moreover, given the history of subsurface oil exploration in the shallow Mississippian-age carbonate reservoirs of the Eastern Kentucky carbonate platform (McFarlan, 1943) and current indicators of oil leaking around abandoned wells (Dugan et al.,2012; Florea, 2013), the region provides for an exceptional field laboratory to test the potential entrainment of sulfur brines from greater depths and the influence of sulfur-rich brines on the dynamics of dissolved inorganic carbon (DIC) in the critical zone (Florea, 2015; Egemeier, 1981; Hill, 1990; Jagnow et al., 2000; Onac et al., 2010). Despite the current understanding of untraditional sulfur-acid driven speleogenesis in karstic systems (Engel et al., 2004; Wynn et al. 2010; Onac et al. 2011; Balci et al., 2012), no study in the region has focused on understanding sulfur cycling and quantifying the contribution of sulfur brines to regional groundwater chemistry. Thus, fifth and last main chapter is dedicated to addressing the potential interaction between oil-related sulfur brines and groundwater at the scale of the regional aquifer system, and its implications on sulfuric-acid-driven carbonates dissolution. Using decadal (2005-2013) data record from Mill Springs (major

ion chemistry for the most part Ca, Mg, Na, $HCO_3$, $SO_4$, Cl) and geochemical modeling (end-member mixing models), the origin of sulfates in groundwater is discussed, the volumetric contribution of sulfur from allochtonous origin to the groundwater chemistry is quantified, and multiple scenarios for sulfur brines entrainment at the scale of the MS and GGC watersheds are tested. Although geochemical evidence suggests the contribution of oil-related brines to groundwater chemistry at the regional scale, non-traditional processes of carbonate dissolution are likely very minimal in the study area, and thus carbonic-acid-driven dissolution still accounts for a considerable proportion of DIC export to the Cumberland River, the regional base flow level.

The broader significance in studying recharge patterns and contaminant fate at the scale of small watersheds (GGC and MS) is to improve the success and the effectiveness of groundwater management plans at larger scales and predicting future changes in water quality in response to current changes in land-use. Understanding and predicting changes in water quality resulting from land-use changes at smaller scales is essential for ensuring that larger scale mitigation goals are met. Given that the Ohio Basin and the Cumberland sub-basin account for more than 30% of nutrients (N and P) inputs in the Gulf of Mexico, broader implications for the management of nutrient levels resulting from intensive farming include the overall mitigation of nitrate levels at the scale of the Mississippi River Basin and the management of the hypoxia zone in the Gulf of Mexico.

Finally, a specific question that has challenged the analytical approach in the understanding of nutrients and carbon dynamics in karst aquifers in the Cumberland region, and which in some sense constitutes the major technical innovation of this dissertation product, is the extraction of dissolved organic carbon (DOC < 3 mg/L in the study area) from water samples considering its

occurrence at levels lower than the natural range in groundwater affected by farming land-use (DOC > 6-7 mg/L). This rigorous analytical challenge was overcome using conservative analytical procedures (cryo-concentration) and advance technology in spectroscopy (Cavity-Ring-Down Spectroscopy). Details on analytical procedures are found in chapter two.

**References**

Anthony, D. (1998) Seasonal effects on the geochemical evolution of the Logsdon River, Mammoth Cave, Kentucky. MSc Thesis, Western Kentucky University, Bowling Green, KY.

Balci, N., Mayer, B., Shanks, W.C. and Mandernack, K.W. (2012) Oxygen and sulfur isotope systematics of sulfate produced during abiotic and bacterial oxidation of sphalerite and elemental sulfur. Geochimica et Cosmochimica Acta, 77, pp.335-351.

Brahana, J.V., Nix, J., Bitting, C., Bitting, C., Quick, R., Murdoch, J., Roland, V., Wets, A., Robertson, S., Scardale, G., North, V. (2014) CAFOs on Karst –meaningful data collection to adequately define environmental risk, with a specific application from the southern Ozarks of northern Arkansas. In: U.S. Geological Survey Scientific Investigations Report 2014–5035. p 97–102

Budd, D.A., Vacher, H.L. (2004) Matrix permeability of the confined Floridan Aquifer, Florida, USA. Hydrogeology Journal 12(5):531–549

Burkholder, J., Libra, B., Weyer, P., Heathcote, S., Kolpin, D., Thorne, P. S., & Wichman, M. (2007) Impacts of Waste from Concentrated Animal Feeding Operations on Water Quality. Environmental Health Perspectives, 115(2), 308–312. http://doi.org/10.1289/ehp.8839

Dale, V.H., Lannom, K.O., Tharp, M.L., Hodges, D.G., Fogel, J. (2009) Effects of climate change, land-use change, and invasive species on the ecology of the Cumberland forests. Canadian Journal of Forest Research 39(2):467–480

Davis, W.M. (1930) Origin of limestone caverns: Geological Society of America Bulletin, v. 41, p 475-628.

Dugan, C.R., Florea, L.J. and Walden, W.D. (2012) A geochemical investigation of springs within the Otter Creek watershed: Wayne County, southeastern Kentucky. In Geological Society of America Abstracts with Programs. v. 44, no. 4, p. 26.

Egemeier, S.J. (1981) *Cavern Development by thermal waters*, National Speleological Society Bulletin, v. 43, no. 2, p. 31-35.

Engel, A.S., Stern, L.A. and Bennett, P.C. (2004) Microbial contributions to cave formation: new insights into sulfuric acid speleogenesis. Geological Society of America. v. 32; no. 5; p. 369–372; doi: 10.1130/G20288.1.

Florea, L.J., Vacher, H.L. (2006) Springflow Hydrographs: Eogenetic vs. Telogenetic Karst. Ground Water 44: 352–361, doi 10.1111/j1745-6584-2005-00158-x

Flore, L.J. (2013) Isotopes of Carbon in a karst aquifer of the Cumberland Plateau of Kentucky, USA, Acta Carsologica 42/2-3, 277-289, Postojna.

Florea, L.J. (2015) Carbon capture and landscape evolution in epigenic karst landscapes modeled using geochemical mass balance. Earth Surface Processes and Landforms.

Groves, C., Meiman, J. (2005) Weathering, geomorphic work, and karst landscape evolution in the Cave City groundwater basin, Mammoth Cave, Kentucky. Geomorphology 67(1):115–126

Groves, C., Anthony, D.M., Meiman, J. (2003) Preliminary investigations of seasonal changes in the geochemical evolution of the Logdson River, Mammoth Cave, Kentucky. Speleogenesis and Evolution of Karst Aquifers.

Groves, C., Bolster, C., Meiman, J. (2005) Spatial and temporal variations in epikarst storage and flow in South Central Kentucky's Pennyroyal Plateau sinkhole plain. US Geological Survey Karst Interest Group Proceedings 64

Hill, C.A. (1990) Sulfuric Acid Speleogenesis of Carlsbad Cavern and Its Relationship to Hydrocarbons, Delaware Basin, New Mexico and Texas, AAPG Bulletin, November 1990, v. 74, no. 11, p. 1685-1694.

Hodne, C.J. (2005) Concentrating on Clean Water: The Challenge of Concentrated Animal Feeding Operations. Iowa Policy Project Report. www.iowapolicyproject.org

Jagnow, D.H., Hill, C.A., Davis, D.G., DuChene, H.R., Cunningham, K.I., Northup, D.E. and Queen, J.M. (2000) History of the sulfuric acid theory of speleogenesis in the Guadalupe Mountains, New Mexico. *Journal of Cave and Karst Studies, 62*(2), pp.54-59.

McFarlan, A.C. (1943) Geology of Kentucky. University of Kentucky, Lexington, KY.

Onac, B.P., Wynn, J.G. and Sumrall, J.B. (2011) Tracing the sources of cave sulfates: a unique case from Cerna Valley, Romania. *Chemical Geology*, *288*(3-4), pp.105-114.

Onac, B.P., Wynn, J.G. and Sumrall, J.B. (2011) Tracing the sources of cave sulfates: a unique case from Cerna Valley, Romania. Chemical Geology, 288(3), pp.105-114.

Renken, R.A., Cunningham, K.J., Zygnerski, M.R., Wacker, M.A., Shapiro, A.M., Harvey, R.W., Metge, D.W., Osborn, C.L. and Ryan, J.N. (2005) Assessing the vulnerability of a municipal well field to contamination in a karst aquifer. Environmental & Engineering Geoscience, 11(4), pp.319-331.

Ryan, M., Meiman, J. (1996) An Examination of Short-term Variations in Water Quality at a Karst Spring in Kentucky. Groundwater 34(1):23–30.

Sasowsky, I.D. and White, W.B. (1994) The role of stress release fracturing in the development of cavernous porosity in carbonate aquifers. Water Resources Research, 30(12), pp.3523-3530.

Vacher, H.L., Mylroie, J.E. (2002) Eogenetic karst from the perspective of an equivalent porous medium. Carbonates and Evaporites 17(2):182–196.

White, W.B. (1988) Geomorphology and Hydrology of Karst Terrains. Oxford University Press, New York.

Wynn, J.G., Sumrall, J.B. and Onac, B.P. (2010) Sulfur isotopic composition and the source of dissolved sulfur species in thermo-mineral springs of the Cerna Valley, Romania. Chemical Geology, 271(1-2), pp.31-43.

## ACKNOWLEDGEMENTS

I am dedicating this work to my Father in Heaven, the author and the finisher of all things, for the inspiration of this dissertation work, for the strength in times of doubt and loneliness, the perseverance that kept me moving when I was ready to give up, the desire to pursue excellence against all odds, for the good and the bad, the nicest and the ugliest moments, for the maturity and the tremendous spiritual and mental growth I have experienced through oppositions and hardships, for the gifts of mentors and friends, the close ones and the not so close…

I am dedicating this work to my earthly Father gone too soon… How I wish you were here to see what I have become! I remember the many dreams you had for me, having a PhD was surely just a tiny part of it. Although you were very tough with me at times, I am thankful for the way you showed me love and for leaving me a legacy of excellence and hardwork. To my mom, for raising us with strong values, teaching us how to share and invite others at our table. I realize more than ever what community really meant now that I am far away. To my siblings and my family all over the world, I have done this for all of us. May this journey give you hope and inspire each one of you to continue pushing back the limits of the possible. The sky is the limit!

I am dedicating this work to Nancy and Chris Williamson. Your support, your care and your unconditional love helped me stand strong when the circumstances around me were pushing me into giving up. Thank you for creating space for rest, authenticity, and acceptance. You are a reminder that friends we make along the road can become more precious than family.

To a chapter of my life ready to be closed, and the new season coming ahead with even bigger challenges, to the dreams and all marvelous plans that are gently kept away from me at this time and those already unravelling.

**Table of Contents**

## LIST OF FIGURES

**FIGURE** **PAGE**

### CHAPTER 1. GENERALITIES ABOUT KARST



### CHAPTER 2. METHODOLOGY

**CHAPTER 3. INFERRING GROUNDWATER FLOW AND RECHARGE FROM TIME SERIES ANALYSIS OF STORM RESPONSES IN THE CUMBERLAND PLATEAU SINKHOLE PLAIN OF SOUTHEASTERN KENTUCKY.**

**CHAPTER 4. LAND-USE AND HYDROLOGIC CONTROLS ON NUTRIENT LOADS IN AQUIFERS DRAINING AGRICULTURAL AND MIXED-USE WATERSHEDS.**

**CHAPTER 5. EFFECTS OF PRESENT AND PAST LAND USE ON CHEMICAL EVOLUTION OF SHALLOW GROUNDWATER IN THE CUMBERLAND SINKHOLE ESCARPMENT OF SOUTHEASTERN KENTUCKY.**

## LIST OF TABLES

**TABLE** **PAGE**

**CHAPTER 2. METHODOLOGY**



**CHAPTER 3. INFERRING GROUNDWATER FLOW AND RECHARGE FROM TIME SERIES ANALYSIS OF STORM RESPONSES IN THE CUMBERLAND PLATEAU SINKHOLE PLAIN OF SOUTHEASTERN KENTUCKY.**

**CHAPTER 4. LAND-USE AND HYDROLOGIC CONTROLS ON NUTRIENT LOADS IN AQUIFERS DRAINING AGRICULTURAL AND MIXED-USE WATERSHEDS.**



**CHAPTER 5. EFFECTS OF PRESENT AND PAST LAND USE ON CHEMICAL EVOLUTION OF SHALLOW GROUNDWATER IN THE CUMBERLAND SINKHOLE ESCARPMENT OF SOUTHEASTERN KENTUCKY.**

# CHAPTER 1:

# GENERALITIES ABOUT KARST

*"Karst areas are among the world's most diverse, fascinating, resource-rich, yet problematic terrains. They contain the largest springs and most productive groundwater supplies on Earth. They provide unique subsurface habitat to rare animals, and their caves preserve fragile prehistoric material for millennia. They are also the landscapes most vulnerable to environmental impacts. Their groundwater is the most easily polluted. Water in their wells and springs can dramatically and rapidly fluctuate in response to surface events…"*

Living on karsts, 2001, American Geological Institute, *AGI Environmental Awareness Series 4.*

## I.1. Generalities about karst: origin and evolution

Karst is produced primarily from the dissolution of underlying soluble rock, typically carbonates (limestone, dolomite, marble) or gypsum. Speleogenesis is the combination of physical (erosion, corrosion, landscape denudation), chemical (dissolution, water rock exchanges, diffusion) and biologic (biogenic and microbially-mediated reactions) mechanisms that lead to the formation of caves. Speleology is the study of cave systems.

### *I.1.1. The origin of karsts*

#### *I.1.1.1. View of cave formation in the 18$^{th}$ and 19$^{th}$ centuries*

Early considerations of the origin of caves (18$^{th}$ century) have associated catastrophic events such as floods and Earth crust deformations as primary causes of caves formation. Catastrophic theorists (Catcott, 1761 and Esper, 1774) associated caves formation to the biblical Deluge. Catcott (1761) in his "*Treatise on the Deluge*" argued that caves resulted from water action which could only have come from floods events with a more violent amplitude than modern streams. Esper (1774) suggested that caves were formed by expansion of gases produced by the decomposition of the bodies of animals drowned by the Flood and deposited in the mass of mud which subsequently hardened to become rock. Only later in the late 18$^{th}$ and early 19$^{th}$ that "uniformitarians" started considering alternative processes such as erosion and rock dissolution to explain caves formation. The major difference with previous theories was the recognition that cave formation could be carried out by normal and long-continuing processes that occur at present-day rates and not necessarily one-time random ones. Hutton (1780) suggested that streams of present-day size had formed cave passages by eroding the rock while it was still new and hence relatively soft. Later on, Brongniart (1817) and De Voisins (1819) attributed the

formation of caves to the removal by water of deposits or inclusions of common salt from within the surrounding rock. Later on, Thirria (1830) and Lyell (1830) recognized the importance of dissolved carbon dioxide in enhancing water power to dissolve carbonate in the *vadose*[1] zone of the karst aquifer. It was only later in the 19th century that Evans (1872) stated the hypothesis of dissolution occurring under the water level in phreatic conditions, especially in caves which contain no evidence of former stream passages and where the dissolving action of vadose water cannot explain the whole process of cave formation.

### *I.1.1.2. Modern views of speleogenesis*

- The importance of the water table

The importance of water table in the development of cave passages was first introduced by Cvijić (1918) who related the development of karsts landforms to subsurface hydrology. Cvijić introduced an hydrologic zonation (dry, transitional and saturated zones) based on location to the water table[2]. According to Cvijić, most groundwater movement take place at or immediately below the water table. Hence the transitional zone could be the major focus of cave development. Grund (1903) provided a more simplistic model of karst aquifers by dividing them broadly into two zones: an unsaturated zone above the water table where most water circulation occurs, and a saturated zone stagnant where water must be stagnant or static and thus not active in cave development.

[1] The vadose zone of an aquifer in the region right above the static water level characterized by constant fluctuations and where the atmosphere to water gas exchanges (and vice-versa) is more prominent.
[2] The water table in a karst aquifer is a theoretical consideration that refers to the static level of water within open cave passages. Kartz (1909) argues that a physical water table cannot be defined for cave aquifers since cave passages are independent of each other.

- Cave hierarchisation: effects of valleys incision
    - Deep flow and deep phreatic dissolution models

Following Grund (1903) and Cvijić (1918) work on the importance of water table zonation in cave development, Davis (1930) provided a cyclic cave formation model based on his view of the "*geomorphological cycle*". However, Davis' view of groundwater flow differed considerably from previous hypotheses of cave formation at shallow depth in the way he visualized slow dissolution development occurring at great depths below the water table. Further, to explain the location of cave passages right above actual water levels in many cave systems, Davis developed a model which takes into account cyclic geomorphologic events such as regional uplift and consequent incision of surface valleys:

"*Davis developed the view that cave passages of explorable size would enlarge close below the water table by modification of once deeper drainage routes when these were raised relative to the land surface. The relative rise could occur in response to regional uplift, as a result of the removal of overlying strata or when the drainage regime was altered by deep incision of surface valleys. The flooded passages that were conceived at greater depth and developed below the water table were in turn raised above the water table and drained. At this stage a new first erosional cycle would begin at depth, associated with a lower drainage route. This view enabled Davis to explain the presence of caves that he considered must have begun to develop below the water table but which were now observed to stand at levels well above the contemporary water table. Once the caves were above the water table the second cave development cycle began, during which the caves could carry water from surface sinks along open passages*." Extract from Klimchouck et al. (2000) Part 2.2 Development of speleogenetic ideas in the 20$^{th}$ century.

– Development of cave around the water table zone

Contrary to Davis, Swinnerton (1929) renewed with Cvijić's view of cave development in the area close to or immediately below the water table. As Davis, he recognized that there is a possible mechanism of cave development associated to sequential erosional cycles (uplift and induced valley incision).

– Drainage hierachisation

Gardner (1935) applied his hypothesis of cave development when studying the genesis of Mammoth Cave (South-Central Kentucky) and Carlsbad Cavern (Southern New Mexico), two cave systems that have little in common beyond their large size. Gardner's view was one of essentially down-dip passage formation commencing in what he called "*carrier beds*" referring to open spaces along limestone bedding planes or sandstone intercalated in limestone, that may serve as the original circulating medium. Gardner's hypothesis required "*downcutting*" by a surface valley to cut through the dipping limestone sequence. Before the Gardner's valley's downcutting hypothesis, interbedding plans were assumed to be saturated by static water (Grund, 1903). Downcutting of the valley led to drainage of the upper saturated zone and subsequent vadose invasion and cave development within the carrier beds. Continuous downcutting might eventually lead to the intersection of a lower carrier bed, at which stage, according to the model, the upper level would be abandoned as its drainage was pirated by caves formed in the lower bed.

- Cave development in the Cumberland Plateau of Southeastern Kentucky
  - Primary control of drainage and water table adjustments

Based on the physical and morphological characteristics of several of the largest caves in that region, Simpson and Florea (2009) hypothesized that drainage hierarchisation and alternance between periods of rapid base-level incision are the major processes explaining cave development in the Southeastern part of the Cumberland Plateau. The overall cave development has been mainly triggered by the water table drop resulting from the Cumberland valley incision. Based on the flow patterns, Sasowky and White (1994) defined the "Cumberland cave development style" as usually composed of 2 drain levels: an abandoned upper level trunk passage above the actual water table and low-level stream passages below the water table which contain the actual draining network of the cave. Those active stream passages generally consist of one or two large master conduits which follow topography contours and connect the whole system to a source down in the valley. However, there are few exceptions: for example, in the *Coral* and *Jugornot* caves that show transridge passages between valleys; cave passages alternate in elliptical or rectangular cross sections.

This bivalent flow path (abandoned upper level and active underground streams) can be attributed to phases of high entrenchment and rapid incisions of river sediments during glacial peaks and to level adjustment of cave streams to reach the river bed. The tall canyons observed in many Cumberland cave systems and the fluvial terraces along the Upper Cumberland River are markers of alternating episodes of river entrenchment and aggradation that shaped the Cumberland karst morphology. Grayson-Gunnar cave, a cave located in Wayne County, Kentucky will be the primary focus of our dissertation work. The Grayson-Gunnar cave system

is a typical example of karst features that have been developed during periods of rapid base levels incision of the Upper Cumberland River's valley.

- The secondary role of the lithology

The geology of the regional karst of the Cumberland Plateau is characterized by thickness variability (20 m to 130 m; Simpson and Florea, 2013) of limestones formation and a complex stratigraphy especially in the Southwestern part. The typical stratigraphy section comprises from the bottom to the top: the St-Louis limestone, the Ste-Genevieve limestone and the Kidder limestone, all separated by physical unconformities. In the Southern part, The Hartselle formation and the Bangor limestone lie on the top of the previous formations, and an abundant chert layer is present in the upper few meters of the St. Louis, and acts as the local barrier for the flow percolating downstream. Where the chert layer is locally present, it may perch or divert groundwater flow toward the spring.

### *I.1.2. Traditional epigenic speleogenetic model: carbonic acid dissolution*

Carbonic acid speleogenesis is defined as the sum of processes occurring in epigenic karst system due to the dissolution of limestone by water containing carbon dioxide. In the classic models of epigenic karst (White, 1988), carbonic acid is the primary source of chemical weathering. Carbonic acid derived from aqueous carbon dioxide acts as an aggressive agent to dissolve $CaCO_3$, which is then transported out of the karst system as calcium and bicarbonate ions. The maximum amount of $CaCO_3$ that can be dissolved, expressed by the maximum calcium concentration (Ca saturation), is determined by the chemical equilibrium between $H_2O$-$CO_2$-$CaCO_3$ phases. Below saturation, the acidic water is able to easily dissolve the carbonate bedrock. Above saturation, no further dissolution can occur. Moreover, carbonates dissolution by

sulfuric acid is an important speleogenetic mechanism in a variety of geologic settings (e.g., geothermal sources). Some epigenic karst systems show strong evidences of sulfuric acid as a dissolution agent (Florea, 2013).

### *I.1.2.1. Equilibrium between carbonates and carbonic acid*

Three different chemical reactions describe $CO_2$-enriched water's attack on calcite surface (Plummer et al., 1978). They are:

$$CaCO_3 + H^+ \leftrightarrow Ca^{2+} + HCO_3^- \quad \text{(Eq.1)}$$

$$CaCO_3 + H_2CO_3 \leftrightarrow Ca^{2+} + 2\ HCO_3^- \quad \text{(Eq.2)}$$

$$CaCO_3 + H_2O \leftrightarrow Ca^{2+} + CO_3^{2-} + H_2O \quad \text{(Eq.3)}$$

Those 3 equations can be combined into the following general reaction

$$CaCO_3 + H_2O + CO_2 \leftrightarrow Ca^{2+} + 2\ HCO_3^- \quad \text{(Eq.4)}$$

Note that for each $Ca^{2+}$ dissolved, one molecule of $CO_2$ is needed. From the previous equations, it can be inferred that the equilibrium between $H_2O$ and $CO_2$ is controlled by the equilibria between $H_2CO_3$, $HCO_3^-$ and $H^+$, which is going to be explained by the following equations (Dreybrodt, 1990; Dreybrodt et al., 1996; Svensson and Dreybrodt, 1992):

$$CO_{2(g)} + H_2O \leftrightarrow CO_{2(aq)} + H_2O \quad \text{(Eq.5)}$$

$$CO_{2(aq)} + H_2O \leftrightarrow H_2CO_{3(aq)} \quad \text{(Eq.6)}$$

$$H_2CO_{3(aq)} \leftrightarrow HCO_3^-{}_{(aq)} + H^+{}_{(aq)} \quad \text{(Eq.7)}$$

$$HCO_3^{-}{}_{(aq)} \leftrightarrow CO_3^{2-}{}_{(aq)} + H^{+}{}_{(aq)} \quad \text{(Eq.8)}$$

$$H_2O \leftrightarrow H^{+}{}_{(aq)} + OH^{-}{}_{(aq)} \quad \text{(Eq.9)}$$

Equation 5 describes the transfer of $CO_2$ from the gas phase into the solution and is defined by the Henry's law (Plummer and Busenberg, 1982):

$$(CO_{2(aq)}) = K_H \times P_{CO2} = K_H \times R \times T \times (CO_{2(g)}) \quad \text{(Eq.10)}$$

Where $K_H$ is Henry's constant in mol / L. atm

$(CO_{2(aq)})$ is the activity of $CO_2$ dissolved

$Pco_2$ is the partial pressure of $CO_2$ in the surrounding atmosphere

R is the gas law constant (R = 0.0826 atm. L / mol. K)

T is the temperature in K

$$CO_{2(aq)} + H_2O \leftrightarrow H_2CO_{3(aq)} \quad \text{(Eq.11)}$$

Equation 11 describes the aqueous $CO_2$ dissolution into water to form carbonic acid. This equation is defined by a constant $K_0$ (mol/L) expressed as follows (Wissbrun et al., 1954):

$$(CO_{2(aq)}) = K_0 \times (H_2CO_{3(aq)}) \quad \text{(Eq.12)}$$

Assuming that there is no further dissociation of $H_2CO_3$, the total activity[3] of carbon species in the water at a given time noted $(H_2CO_3^{*})$ is the sum of the actual $CO_{2(aq)}$ and the activity of $H_2CO_3$ yielded by $CO_{2(aq)}$ dissolution into water (Equation 13):

$$(H_2CO_3^{*}) = (CO_{2(aq)}) + (H_2CO_{3(aq)}) = (1 + 1/K_0) \times (CO_{2(aq)}) \quad \text{(Eq.13)}$$

[3] In this section, species are quantified as activities. Activities (i) are related to concentrations [i] by the coefficients $\gamma_i$. (i) = $\gamma_i$. [i]

Considering $1/K_0 \approx 0.003$ (Wissbrun et al., 1954), $(CO_{2(aq)}) \approx (H_2CO_3^*)$

$$H_2CO_{3(aq)} \leftrightarrow HCO_3^-{}_{(aq)} + H^+{}_{(aq)} \quad \text{(Eq.14)}$$

$$HCO_3^-{}_{(aq)} \leftrightarrow CO_3^{2-}{}_{(aq)} + H^+{}_{(aq)} \quad \text{(Eq.15)}$$

Equations 14 and 15 express equilibria between $H_2CO_3$, $HCO_3^-$, $CO_3^{2-}$ and $H^+$. Equation 14 describes $H_2CO_3$ dissociation into $HCO_3^-$ and $H^+$ and is defined by constant $K_1$ (mol/L) expressed with the following mass action law (Plummer and Busenberg, 1982):

$$K_1 = \frac{(H^+) \times (HCO_3^-)}{(HCO_3^*)} = \frac{1}{1 + K_0} \times \frac{(H^+) \times (HCO_3^-)}{(H_2CO_3)} \quad \text{(Eq.16)}$$

Equation 15 describes the next dissociation step and is defined at equilibrium by a constant $K_2$ (mol/L; Plummer and Busenberg, 1982)

$$K_2 = \frac{(H^+) \times (CO_3^{2-})}{(HCO_3^-)} \quad \text{(Eq.17)}$$

$$H_2O \leftrightarrow H^+ + OH^- \quad \text{(Eq.18)}$$

Equation 18 describes the dissociation of water and is defined by a constant $K_w$ (mol/L) expressed as follows (Harned and Hamer, 1933):

$$(H^+) \times (OH^-) = K_w \quad \text{(Eq.19)}$$

### *I.1.2.2. Sources of acidity: equilibrium between $H_2CO_3$, $HCO_3^-$, $CO_3^{2-}$ and $H^+$*

As previously stated, the equilibrium between $H_2CO_3$, $HCO_3^-$, $CO_3^{2-}$ and $H^+$ is a controlling factor of carbonate dissolution into groundwater. This equilibrium is governed by pH and less by temperature and ionic strength. Assuming that the total concentration of carbon in given water in equilibrium with $CO_2$ is given by:

$$C_T = [H_2CO_3^-] + [HCO_3^-] + [CO_3^{2-}] \quad \text{(Eq.20)}$$

The molar fraction of each species can therefore be defined as following:

$$\alpha_0 = \frac{[H_2CO_3^-]}{C_T} \quad \text{(Eq.21)}$$

$$\alpha_1 = \frac{[HCO_3^-]}{C_T} \quad \text{(Eq.22)}$$

$$\alpha_2 = \frac{[CO_3^-]}{C_T} \quad \text{(Eq.23)}$$

Figure 1 is a representation of the control of pH on the equilibrium and the stability of each species. For pH < 4, theoretically there is no existing $HCO_3^-$ and $CO_3^{2-}$ in water. With increasing pH, $H_2CO_3$ progressively dissociates into $HCO_3^-$. Therefore $HCO_3^-$ is the main existing species for neutral to slightly basic waters (6< pH <8.3), which is the case in most natural karst waters. For pH > 8.3, $HCO_3^-$ starts to dissociate until at pH ≈ 10, where $CO_3^{2-}$ becomes dominant.

## I.2. Karst hydrogeology

### *I.2.1. Conceptual models*

#### *I.2.1.1. Darcy Law*

In 1856, Henry Darcy established an empirical relationship that describes the flow of water through a porous media known as Darcy's Law based on his experience with water flow in tubes and filters of sand. Assuming constant hydraulic gradient (unconfined aquifer) and uniform flow (laminar conditions), the average flow rate (Q) is a function of the permeability of the media (K), the area of the cross-sectional sectional perpendicular to the flow (A), the flow length (L) and the difference in hydraulic head between inflow and outflow ($h_2 - h_1$) as stated by the following equation.

$$Q = K \times A \times \frac{h_2 - h_1}{L} \quad \text{(Eq.24)}$$

### *I.2.1.2. The equivalent porous model*

The equivalent porous model or single-porosity model has been widely used in hydrogeology to characterize aquifers in sedimentary and alluvial settings. The model assumes 1) that the aquifer is formed of porous material, in which space is uniformly distributed (Renken et al., 2005), 2) a laminar flow (Vacher and Mylroie, 2002). The pore spaces consist of parallel capillary tubes in a cube so that the total discharge through the volume is the integration of the specific discharge in every single capillary tube (Fig. 3)

Assuming that each capillary tube has a constant diameter *D*, the specific area of each tube is given by:

$$A_t = \frac{\Pi \times D^2}{4} \quad \text{(Eq.25)}$$

If *N* is the total number of tubes, the total porosity will be expressed as it follows:

$$n = \frac{N \times A_t}{A} = \frac{\Pi \times N \times D^2}{4A} \quad \text{(Eq.26)}$$

The total surface area can be expressed as a function of the porosity, the total number of tubes and the size of each tube:

$$A = \frac{\Pi \times N \times D^2}{4n} \quad \text{(Eq.27)}$$

The application of the Darcy's Law (Eq. 24) yields the total discharge according to the following equation:

$$Q = K \times A \times \frac{dh}{dL} = K \times \frac{\Pi \times N \times D^2}{4n} \times \frac{dh}{dL} \quad \text{(Eq.28)}$$

dh/dL is the hydraulic gradient (head differences versus elevation differences)

Q is a function of the specific discharge in each tube $q_i$

$$Q = q_i \times N \quad \text{(Eq.29)}$$

Thus the specific discharge in each tube is given by:

$$q_i = \frac{Q}{N} = K \times \frac{\Pi \times D^2}{4n} \times \frac{dh}{dL} \quad \text{(Eq.30)}$$

### *I.2.2. Hydrogeology of carbonate aquifers*

The hydrogeology of carbonate rocks is complex. Carbonate formations are characterized by anisotropy, continuously evolving porosity and permeability, and a wide range of depositional environments. Although the equivalent porous medium model is assumed to be suitable to the majority of fractured and sedimentary media, this model has many limitations in its applicability to karstic settings (conduits and caves) where flows are highly turbulent especially following storm events (Vacher and Mylroie, 2002). Due to the high connectivity with surface recharge, the distribution in flow regimes in epigenic karsts is highly dependent on climate conditions. The challenges of applying common hydrogeological models to the study of karst aquifers are mainly related to 1) the anisotropy i.e. large range of hydraulic properties (porosity and permeability); 2) the variety of depositional environments, and 3) post-depositional processes further affecting original hydraulic properties.

To avoid simplifying the heterogeneity and the anisotropy of karst aquifers, further models were introduced to explain groundwater flows in karst aquifers. Vacher and Mylroie (2002) introduced the concept of dual-porosity in eogenetic karst, which consists of a combination of matrix or primary porosity (storage system) and conduit macroporosity (transmitting system), with a dominance of the storage term (matrix porosity) in the groundwater flow at the spring. Renken at al. (2005) further introduced the concept of triple-porosity model in their study of the Biscayne aquifer in the Floridan platform, including fractures and bedding planes porosity as a third term. Florea and Vacher (2006) classified South-Central Kentucky carbonates platforms within an age range of $10^2$ Ma and a matrix permeability ranging between $10^{-8}$ and $10^{-7}$ Ma, which is closer to the values obtained in other telogenetic (mature) carbonate platforms like the Ozark Plateau (Arkansas) and the Potosi Dolomite (Missouri). In the study of the Cumberland platform, the triple porosity model (fractures, bedding planes, matrix) will be considered. However, because of the platform is relatively mature in comparison to the Floridan platform (Florea and Vacher, 2006), the matrix porosity component will be considered negligible.

#### *II.2.2.1. Anisotropy*

Karst aquifers feature a wide range of hydraulic properties depending on the type of surrounding bedrock. Brahana et al. (1988) first distinguished between carbonate formations using the total porosity (%) and the pore size (mm). Figure 4 shows the total porosity, pore sizes and hydraulic conductivity (K) of several types of carbonate settings. The hydraulic conductivity is estimated using average well yields (m/day) in different formations. The dashed line is a theoretical line defined by Ford (1980) to differentiate conditions favoring the development of caves features (below the line) from conditions hindering their development (above the line). If the dissolution

is concentrated only along zones of high permeability (primary pores), then pores will develop in restricted zones of the formation, therefore hindering the development of karst features. However, if the dissolution is widely diffused, then secondary porosity occurs, which is more likely to produce karst features.

Vacher and Mylroie (2002) attributed the differences in hydrologic response between old and modern systems to the degree of burial and diagenesis. They distinguish eogenetic karsts (where limestones have not yet been buried) from telogenetic systems representing post-burial stages.

Budd and Vacher (2004) provided a classification of karst systems based on permeability (matrix, fracture, channel) and the percentage contribution of each hydraulic features on the water flow. Very mature Cenozoic systems (e.g., Biscayne, Upper Floridan, and Bahamas platforms) exhibit consistently higher matrix permeability ($10^{-11}$ – $10^{-14}$ $m^2$) compared to Mesozoic (e.g., Edwards aquifer, TX) and Paleozoic systems (e.g., Mammoth cave system, KY) which show much lower permeability values ($10^{-15}$ – $10^{-20}$ $m^2$). Water flow primarily occurs through fractures in Paleozoic, Mesozoic and Cenozoic systems. However, matrix porosity may control 3 to 7% of the flow in modern systems.

Following the work of Vacher and Mylroie (2002) and Budd and Vacher (2004) who established a direct correlation between the age of carbonates systems, their degree of burial, and their hydraulic properties (porosity and permeability), Florea and Vacher (2006) provided a classification of eogenetic and telogenetic systems based on the flashiness of spring response to storms, hydraulic properties (matrix porosity), and relative age of cave formations (Fig. 5).

### *II.2.2.2. Depositional environments*

The type of depositional environment of carbonate sediments determines the original porosity and permeability of the resulting cave formation. Modern marine carbonates sediments exhibit an original matrix porosity ranging from 40% to 70% (Brahana et al., 1988). However, most limestones found in post-depositional environments where cementation, compaction and regional uplift may have considerably decreased porosity, will exhibit values inferior to 10%. Depositional environments will also affect the geochemical processes originating carbonate deposits and therefore their texture. For example, travertines, which are carbonates deposits commonly found around tropical springs, will be formed through physico-chemical precipitation controlled by changes in $CO_2$ pressure and exhibit an oolitic texture. A majority of bioclastic limestones are formed through biological precipitation of limestones in marine environments, and coral limestones mainly form in coastal environments.

### *II.2.2.3. Post-depositional processes*

Carbonate rocks show a continually evolving porosity and permeability (second porosity) due to post-depositional processes such as karstification (increasing porosity), diagenesis (decreasing porosity) and other geological and geochemical mechanisms that are likely to affect hydrogeological behaviors. More generally, processes controlling the porosity of carbonates aquifers are:

- **Physical processes** such as diagenesis, which includes compaction, cementation and fluid circulation (recrystallization).
- **Geochemical processes** such as dissolution, weathering, precipitation, dolomitisation (enrichment in Mg), fluid chemistry (pH, $Pco_2$)

- **Structural and tectonic processes**: uplifting, metamorphism, faulting which may cause an opening of fractures and increase fracture density. Structural and tectonic process are major contributors to the secondary porosity in carbonates aquifers.
- **Hydrologic processes** mostly fluid circulation (water, gas, vapors). The existence of fluid circulation paths will also affect the anisotropy of carbonate sediments.
- **Biological factors** primarily in relation with the activity sulfate–reducing bacteria in carbonate sediments affected by petroleum migration. The oxidation of hydrocarbons by sulfates under anaerobic conditions and the mediation of sulfur-reducing bacteria generate sulfide ($H_2S$ or HS). When dissolved into water, sulfide generates sulfuric acid that is involved in the dissolution of carbonates, and the formation of gypsum as a secondary mineral. Gypsum is less dense than carbonates, therefore its deposition along cave walls creates voids in sediments (secondary porosity).

*II.2.2.3.1. Dolomitisation*

Dolomitisation summarizes all geochemical processes involving the progressive replacement of Ca by Mg in the original structure of the $CaCO_3$ mineral. The change of density created by the replacement of Ca by Mg generates an enhancement of porosity and permeability of the mineral. Major dolomitisation processes affecting carbonate evolution are now known to occur at the interface between fresh and saline water in brackish environments.

*II.2.2.3.2. Diagenesis*

Diagenetic processes involved in karstification include compaction, cementation, pressure solution and metamorphism. Compaction includes both mechanical process (grain

rearrangement) and chemical process (pressure dissolution at grain-to-grain contact). Cementation happens following the cooling of pressure fluids inside intergranular voids or mineral deposition from moving groundwater between grains. Vacher and Mylroie (2002) differentiated karst formations based on diagenetic processes from which they originate (Fig. 6). Using a two-dimensional diagram with porosity (%, y-axis) and pore size (mm, x-axis), they were able to represent the evolution of a carbonate platform from early stage of deposition (eogenetic karst) to postburial stages (telogenetic karst). Eogenetic formations represent early stages of diagenesis during which limestones are not yet deeply buried. This evolution stage is typical of small tropical platforms of Quaternary ages (Bahamas, Bermuda) and continental margins (Southern Florida). On the contrary, telogenetic karsts are formed through post-burial processes followed by uplift and erosion (Fig. 6). Typical telogenetic formations include pre-Quaternary continental deposits in Texas (Edwards aquifer), Missouri (Potosi dolomite), and South-Central Kentucky (Mammoth cave system).

Mylroie et al. (1995) differentiated karst development features in eogenetic platforms (islands) in three categories based on sea level changes, the type of recharge and the dynamic of the freshwater/saltwater mixing line (dissolution/precipitation front): simple carbonate island, carbonate cover island and carbonate rimmed-islands. The evolution of a carbonate system from the eogenetic stage to the telogenetic stage always involves a change in hydraulic characteristics mainly related to the formation of secondary porosity during uplift and fracturing.

### *II.2.3. Hydraulic models suitable to carbonates systems*

Recent studies in karst systems have shown huge limitations in the estimation of flow rates and contaminants transfer using general flow models such the Darcian model and the equivalent

porous medium model (Worthington et al., 2002; Renken et al., 2005). Recent work in carbonate aquifers have emphasized the need to consider multi-porosity conceptualizations (Quinlan et al., 1996; Mohrlok and Teutsch, 1997; White, 1999; Worthington, 1999; Halihan et al., 1999; Halihan et al., 2000; Worthington et al., 2000).

#### *II.2.3.1. Double-porosity system*

The dual-porosity conceptualization (Fig. 7) defines eogenetic karst as a combination of conduit and matrix porosity with a dominance of matrix porosity, and telogenetic karst as a system in which secondary elements (channels/conduits and fractures) dominate the flow. In the conceptual model, the matrix porosity plays the role of the aquifer storage medium, and the tubes/conduits porosity (also refers to as macroporosity) is the transmitting system (flow system).

In the following, the eogenetic karst will be considered as system with a dominance of conduit/tube (porosity $Ø_t$ and permeability $K_t$) and matrix ($Ø_m$, $K_m$). The equivalent system is considered as parallel combination of two single flow systems (Fig. 8). Considering *dh* as the hydraulic potential, the total hydraulic potential is the sum of single hydraulic potential in each single flow system (box). If $dh_1$ is the hydraulic potential in the tube system and $dh_2$ the hydraulic potential in the matrix system, the total hydraulic potential is given by:

$$dh = dh_1 + dh_2 \qquad \text{(Eq.31)}$$

The specific discharge in each tube $q_i$ is been established for a single continuum system using the following equation:

$$qi = K \times \frac{\Pi \times D^2}{4Ø} \times \frac{dh}{dL} \rightarrow dh = \frac{\Delta L \times q_i}{K} \times \frac{4Ø}{\Pi D^2} \qquad \text{(Eq.32)}$$

Applying equation 32 to each single system, the following equation is obtained:

$$q_{tube} = K_t \times \frac{\Pi \times D^2}{4\emptyset_t} \times \frac{dh_1}{dL} \rightarrow dh_1 = \frac{\Delta L \times q_{\text{tube}}}{K_t} \times \frac{4\emptyset_t}{\Pi D^2} \quad \text{(Eq.33)}$$

$$q_{matrix} = K_m \times \frac{\Pi D^2}{4\emptyset_m} \times \frac{dh_2}{dL} \rightarrow dh_2 = \frac{\Delta L \times q_{\text{matrix}}}{K_m} \times \frac{4\emptyset_m}{\Pi D^2} \quad \text{(Eq.34)}$$

Replacing equations 33 and 34 into equation 31,

$$\frac{\Delta L \times q_i}{K} \times \frac{4\emptyset}{\Pi D^2} = \frac{\Delta L \times q_{\text{tube}}}{K_t} \times \frac{4\emptyset_t}{\Pi D^2} + \frac{\Delta L \times q_{\text{matrix}}}{K_m} \times \frac{4\emptyset_m}{\Pi D^2} \quad \text{(Eq.35)}$$

Considering a uniform flow through the system ($q_{tube} = q_{matrix} = q_i$), equation 35 becomes:

$$\frac{\Delta L \times q_i}{K} \times \frac{4\emptyset}{\Pi D^2} = \frac{\Delta L \times q_i}{K_t} \times \frac{4\emptyset_t}{\Pi D^2} + \frac{\Delta L \times q_i}{K_m} \times \frac{4\emptyset_m}{\Pi D^2} \quad \text{(Eq.36)}$$

Through simplification,

$$\frac{\emptyset}{K} = \frac{\emptyset_t}{K_t} + \frac{\emptyset_m}{K_m} \quad \text{(Eq.37)}$$

Thus,

$$K = \emptyset \times \left(\frac{\emptyset_t}{K_t} + \frac{\emptyset_m}{K_m}\right)^{-1} \quad \text{(Eq.38)}$$

Assuming a low flow resistance in tube/conduits, $K_t \rightarrow \infty$, therefore K may be given by:

$$K = \emptyset \times \frac{K_m}{\emptyset_m} = \emptyset \times \frac{K_m}{1-\emptyset_t} \quad \text{(Eq.39)}$$

***II.2.3.2. Triple-porosity system***

Budd and Vacher (2004) introduced the concept of triple porosity to characterize fractured porous aquifer in the unconfined region of the Upper Floridan system. Later on, Renken et al. (2005) used the triple-porosity concept in their study of the Biscayne aquifer, taking into account the conduits, fractures and matrix porosity. In the following, consider the telogenetic karst as

system featuring matrix (porosity $Ø_m$ and permeability $K_m$), conduit/tube ($Ø_t$, $K_t$) and fracture ($Ø_f$, $K_f$) flow media. Thus, the equivalent system is considered as parallel combination of three single flow systems (Fig. 9). In this case, the system is similar to the double-porosity system with the addition of the fracture porosity.

Therefore, the equivalent permeability of the system is described by:

$$K = \left( \frac{Ø_t}{K_t} + \frac{Ø_f}{K_f} + \frac{Ø_m}{K_m} \right)^{-1} \quad \text{(Eq.40)}$$

**References**


Brahana, J.V., Thrailkill, J., Freeman, T. and Ward, W.C. (1988). Carbonate rocks. Hydrogeology. The Geological Society of North America, Boulder Colorado. 1988. pp.333-352.

Brongniart, A. (1817). Caverne. In : Dictionnaire des sciences naturelles. V.7. Strasbourg. pp.298-309.

Budd, D.A. and Vacher, H.L. (2004). Matrix permeability of the confined Floridan Aquifer, Florida, USA. Hydrogeology Journal, 12(5), pp.531-549.

Busenberg, E. and Plummer, L.N., 1982. The kinetics of dissolution of dolomite in CO2-H2O systems at 1.5 to 65oC and 0 to 1 atm PCO2. American Journal of Science, 282(1), pp.45-78.

Catcott, A. (1761). A Treatise on the Deluge: Containing IV. Natural Proofs of the Deluge, Deduced from a Great Variety of Circumstances: London, M. Withers., 296 p.

Cvijic, J. (1918). Hydrographie souterraine et évolution morphologique du karst. Recueil des travaux de l'Institut de Géographie Alpine, 6(4), pp.375-426.

Davis, W.M., 1930. Origin of limestone caverns. Bulletin of the Geological Society of America, 41(3), pp.475-628.

De Voisins, J.F.D.A. (1819). Traité de géognosie (Vol. 1). F.G. Levrault, eds. v.2, pp.382-383.

Dreybrodt, W. "The role of dissolution kinetics in the development of karst aquifers in limestone: a model simulation of karst evolution." The Journal of geology 98, no. 5 (1990): 639-655.

Dreybrodt, W., Lauckner, J., Zaihua, L. , Svensson, U., and Buhmann, D. 1996. The kinetics of the reaction $CO_2 + H_2O \rightarrow H^+ + HCO_3^-$ as one of the rate limiting steps for the dissolution of calcite in the system $H_2O$-$CO_2$-$CaCO_3$. Geochimica et Cosmochimica Acta 60(18): 3375-3381.

Esper, J.F. (1774). Ausführliche Nachricht von neu entdeckten Zoolithen…: Nurnberg, Knorr. 148 p. pp.100-107.

Evans, F.G. (1872). The Carboniferous limestone. Report and Transactions. Cardiff Naturalists' Society 3(1): pp.39-47.

Florea, L.J. and Vacher, H.L. (2006). Springflow hydrographs: eogenetic vs. telogenetic karst. Groundwater, 44(3), pp.352-361.

Ford, D.C. (1980). Threshold and limit effects in karst geomorphology. In Coates, D.R., and Vitek, J.D., eds. Thresholds in Geomorphology. London: Allen and Unwin, pp.345-362.

Gardner, J.H. (1935). Origin and development of limestone caverns. Bulletin of the Geological Society of America, 46(8), pp.1255-1274.

Grund, A. (1903). Die Karsthydrographie: Studien aus Westbosnien: Geographische Abhandlungen herausgegeben von A. Penck 9. Teubner.

Halihan, T., Mace, R.E. and Sharp Jr, J.M. (2000). Flow in the San Antonio segment of the Edwards aquifer: matrix, fractures, or conduits. Groundwater flow and contaminant transport in carbonate aquifers: pp.129-146.

Halihan, T., Sharp Jr, J.M. and Mace, R.E. (1999). Interpreting flow using permeability at multiple scales. Karst modeling: Karst Waters Institute Special Publication 5: pp.82-96.

Harned, H.S. and Hamer, W.J., 1933. The ionization constant of water. Journal of the American Chemical Society, 55(6), pp.2194-2206.

Hutton, J. (1780). A Tour to the Caves. In: The environs of Ingleborough and Settle, in the West-Riding of Yorkshire…: London, Richardson and Urquhart, 49 p. pp.38-39.

Klimchouk, A. and Ford, D. (2000). 3.1. Types of karst and evolution of hydrogeologic setting. In: Speleogenesis. Evolution of Karst Aquifers. Huntsville: National Speleological Society, pp.47-53.

Lyell, C. (1830). Principles of geology. v.1: Murray, London. p.16

Mohrlok, U. and Teutsch, G. (1997). Double continuum porous equivalent (DCPE) versus discrete modelling in karst terranes. In Proceedings of the International Symposium and Field Seminar on Karst. pp.319-326.

Mylroie, J.E., Carew, J.L. and Vacher, H.L. (1995). Karst development in the Bahamas and Bermuda. Geological Society of America Special Papers, 300, pp.251-267.

Plummer, L.N., Wigley, T.M.L. and Parkhurst, D.L. (1978). The kinetics of calcite dissolution in CO2-water systems at 5 degrees to 60 degrees C and 0.0 to 1.0 atm CO2. American journal of science, 278(2): pp.179-216.

Quinlan, J.F., Davies, G.J., Jones, S.W. and Huntoon, P.W. (1996). The applicability of numerical models to adequately characterize ground-water flow in karstic and other triple-

porosity aquifers. In Subsurface Fluid-Flow (Ground-Water and Vadose Zone) Modeling. ASTM International.

Renken, R.A., Cunningham, K.J., Zygnerski, M.R., Wacker, M.A., Shapiro, A.M., Harvey, R.W., Metge, D.W., Osborn, C.L. and Ryan, J.N. (2005). Assessing the vulnerability of a municipal well field to contamination in a karst aquifer. Environmental & Engineering Geoscience 11(4): pp.319-331.

Sasowsky, I.D. and White, W.B. (1994). The role of stress release fracturing in the development of cavernous porosity in carbonate aquifers. Water Resources Research 30(12): pp.3523-3530.

Simpson, L.C. and Florea, L.J. (2009). The Cumberland Plateau of Eastern Kentucky. Caves and Karst of America, 2009, p.70.

Svensson, U. and Dreybrodt, W., 1992. Dissolution kinetics of natural calcite minerals in CO2-water systems approaching calcite equilibrium. Chemical Geology, 100(1-2), pp.129-145.

Swinnerton, A.C. (1929). The caves of Bermuda. Geological Magazine, 66(2): pp.79-84.

Thirria, C.É. (1830). Notice sur le terrain jurassique du département de la Haute-Saône et sur quelques-unes des grottes qu'il renferme. Mémoires de la Société d'Histoire Naturelle de Strasbourg 1(62): pp.41-42.

Vacher, H.L. and Mylroie, J.E. (2002). Eogenetic karst from the perspective of an equivalent porous medium. Carbonates and Evaporites 17(2): p.182.

White, W.B. (1999). Conceptual models for karstic aquifers. In: Palmer, A.N., Palmer, M.V., Sasowsky, I.D. (eds) Karst modeling. Karst Waters Institute Special Publication (5): pp.11–16.

White, W.B., (1988). Geomorphology and hydrology of karst terrains 551(447).

Wissbrun, K.F., French, D.M. and Patterson Jr, A., 1954. The true ionization constant of carbonic acid in aqueous solution from 5 to 45. The Journal of Physical Chemistry, 58(9), pp.693-695.

Worthington, S.R. (1999). A comprehensive strategy for understanding flow in carbonate aquifers. In Palmer, A.N., Palmer, M.V., Sasowsky, I.D. (eds) Karst modeling. Karst Waters Institute Special Publication (5): pp.30-37.

Worthington, S.R., Ford, D.C. and Beddows, P.A. (2001). Porosity and permeability enhancement in unconfined carbonate aquifers as a result of dissolution. In SPELEO Brazil 2001-13th International Congress of Speleology.

Worthington, S.R., Schindel, G.M. and Alexander Jr, E.C. (2002). Techniques for investigating the extent of karstification in the Edwards Aquifer, Texas. In Martin, J.B., Wicks, C.M., Sasowsky, I.D. (eds) Hydrogeology and biology of post-Paleozoic carbonate aquifers. Karst Waters Institute Special Publication 7: pp.173-175

**Figures**

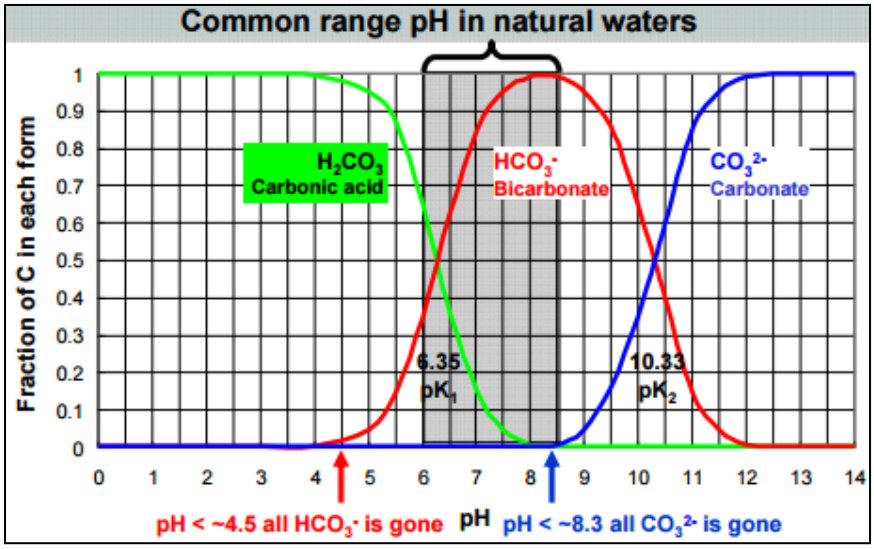


Figure 1: Relative speciation (%) of $H_2CO_3$, $HCO_3^-$ and $CO_3^{2-}$ as a function of pH in the solution. This example is made assuming a very dilute karst water (ionic strength < 0.1) at T=15°C in a close system.

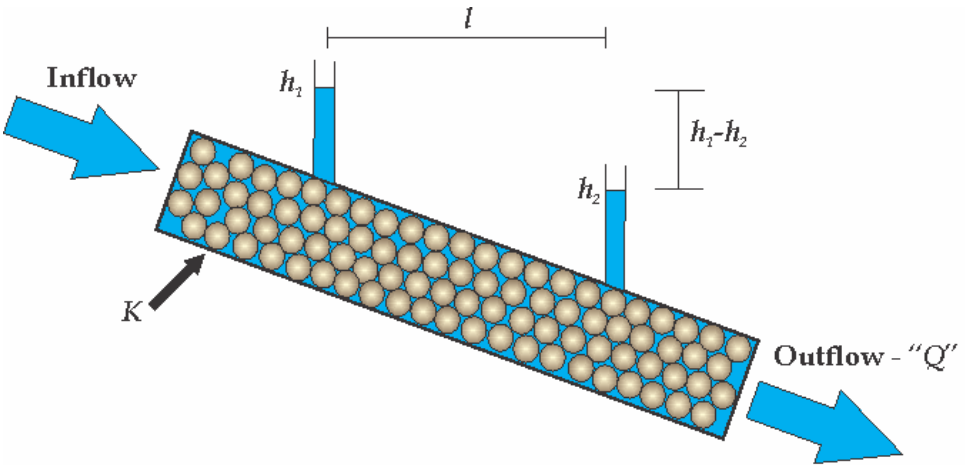


Figure 2: Basic Darcy's flow model assumes a constant hydraulic gradient and linear flow.

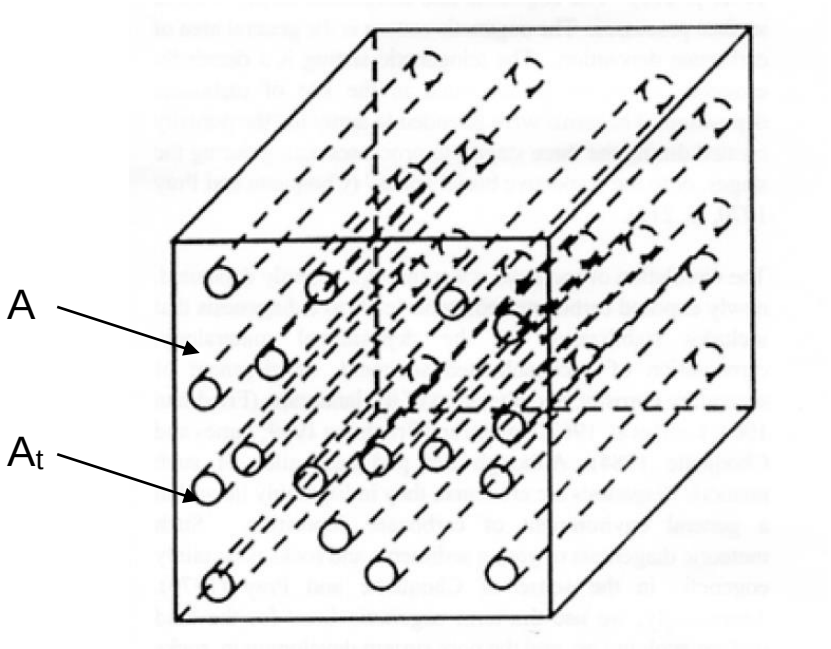


Figure 3: Diagram showing the equivalent porous medium with a tube density occupying 40% of the block (adapted from Vacher and Mylroie, 2002). A is the total surface area; $A_t$ is the specific area of each tube.

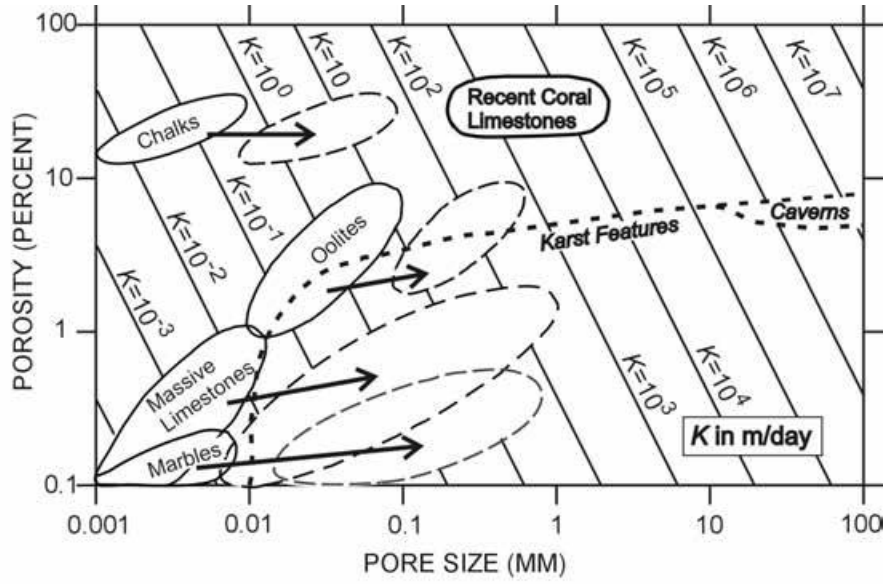


Figure 4: Primary and secondary porosity, pores size, and hydraulic conductivity of carbonates rocks, features and caverns (Brahana et al., 1988).

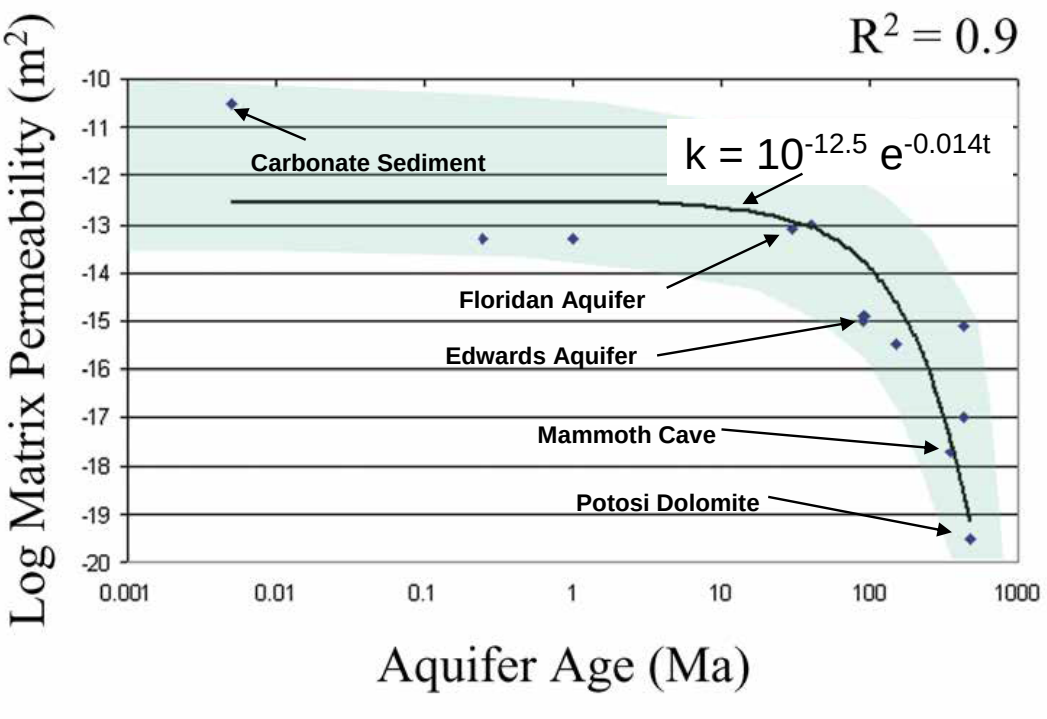


Figure 5: Matrix permeability of carbonate aquifers as an exponential function of aquifer age ($\log K = A.\ e^{-\alpha T}$). Adapted from Florea and Vacher (2006).

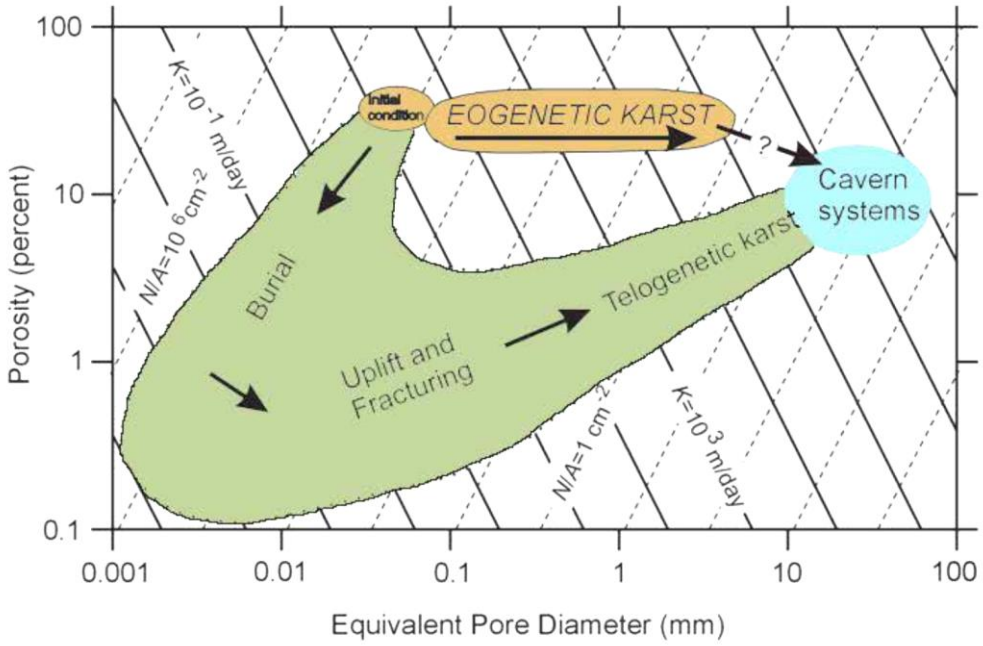


Figure 6: Classification of eogenetic and telogenetic karst based on degree of diagenetic burial and uplift. Adapted from Vacher and Mylroie (2002). Eogenetic karst from the perspective of an equivalent porous medium.

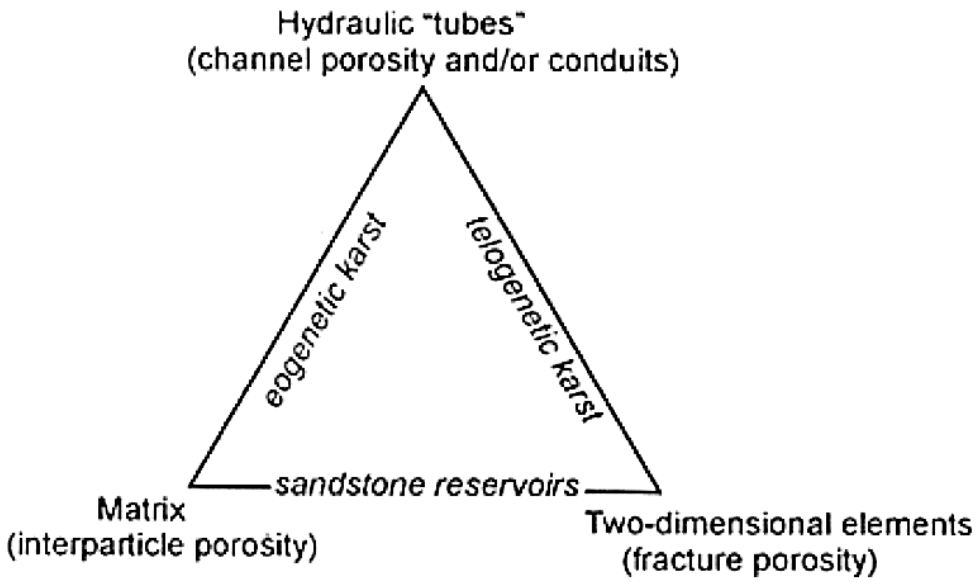


Figure 7: Concept triangle showing variables of double-porosity systems. The triangle is intended to show conceptual mixtures and not to position mixtures quantitatively as in a diagram of phases.

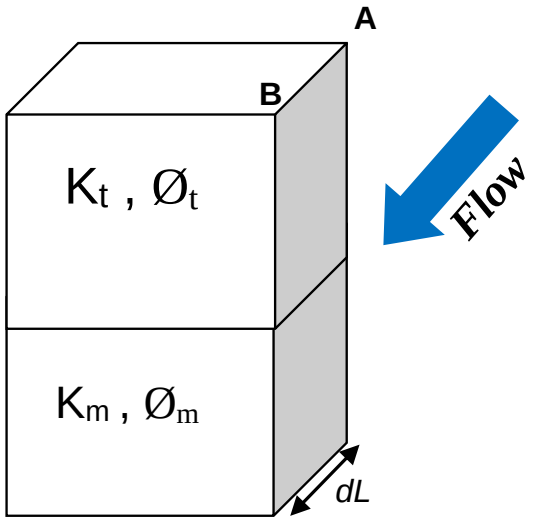


Figure 8: Diagram representing the eogenetic karst as a parallel combination of conduit/tube ($Ø_t$, $K_t$) and matrix ($Ø_m$, $K_m$) media.

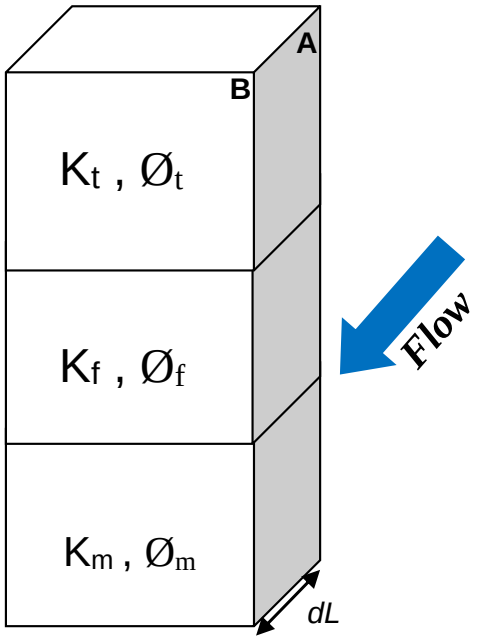


Figure 9: Diagram representing the eogenetic karst as a parallel combination of matrix ($Ø_m$, $K_m$), conduit/tube ($Ø_t$, $K_t$) and fracture ($Ø_f$, $K_f$) media.

# CHAPTER 2:

# METHODOLOGY

*"A specific question that has challenged our analytical approach in the understanding of nutrients and carbon dynamics in karst aquifers in the Cumberland region, and which in some sense constitutes the major technical innovation of this dissertation product, is the extraction of low concentrated dissolved organic carbon (DOC < 3 mg/L). Using conservative analytical procedures (cryo-concentration) and advance technology in spectroscopy (Cavity-Ring-Down Spectroscopy), this rigorous analytical challenge was overcome."*

## I.1. Site description

Two sites were selected within the study based on their locations and the geochemical lines of evidence of carbonic acid and sulfuric acid speleogenesis. The first site, the Grayson-Gunnar Cave System (GGC – Fig. 1), an 11-km-long cave system located in the study area, is a unique site to examine geochemical features of a system, which was formed primarily to carbonic acid dissolution—in other terms, a system that does not show any evidence of sulfuric acid speleogenesis within its watershed (12 $km^2$). Surveyed passages include two branches of an underground stream. The south branch of this watershed includes low-density grazing and residential septic tanks. The north branch of this watershed includes a CAFO (Concentrated Animal Feeding Operation) for poultry. Thus, this system will be used to address the estimation of carbon and nutrients loads in an aquifer strongly influenced by varying surface land-uses.

The second site is the Mill Springs System, a 7.1-square mile (18.3 $km^2$) karst system delineated west by the Kentucky State Road 1275 and east by the State Road 90 (Fig. 2) and is found within the fine to medium-grained thick Reelsville Limestones. Although no cave passage has been mapped in the area, dye trace studies revealed potential flow paths from surface recharge (sinkholes located up to 2 miles south of the major spring) to the springs and a regional flow gradient converging towards the Cumberland River (Fig. 2). The watershed is primarily forested (79.1%), secondarily agricultural -corn and soybean (18.5%) and residential (<2.5%; KWD report 2012). A CAFO has been identified in the southwestern part of the recharge area (Hannah Hills), but no connection to the regional flow paths has been found. The land-use distribution and long-term quarterly data (2005-2013) available for the MS system provides for an exceptional field laboratory to 1) study the fractional end-member mixing of various geochemical sources (road salts, oil-related sulfur brines) and their potential influence sulfuric

acid dissolution and 2) to test the influence of sulfur-rich brines on the dynamics of inorganic carbon in the critical zone.

## I.2. Groundwater sampling and monitoring

### *I.2.1. High-frequency monitoring*

At the spring for GGC (Fig. 1), an YSI EXO2-sonde was deployed in a pool close to the spring to measure integrated average values of temperature (T), pH, dissolved oxygen (DO), specific conductance (SpC), turbidity, and phycocyanin (a form of chlorophyll) during a 10-minute interval continuously during one year (from May 2015 to May 2016) with a monthly calibration. An In-Situ Aqua Troll was deployed at the same location to collect hourly values of water level, SpC and temperature.

### *I.2.2. Discrete measurements*

#### *I.2.2.1. Water level and Discharge*

Water level (m) and surface velocity (m/s) measurements were performed at a flowing stream in the vicinity of the spring on a weekly basis using a Type-A current meter. Discharge values (in $m^3/s$) were then computed using standard USGS stream gauging protocols the "*mean-section*" method provided by Rantz (1982).

In this method, the elemental strip is taken between two verticals and the mean depth ($d_m$) is taken as the average of the depths in the two verticals. The width of the strip is the distance b between the two verticals. The velocity is the strip is taken as the average of the mean velocity determined in the two verticals (Fig. 3). The discharge in the elemental strip is given by the equation

$$\Delta Q = b \times d_m \times V_m \quad \text{(Eq.1)}$$

Where $d_m$ and $V_m$ are the mean depth and the mean velocity measured for an elemental strip.

For strip 3, $d_m$ and $V_m$ are given by the following equations:

$$d_m = \frac{d_2 + d_3}{2} \quad \text{(Eq.2)}$$

$$V_m = \frac{V_2 + V_3}{2} \quad \text{(Eq.3)}$$

The stream discharge is given by:

$$Q = \sum \Delta Q \quad \text{(Eq.4)}$$

In shallow and narrow streams, as it is the case for the GGC discharging stream, $d_m << b$ (max $d_m \leq 0.1$ m), the velocity is not expected to vary considerably within the vertical depth. Therefore the velocity measured at the surface is assumed to be representative of the velocity at any point along a chosen vertical strip.

#### *I.2.2.2. Precipitation data*

Precipitation data were obtained from the USGS water data base (https://waterdata.usgs.gov). A 30-minutes interval precipitation data recorded at the Beaver Creek Station (station 03413200), located less than 4 miles away from the GGC spring near Monticello, KY was used. The station is maintained by the USGS and data are recorded on a real-time basis using a Belfort Weighing Bucket rain gage.

### *I.2.2.3. Physico-chemical variables*

Discrete measurements of temperature (T), pH, dissolved oxygen (DO), and specific conductance (SpC) were collected using an YSI Pro Plus sonde on a weekly basis at the GGC spring (May – August 2015) and at chosen locations along the Northern and Southern branches (PLP passage and H passage respectively) of a monthly basis.

### *I.2.2.4. Dissolved analytes*

To achieve the goal of assessing end-members mixing sources in a system formed through carbonic acid speleogenesis (GGC), a detailed investigation was performed on dissolved ions, including nutrient concentrations (nitrogen species and phosphates), concentrations and isotopic ratios of both organic and inorganic carbon, and trace metals from the spring and the two contributing end-members (northern branch and southern branch; Fig. 1) that accounts for the spring discharge. Discrete water samples were collected on a weekly basis from May to August 2015 at the above three locations. All samples were pumped through a 0.45 µm-cellulose filter. Following sampling and storage, water samples were transported to the field house (Fig. 1) and analyzed for nutrient speciation ($NO_3^-$, $NO_2^-$, $NH_4^+$ and $PO_4^{3-}$) within 48 hours. Samples collected for major ions, dissolved organic carbon (DOC), dissolved inorganic carbon (DIC), metals and carbon isotopes were stored in a refrigerator at 4°C and further shipped to the Ball State University Environmental Geology Laboratory for analyses.

#### *I.2.2.4.1. Major ions*

Samples for cations and anions analyses were collected in 250 mL HDPE bottles. Cations and anions (except bicarbonate) were analyzed using a Dionex 3000 ion chromatograph at the BSU

Organic Chemistry laboratory, and stored at 4°C until the time of analysis. For cations analysis, 2 mL of 6N nitric acid $HNO_3$ was added to each bottle before sampling to avoid flocculation and precipitation of metal colloids prior to analysis. Cations and anions were analyzed using Dionex 3000 liquid chromatography.

*I.2.2.4.2. Total Alkalinity*

For total alkalinity measurements, Gran titrations were performed in-situ using HACH kits on filtered and unfiltered water samples to discriminate between contributions to alkalinity from dissolved and particulate inorganic carbon (DIC and PIC). The principle of Gran titration is to add an increasing volume of 16 N of nitric acid to a 100 mL water sample at a given temperature in a step-wise fashion, and follow the corresponding increase in pH. The point of inflection or point of change in color corresponds to the equilibrium between acid species ($H^+$) and all the alkaline species ($HCO_3^-$, $CO_3^{2-}$ and $OH^-$) present in the water sample (Fig. 4). The values of acid volume and pH added were then entered in the USGS alkalinity calculation website (https://or.water.usgs.gov/alk/) to determine the value of total alkalinity (expressed in mg/L of equivalent $CaCO_3$), and its speciation into bicarbonates (mg/L of equivalent $HCO_3^-$), carbonates (mg/L of equivalent $CO_3^{2-}$), and hydroxides (mg/L of equivalent $OH^-$).

*I.2.2.4.3. Nutrients: Dissolved Inorganic Nitrogen speciation and orthophosphates.*

Samples for Dissolved Inorganic Nitrogen speciation and orthophosphates were collected using a 0.45 µm-cellulose filter in 250 mL high-density polyethylene bottles. Speciation of nitrogen ($NO_3^-$, $NO_2^-$, $NH_4^+$) and orthophosphate ($PO_4^{3-}$) was performed within 48 hours at the field house using a colorimetric titration on a HACH DR2800 portable spectrophotometer. The instrument was calibrated for $NO_3^-$ and $PO_4^{3-}$ titration. However, due to the instability of $NO_2^-$

and $NH_4^+$ species in water samples, it is unusual to build calibration curves for their titration. Thus $NO_2^-$ and $NH_4^+$ values were directly reported as read from the spectrophotometer.

To obtain the $NO_3^-$ calibration curve, a 100 mg/L N-$NO_3^-$ standard solution was successively diluted into 10 mg/L, 5 mg/L, 3 mg/l, 2.5 mg/L, 2 mg/L solutions respectively. For each concentration a standard titration was preformed and the values yielded by the DR2800 spectrophotometer were recorded and developed into a graph. With a regression coefficient of 0.96, the power function was the best fit for the calibration (Fig. 5).

A similar calibration was performed for orthophosphate species by successively dissolving a 10 mg/L P-$PO_4^{3-}$ standard solution into 5mg/L, 2.5 mg/L, 1 mg/L, 0.5 mg/l and 0.25 mg/L solutions respectively and plotting the yielded values along with the known standard concentrations of the diluted samples. A linear fit with a regression coefficient of 0.97 is the best fit for the data (Fig. 6).

*I.2.2.4.4. Dissolved Inorganic Carbon*

Samples collected for dissolved inorganic carbon (DIC) were all filtered using a 0.45 µm-cellulose filter to remove the particulate carbon and stored in 40 mL glass vials with septum using the complete filling with no air standard method. Due to very high volatility of dissolved $CO_2$ and to preserve the DIC content and avoid further exchange of $CO_2$ with the ambient atmosphere during or immediately after sampling, 2 mg of NaOH powder (N/44 standard) were added to the 40 mL vials before collection of water sample. Samples were analyzed for DIC through the Sievers 900 $CO_2$ purging system at the Ball State University Organic Chemistry laboratory. The DIC was purged out of each sample in the form of $CO_2$ gas using a combined persulfate and UV oxidation process. The $CO_2$ gas was then mixed with pure water and the

equivalent DIC concentration was detected as a change in specific conductivity of the pure water solution, and reported as mg of DOC per liter of water or part per mil.

*I.2.2.4.5. Dissolved Organic Carbon*

Dissolved Inorganic Carbon (DOC) samples were all filtered using a 0.45 µm-cellulose filter to remove the particulate carbon. DOC samples were collected in 250 mL HDPE bottles. During sampling, sample bottles were completely filled without air and kept at a temperature below 14°C. DOC content was measured using a Sievers 900 carbon analyzer. Following DIC measurements, water samples were acidified with $H_2PO_3$ and purged with N gas to remove any non-purgeable DIC fraction prior to the measurement of DOC. The remaining organic carbon is oxidized to $CO_2$, which is released from the sample dissolve into pure water. The equivalent DOC is detected as a change in specific conductivity of the pure water solution, and reported as mg/L or ppm DOC.

*I.2.2.4.6. Dissolved Organic Carbon aromaticity: Specific UV Absorbance.*

The Specific Ultra-Violet Absorbance at 254-nanometer wavelength ($SUVA_{254}$) was used to assess the DOC aromaticity. $SUVA_{254}$ is defined as the UV radiation length absorbed at 254 nanometers by a given molecule. $SUVA_{254}$ is an "average" absorptivity scale for all the molecules in a water sample that comprise aromatic fractions of DOC (hydrophobic and hydrophilic) and has been used as a surrogate measurement for DOC aromaticity. It is now proven that a strong correlation exists between molar absorptivity ($\lambda$= 254 nm) and aromatic carbon content of aquatic humic substances (non-decomposed organic substances) in a variety of terrestrial environments (Weishaar et al. 2003; Fig. 7) meaning that aromatic carbon content and

the UV absorbance (UVA) are good indicators of DOC reactivity in a number of environmental processes (Fig. 7).

According to Potter and Wimsatt (2009), SUVA calculation requires both the DOC and UVA measurements. The DOC concentration was determined using the Sievers 900 TOC analyzer as detailed in section *II.2.2.4.5*. The UVA measurement requires that the water sample be passed through a 0.45-µm cellulose filter and transferred to a quartz cell. It is then placed in a spectrophotometer to measure the UV absorbance at 254 nm and reported in $cm^{-1}$.The SUVA is then calculated by dividing the UVA of the water sample (in $cm^{-1}$) by the DOC concentration of the sample (in mg/L) and then multiplying the result by 100 cm/M. SUVA is reported in units of L/mg-M. The EPA method for SUVA calculation is summarized by the following equations:

$$SUVA\ (L/mg.m) = UVA\ (cm^{-1}) / DOC\ (mg/L) * 100\ cm/m \quad (Eq.5)$$

$$UVA = A / d \quad (Eq.6)$$

Where UVA is the calculated UV absorbance of the sample in absorbance units ($cm^{-1}$), A is the measured UV absorbance at 254 nm of the sample that is filtered through a 0.45-µm cellulose filter media, and d is the quartz cell path length in cm.

### *I.2.2.5. Isotopes: $\delta^{13}$C-DIC, $\delta^{13}$C-DOC*

#### *I.2.2.5.1. $\delta^{13}$C-DOC analysis*

Samples for $\delta^{13}$C-DOC were collected in 1 L HDPE (High Density Polypropylene) bottles with no headspace, using a 0.45-µm filter to remove particulate and suspended matter and preserved with 1 mL of 12 N HCl and a Parafilm barrier.

A method for $\delta^{13}$C-DOC measurement in stream water with low DOC concentrations (< 20 µmol of $CH_2O$ for equivalent 150–200 mL of stream water or < 3 mg of equivalent DOC per liter of water) is provided by Gandhi et al. (2004). In such case, sample preparation prior to isotope analysis includes three major steps originally described in the literature for enzyme extraction from protein solutions (Virgen-Ortíz et al., 2012): 1) acidification to remove volatile DIC, 2) evaporative condensation (also referred to as lyopholization, cryoconcentration or cryopreservation), and 3) combustion (Fig. 8).

*Acidification*

Prior to the evaporative condensation, samples were acidified with 1mL of HCl to purge any remaining volatile DIC in the form of $CO_2$ gas.

*Cryo-concentration*

Cryo-concentration has been widely used for the conservation of a wide range of biological materials (Day and Stacey, 2007). In the analytical procedure, however, the choice of cryo-concentration over another concentration technique arose from the need to preserve the organic carbon in samples that were already consistently depleted in organic carbon (average range: 0.10 to 2.20 mg/L) with regards to the average content in freshwater (average range of 0.7 to 7 mg/L in groundwater and rivers across the US; Perdue and Ritchie, 2003).

The goal of cryo-concentration was to concentrate the DOC content of water samples up to 3000 µg/L which is the detection limit for the PICARRO Cavity-Ring-Down spectrophotometer (CRDS) combustion module ($\delta^{13}$C-DOC). The advantage of cryo-concentration compared to common evaporative concentration techniques is that it produces better yields for concentrates by preserving the purgeable fraction of DOC from loss during the evaporation process. A 79.8% average DOC recovery was estimated through cryo-concentration for all samples, which is even

higher than the yield obtained for DOC extraction in freshwater through common solid-phase extraction techniques such as XAD resins (yield = 56-60%; Aiken et al. 1992; Malcom and MacCarthy, 1992).

Prior to analysis, 2 glass flasks of 1200 ml countenance were filled with 500 mL sample each. Flasks were previously rinsed with ultra-pure deionized water to limit any carbon contamination into the samples. Samples were then frozen using liquid Nitrogen. Water samples were equally homogenized on the surface of the flask during freeze-drying to insure a good distribution of the sample and higher carbon recovery. Samples were then loaded on the condensative module operating on ice-air exchange mechanism (sublimation). The precipitation that occurs during the condensative process allows the organic carbon to be preserved during the sublimation (ice-vapor exchange) process. The condensation is done in 2 steps: the 1200 ml flask is placed on the condensator for 40 to 72 hours. The recovered solid is then dissolved using nanopure water and carefully poured into a 300 mL flask which is then placed on the condensator for additional 48 hours. The yielded resin is preserved at 4°C fridge before loading into the combustion module of a Picarro CRDS spectrophotometer for $\delta^{13}$C-DOC analysis.

*Combustion*

Isotope measurements of DOC content were performed using the Picarro CRDS (Fig. 9) and the methodology provided by Gupta et al. (2009). Resin obtained from evaporative condensation is injected through a 9.5 mm septum-sealed port into a combustion chamber where it reacts with a dry gas ($N_2$) at 140°C. The resulting water vapor ($H_2O$ gas) and secondary gases (primarily $CO_2$ and $N_2O$) are then carried by a stream of helium through a thermally-inert cylinder (walls made of copper, quartz chips, quartz wool) at 650°C. The homogeneous mixture of the sample and dry gas flows to the gas-phase instrument at a constant flow rate via a three-way valve, where its

isotopic content ($^{13}C/^{12}C$ of $CO_2$ gas) is repeatedly measured as a function of the decay time and the reflection of a laser light inside the cylinder (depletion spectroscopy). The isotopic content is then standardized into a carbon isotope ratio $\delta^{13}C$-DOC using an element of known carbon content (Cretaceous marine Pee Dee Belemnite PDB, $^{13}C/^{12}C = 0.0112372$) and the following relation:

$$\delta^{13}C\text{-DOC} = [((^{13}C/^{12}C_{sample}) / (^{13}C/^{12}C_{standard})) - 1] \text{ X } 1000 \quad \text{(Eq.7)}$$

*I.2.2.5.2. $\delta^{13}C$-DIC in groundwater*

Samples for $\delta^{13}C$-DIC were filtered using a 0.45 µm-cellulose filter and collected in a 30 mL borosilicate vial sealed with parafilm. To prevent any biological reaction susceptible of changing the DIC content upon sampling, vials were rinsed with HCl, autoclaved at 500°C and preserved with copper (II) sulfate prior to sampling. Analytical procedures for DIC were derived from Capasso et al. (2005). Samples are acidified and volatile DIC species are transformed into $CO_2$. Water samples are then directly injected by syringe into 5.9 ml vials with screw caps which have a piercable rubber septum. A carrier gas ($N_2$) is flushed into the vials through a syringe that simultaneously dispenses a fixed amount of phosphoric acid ($H_3PO_4$) purging out any residual non-labile DIC in form of $CO_2$ gas. The resulting $CO_2$ is purged into a distilled water solution. After equilibrium is reached (usually in less than 24 h at a temperature of 70°± 0.1°C), the sample is loaded into a Picarro CRDS. The isotope content of DIC is analyzed using the same procedure provided for DOC isotope, except that samples are introduced in the combustion chamber in liquid form.

### *I.2.2.6. Metals*

Samples for metals analyses were collected in 250 mL HDPE bottles and analyzed using Inductively Coupled Plasma Mass Spectrometry (ICPMS) at the Muncie Water Quality Division Laboratory.

## References


Aiken, G.R., McKnight, D.M., Thorn, K.A., Thurman, E.M. (1992) Isolation of hydrophilic organic acids from water using nonionic macroporous resins. Org. Geochem., 18, 567-573.

Blair R.J., Ray J.A., O'dell P.W., Marbert B.S., Goodmann P.T. (2012) Integrated Surface Water and Groundwater Assessment of Large Springs in the Green River Basin (BMU4, Round 2). Project Report 0503. Kentucky Division of Water.

Capasso, G., Favara, R., Grassa, F., Inguaggiato, S. and Longo, L. (2005) On-line technique for preparing and measuring stable carbon isotope of total dissolved inorganic carbon in water samples (d13CTDIC). Annals of Geophysics, 48(1).

Day, J.G. and Stacey, G. (2007) Cryopreservation and freeze-drying protocols (Vol. 368). Springer Science & Business Media.

Gandhi, H., Wiegner, T.N., Ostrom, P.H., Kaplan, L.A. and Ostrom, N.E. (2004) Isotopic (13C) analysis of dissolved organic carbon in stream water using an elemental analyzer coupled to a stable isotope ratio mass spectrometer. Rapid Communications in Mass Spectrometry, 18(8), pp.903-906.

Gupta, P., Noone, D., Galewsky, J., Sweeney, C. and Vaughn, B.H., (2009) Demonstration of high-precision continuous measurements of water vapor isotopologues in laboratory and

remote field deployments using wavelength-scanned cavity ring-down spectroscopy (WS-CRDS) technology. Rapid communications in mass spectrometry, 23(16), pp.2534-2542.

Malcolm, R.L., MacCarthy, P. (1992) Quantitative evaluation of XAD-8 and XAD-4 resins used in tandem for removing organic solutes from water, Environ. Intern., 18, 597-607.

Perdue, E.M. and Ritchie, J.D. (2003) Dissolved organic matter in freshwaters. Treatise on geochemistry, 5, p.605.

Potter, B.B. and Wimsatt, J.C. (2009) Determination of total organic carbon and specific UV absorbance at 254 nm in source water and drinking water. N.E.R. Laboratory, O.O.R.A. Development, U.S.E.P.A Cincinnati, Ohio 45268.

Rantz (1982) Measurement and computation of streamflow, v. 1, Measurement of stage and discharge. United States Geological Survey Water Supply Paper 2175: 284.

Virgen-Ortíz, J.J., Ibarra-Junquera, V., Osuna-Castro, J.A., Escalante-Minakata, P., Mancilla-Margalli, N.A. and Ornelas-Paz, J.D.J., 2012. Method to concentrate protein solutions based on dialysis–freezing–centrifugation: Enzyme applications. Analytical biochemistry, 426(1), pp.4-12.

Weishaar, J.L., Aiken, G.R., Bergamaschi, B.A., Fram, M.S., Fujii, R. and Mopper, K. (2003) Evaluation of specific ultraviolet absorbance as an indicator of the chemical composition and reactivity of dissolved organic carbon. *Environmental science & technology*, *37*(20), pp.4702-4708.

Zare, R.N., Kuramoto, D.S., Haase, C., Tan, S.M., Crosson, E.R. and Saad, N.M., 2009. High-precision optical measurements of 13C/12C isotope ratios in organic compounds at natural abundance. Proceedings of the National Academy of Sciences, 106(27), pp.10928-10932.

**Figures**

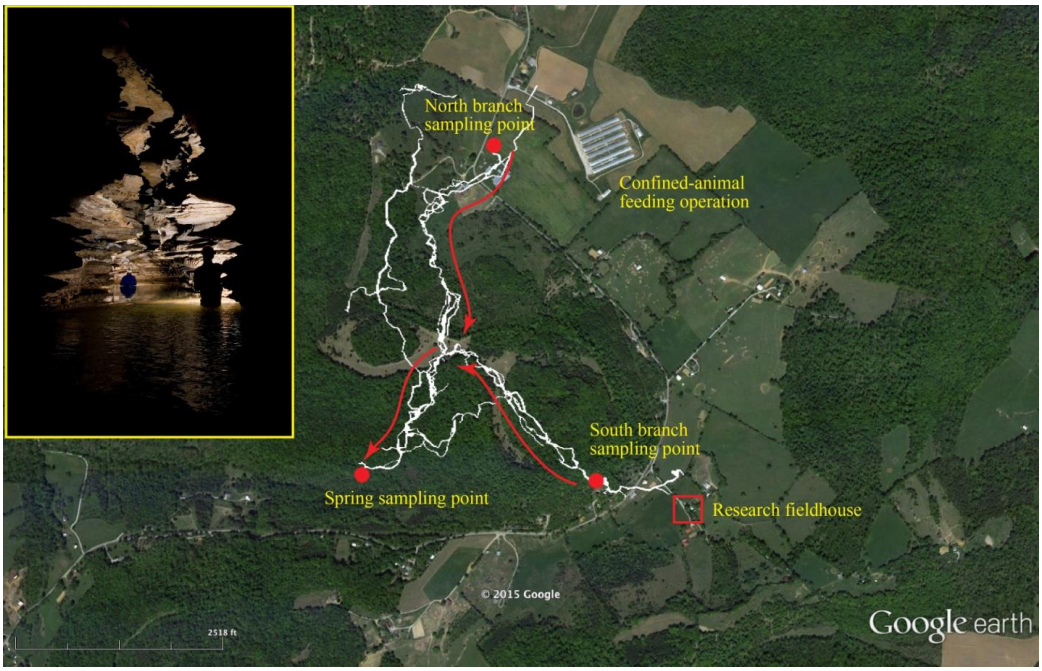


Figure 1: Surveyed passages of Grayson-Gunnar Cave are shown in white and are courtesy of members of the Greater Cincinnati Grotto of the National Speleological Society. Red arrows illustrate primary groundwater flow paths. Red dots are the selected sites for data collection from each fork of the cave and from the combined flow at the spring. The research field house that will serve as a base of operations is shown in the red square. The inset image by Robert Coomer is of the main stream upstream from the spring.

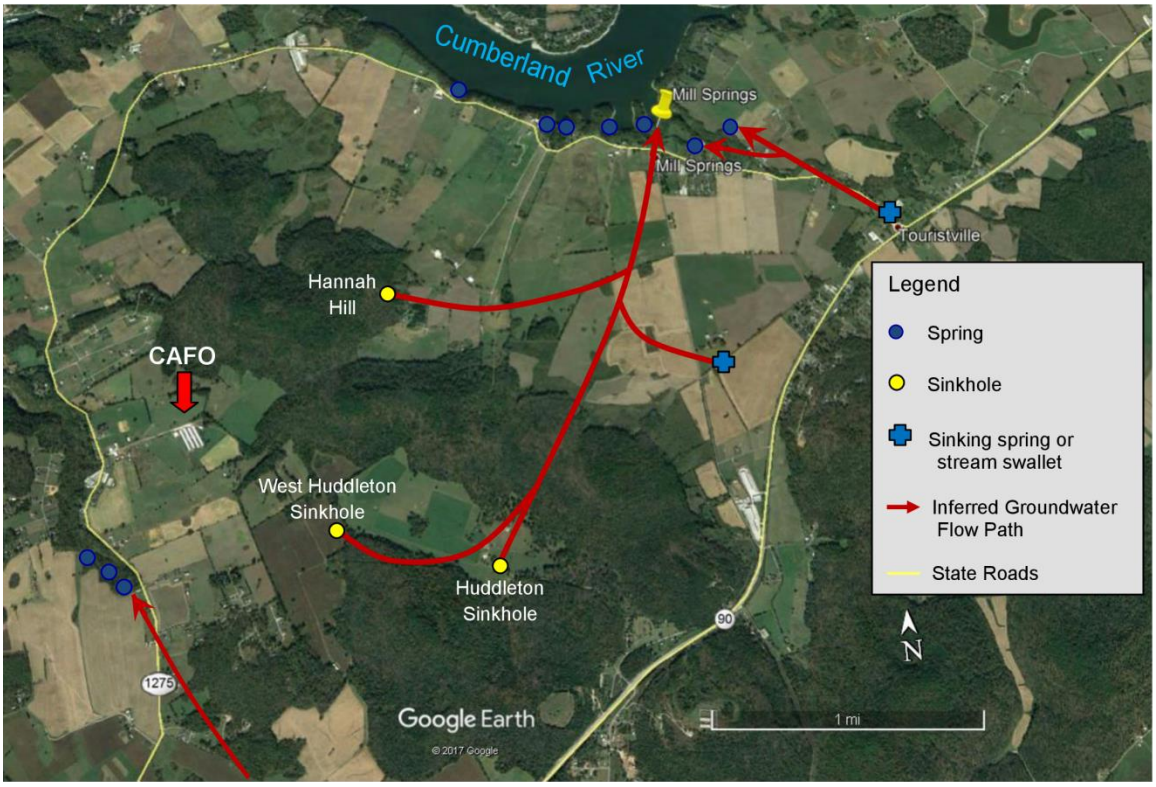


Figure 2: Inferred groundwater flow paths from preliminary Groundwater Tracing conducted by the Kentucky Division of Water within the Mill Springs recharge basin. Red arrows illustrate generalized pathways between tracer injections in sinkholes and dye recovery at Mill Springs.

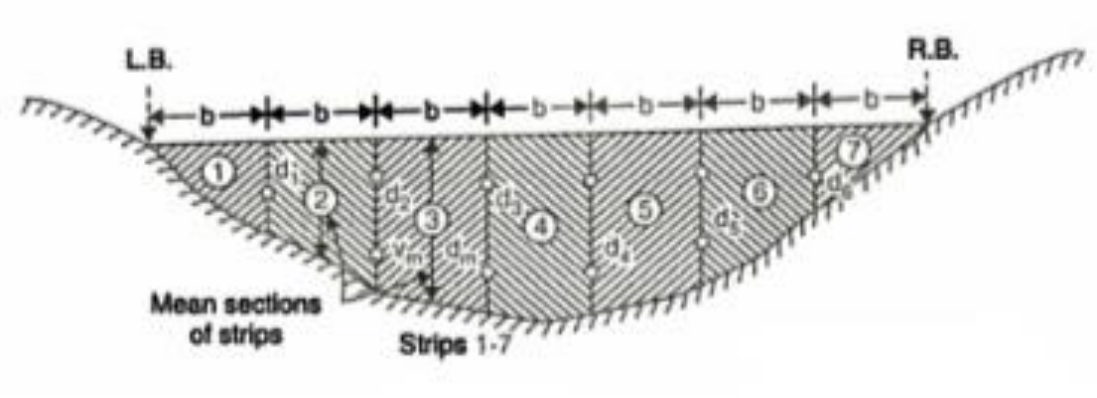


Figure 3: Principle of discharge calculations using the mean-section method (Rantz, 1982).

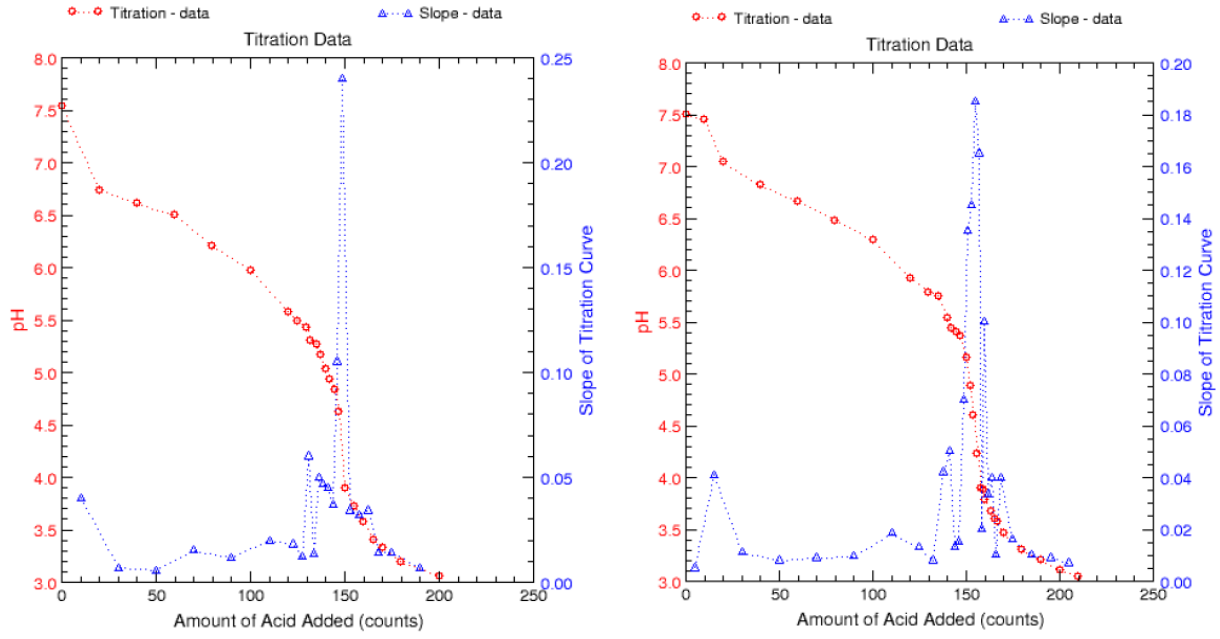


Figure 4: Titration curves obtained using the Grant inflection point method on a sample collected at the GGC discharging stream on the 06-05-2015. The left graph represents the filtered sample and the right represents the unfiltered.

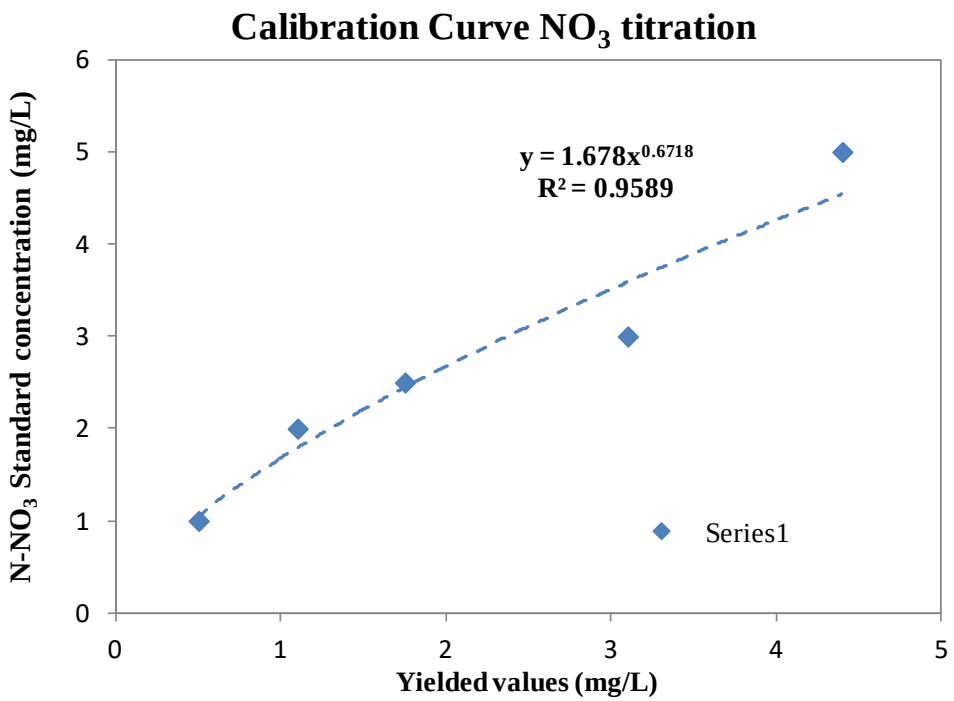


Figure 5: Calibration curve obtained for nitrate species.

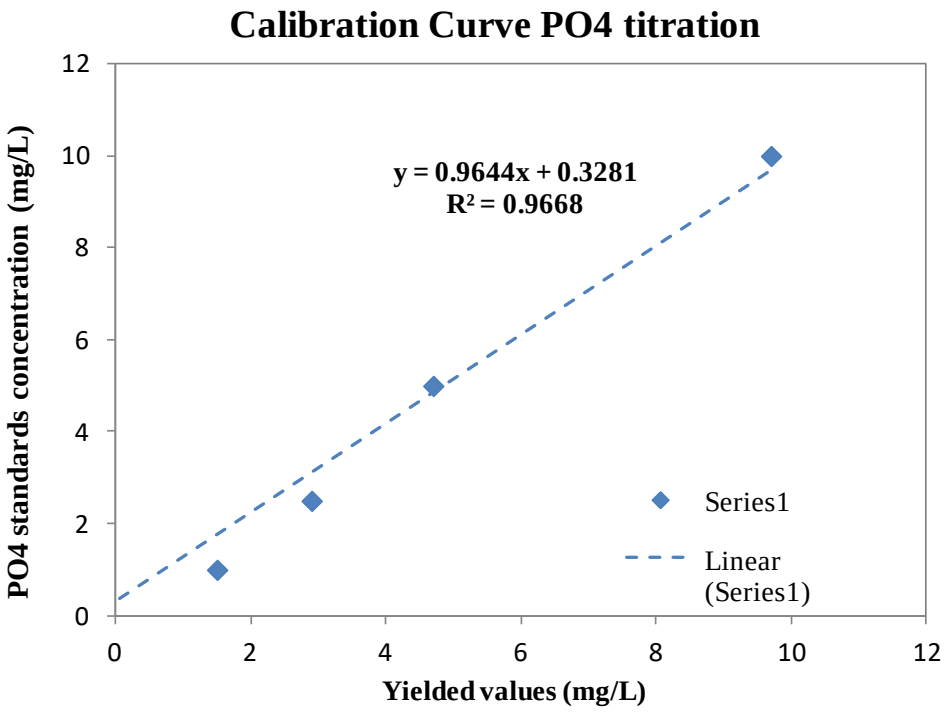


Figure 6: Calibration curve obtained for orthophosphate species.

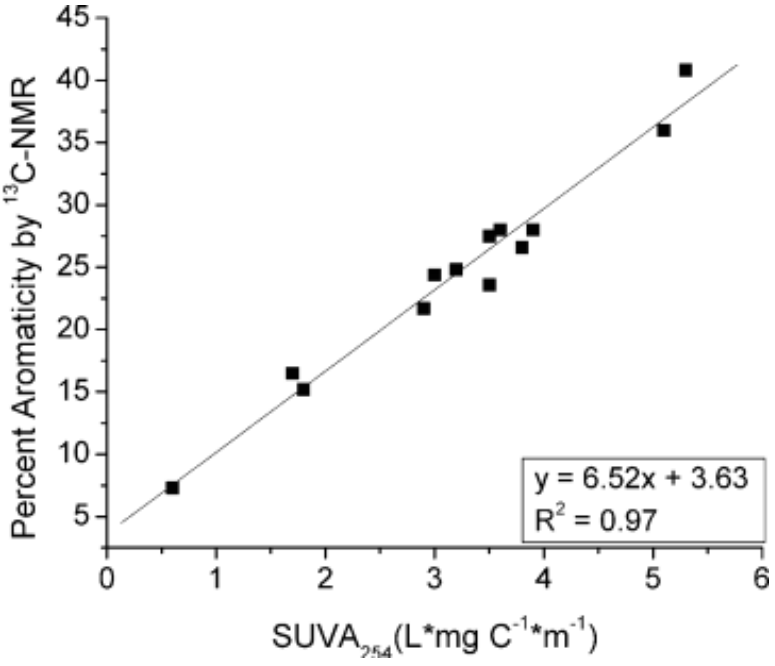


Figure 7. Linear correlation obtained between $SUVA_{254}$ and percent aromaticity from various samples collected in a variety of terrestrial environments including the United States and Antarctica. Data suggest that UV absorbance is a good indicator of the content in aromatic fractions of the Natural Organic Matter.

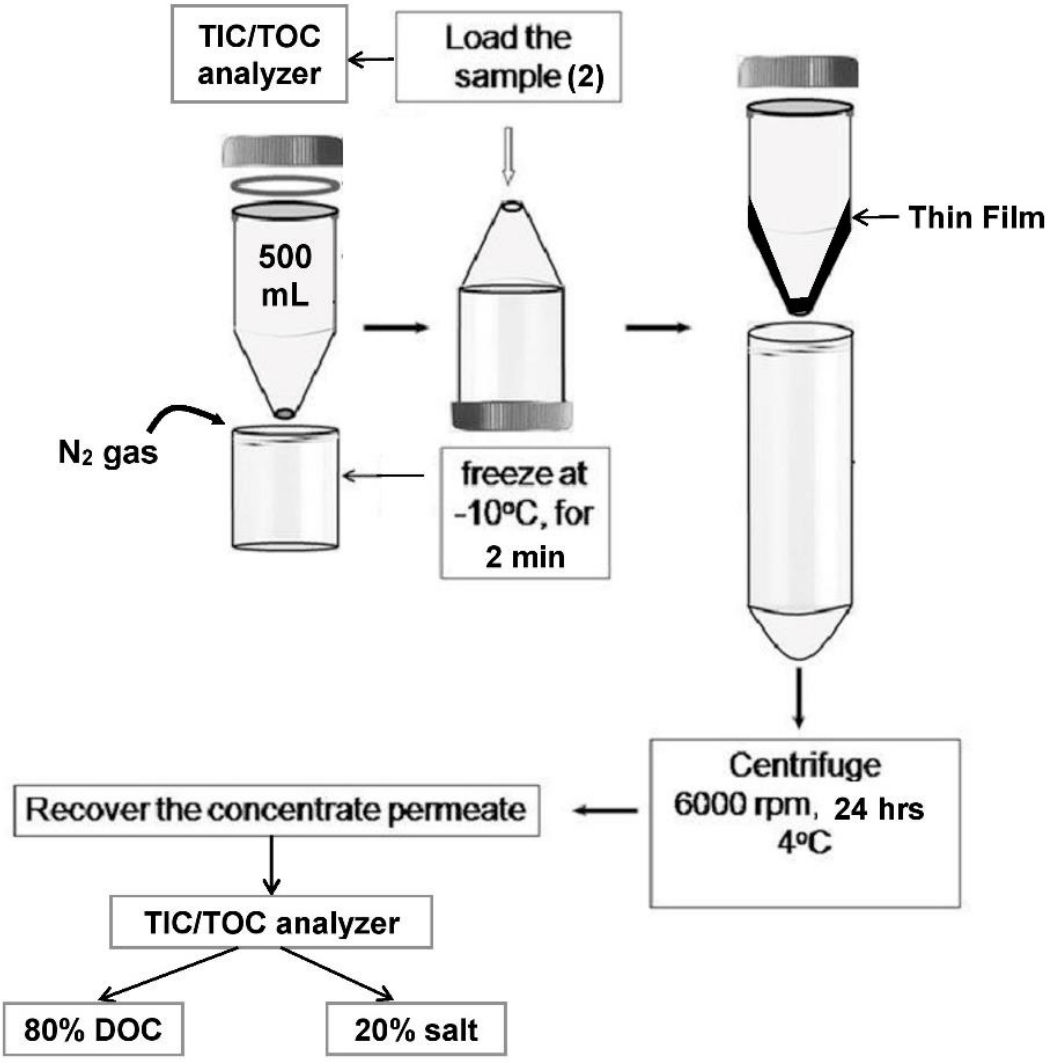


Figure 8: Schematical representation of the Dissolved Organic Carbon extraction process prior to analysis for stable isotope ($\delta^{13}$C-DOC). Adapted from Virgen-Ortíz et al. (2012)

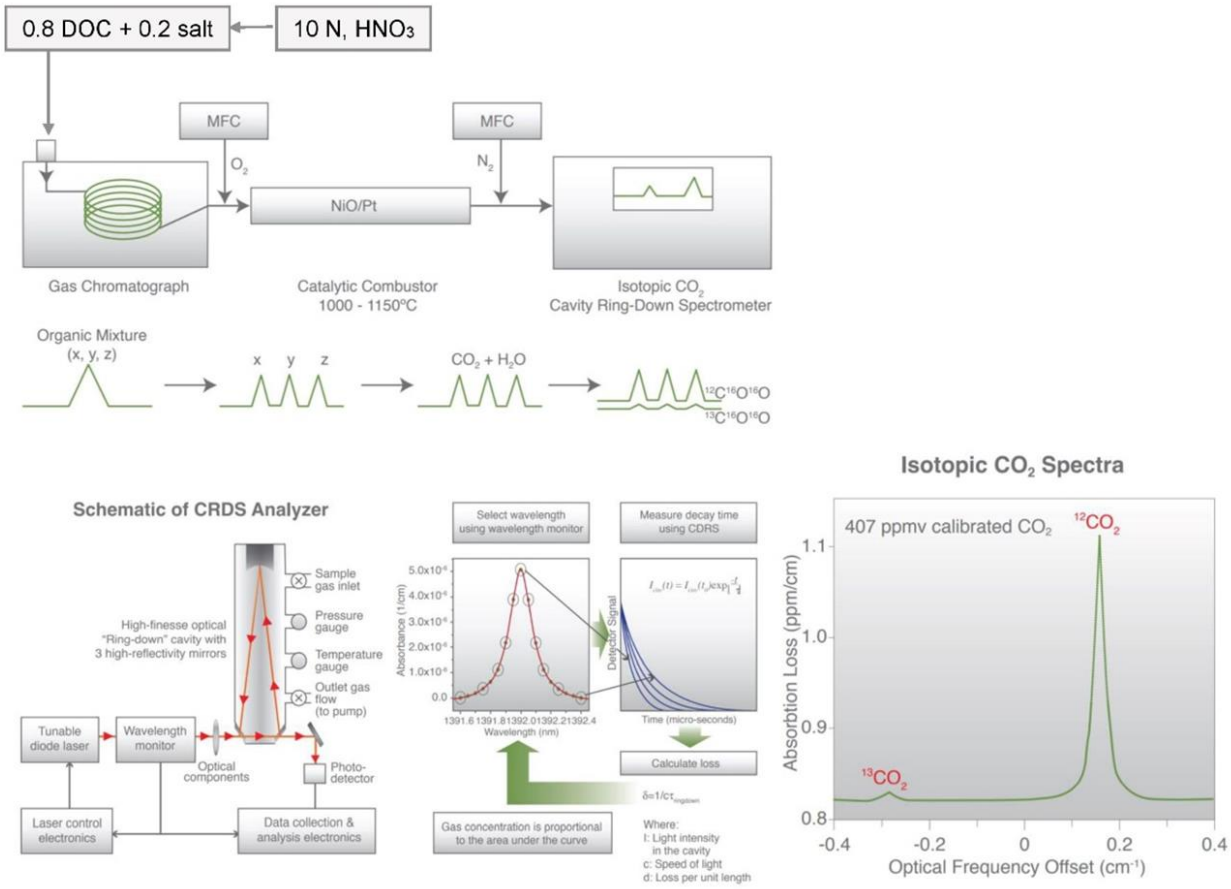


Figure 9: Schematic representation of stable isotope analysis of organic carbon using Cavity Ring-Down Spectrometry. Adapted from Zare et al. (2009).

# Tables

Table 1: A summary of water sampling and analysis protocol (Implemented for the summer 2015 sampling phase at GGC)

| Order | Parameters | | Filtration | Sampling method | Container | Duplicate | Prewashing | Conservation agent | Analysis |
|---|---|---|---|---|---|---|---|---|---|
| 1 | Cations | Ca, Mg, Na, K , Mn, Fe, Al, As | No | Classic filling | 250 ml high-density polyethylene bottles | | No | HNO3 | Ion Chromatography |
| 2 | Anions | Br, F, Cl, SO4 | No | Classic filling | 250 ml high-density polyethylene bottles | | No | No | Ion Chromatography |
| 3 | Total Alkalinity | $HCO_3$, $CO_3$ | No | Hach Alkalinity titration (acid titration) **in-situ** | Test tube | 1 filtered | prerinced with water sample | No | USGS alkalinity calculation (Inflection point) |
| 4 | DIC/DOC | DIC | 0.45 µm filter | Seringue filling with no air | 40 mL vials, glass with silicone septa | 1 | Rinced with HCl +Heated at 500°C | Cupper Sulfate (CuS) | Sievers 900 TIC analyzer (Inorganic $CO_2$ purge) |
| | | DOC | 0.45 µm filter | Seringue filling with no air | 40 mL vials, glass with silicone septa | 1 | Rinced with HCl +Heated at 500°C | 2000µL HNO3 | Schimadzu TOC analyzer* |
| 4 | Nutrients | Total Nitrogen | 0.45 µm filter | Seringue filling with no air | 40 mL vials, glass with silicone septa | 1 | Rinced with HCl +Heated at 500°C | 2000µL HNO3 | Schimadzu TOC analyzer (unspeciated N) |
| | | $NO_3$, $NO_2$, $NH_3$ | 0.45 µm filter | Seringue filling with no air | 250 ml high-density polyethylene bottles | | No | No | colorimetric titration on HACH DR 2800 spectrophotometer |
| | | Orthophosphate PO4 | 0.45 µm filter | Seringue filling with no air | 250 ml high-density polyethylene bottles | | No | No | colorimetric titration on HACH DR 2800 spectrophotometer |
| 5 | Isotopes | $\delta^{13}C$ (DIC) | 0.45 µm filter | Seringue filling with no air | 40 mL vials, glass with silicone septa | 1 | Rinced with HCl +Heated at 500°C | CuS+ 2000 µL of standard NaOH | Picarro δC analyzer |
| | | $\delta^{13}C$ (DOC) | 0.45 µm filter | Seringue filling with no air + Evaporation + Acidification | 1 L low-density polypropylene (Nalgene) bottle | 1 | Rinced with HCL | 1 mL of 12N HCl | Picarro δC analyzer |

# CHAPTER 3:

# INFERRING GROUNDWATER FLOW AND RECHARGE FROM TIME SERIES ANALYSIS OF STORM RESPONSES IN THE CUMBERLAND PLATEAU SINKHOLE PLAIN OF SOUTHEASTERN KENTUCKY.

Hydrogeol J. (2018) 26: 2649. https://doi.org/10.1007/s10040-018-1837-8
Received: 16 November 2017; Accepted: 22 July 2018; Published: 06 August 2018
Tagne, G.V.[1], Dowling, C.[2]
[1,2] Department of Geological Sciences, Ball State University, 2000 W University Ave, Muncie, IN 47306, USA.

**Abstract**

Epigenic karsts exhibit strong connectivity to surface recharge. In land-use dominated by extensive agriculture and farming, epigenic karst aquifers are highly vulnerable to surface contaminants from point and non-point sources. Currently, the karstic landscapes of the Southeastern Kentucky platform are impacted by a rapid proliferation of confined animal feeding operations. The analyses of karst aquifer responses to storm events provide qualitative information regarding aquifer recharge flow paths and groundwater residence time, and the knowledge of spatial and temporal variations in recharge and flow is crucial to the understanding of the fate of surface contaminants. Time series correlation analyses on long-term physicochemical data recorded at the outlet of Grayson Gunnar Cave, an epigenic karst system located along the Cumberland escarpment in Southeastern Kentucky, revealed the existence of two separate conduit branches responding 4 to 8 hours apart from each other. Recorded storm response times range from 4 hours for flushing and dilution to 7 hours for recovery. The fastest responding branch accounts for the majority (80%) of the spring discharge. An estimated volume of 6 million liters is discharged from both branches during major storms. As evidenced by groundwater residence time (7 days), recharge is likely characterized by localized infiltration of rain water from subsurface sinkhole to the conduits with no contribution of regional or lateral groundwater flow.

Keywords: Karst · Groundwater flow · Contamination · Time series analysis · Kentucky

## I. Introduction

A large fraction of surface contaminants from intensive agricultural and farming landscapes can be transferred through streams and shallow aquifers within a few hours following precipitation and major discharge events (Hooda et al. 2000). Epigenic karsts, the upper boundary of a karst

system that has enhanced porosity, similar to a vadose zone in carbonate rocks, are vulnerable to surface contaminants because their strong hydrological connection with meteoric recharge through sinkholes, karst windows, springs, and caves (White 1988; Ford and Williams 2007), and secondary porosity enhancement through carbonate dissolution, thus raising specific concerns for water quality and water resource protection (Mull et al. 1988; Brahana et al. 2014). In addition, the proliferation of confined-animal feeding operations (CAFOs) on epigenic karst terranes in recent years has raised new concerns about the vulnerability of karst aquifers to point (e.g., manure lagoons) and non-point (e.g., manure-fertilized croplands) sources of contamination from animal wastes (Brahana et al. 2014).

The analysis of aquifer response to storms and the estimation of recharge and flow paths provide valuable information to the understanding of contaminant transfer in groundwater. Time series correlation analyses have been widely used in karst hydrogeology to quantify aquifer response time and estimate surface contaminants transfer patterns following major storm events (Padilla and Pulido-Bosch 1995; Larocque et al. 1998; Massei et al. 2006; Fiorillo and Doglioni, 2010). Using time series correlation analyses on specific conductivity and discharge at the South Spring System (SSS), an epigenic karst located in the Maynardville limestones (Cambrian age) in Tennessee (Fig. 1) Desmarais and Rojstaczer (2002) differentiated the spring response into 3 stages: flushing, dilution, and recovery (Fig. 3). During the flushing phase, the groundwater storage water is pushed out by the incoming surface recharge into the spring. This phase is characterized by a peak in specific conductivity, marking the arrival of the groundwater storage water at the spring. The dilution phase is characterized by a prolonged decrease in specific conductivity, marking the dilution of the groundwater by the newly infiltrated storm water. Using cross-correlation analyses between rainfall (input signal) and water level, specific

conductance, and turbidity (as outputs signals), Massei et al. (2006) assessed the dynamics of the Hannetot epigenic karst aquifer in Late Cretaceous Age chalks of the Lower Seine Valley (Haute-Normandie, France). The study revealed low aquifer inertia (short memory effect) for water level and turbidity and a much higher aquifer inertia (longer memory effect) for specific conductivity. The results also revealed the occurrence of two primary flow paths for recharge water: a faster and highly reactive flow path marking the rapid flush of turbid surface water through the groundwater conduit system following major rainfall events, and a slower one related to a delayed infiltration of storm-derived water through the matrix and the fissures of the epikarst. Water levels revealed a non-linear behavior of the system in response to direct rainfall, therefore suggesting that the discharge at the spring may be controlled by the dynamics of the epikarst (storage and progressive release of rainwater).

Similarly to Massei et al. (2006), other studies have also highlighted the importance of the epikarst (vadose zone) in controlling recharge mechanisms in eogenetic (young) karst systems where the conduit development is limited (Groves et al. 2005; Perrin et al. 2003). However, in telogenetic (mature) karsts where conduit development is evolved and matrix permeability is considerably low, studies have highlighted the importance of conduit development and macroporosity in defining karst aquifer behavior in response to storm events (Vacher and Mylroie 2002; Budd and Vacher 2004; Florea and Vacher 2006). In those mature systems (e.g., South Spring system described by Desmarais and Rojstaczer 2002), the majority of the spring discharge is derived from stored groundwater in the aquifer compartments (95% estimated for the South Spring system). Thus conduit-flow-dominated systems tend to exhibit flashier responses to storms due to a high groundwater storage capacity ($2 \times 10^6$ liters estimated at the South Spring system) and fast recharge through a well-interconnected conduit network. In

contrast, relatively young carbonate platforms (e.g., Timavo Spring System, Upper-Triassic Northwestern Kras of Slovenia; Doctor et al. 2006) are characterized by low conduit development. Hence, spring discharge is primarily sustained by slow and diffuse recharge through the pores of the matrice (41 to 58% of the total recharge at the Timavo Spring System) and explaining smoother spring behavior in response to storms. The Grayson-Gunnar cave (GGC) system (Fig. 2) is classified as a branched network (well interconnected mature conduit-flow-dominated network with very few closed loops) according to Palmer (1991), therefore the macroporosity and the morphology of the conduit system are predicted to exert a major control on the spring behavior.

Several studies have used physical and chemical data to assess aquifer recharge and characterize spring response to storms in karstic environments in the Central Kentucky and Southern Appalachian regions (Shuster and White 1971; Scanlon 1989; Ryan and Meiman 1996; Desmarais and Rojstaczer 2002). The primary focus of this study will consist of analyzing long-term physical and chemical data collected at three specific locations in the GGC system in order to 1) identify the aquifer's reactive compartments during major storms and 2) differentiate their contributions to the spring discharge based on evidence from time-series analysis (specific conductivity, turbidity, fluorescent dissolved organic matter –fDOM), major ion chemistry, and mass-balance calculations. The goal of the study is to improve the understanding of karst aquifer dynamics in the Cumberland Plateau of Southeastern Kentucky, a physiographic region that has received less attention in comparison to the contiguous and relatively more evolved carbonate platform of Central Kentucky – Mammoth Cave and Inner Bluegrass regions (Felton and Currens 1994; Hess and White 1988; Groves et al. 2005; Ryan and Meiman 1996; Anthony 1998; Groves et al. 2003). The analysis of the GGC aquifer response to storms and the

knowledge of recharge and subsurface flow paths will provide valuable information for understanding contaminants transfer in the Cumberland sinkhole plain.

## II. Study area

### *II.1. Geology*

Karst features in Southeastern Kentucky are developed along the edge of the Cumberland Plateau and belong to a continuum starting on the east side of the Appalachian Mountains on the Kentucky and Tennessee border and extending in the South through Alabama. The karst of the Cumberland Plateau in Kentucky is developed in Mississippian carbonates, which are locally overlain by Pennsylvanian siliciclastic caprocks (Simpson and Florea 2009). The cave forming limestones are the thick-bedded, fine-grained St Louis limestone, overlaid by the shallow-water, light-colored, oolitic, and locally cross-bedded Ste Genevieve limestones (Fig. 1). The Ste Genevieve formation is regionally covered by the Slade (calcarenite and dolostone) and the Paragon (dark shale) formations. A mature karst landscape has developed in Mississippian-age carbonates of the Slade Formation (Ettensohn et al. 1984). Deeply incised valleys connect the uplands of the Cumberland Plateau to the underlying sinkhole plain (Anthony and Granger 2007) and likely control the regional groundwater flow. The Cumberland River constitutes the regional base flow level where all the underground cave streams converge.

This study focuses on Grayson-Gunnar Cave (GGC), an 11-km-long cave system at the edge of the Cumberland Escarpment of Southeastern Kentucky. The active cave is an epigenic karst system primarily developed in the St. Louis and Ste. Genevieve Formations. The Grayson-Gunnar spring outlet is located at the lower limit of the St Louis limestones at the contact with the Salem-Warsaw formation (Fig. 1). Based on the classification by Palmer (1991) and cave

surveys, it is a mature karst with two flowing conduits or branches (Northern and Southern Branches) with strong connections to surface input and is dominated by conduit flow (Fig. 2).

### *II.2. Land use*

The adjoining region of the Cumberland Escarpment of southeast Kentucky is a part of the Interior Lowland Plateaus Physiographic Province, a region mainly covered by secondary-growth forests and agricultural and low pasture lands. Dale et al. (2009) estimated land cover distribution to be 52.5% forested, 25.8% mixed upland, 10.1% transitional cover, 7.8% cleared land, 3.5% pastures and non-forested, and 0.3% urban. Agricultural land-use in the study area is primarily dominated by open pasture with low-density grazing on the Plateau and row-crop (corn and soybean) production on the plain. Increasingly, confined-animal feeding operations (CAFOs) have encroached in the region and have generated societal controversies (personal communication with locals). In the GCC system, the Southern branch recharge area is connected to a low-density grazing and residential land cover, and the Northern branch recharge basin includes fertilized croplands (corn) and a CAFO (poultry).

### *II.3. Climate*

The climate of South-Central Kentucky is classified as a humid subtropical climate (Peel et al. 2007). In 2015, the average annual temperature was estimated at 15 ± 0.01°C (Kentucky Mesonet website http://www.kymesonet.org at the Albany station, Clinton County, KY) with an average annual minimum of 9 ± 0.01°C and an average annual maximum of 21 ± 0.01°C. The region experiences four distinct seasons. Winters are cool to cold (winter minimum peaked at -16 ± 0.01°C on 23 January 2015) with mild periods. Summers are hot and humid (summer

maximum peaked at 33 ± 0.01°C on 18 July 2015) with variable spring and fall seasons. Precipitation is common year round (average annual precipitation = 1,470 mm) with higher summer values (620 mm recorded between May and August 2015) and a lower winter range (430 mm recorded between October 2015 and January 2016). Summer and fall precipitation events are driven by warm air and tropical moisture from the Gulf of Mexico, while winter rainfall mostly is derived from continental polar air masses coming from the Northern Great Plains and the Great Lakes area (Florea 2013). Re-evaporation and convection of local air masses drive spring and early summer rainfall events. The climate is moderated by the surrounding mountain range of the Cumberland Plateau.

## III. Methods

### *III.1. Physico-chemical data*

A YSI EXO2 sonde was deployed in a pool near the spring at GGC (Fig. 2) to measure dissolved oxygen (DO), temperature (T), specific conductivity (SPC), Total Dissolved Solutes (TDS), turbidity, Total Suspended Solids (TSS), chlorophyll, Phycocyanin (Blue-Green Algae content), fluorescent dissolved organic matter (fDOM), pH, and oxidation-reduction potential (ORP) at 10-minute intervals. More than 39,000 data points were collected between May 2015 and February 2016. An In-Situ Aquatroll 200 sonde deployed at the same location collected simultaneously values of water level, specific conductivity, and temperature. Temperature and specific conductivity records are unavailable for a few days (18-20 December 2015) due to a battery failure.

### *III.2. Discharge*

Discrete measurements of water levels and flow velocities were performed at the spring on a weekly basis from 16 May to 02 August 2015 using a Type A current meter. Flow velocity measurements were then converted into point discharge values and integrated to the spring flow section using standard USGS stream gauging protocols (Rantz 1982). Discrete measurements of water levels and discharge were used to establish a rating curve (Fig. 4). The established stage-discharge regression was used to estimate instantaneous discharge based on 10-minute-interval measurements of water level from the Aquatroll sonde displayed near the spring.

### *III.3. Precipitation and Potential evapotranspiration*

Precipitation data (30-minute interval) were extracted from the USGS Water Watch database (http://waterwatch.usgs.gov/) at the Beaver Creek gauging station, located 10 km north of the GGC spring. Complementary average monthly precipitation data, average low-temperature and average high-temperature data (monthly average calculated from 1961 to 1990) were also obtained from the U.S. climate data website (www.usclimatedata.com) for the corresponding location.

Daily potential evapotranspiration (PET) was estimated using the Priestly-Taylor PET online model (http://onlinecalc.sdsu.edu/onlinepriestleytaylor.php). Input data extracted from the Kentucky Mesonet database (http://www.kymesonet.org) at the Albany station (Clinton County) included: average daily temperature (°Fahrenheit), daily humidity (%), daily precipitation (inch), and daily solar insolation ($MJ/cm^2$). Data were converted into appropriate units (air temperature in °Celsius, and net solar radiation in $Cal/cm^2/day$) prior to uploading into the online Priestly-Taylor PET calculation model. In addition to daily solar insolation ($Q_n$), the model takes into

account the mass density of water (ρ), the heat of vaporization (λ), and Penman's ratio (α), as shown by equation 1. The model yields daily PET (cm/day) as outputs.

$$PET = 1.26 \times \alpha \times \frac{1}{\alpha+1} \times \frac{Q_n}{\rho \times \lambda} \quad \text{(Eq. 1)}$$

The previous equation is valid under humid climate, assuming that inputs fall within the following ranges: air temperature (0-40°C) and net radiation (100-1000 Cal/cm$^2$/day). For this reason, net radiation values under 100 Cal/cm$^2$/day (occurring during some very low sunlight winter days) have been extrapolated to a minimum value of 100 Cal/cm$^2$/day, which introduces an error of ± 15% in the estimation of PET. This value is consistent with previous studies that predicted a similar range of error (15 to 20%) in the estimation of daily and annual mean PET using insolation-based methods in the Southeastern United States (Amatya et al. 1995; Lu et al. 2003).

### *III.4. Chemistry data*

Discrete samples were collected for major ions from May 16 to August 02, 2015. Sampling was performed on a weekly basis at the GGC spring and on a monthly basis at two other locations along the contributing tributaries namely the Northern branch and the Southern branch (Fig. 2). Samples were passed through a 0.45 µm-cellulose membrane filter, collected in 250 mL HDPE bottles, and stored at 4°C at a temporary field facility until shipment for analysis. For cations analysis, 2 mL of 6N nitric acid was added to each bottle prior to sampling to avoid flocculation and precipitation of metal colloids. Cations and anions (except bicarbonate) were analyzed using a Dionex 3000 ion chromatograph at the Ball State Organic Chemistry Laboratory. Bicarbonate ions were measured by total alkalinity Gran titrations performed in-situ using HACH kits on

filtered and unfiltered water samples. Speciation among bicarbonate, carbonate, and hydroxide ions was then performed using the USGS alkalinity calculation website. Instantaneous measurements of temperature (T), pH, dissolved oxygen (DO), and specific conductivity were performed at each sampling location using a YSI Pro Plus.

### *III.5. Serial correlation: autocorrelation and cross-correlation analyses*

Serial correlation analyses were performed using SPSS Statistics software (v. 23) to assess relationships and time dependency among time series of variables (namely specific conductivity, temperature, turbidity, chlorophyll, fDOM, precipitation, and discharge). Data from the EXO2 and Aquatroll sondes (initially collected at a 10-minute- interval) were discretized to fit the interval of precipitation from the USGS water watch (30-minute-interval) and normalized prior to the analyses. Autocorrelation analysis was performed by pairing a given time-series (e.g. specific conductivity) with itself at increasing time increments (lags). Cross-correlation analysis was performed by pairing two different time-series (e.g. specific conductivity and discharge) at increasing time increments. Serial correlations were presented graphically in the form of bar chart histograms (correlograms). These correlograms are referred to as autocorrelograms (for autocorrelation) and cross-correlograms (for cross-correlation). The value of the correlation coefficient (y-axis) is given for different time lags (x-axis).

Precipitation is used as an input variable for cross-correlation analyses following the work of Padilla and Pulido-Bosch (1995), Eisenlohr et al. (1997), Massei et al. (2006), and Fiorillo and Doglioni (2010). Because rainfall does not present any memory effect, autocorrelation functions derived from precipitation usually exhibits a Dirac delta function $\delta(t)$ ($\delta(t) = 1$ for $t = 0$ and $\delta(t) \rightarrow 0$ for $t \neq 0$; Fig. 5). Mangin (1984) suggests a value of 0.2 for the autocorrelation coefficient

as a standard to compare memory effects among multiple variables (Fig. 5). A longer time for the autocorrelogram to reach a coefficient of 0.2 suggests a longer memory effect (higher aquifer inertia). The absolute value of the slope of the fitting function indicates the rate of decrease of the autocorrelation for the given variable. In reality, any value of the autocorrelation coefficient could be used as a standard for comparison as long as it assesses the rate of decrease of the autocorrelogram (Fig. 5). The rate of decrease of the autocorrelation function can be assessed by applying a regression fitting function (Massei et al. 2006). A higher absolute value of the slope indicates a fast decrease of the autocorrelation function and thus a short memory (low aquifer inertia) of the system with respect to a previously recorded disturbance – e.g., storm, rainfall event (Fig. 5). On the contrary, a smaller absolute value of the slope indicates a slow decrease of the autocorrelation function and therefore a longer memory (Fig. 5).

## IV. Results

### *IV.1. Seasonal fluctuations in aquifer recharge*

Figure 6 summarizes data collected during a series of storms in summer 2015 (May to August 2015) and winter 2016 (November 2015 to February 2016). Precipitation and PET are daily values from the Kentucky Mesonet database. Precipitation is higher during summer months (max daily P = 68.6 mm, average daily P = 5.9 mm) than during winter months (max daily P = 38.1 mm, average daily P = 4.1 mm). PET is higher in the summer (max daily PET = 11.8 mm, min daily PET = 8.8 mm, median daily PET = 8.3 mm) than winter (max daily PET = 5.9 mm, median daily PET = 2.2 mm, average daily PET = 2.4 mm).

The established stage-discharge rating curve (Fig. 4) exhibits both exponential (Q-*expo*) and linear (Q-*linear*) fits as shown in Table 1. The exponential fit [$Q = (2 \times 10^{-7}) \times 10^{(15.72 \times H)}$] yields

a better estimation of discharge at low stage (water level < 0.8 m; $R^2 = 0.82$). On the contrary, the linear rating curve [$Q = 4.13 \times H - 3.36$] is a better fit for the estimation of discharge at high stage (water levels ≥ 0.8 m; $R^2 = 0.93$). Therefore, water levels from the Aquatroll sonde were converted to discharge using an exponential fit at low stage and a linear fit for higher stages. A standard error of 10 % (average value for high discharge events, $Q > 0.1$ $m^3/s$) is estimated for discharge calculations at high flow using the linear fit, which is lower than the error obtained using the exponential fit (average value = 17%). The use of a linear relationship minimizes the error associated with the estimation of discharge for high flow conditions. At higher stages and under uniform flow conditions, the stage-discharge relationship is likely controlled by the shape and the morphology of the channel (Braca 2008), the slope of the stage-discharge regression is constant, mimicking the normal slope of the streambed, thus defining linear regression as shown in the inset of Fig. 4.

Spring discharge varies within the same range for both seasons (max Q summer = 1.4 $m^3/s$, max Q winter = 1.6 $m^3/s$, min Q summer = 0.04 $m^3/s$, min Q winter = 0.06 $m^3/s$). In winter, discharge appears to be correlated to cumulative precipitation and precedent moisture conditions: the highest discharge (Q = 1.66 $m^3/s$ on 25 December 2015) occurs following extended rainfall over a short period of time (cumulative rainfall = 31.5 mm from 22-25 December 2015). In summer, the effect of precipitation and moisture conditions on discharge is mitigated by temporal variations in evapotranspiration. The highest peak in precipitation (P = 68.6 mm on 29 September 2015) yielded a discharge of 0.8 $m^3/s$, while a more moderated rainfall event (P = 46.2 mm on 14 July 2015) led to a higher discharge (1.36 $m^3/s$).

### *IV.2. Long-term physical data*

Table 2 presents the results of the analysis of the specific conductivity signal for 11 large storms ($Q_{max}$ > 0.5 $m^3/s$) recorded in summer 2015 and winter 2015. The base flow upper threshold is defined at 0.08 $m^3/s$, and all the discharge variations under that value are considered as being part of the noise in the base flow record of the instrument. The majority of the largest storms ($Q_{max}$ > 0.5 $m^3/s$) occurred in the months of July (summer storms) and December 2015 (winter storms). Storm events show an average total duration of 4 hours (min = 1.92 hours and max = 7.92 hours, Table 2). While the first response in specific conductivity is almost instantaneous during the summer (first peak occurs on average 0.14 hours (8 min) after peak in discharge), the first response in specific conductivity occurs 1 to 2 hours following the peak in discharge in the winter. The same pattern is observed for the second response with a relatively faster peak during the summer (average = 1.68 hours) compared to the winter (average = 3.28 hours). Overall, the flushing phase lasts from 2 hours (summer) to 4.5 hours (winter). The dilution lasts half the time for summer storms (2.4 hours) as it does for winter storms (4 hours). The average recovery time is identical for both seasons (7 hours). However, the recovery period is more extended during the winter when comparing individual storms with similar amplitude ($Q_{max}$).

Figures 7a and 7b present time series of physicochemical parameters recorded by the EXO2 sonde (temperature, specific conductivity, turbidity, chlorophyll, fDOM) during summer and winter respectively. Time-series records are plotted with discharge and precipitation. The response of all the above variables is proportional to the amplitude of the discharge peak for all the individual storm events (summer and winter), thus showing a linearity between the rise in discharge and physicochemical changes. A description of the physicochemical changes is further

done using an approach “by parameter” for specific conductivity, temperature, turbidity, chlorophyll and fDOM.

### *IV.2.1. Specific conductivity*

The specific conductivity (SPC) first increases following the rise in discharge, then decreases to a minimum value once the peak in the discharge is attained (Fig. 7). The SPC signal shows a stable and constant record of two peaks in SPC following the arrival of storm water (Fig. 8a). This pattern is observable for all the 11 recorded storms independent of the intensity of the storm and the season (Fig. 7). However, the time delay between the first and second peaks in SPC varies with storm intensity and seasonality (Table 2). The average difference in amplitude between the two peaks (20 to 40 µS/cm) lies well above the range expected for an instrumental artifact (< 1 µS/cm). The analysis of the SPC signal reveals that the first peak in SPC occurs 8 minutes to 1 hour following the peak in discharge, marking the end of the flushing phase (F1; Fig. 8a). The first peak in SPC is followed by a steep decrease marking a dilution (D1; Fig. 8a). The second peak in SPC tends to occur within 1 to 3 hours following the first peak, marking the second flushing (F2; Fig. 8a). The second peak is then followed by a dilution (D2; Fig. 8a) that lasts between 2 and 4 hours. The dilution is followed by a long recovery (6 to 7 hours) characterized by a slow increase in SPC, marking the system’s return to pre-storm conditions (R; Fig. 8a).

### *IV.2.2. Temperature*

Spring water temperature is overall constant (14°C on average) in summer (Fig. 7a) and winter (Fig. 7b). However, there is a general tendency towards an increase (< 0.5°C) indicating a slight

warming from late spring toward summer. The temperature increases a few hours following the arrival of stormwater at the GGC spring in summer (<1°C for smaller storms Q < 0.5 $m^3/s$; and 2 to 3°C for larger summer storms, Q > 0.5 $m^3/s$). The record of temperature also shows a small drop (0.2°C) prior to the increase for small summer storms.

### *IV.2.3. Turbidity, chlorophyll, and fDOM*

Turbidity, chlorophyll, and fDOM all increase proportionally to the discharge for each individual storm event recorded in summer and winter (Fig. 7a, Fig. 7b). Time-series graphs also show a slower return to base flow conditions (long recovery) for all the above parameters in summer and winter. In summer, turbidity increases 200 to 300 Formazin Nephelometric Units (FNU) on average following the arrival of storm water with a maximum value of 350 FNU following larger storms. In winter, increases in turbidity following major storms occur at a lower amplitude compared to the summer (<100 FNU, except for storms 9 and 10) with lower values recorded during base flow conditions (0 FNU) compared to the summer (50 FNU). Fluorescent dissolved organic matter varies within a range of 2 to 16 Relative Fluorescence Units – RFU (summer and winter), with an increase in amplitude of 4 to 6 RFU following the arrival of storm water at the spring, and a maximum peak at 16 RFU during larger storms. Chlorophyll shows the least variability among other variables with an increase of 50 to 100 RFU following summer storms. The increase is even less significant during the winter (<30 FNU).

## *IV.3. Autocorrelation and cross-correlation analyses*

For the study of the GGC aquifer response, autocorrelation analyses are used to assess the time dependency between consecutive storm events and seasons (system memory; Fig. 9A and 9B).

Cross-correlation analyses are used to show dependence among variables and estimate lag times between paired values of two or more variables. Figure 10 displays cross-correlation matrices obtained using 7 independent variables (precipitation, discharge, SPC, temperature, turbidity, chlorophyll, fDOM,) recorded at a 10 minute-intervals during summer (10 June to 9 August 2015; Fig. 7a) and winter 2015 (27 November 2015 to 17 February 2016; Fig. 7b) at the GCC spring.

Lag times are obtained by multiplying the value of the lag number corresponding to the highest (or lowest) peak of the correlogram by a 30-minute interval. The middle vertical line represents the ‘’0’’ time lag. Upper and lower horizontal lines delineate the 95% confidence interval. Outliers located above the confidence interval indicate a positive correlation between the independent variable (in ordinate) and the dependent variable (in abscise) at the corresponding lag. Below the confidence interval, outliers indicate a negative correlation between the independent variable and the dependent variable at the corresponding lag. A standard error of 0.012 is estimated for correlation coefficients (y-axis).

### *IV.3.1. Autocorrelation functions*

The shape of the autocorrelation function (ACF) of precipitation describes a Dirac delta function (Fig. 9A,f and 9B,f). The precipitation ACF decreases progressively from an initial maximum to a minimum within 7 hours. With the exception of fDOM (Fig. 9A,e), all the physicochemical variables exhibit limited periodicity, low amplitude of variations (majority of spectrum occurs within the ± 0.2 range), and low memory (Fig. 9A,a-d and Fig. 9B,a-e) following the characteristics of the rainfall signal (Dirac function; Fig. 9B,f), thus suggesting that the physicochemical response is driven by inputs from precipitation. The extent of the memory

effect ranges from 30 min (turbidity) to one hour (SPC, temperature and chlorophyll; Fig. 9A) during summer. Overall, a longer memory is observed during winter (1.5 hours for SPC and 3 hours for temperature and chlorophyll; Fig. 9B).

### *IV.3.2. Cross-correlation functions*

Cross-correlation functions (CCFs) (Fig. 10) reflect the interdependence between physicochemical response (SPC, temperature, turbidity and fDOM) and rainfall (P) inputs as suggested by ACFs (Fig. 9A and 9B). Figures 7a and 7b show that physicochemical changes also follow changes in discharge, thus Fig. 10 also assumes causality between discharge (Q) and physical variables. Although the majority of CCFs' spectra occurs between the +0.2/-0.2 range, CCFs between Q and SPC, temperature, turbidity and fDOM spectrums exhibit significant outliers that provide valuable information regarding dependence among variables. The CCF between discharge (Q) and SPC (Fig. 10b) shows significant outliers (negative correlations) at lags 1 (t = 0.5 hour) and 13 (t = 6.5 hours) and has an estimated period of 12 lags (i.e. dt = 6 hours) between peak amplitudes. The summer CCF between Q and temperature (Fig. 10c) also shows significant outliers (positive correlations) at lag 1 (t = 0.5 hour) and 13 (t = 6.5 hours), and the same period (dt = 6 hours) as the previous CCF (Q and SPC). The CCF between Q and turbidity (Fig. 10d) shows similar periodicity (dt = 4 hours) estimated using significant positive outliers at lags 9 (t = 4.5 hours) and 17 (t = 8.5 hours). The CCF between Q and fDOM (Fig. 10e) also mimics the periodicity of the Q-turbidity CCF (dt = 4 hours) with significant outliers at lag 8 (t = 4 hours) and 15 (t = 8 hours). Although Q-turbidity and Q-fDOM CCFs exhibit the same range in periodicity with Q-SPC and Q-T CCFs, there are significant shifts in the phase (frequency delay ($\tau$): $\tau$ = 4 hours and $\tau$ ' = 3 hours) with regards to the latter. Cross-correlation

between SPC and temperature (Fig. 10f) shows a symmetric behavior with similar changes in amplitudes on both sides of the spectrum likely reflecting the simultaneous responses of the two variables with changes in discharge (Fig. 10b and 10c) and the similarity in frequencies of the two spectrums.

### *IV.4. Major ions chemistry and carbon dioxide partial pressure.*

Table 3 shows major ions data ($Ca^{2+}$, $Mg^{2+}$, and $HCO_3^-$), computed molar ratios (Ca/Mg and $Ca/HCO_3$), carbon dioxide partial pressure and saturation indexes for calcite and dolomite minerals for three locations within the aquifer (GCC spring, Northern branch, and Southern branch). Calcium and magnesium ions are the predominant cations at three sites, both accounting for 61% of total cations content at the spring, 57% at the Northern branch, and 61% at the Southern branch. Bicarbonate ions largely dominate the anions at all locations ($HCO_3^-$ = 98% of total anion content). Molar $Ca/HCO_3$ ratios are significantly higher (P-value = 0.06) in the Northern branch (NB average = 0.43 ± 0.07) compared to the Southern branch (SB average = 0.36 ± 0.06; Table 3). Spring samples show near saturation with respect to calcite (-1 < calcite SI < -0.5; average = -0.7). Spring samples are closer to saturation with calcite than with dolomite (SI calcite > SI dolomite) and combined with Ca/Mg ratios (1.7 to 3.5) suggest the groundwater has contact dominantly with calcite-bearing bedrocks. Values of SI calcite and SI dolomite also reveal a decreasing trend from the flowing branches (NB and SB) to the spring, suggesting a process of desaturation at the contact with the atmosphere. With the absence of evidence for calcite supersaturation (SI calcite < 0), calcite precipitation at the spring is unlikely to occur, thus desaturation may occur through evaporation. Moreover, changes in temperature and $Pco_2$ along the flow lines between the conduits and the spring are not significant enough (T = 14.2 ± 0.2 °C;

$Pco_2$ = 2.03 ± 0.02) to drive changes in water composition driven by $CO_2$ degassing and mineral precipitation at the spring.

$$Ca\,CO_3 + H_2CO_3 \rightarrow Ca^{2+} + 2\,HCO_3^- \quad \text{(Eq. 2)}$$

$$Ca\,Mg\,(CO_3)_2 + 2\,H_2CO_3 \rightarrow Ca^{2+} + Mg^{2+} + 4\,HCO_3^- \quad \text{(Eq. 3)}$$

In the classic models of epigenic karst (White 1988), carbonic acid is the primary source of chemical weathering (Equations 2 and 3). Thus, the dissolution of carbonate minerals is likely the primary contributor of $Ca^{2+}$, $Mg^{2+}$, and $HCO_3^-$ to the GGC spring water. However, individual major ions do not display major differences between the Northern and the Southern branch either in calcium (P-value = 0.25; *paired two-samples for means t-test*), magnesium (P-value = 0.64), or bicarbonate concentrations (P-value = 0.93). Thus, to illustrate differences in carbonate dissolution among Northern branch, Southern branch, and spring locations at GGC, samples from the three locations are plotted in a two-dimensional diagram (Fig. 11) showing the relation between $Ca^{2+}$ + $Mg^{2+}$ (y-axis) and $HCO_3^-$ (x-axis). Based on molar balances of equations 2 and 3, calcite dissolution yields a (Ca+Mg)/$HCO_3$ molar ratio of 0.5, and dolomite dissolution yields a (Ca+Mg)/$HCO_3$ ratio of 0.25.

## V. Discussion

The data suggest that the two contributing conduit branches (NB and SB) are responding at different time intervals. Time-series analyses of long-term physicochemical variables (discharge, specific conductivity, temperature, turbidity, fDOM) and major ion data provide means to quantify aquifer compartments (NB, SB, epikarst, and groundwater storage) response time and to differentiate between the two conduit branches.

### *V.1. Dynamics of the Northern and the Southern Branches*

Specific conductivity time series shows the occurrence of two peaks (Fig. 7 and Fig. 8) following major storm events, which suggests that the NB and the SB respond differently. Identifying the flow dynamics of each branch is essential to the estimation of the transit time of surface contaminants in relation to the heterogeneous surface land-use distribution.

Samples from the 3 locations (NB, SB and GCC spring; Table 3) reveal significant differences in SPC (P-value = 0.21; *unpaired two-samples for means t-test*) between the Northern and the Southern branches, with relatively low values (by 2 to 6 µS/cm) at the Southern branch compared to the Northern one for 3 recorded events (05/16/15, 07/03/15, 08/02/15). The interpretation of SPC time-series shows that, for all recorded storm events, higher peak values are always recorded for the faster branch, while lower peak values are recorded for the slower branch (Fig. 7). Data from Table 3 display significantly higher SPC values at the NB, indicating that the NB is most likely the fastest responding branch, while the SB is the slowest one.

Cave surveys at GGC (Fig. 2) have shown that the SB is connected at the surface to a residential land cover, and the NB is covered by forests, agriculture, and farms (including CAFO). Because the land-use in the Northern half of the GGC recharge basin (NB) is relatively similar to land cover at the Big Spring system (BSS) in the Mammoth Cave Region (relatively pristine with regards to human settlement), levels of surface contaminants in both groundwater basins are predicted to be similar. Turbidity ranges from values <10 NTU to 40 NTU at the BSS (Ryan and Meiman 1996), within the expected range for non-point sources inputs in streams and groundwater draining primarily agricultural lands (<100 NTU; Collins and Jenkins 1996). However, turbidity values at the GGC are relatively high (average range = 50 to 400 NTU; record of 650 NTU during a major storm event of December 2015; Fig. 7b) in comparison to the

anticipated values for diffuse infiltration from non-point sources (e.g., runoff from agricultural land). Thus, the elevated range of turbidity in GGC suggests the occurrence of localized (point-source) infiltration from the Southern residential (semi-urban) portion of the GGC recharge basin as supported by the work done by Coulter et al. (2004). Potential sources of turbidity in that portion of the basin may include: 1) direct seepage under solid waste disposal sites into the cave, and 2) suspended particles from fecal origin (leakage under septic systems). Moreover, observations of time-series turbidity signal at the GGC spring (Fig. 7a and 7b) suggest that the slowest responding branch is responsible for the highest peaks in turbidity and fDOM, while the fastest responding branch is responsible for the lowest peaks in turbidity and fDOM. Combining the above evidence, the NB (primarily agricultural and forested land cover with no evident source of turbidity) accounts for the fastest response (low turbidity and fDOM). The Southern branch, on the other hand, shows potential sources of turbidity (solid waste disposal sites) and fDOM (septic systems) at its surface, thus could be responsible for the slowest response (highest turbidity and fDOM peaks on time-series records).

Additionally, the interpretation of major ion chemistry, carbon dioxide content and temperature (Table 3) further complements evidence that the NB responds faster. Table 3 shows that there are no significant differences in values of $Pco_2$ and temperature between 2 flowing conduit branches (NB and SB) and the spring, indicating that changes in environmental conditions that occur along these flow lines are not significant enough to drive changes in major ion chemistry (either through $CO_2$ degassing or mineral precipitation) at the spring. At the given temperature range ($T > 10°C$) and carbon dioxide partial pressure (median $P_{CO2} \approx 2$; Table 3), the solubility of calcite exceeds that of dolomite and will dissolve faster than dolomite (Wigley 1973). Moreover, for the given values of SI calcite (<0) and carbon dioxide partial pressure at the

spring (below the atmospheric $P_{CO2}$ value of 3.5), calcite precipitation can not occur at the spring.

The residence time and dissolution kinetics between calcite and dolomite (relatively faster dissolution of soluble calcite and slower dissolution of less soluble dolomite) may help to interpret the distribution of major ion concentrations at the GCC spring (Fig. 11). Figure 11 shows that the chemistry of samples from the NB reflects evidence of calcite dissolution (faster kinetics), and, combined with values of SI calcite (-1 < SI calcite < -0.2), suggests a faster equilibrium between groundwater and carbonates (less than 3 weeks) and a shorter residence time in the NB conduit. On the other hand, GCC spring samples follow a trend that reflects dolomite dissolution. Given that dolomite will dissolve slower under given the $Pco_2$ and temperature conditions, the chemistry of spring samples (Fig. 11) reflects a longer residence time and prolonged interaction between the groundwater and carbonates. It is also implied that the trend towards dolomite dissolution observed at the spring derives from infiltration through the SB (longer residence time).

Overall, the evidence from long-term physical data (SPC, turbidity, fDOM), major ions (Ca, Mg, and $HCO_3$) and environmental conditions ($P_{CO2}$ and temperature) highly suggest that NB responds faster than the SB, which reacts relatively slower.

### *V.2. Volumetric contributions to the spring discharge*

For a given storm event, volumetric contributions of the NB and the SB to the spring discharge can be estimated using mass balance calculations and known solute concentrations ($Ca^{2+}$, $Mg^{2+}$, $HCO_3^-$) at the spring ($C_S$), the Northern branch ($C_{NB}$) and the Southern branch ($C_{SB}$) (Dreiss 1989; Desmarais and Rojstaczer 2002). It is assumed that: 1) the spring discharge is the sum of

discharges from the two contributing branches (Equation 4), and 2) there is a complete mixture of the fluxes from the Northern and Southern branches at the spring (Equation 5):

$$Q_S = Q_{SB} + Q_{NB} \quad \text{(Eq. 4)}$$

$$Q_S \times C_S = Q_{SB} \times C_{SB} + Q_{NB} \times C_{NB} \quad \text{(Eq. 5)}$$

where $Q_S$, $Q_{SB}$, and $Q_{NB}$ are discharge values as measured at the GGC spring, the Southern and Northern branches respectively; $C_S$, $C_{SB}$, and $C_{NB}$ are given solute concentrations at the spring, the Southern and Northern branches respectively (Table 3).

The flux of dissolved solutes (Q × C) transported through a given conduit is the unit mass of solutes (ΔM) transferred per unit of time ΔT (Equations 6, 7 and 8).

$$Q \times C = \Delta M \times (\Delta T)^{-1} \quad \text{(Eq. 6)}$$

$$Q_{NB} \times C_{NB} = \Delta M_{NB} \times (\Delta T_{NB})^{-1} \quad \text{(Eq. 7)}$$

$$Q_{SB} \times C_{SB} = \Delta M_{SB} \times (\Delta T_{SB})^{-1} \quad \text{(Eq. 8)}$$

Paired samples t-tests show that there is no statistical difference in $Ca^{2+}$, $Mg^{2+}$, and $HCO_3^-$ concentrations between NB and SB (p-values = 0.25; 0.64; 0.93 respectively), indicating that carbonate dissolution provides the same amount of dissolved solutes ($Ca^{2+}$, $Mg^{2+}$, $HCO_3^-$) to the groundwater flowing through both conduit branches (Equation 9).

$$\Delta M_{NB} \approx \Delta M_{SB} \quad \text{(Eq. 9)}$$

In addition, the combined interpretation of long-term physical and major ion data suggests that the response of the Northern branch to storms is faster than the Southern branch, therefore

$$\Delta T_{NB} << \Delta T_{SB} \quad \text{(Eq. 10)}$$

which leads to equations 11 is:

$$Q_{SB} \times C_{SB} << Q_{NB} \times C_{NB} \quad \text{(Eq. 11)}$$

Therefore, equation 5 can be rewritten (Equation 12), suggesting that the majority of the flux of solutes at the GGC spring is derived from the NB.

$$Q_S \times C_S \approx Q_{NB} \times C_{NB} \quad \text{(Eq. 12)}$$

Equation 12 is further rearranged:

$$Q_{NB} = Q_S \times \frac{C_S}{C_{NB}} \quad \text{(Eq. 13)}$$

According to Equations 4 and 13,

$$Q_{SB} = Q_S - Q_{NB} = Q_S - Q_S \times \frac{C_S}{C_{NB}} \quad \text{(Eq. 14)}$$

and leads to Equation 15:

$$Q_{SB} = Q_S \times (1 - \frac{C_S}{C_{NB}}) \quad \text{(Eq. 15)}$$

To determine the volumetric proportions of the SB (%Vol SB) and of the NB (%Vol NB), Equations 16 and 17 are derived from the previous expressions of $Q_{NB}$ (Equation 13) and $Q_{SB}$ (Equation 15):

$$\%SB = \frac{Q_{SB}}{Q_S} \times 100 = (1 - \frac{C_S}{C_{NB}}) \times 100 \quad \text{(Eq. 16)}$$

$$\%NB = \frac{Q_{NB}}{Q_S} \times 100 = \frac{C_S}{C_{NB}} \times 100 \quad \text{(Eq. 17)}$$

Equations 16 and 17 are used to estimate contributions of each branch (NB and SB) at the GGC spring for 3 major summer storm events (16 May, 03 July and 02 August 2015; Table 4). Because molar concentrations of dissolved solutes ($Ca^{2+}$, $Mg^{2+}$, $HCO_3^-$) vary over time, molar ratios (Ca/Mg, $Ca/HCO_3$) are used in mass balance calculations (Table 4). The ratios are

relatively constant in groundwater discharging from limestone: Ca/Mg = 1 in spring waters discharging from dolomite-rich limestones (Shuster and White 1971); Ca/Mg ranges from 2.6 to 2.8 in water discharging from the calcite-dominant Maynardville Limestone (Desmarais and Rojstaczer 2002); $Ca/HCO_3 \sim 0.5$ in waters that equilibrated with calcite, and 0.25 for dolomite equilibrium (Fig. 11).

With the exception of the storm event recorded on 03 July 2015 (wettest month of that year), the contribution of the SB at the spring remains significantly lower (22% on average) than that of the NB (78% average). Moreover, the contribution of the Northern branch remains consistently high during both low flow ($Q_s$ = 0.09 $m^3/s$; 16 May 2015) and high flow conditions ($Q_s$ = 0.58 $m^3/s$; 02 August 2015), suggesting that the NB is the primary feeding branch for the GGC spring, independent of the flow conditions. Moreover, estimates of the total volume discharged at the spring during major storms yield an average value of 1 billion liters of water, with 6 million liters of water discharge from stored groundwater on average (Table 5). Based on previous estimates of the volumetric contributions of each branch at the spring, the NB stored groundwater likely accounts for an average of 5 million liters (78%) and the SB storage releases the remaining 1 million liters (22%).

### *V.3. Residence time*

It is inferred from the major ion chemistry (Fig. 11) that groundwater chemistry within the GGC system is characterized by two end-member mixing waters. The first end-member is represented by groundwater showing fast equilibrium with carbonates (calcite dissolution) and a short residence time. The second water type reflects a longer residence time and prolonged contact with limestone. The relative contributions of new water (storm water that transitioned through

the karstic system fast enough to prevent prolonged interaction with carbonates and/or mixing with stored groundwater) and old water (groundwater storage with longer residence time) to the spring is estimated using a methodology provided by Desmarais and Rojstaczer (2002) that consists of the integration of the area below the discharge curve (Fig. 12) during the dilution phase (Q-new). Assuming that spring water composition is the mixing of both fast surface recharge (Q-new; storm water) and groundwater storage (Q-old), the proportion of old conduit water (Q-old) is then obtained by subtracting the fast recharge (Q-new) from the total discharge (Qtotal – Q-new). On average (Table 2), it is estimated that 35% of the total volume of water discharging at the spring during major storms is old water from the groundwater storage (Table 5). Moreover, the age distribution of groundwater is expected to vary based on the relative age of each end-member (Q-new and Q-old) and their respective mixing proportions (Kazemi et al. 2006). Thus, the average spring water residence time (RT) can be expressed as a volumetric percentage of the two end-member sources according to the following equation:

$$RT = [\%Vol\ (Q\text{-}old) \times RT\ (Q\text{-}old)] + [\%Vol\ (Q\text{-}new) \times RT\ (Q\text{-}new)] \quad \text{(Eq. 18)}$$

Where %Vol are the respective volumetric contributions of old and new water to the spring. Considering that 35% of spring water derives from groundwater storage, equation 18 can be rewritten as follow:

$$RT = 0.35 \times RT\ (Q\text{-}old) + 0.65 * RT\ (Q\text{-}new) \quad \text{(Eq. 19)}$$

Because the solubility of calcite in waters in equilibrium with $CO_2$ gas under partial atmospheric conditions ($P_{CO2} \leq 1$ atm) occurs within a time range of 5 to 16 days (Segnit et al. 1962), the estimated maximum residence time for “old” water that has reached near equilibrium with calcite (-1< SI calcite <-0.2; Table 3) is 3 weeks or less. Moreover, a residence time for “new” water can be estimated using the timing of surface water infiltration (30 minutes to 6

hours; Table 6). Thus, based on equation 20, the water discharging at the spring following a given storm has an average residence time of 2 to 7 days. This range is consistent with subsurface residence time (2 to 6 days) in conduit-fed springs where the majority of discharge is provided by storm runoff (Jacobson and Langmuir 1970).

### *V.4. Timing and mechanisms of recharge*

The interpretation of time series analyses of physicochemical response provides information regarding recharge patterns and storm water transit time through the flowing karstic branches (NB and SB) and the epikarst compartments following summer and winter storms. The discharge signal in response to rainfall (Fig. 10a) shows complex non-periodical patterns suggesting that the aquifer recharge is not solely controlled by the amount of instantaneous rainfall, but other factors such as antecedent moisture (relative wetness or dryness of the karstic system) may introduce some noise in the precipitation to discharge signal conversion (Massei et al. 2006). Among all the physicochemical variables, SPC and temperature show the most significant responses to changes in discharge (Fig. 10b and 10c) based on values of outliers beyond the ±0.2 range.

The CCF between SPC and temperature (Fig. 10f) looks symmetric, thus suggesting that the two variables are interdependent and could be the result of a common cause, likely the discharge (Fig. 10b and 10c). Moreover, the SPC and temperature spectrums exhibit the same period (dt = 6 hours), which corresponds to the range expected for the delay in responses between the Northern and the Southern branches (Table 2). The first variation in the SPC and temperature spectrums (lag 1; Fig. 10b and 10c) exhibit the highest amplitude, reflecting fast infiltration of storm water through the Northern conduit compartment with no mixing with groundwater

storage. On the contrary, due to slower flow dynamics in the Southern Branch, there is some proportion of stored groundwater mixing with recharge in the SB, as suggested by low-amplitude variations in SPC and temperature (diluted signal) observed later in the SPC and temperature spectrums (lag 12; Fig. 10b and 10c). The existence of a similar range of periodicity (dt = 4 hours) for the turbidity and fDOM spectrums (Fig. 10d and 10e) reveals that the latter variables are also responding to the same cause (discharge) as SPC and T but at a different frequency. However, the frequencies of the turbidity and fDOM spectrums are off by 3 to 4 hours ($\tau$ and $\tau$'; Fig. 10d and 10e) with regards to the response of the conduit compartment (SPC and temperature spectrums), thus the earlier variables may reflect the response of a different aquifer compartment, likely the epikarst.

The slower reactivity of the epikarst compartment in comparison to the NB and SB conduits can be explained by a slow infiltration of storm water through the overlying caprocks (Paragon shales; Fig. 1). The frequency delay ($\tau$) observed in the Q-turbidity cross-correlogram (Fig. 10d) may mark the slow mobilization of suspended sediments by the incoming storm water moving through fractures in the epikarst. Retention mechanisms (particles deposition and retention on matrix grains) may also occur during the latter process, causing a delay in the response of the epikarst in relation to the NB and SB. The frequency delay ($\tau$') that characterizes the Q-fDOM cross-correlogram (Fig. 10e) could reflect the influence of biological mechanisms (microbially-mediated decomposition or uptake of organic matter) that may interfere with the fate of organic compounds during storm water infiltration through the soil and the epikarst.

Overall, the aquifer dynamics in response to storms features two main phases: 1) a rapid infiltration of storm water through the conduit system (30 minutes for the NB up to 6 hours for the SB; Fig. 10b and 10c), and 2) the slow response of the epikarst compartment characterized by

the late arrival of both particulate and dissolved organic contents at the spring 3 to 4 hours following the response of the conduit branches (Fig. 10d and 10e).

### *V.5. A conceptual model of recharge: effect of antecedent moisture*

The rapid responses of physicochemical variables to individual storms and the shape of the autocorrelation functions (mimicking the Dirac function for the majority of the variables; Fig. 9A) support the notion that the GGC aquifer recharge is primarily driven by inputs from precipitation (Fig. 13). The relatively short groundwater residence time (< 7 days) indicates that the rain water feeding the spring has only moved a short distance downstream and entered the carbonate system through subsurface sinkhole and macroporous fractures/conduits and that no regional groundwater flow or lateral flow (residence time in the order of months) contributes to the spring discharge. However, the lack of clear correlation between discharge and precipitation (Fig. 10a) reveals that the aquifer recharge is not solely controlled by the amount of instantaneous rainfall. Massei et al. (2006) attributed the non-linearity in the discharge-precipitation relationship to the effect of antecedent moisture (such as soil and epikarst saturation). In the winter, increased soil moisture, combined with stored groundwater and lower average evapotranspiration (Fig. 6) are likely facilitating the occurrence of a flushing mechanism (Ryan and Meiman 1996; Fig. 13a). Moreover, high antecedent moisture during winter may also limit the ability of the aquifer to recover from the storm and accounts for a slower return to base flow conditions following a storm, as shown by longer memory effect (higher aquifer inertia) in winter ACFs (Fig. 9B) in contrast to summer ACFs (Fig. 9A). Because the entire stored groundwater volume stored in the system ($5 \times 10^6$ liters on average; Table 5) needs to be displaced before the arrival of storm water in the winter, storm water infiltration through the

conduit is estimated to last on average 2 hours longer in winter compared to summer (Table 6). On the contrary, during summer storms, the combined effect of low moisture conditions, low groundwater reserve, and high average evapotranspiration (Fig. 6) during summer may hinder flushing (Fig. 13b) and cause a faster storm water infiltration through the GCC (Table 6). Consequently, the average duration of storms is relatively longer during winter compared to summer (Table 6).

## VI. Conclusion

Overall, the study of the spring response at the Grayson-Gunnar Cave system highlights a separated response of two flowing branches. The Northern Branch, likely the fastest responding branch, accounts for 5 million liters of stored groundwater discharging at the spring following a major storm. The Southern Branch responds 4 to 8 hours after the NB and accounts for an average of 1 million liters of stored groundwater discharging at the spring. Average response times range from 4 hours for flushing and dilution to 7 hours for recovery and return to pre-storm base flow conditions following a major storm. This study also highlights the control of climate (precipitation distribution and evaporation) and antecedent saturation of the aquifer in the recharge process in mature and primarily conduit-fed karst aquifers such as the GGC. It takes about 2 hours for the entire groundwater reserve to be emptied prior to the infiltration of storm water during highly saturated conditions (winter). Complex water-rock interactions occurring within the epikarst are likely reinforcing the heterogeneous response of the karst system thus making it difficult to properly interpret the signals from surface variables (e.g., SPC, turbidity). Further analysis of the fate of nutrients and carbon within the vadose zone may improve the

understanding of epikarst processes and provide a better constraint on the hydrological characteristics of this karstic system.

**Acknowledgements**

We are thankful to Harry Goepel for providing housing in Kentucky during sampling. We acknowledge the Greater Cincinnati Grotto of the National Speleological Survey that has allowed the use of surveys data from the Grayson-Gunnar Cave. We expand our gratitude to Gary and Synda Heikkinen (and the wonderful dogs) for granting us access to the Grayson-Gunnar Cave property. A special gratitude to Bill Walden, for valuable information and emotional support he gently provided during our stay in Monticello, KY. We acknowledge Dr Michael E. Perdue for graciously allowing us the use of the instrumentation at the Organic Chemistry Lab (Ball State University) and to Shamus Driver for his tremendous help with the analyses. Last but not least, we want to thank the following organizations for granting funding for this project: the National Speleological Society through the 2015 Ralph Stone Research Grant, the Cave Research Foundation through the 2015 Phillip M. Smith Graduate Research Grant, and the Geological Society of America through the 2015 Student Research Grant.

**Funding information**

We want to thank the following organizations for granting funding for this project: the National Speleological Society through the 2015 Ralph Stone Research Grant, the Cave Research Foundation through the 2015 Phillip M. Smith Graduate Research Grant, and the Geological Society of America through the 2015 Student Research Grant.

**References**

Amatya, DM, Skaggs, RW, Gregory, JD (1995) Comparison of methods for estimating REF-ET. Journal of irrigation and drainage engineering 121(6):427-435.

Anthony D (1998) Seasonal effects on the geochemical evolution of the Logsdon River, Mammoth Cave, Kentucky. MSc Thesis, Western Kentucky University, Bowling Green

Anthony DM, Granger DE (2007) A new chronology for the age of Appalachian erosional surfaces determined by cosmogenic nuclides in cave sediments. Earth Surface Processes and Landforms 32:874–887

Braca G (2008) Stage-discharge relationships in open channels: Practices and problems. Univ. degli Studi di Trento, Dipartimento di Ingegneria Civile e Ambientale

Brahana JV, Nix J, Bitting C, Bitting C, Quick R, Murdoch J, Roland V, Wets A, Robertson S, Scardale G, North V (2014) CAFOs on Karst –meaningful data collection to adequately define environmental risk, with a specific application from the southern Ozarks of northern Arkansas. In: U.S. Geological Survey Scientific Investigations Report 2014–5035. p 97–102

Budd DA, Vacher, HL (2004) Matrix permeability of the confined Floridan Aquifer, Florida, USA. Hydrogeology Journal 12(5):531–549

Collins R, Jenkins A (1996) The impact of agricultural land use on stream chemistry in the Middle Hills of the Himalayas, Nepal. Journal of Hydrology 185(1–4):71–86

Coulter, CB, Kolka, RK, Thompson, JA (2004) Water quality in agricultural, urban, and mixed land use watersheds. Journal of the American Water Resources Association, 40(6):1593-1601.

Crawford NC (1982) Hydrogeologic problems resulting from development upon karst terrain, Bowling Green, Kentucky. United States Environmental Protection Agency

Dale VH, Lannom KO, Tharp ML, Hodges DG, Fogel J (2009) Effects of climate change, land-use change, and invasive species on the ecology of the Cumberland forests. Canadian Journal of Forest Research 39(2):467–480

Desmarais K, Rojstaczer S (2002) Inferring source waters from measurements of carbonate spring response to storms. Journal of Hydrology 260(1):118–134

Doctor DH, Alexander, EC, Petrič M, Kogovšek J, Urbanc J, Lojen S, Stichler W (2006) Quantification of karst aquifer discharge components during storm events through end-member mixing analysis using natural chemistry and stable isotopes as tracers. Hydrogeology Journal 14(7):1171–1191

Dreiss SJ (1989) Regional scale transport in a karst aquifer: 1. Component separation of spring flow hydrographs. Water Resources Research 25(1):117–125

Eisenlohr L, Bouzelboudjen M, Király L, Rossier Y (1997) Numerical versus statistical modelling of natural response of a karst hydrogeological system. Journal of hydrology 202(1): 244–262

Ettensohn FR, Rice CR, Dever GR, Chesnut DR (1984) Slade and Paragon Formations; New stratigraphic nomenclature for Mississippian rocks along the Cumberland Escarpment in Kentucky. U.S. Geological Survey Bulletin 1605–B: 37

Felton GK, Currens JC (1994) Peak flow rate and recession-curve characteristics of a karst spring in the Inner Bluegrass, central Kentucky. Journal of Hydrology 162(1–2):99–118

Fiorillo F, Doglioni A (2010) The relation between karst spring discharge and rainfall by cross-correlation analysis (Campania, southern Italy). Hydrogeology Journal 18(8):1881–1895

Florea LJ (2013) Selective recharge and isotopic composition of shallow groundwater within temperate, epigenic carbonate aquifers. Journal of hydrology 489:201–213

Florea LJ, Vacher HL (2006) Springflow Hydrographs: Eogenetic vs. Telogenetic Karst. Ground Water 44: 352–361, doi 10.1111/j1745-6584-2005-00158-x

Ford DC, Williams P (2007) Karst Hydrogeology and Geomorphology. John Wiley & Sons

Groves C, Anthony DM, Meiman J (2003) Preliminary investigations of seasonal changes in the geochemical evolution of the Logdson River, Mammoth Cave, Kentucky. Speleogenesis and Evolution of Karst Aquifers.

Groves C, Bolster C, Meiman J (2005) Spatial and temporal variations in epikarst storage and flow in South Central Kentucky's Pennyroyal Plateau sinkhole plain. US Geological Survey Karst Interest Group Proceedings 64

Hallberg GR, Libra RD, Hoyer BE (1985) Nonpoint source contamination of ground water in karst-carbonate aquifers in Iowa. Perspectives on Nonpoint Sources Pollution. U.S. Environmental Protection Agency 440/5-85-001. p 109–114

Hess JW, White WB (1988) Storm response of the karstic carbonate aquifer of southcentral Kentucky. Journal of Hydrology 99(3–4):235–252

Hooda PS, Edwards AC, Anderson HA, Miller A (2000) A review of water quality concerns in livestock farming areas. Science of the Total Environment 250(1):143–167

Jacobson, RL, Langmuir, D (1970) The chemical history of some spring waters in carbonate rocks. Groundwater 8(3): pp.5-9.

Kazemi, GA, Lehr, JH, Perrochet, P (2006) Groundwater age. John Wiley & Sons eds.

Larocque M, Mangin A, Razack M, Banton O (1998) Contribution of correlation and spectral analyses to the regional study of a large karst aquifer (Charente, France). Journal of Hydrology 205(3–4):217–231.

Lu, J, Sun, G, McNulty, SG, Amatya, DM (2003) Modeling actual evapotranspiration from forested watersheds across the Southeastern United States. Journal of the American Water Resources Association 39(4):886-896.

Mangin A (1984) Pour une meilleure connaissance des systèmes hydrologiques à partir des analyses corrélatoire et spectrale (Correlation and spectral analyses to better understand hydrologic systems). Journal of hydrology 67(1–4):25–43

Massei N, Dupont JP, Mahler BJ, Laignel B, Fournier M, Valdes D, Ogier S (2006) Investigating transport properties and turbidity dynamics of a karst aquifer using correlation, spectral, and wavelet analyses. Journal of hydrology 329(1):244–257

Meiman J (1991) The effects of recharge basin land-use practices on water quality at Mammoth Cave National Park, Kentucky. National Cave Management Proceedings, Bowling Green, Kentucky:105–115

Mull DS, Liebermann TD, Smoot JL, Woosley Jr. LH, Mikulak RJ (1988) Application Of Dye-Tracing Techniques For Determining Solute-Transport Characteristics Of Ground Water In Karst Terranes. U.S. Environmental Protection Agency EPA904/6-88-001. p 103

National Speleological Society Annual Report 2005. The Exploration and Survey of Grayson Gunnar Cave.

Padilla A, Pulido-Bosch A (1995) Study of hydrographs of karstic aquifers by means of correlation and cross-spectral analysis. Journal of Hydrology 168(1-4):73–89

Palmer AN (1991) Origin and morphology of limestone caves. GSA Bulletin 103(1):1–21. doi: https://doi.org/10.1130/0016-7606

Peel MC, Finlayson BL, McMahon TA (2007) Updated world map of the Köppen-Geiger climate classification. Hydrology and earth system sciences discussions 4(2):439–473

Perrin J, Jeannin PY, Zwahlen, F (2003) Implications of the spatial variability of infiltration-water chemistry for the investigation of a karst aquifer: a field study at Milandre test site, Swiss Jura. Hydrogeology Journal, 11(6):673–686

Rantz SE (1982) Indirect Determination of Peak Discharge. In: Measurement and computation of streamflow, Volume 1, Measurement of stage and discharge. United States Geological Survey Water Supply Paper 2175. p 284

Ryan M, Meiman J (1996) An Examination of Short-term Variations in Water Quality at a Karst Spring in Kentucky. Groundwater 34(1):23–30

Scanlon BR (1989) Physical controls on hydrochemical variability in the inner bluegrass karst region of central Kentucky. Groundwater 27(5):639–646

Segnit, ER, Holland, HD, Biscardi, CJ (1962) The solubility of calcite in aqueous solutions: I. The solubility of calcite in water between 75° and 200° at CO2 pressures up to 60 atm. Geochimica et Cosmochimica Acta 26(12):1301-1331.

Shuster ET, White WB (1971) Seasonal fluctuations in the chemistry of lime-stone springs: A possible means for characterizing carbonate aquifers. Journal of Hydrology 14(2):93–128

Simpson LC, Florea LJ (2009) The Cumberland Plateau of Eastern Kentucky. In: Caves and Karst of America. National Speleological Society. p 70–79

Vacher HL, Mylroie JE (2002) Eogenetic karst from the perspective of an equivalent porous medium. Carbonates and Evaporites 17(2):182–196

White WB (1988) Geomorphology and Hydrology of Karst Terrains. Oxford University Press, New York

Wigley, TML (1973) The incongruent solution of dolomite. Geochimica et Cosmochimica Acta 37(5):1397-1402.

**Figures**

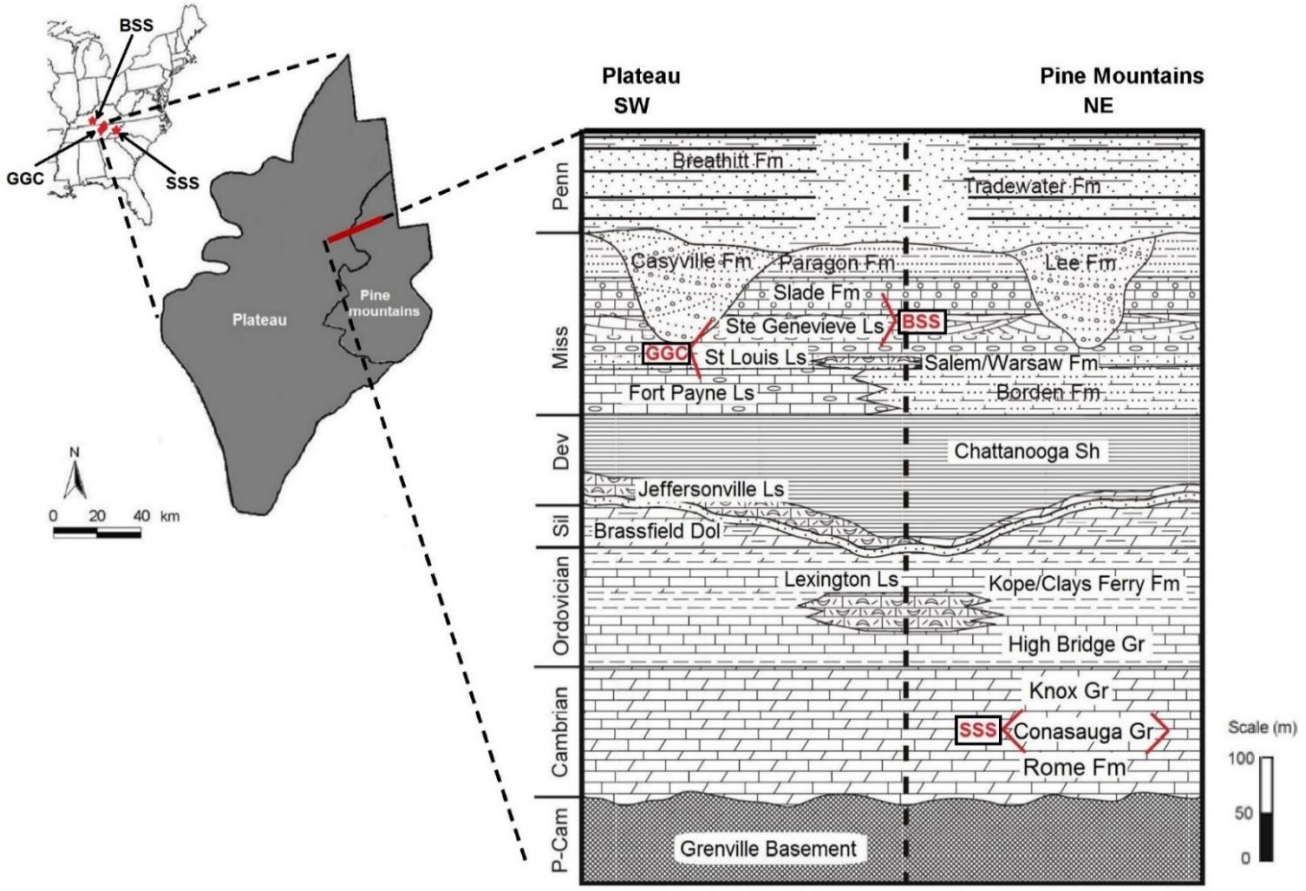


Figure 122: Location map of the Cumberland Plateau (Southeastern Kentucky and Northern Tennessee) and the generalized stratigraphic cross-section of the region (adapted from Simpson and Florea, 2009) based on a theoretical transect (red line) extending from the Plateau (SW) to the Pine Mountains (NE). The *GGC* is located in reference to the Big Spring system (BSS) in the Mammoth Cave Region (Ste Genevieve Ls), and the South Spring system (SSS) in the Maynardville Ls (NE Tennessee; Desmarais and Rojstaczer 2002). Included abbreviations: Dol = Dolomite; Fm = Formation; Gr = Group; Ls = Limestones; Sh = Shales; Sil = Silurian; Dev = Devonian; Miss = Mississippian; Penn = Pennsylvanian

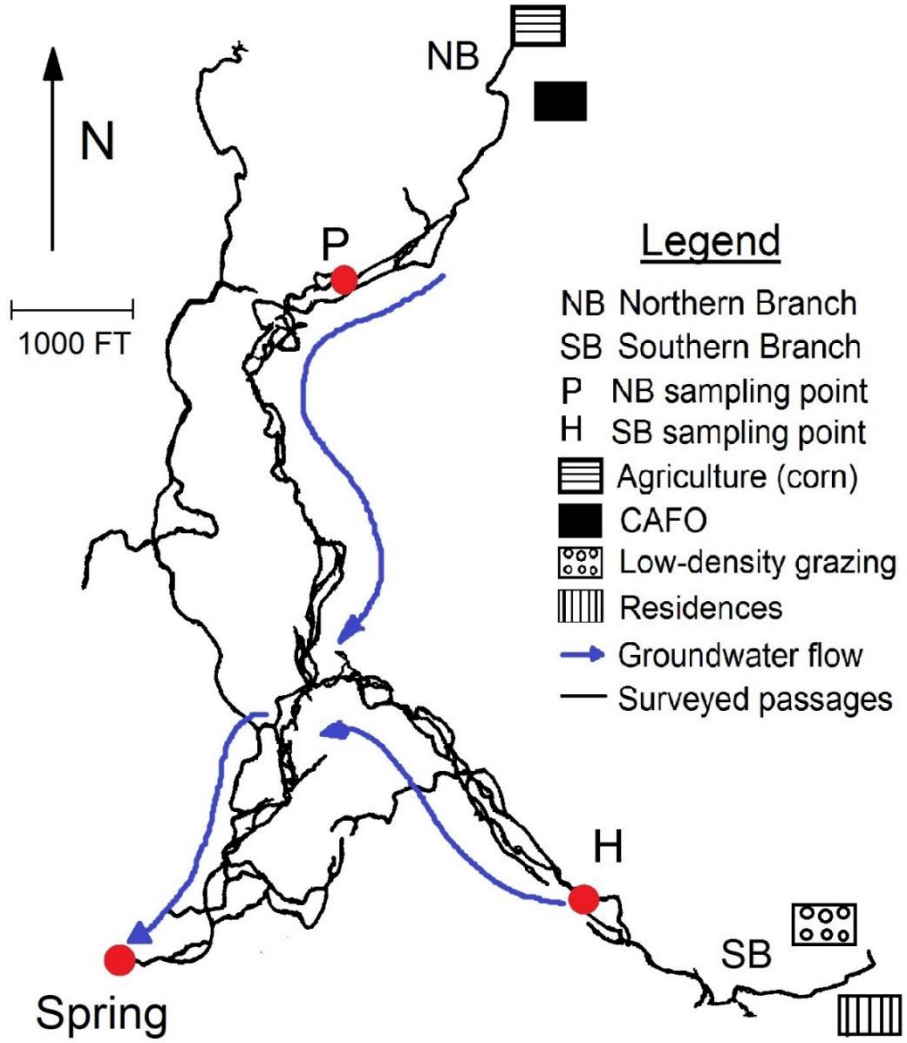


Figure 2: Surveyed passages of the Grayson-Gunnar Cave System. Blue arrows illustrate primary groundwater flow paths. Red dots are the selected sites for data collection from each fork of the cave and from the combined flow at the spring. Courtesy of members of the Greater Cincinnati Grotto of the National Speleological Society (NSS, 2005)

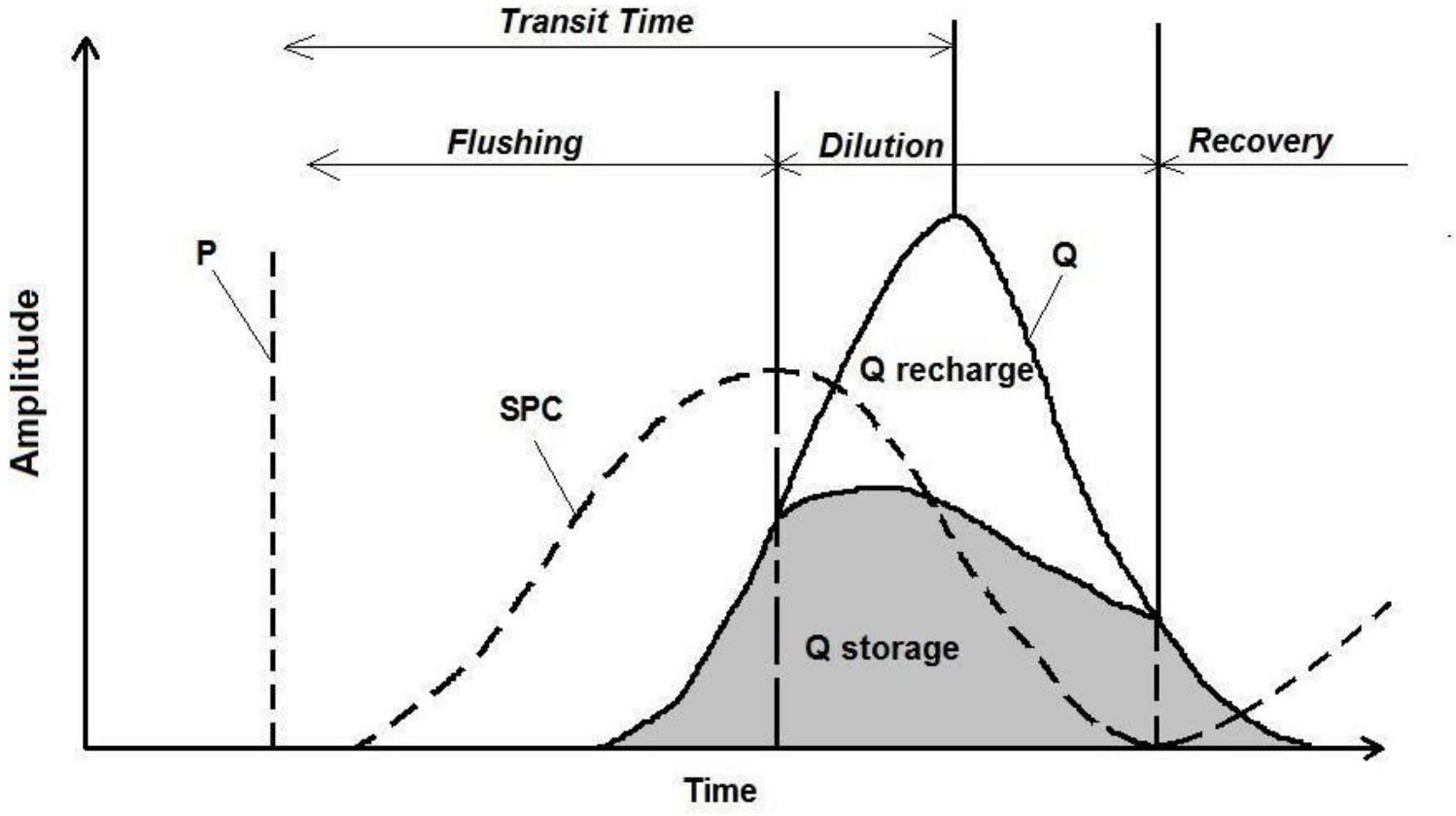


Figure 3: A conceptual model of an epigenic karst aquifer's response to storm events. Time correlation between specific conductivity (*SPC*) and discharge (*Q*) differentiate among flushing, dilution and recovery phases. The *flushing* (or the arrival of storage groundwater '*Q storage'* at the spring) occurs within the time lag between the rise in specific conductivity (SPC) and the peak in SPC. The *dilution* (or the arrival of the surface recharge '*Q recharge'* at the spring) occurs within the time lag between the peak in SPC and the low in SPC. The *transit time* is defined by Mangin (1984) as the time delay between peak precipitation and peak discharge. Adapted from Desmarais and Rojstaczer (2002)

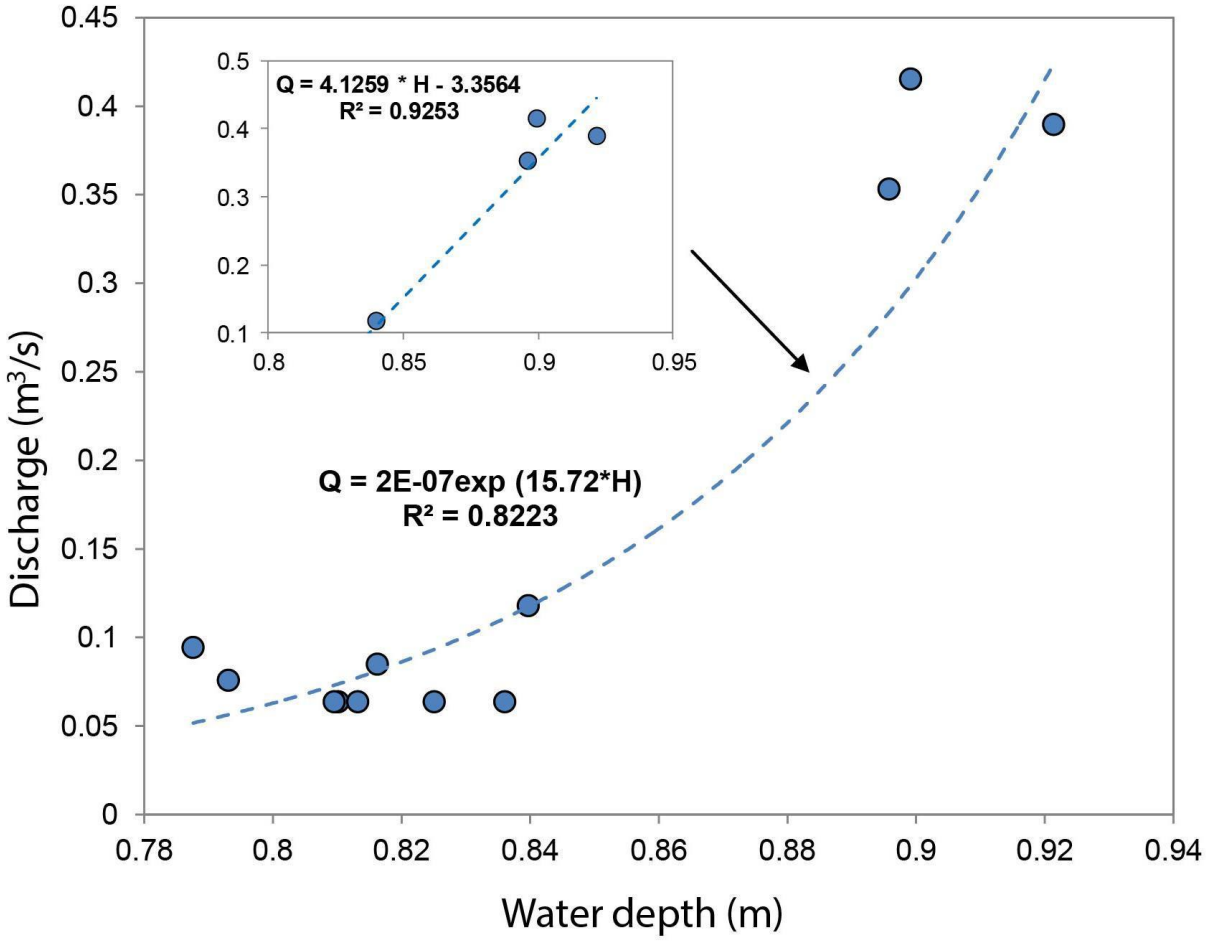


Figure 4: Stage-discharge regression established for the GGC system. The general exponential fit is used to estimate the discharge at low stage (H < 0.8 m; $R^2 = 0.82$). **Inset:** a linear extrapolation provides a better regression ($R^2 = 0.93$) at high stages (H > 0.8 m)

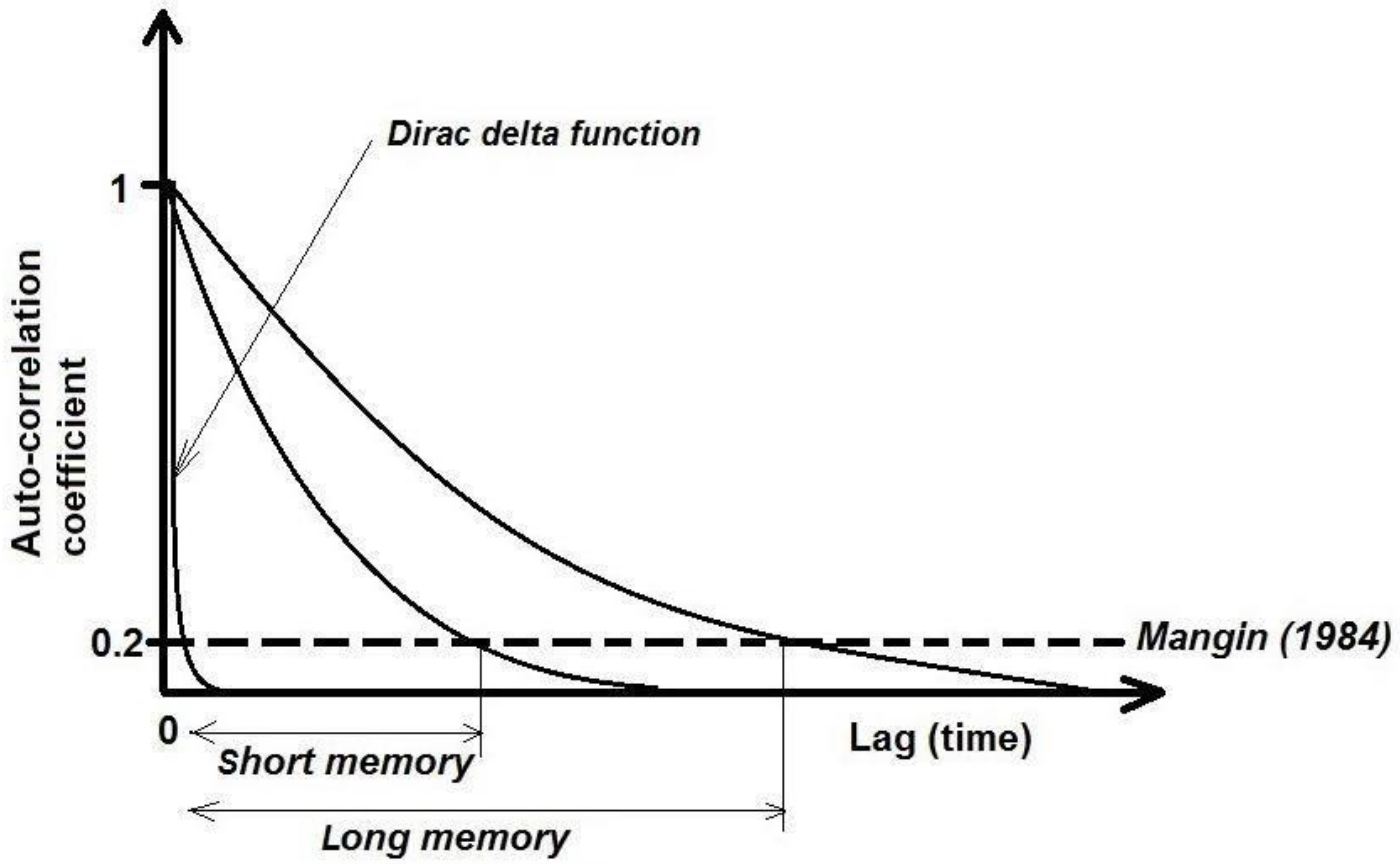


Figure 5: Example of a logarithmic autocorrelogram function obtained for a given variable time series. The rate of decrease of the autocorrelogram is used to estimate the extent of the memory effect (Mangin 1984)

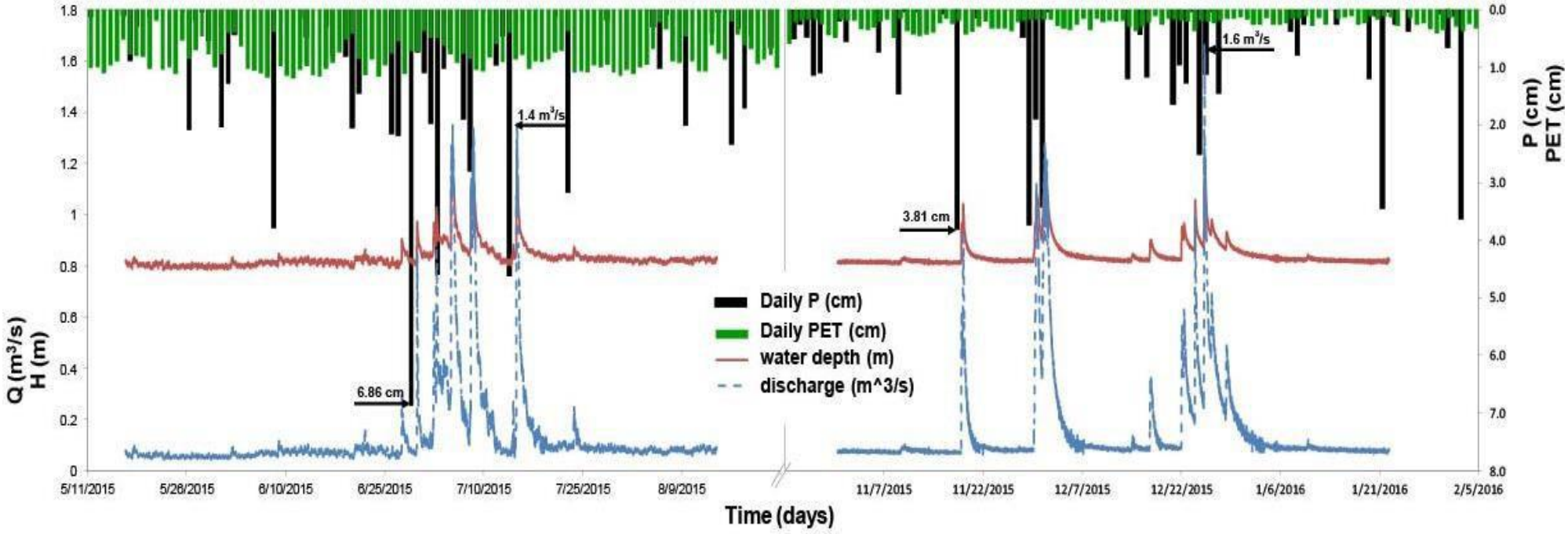


Figure 6: Long-term record of instantaneous discharge (*Q*), water level (*H*), daily Potential Evapotranspiration (*PET)*, and daily Precipitation *P*

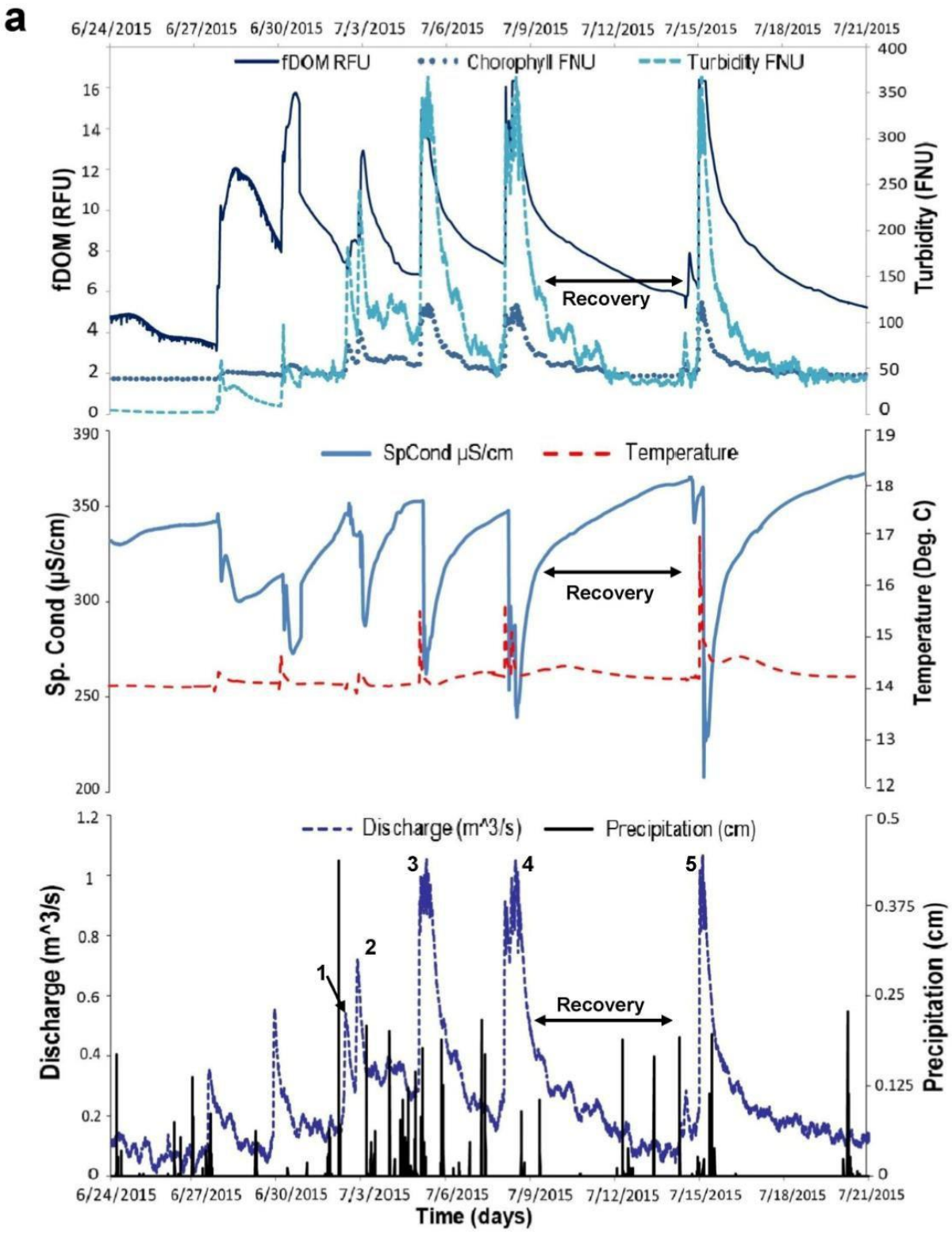


Figure 7a: Physicochemical response to storm events (Summer 2015). Displayed lag numbers range from -20 to +20 (x-axis)

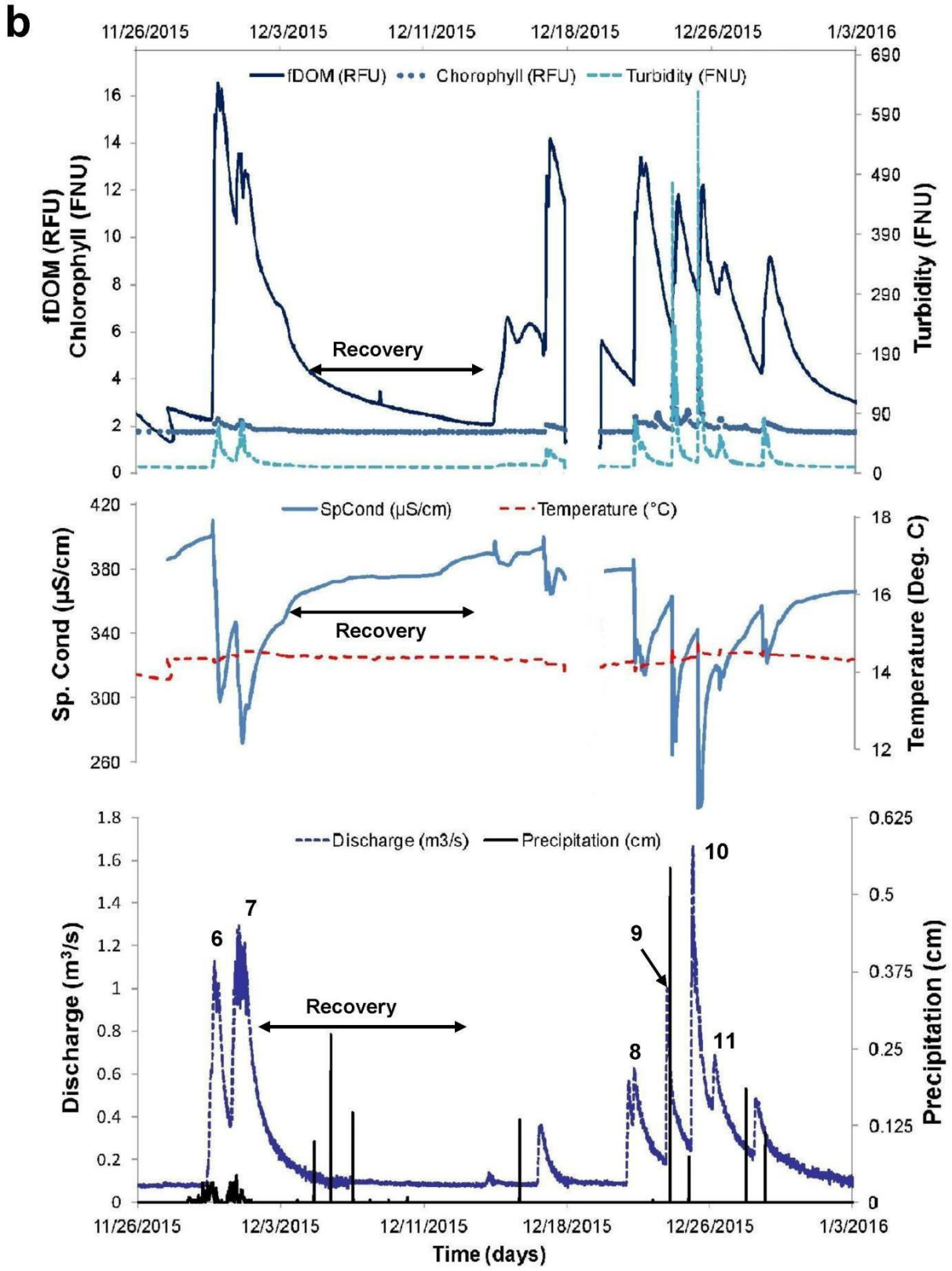


Figure 7b: Physicochemical response to storm events (Winter 2015). Displayed lag numbers range from -20 to +20 (x-axis)

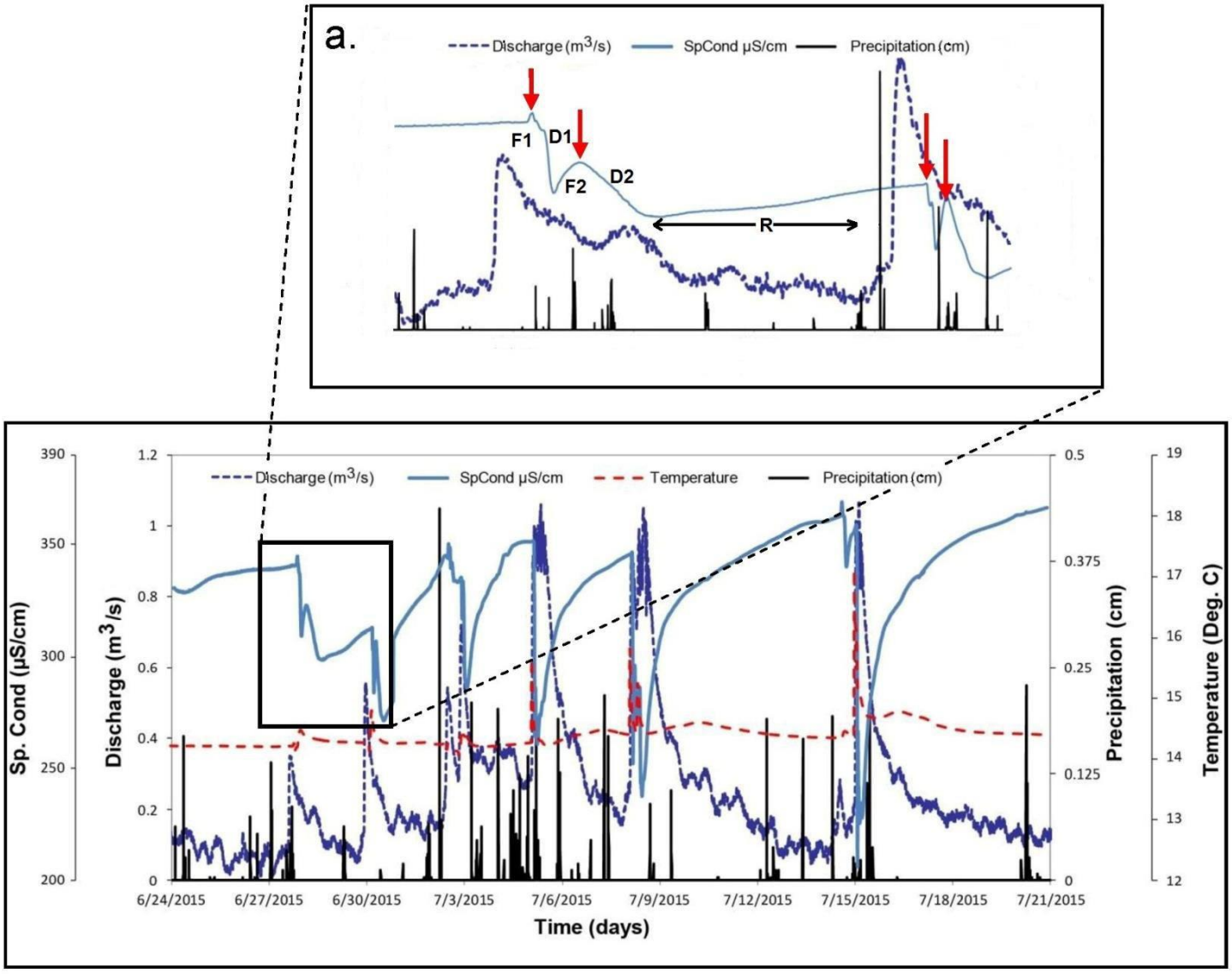


Figure 8: Evolution of specific conductivity and temperature during summer storm events as recorded by the EXO2 sonde displayed near the entrance of the Grayson-Gunner cave (bottom). **a** Zoom on the double peak in the specific conductivity signal (*red vertical arrows*). F1: First Flush; D1: First Dilution; F2 Second Flush; D2: Second Dilution; R: Recovery

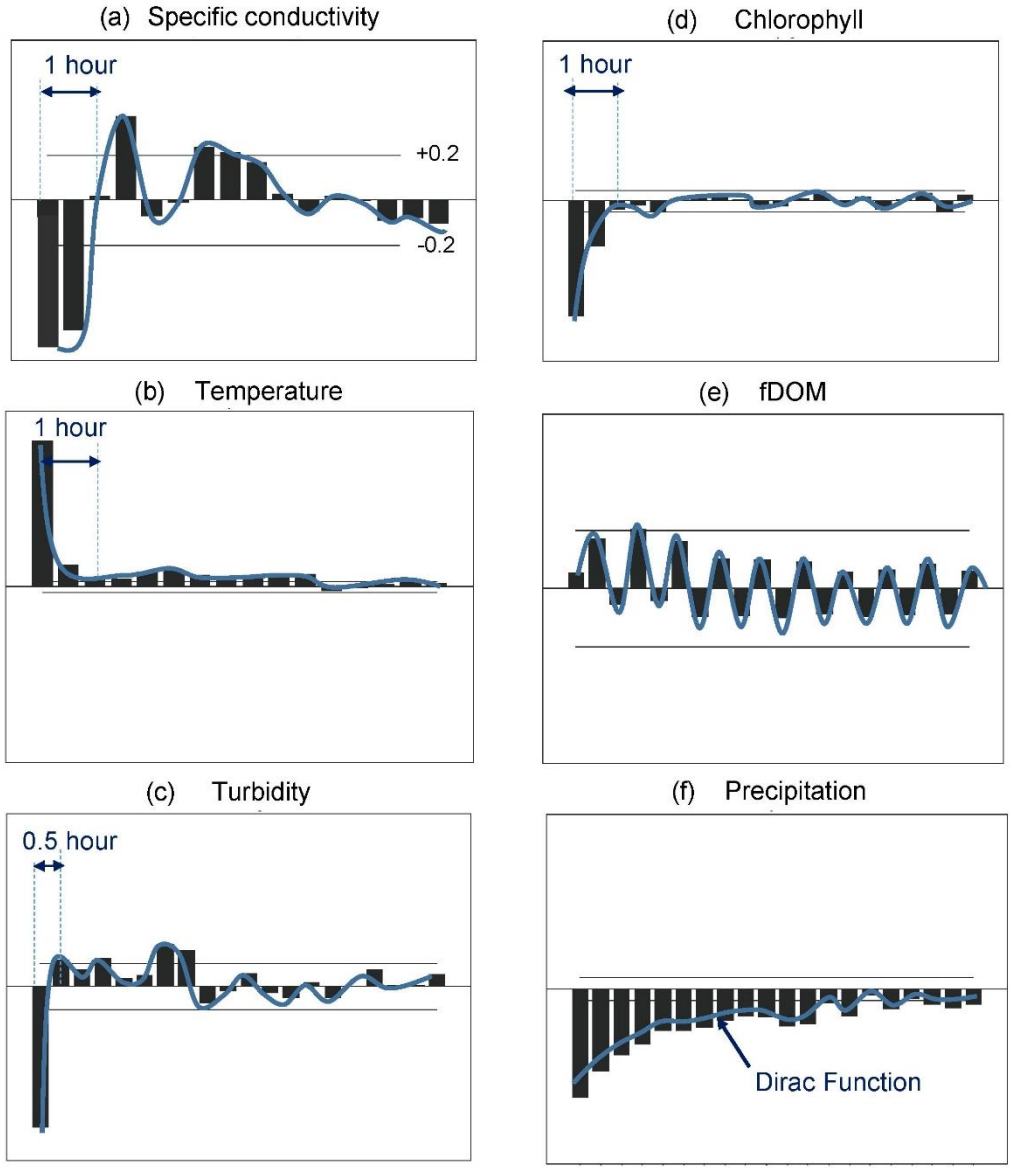


Figure 9A: Summer autocorrelation functions obtained using 30-minute-interval time-series from 6/10/2015 to 8/9/2015 (summer 2015) suggest that physicochemical changes are driven by inputs from precipitation (Dirac functions) The memory effect is estimated using the ±0.2 threshold (Mangin, 1984). The specific conductivity spectrum was zoomed in to highlight the ±0.2 fluctuation range

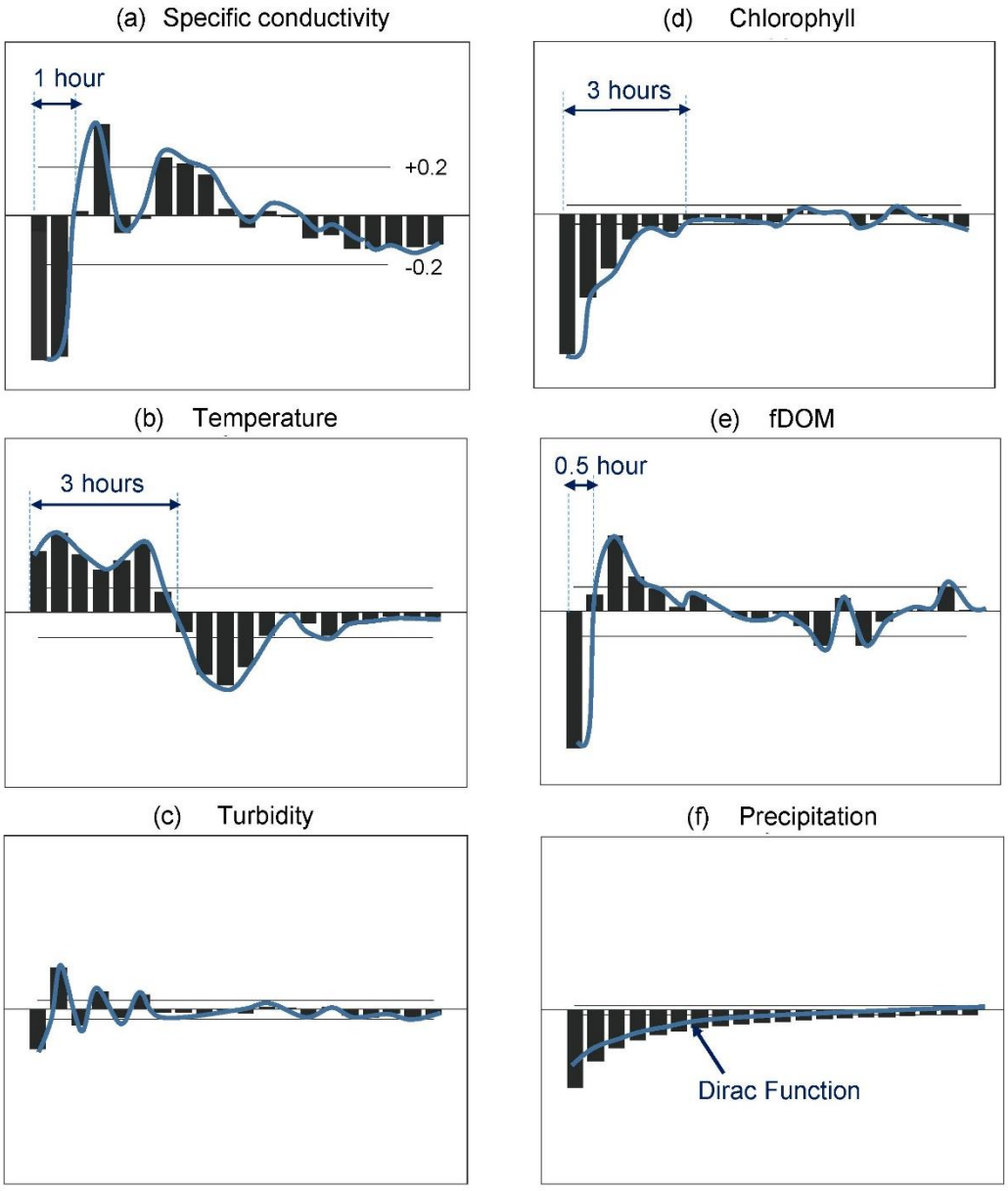


Figure 9B: Winter autocorrelation functions obtained using 30-minute-interval time-series from 11/27/2015 to 02/17/2015 (winter 2015) suggest that physicochemical changes are driven by inputs from precipitation (Dirac functions). The memory effect is estimated using the ±0.2 threshold (Mangin, 1984)

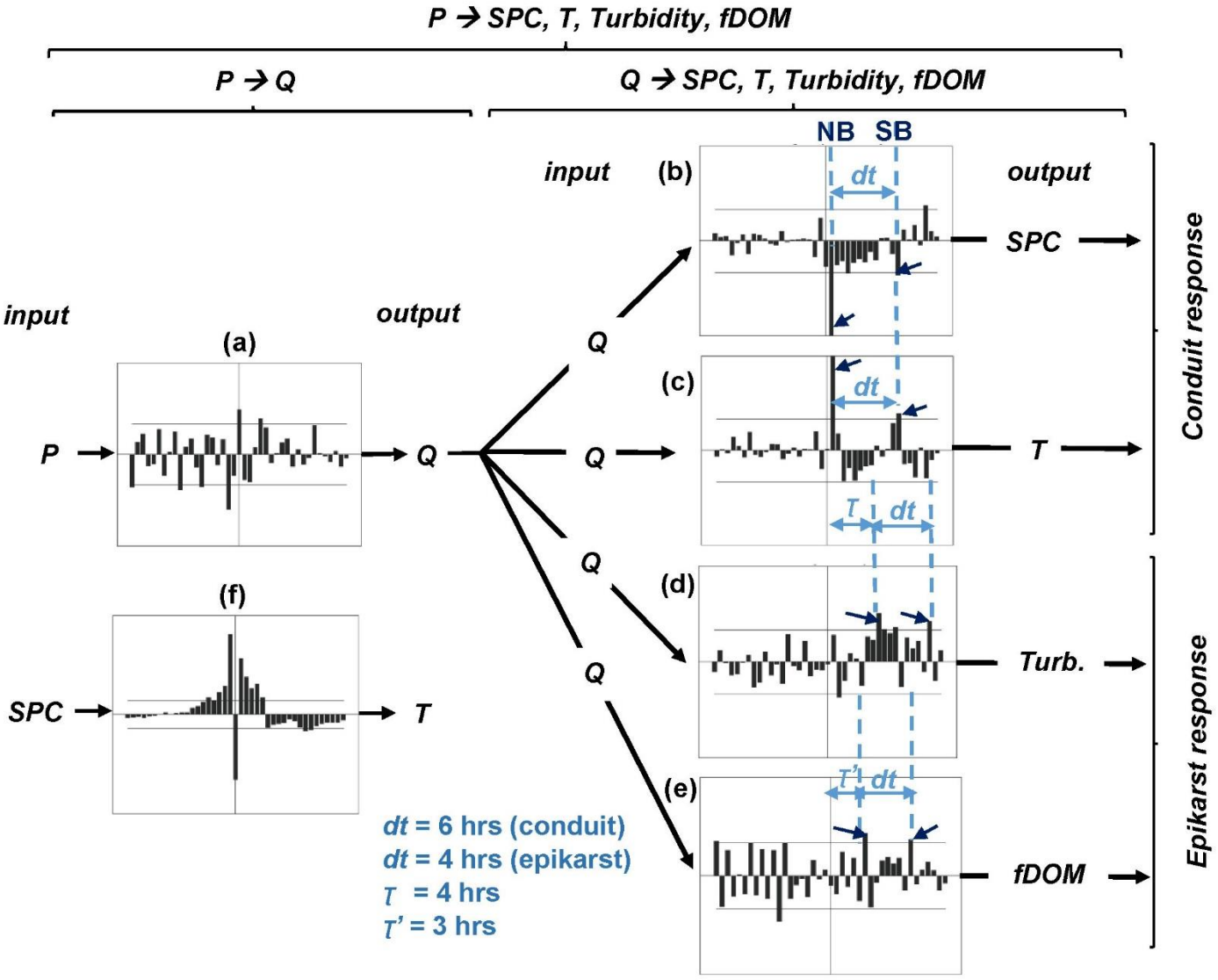


Figure 10: Cross-correlation functions obtained using 30-minute-interval time-series (summer data only). (a) cross-correlogram between precipitation (P) and discharge (Q); (b) Q - Specific Conductivity (SPC); (c) Q - temperature (T); (d) Q - turbidity (Turb.); (e) Q - fDOM; (f) SPC - T

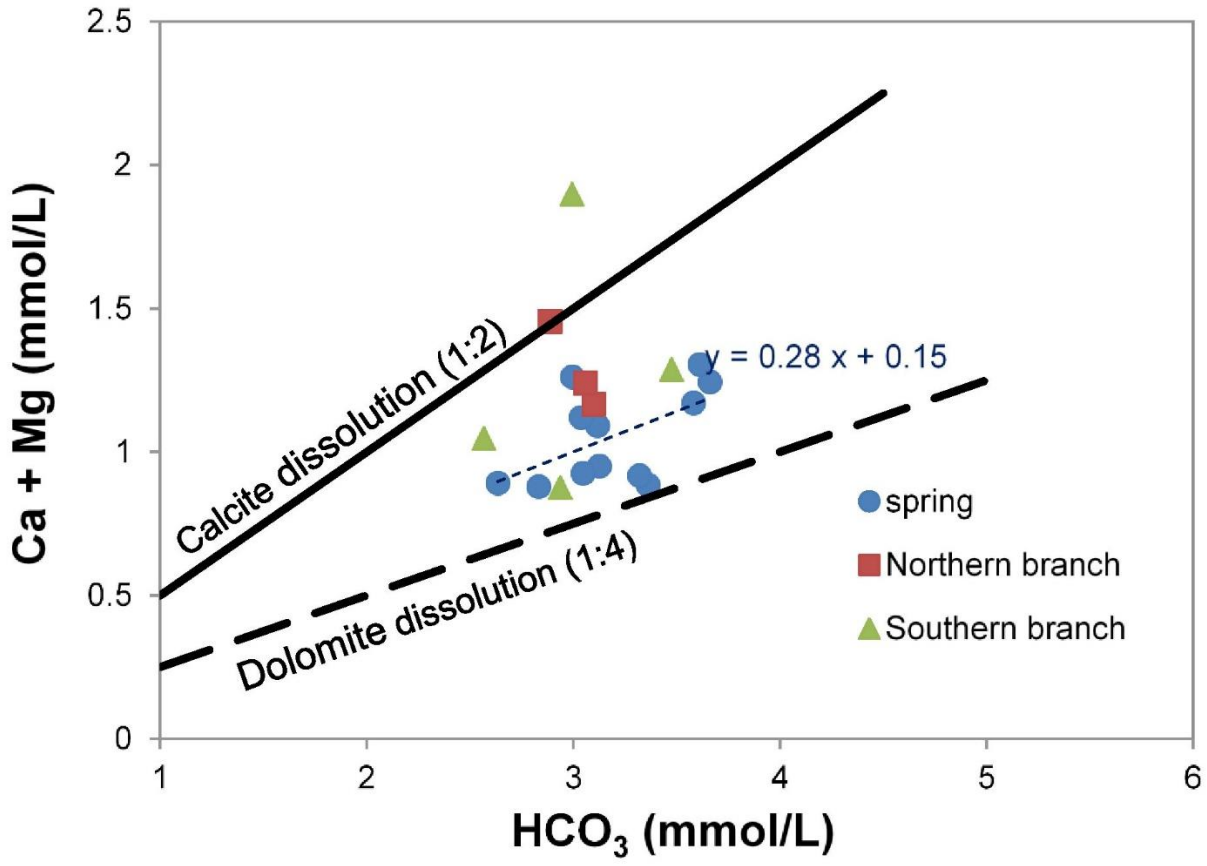


Figure 11: Plot of Ca+Mg (mmol/L) against $HCO_3$ (mmol/L). Samples from the Northern Branch, the Southern Branch and the GCC spring and represented by squares, triangles and circles respectively

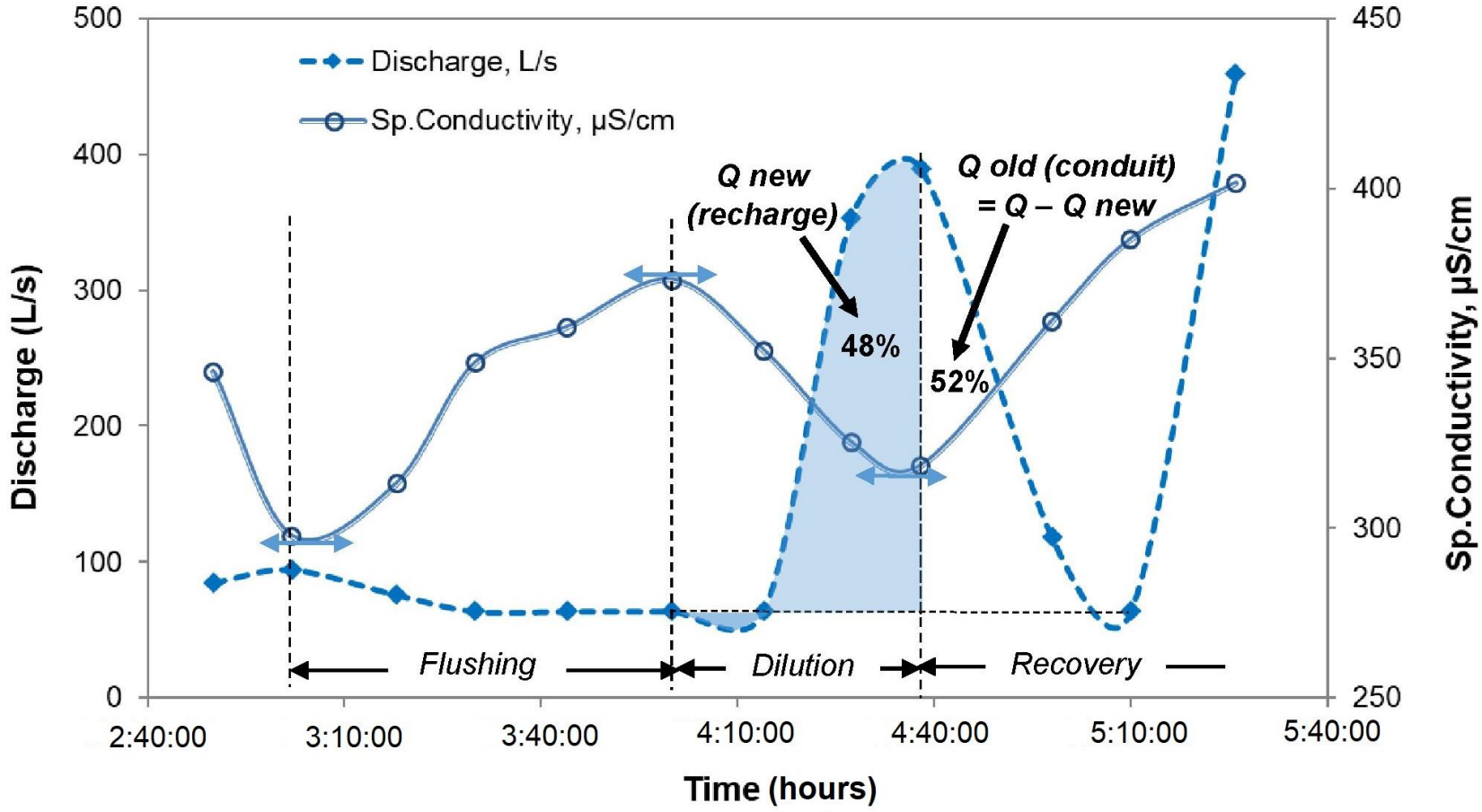


Figure 12: Volumetric percentages of new water (Q-new; storm water) and old water (Q-old; groundwater reserve volume) from 10-minute interval record of summer storm # 4 (7/7/2015; Table 2) using the integration of the discharge curve as proposed by Desmarais and Rojstaczer (2002). A volume of $1.69 \times 10^6$ liters of storm water (48% of the total discharge) reaches the spring during dilution. A volume of $1.83 \times 10^6$ liters of groundwater storage (52% of total discharge) is estimated by subtracting Q-new from Q-total

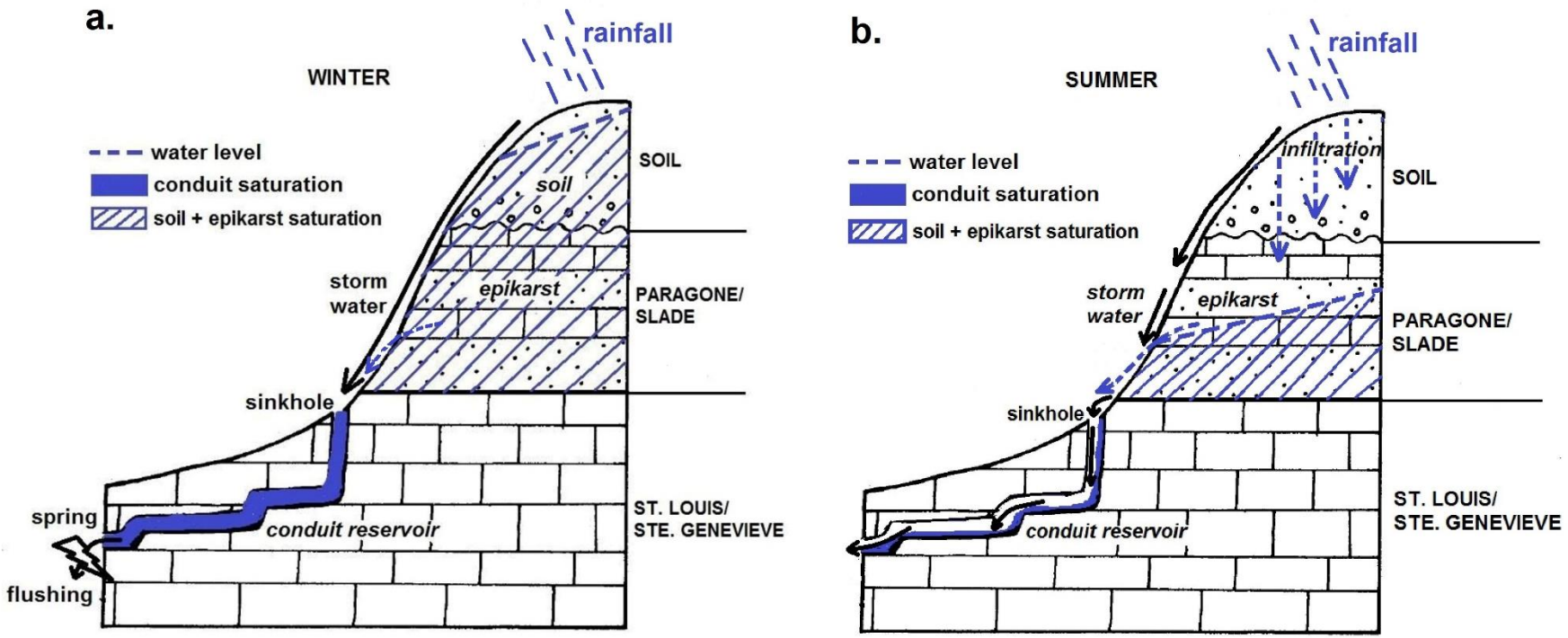


Figure 13: A conceptual model of groundwater flows in the GGC system. The *groundwater storage* is considered one single entity (although there are 2 conduit branches in the system). **a** Cumulative *rainfall* combined with antecedent moisture and aquifer saturation during the *winter* result in the *flushing* of the high volume of groundwater storage by the incoming *storm water*. **b** High evaporation and low antecedent moisture during the *summer* lead to the direct infiltration of *storm water* through surface runoff and conduit system. Modified from Ryan and Meiman (1996)

**Tables**

Table 1: Discharge (*Q*) calculated as a function of water level (H) using the exponential fit (*Q-expo*) and the linear fit (*Q-linear*). Yielded values are compared to the actual discharge measurements at the spring (*Q*). Exponential fit yields good estimation of the discharge at low flow conditions ($Q < 0.1$ $m^3/s$) and tends to underestimate the actual discharge at high flow ($Q > 0.1$ $m^3/s$). On the contrary, linear fit yields a better estimation of discharge at high flow

| Sample date | Q ($m^3/s$) | H (m) | Q-expo | Q-linear |
|---|---|---|---|---|
| 05/16/2015 | 0.085 | 0.82 | 0.075 | 0.011 |
| 05/22/2015 | 0.094 | 0.79 | 0.048 | -0.107 |
| 05/30/2015 | 0.076 | 0.79 | 0.052 | -0.084 |
| 06/05/2015 | 0.064 | 0.81 | 0.068 | -0.014 |
| 06/12/2015 | 0.064 | 0.83 | 0.086 | 0.048 |
| 06/20/2015 | 0.064 | 0.81 | 0.067 | -0.016 |
| 06/27/2015 | 0.064 | 0.81 | 0.071 | -0.001 |
| 07/03/2015 | **0.415** | 0.90 | 0.275 | **0.353** |
| 07/03/2015 | **0.353** | 0.90 | 0.261 | **0.339** |
| 07/09/2015 | **0.390** | 0.92 | 0.391 | **0.445** |
| 07/19/2015 | **0.119** | 0.84 | 0.108 | **0.108** |
| 07/25/2015 | 0.064 | 0.84 | 0.102 | 0.093 |

Table 2: Specific conductivity (SPC) hydrograph decomposition for large storms (peak Q > 0.5 $m^3/s$) in *summer* 2015 and *winter* 2015

| Event number | Storm date | $Q_{max}$ ($m^3/s$) | Flushing | | Dilution (hours) | Recovery (hours) | Total duration (hours) |
|---|---|---|---|---|---|---|---|
| | | | Time to 1st peak (hours) | Delay to 2nd peak (hours) | | | |
| 1 | 07/02/2015 | 0.58 | 0.00 | 1.20 | 0.72 | 0.00 | 1.92 |
| 2 | 07/02/2015 | 0.88 | 0.00 | 1.44 | 2.88 | 0.24 | 4.32 |
| 3 | 07/04/2015 | 1.14 | 0.00 | 2.40 | 1.20 | 0.24 | 3.60 |
| 4 | 07/07/2015 | 1.31 | 0.00 | 2.40 | 5.52 | 30.00 | 7.92 |
| 5 | 07/14/2015 | 1.36 | 0.72 | 0.96 | 1.68 | 5.76 | 3.36 |
| 6 | 11/30/2015 | 1.04 | 1.00 | 3.12 | 6.24 | 0.59 | 10.36 |
| 7 | 12/01/2015 | 1.28 | 1.25 | 1.20 | 6.96 | 22.56 | 9.41 |
| 8 | 12/22/2015 | 0.63 | 0.53 | 4.56 | 5.04 | 7.44 | 10.13 |
| 9 | 12/24/2015 | 0.97 | 2.26 | 1.92 | 1.68 | 4.32 | 5.86 |
| 10 | 12/25/2015 | 1.66 | 0.65 | 1.92 | 2.40 | 0.50 | 4.97 |
| 11 | 12/26/2015 | 0.69 | 1.67 | 6.96 | 2.16 | 4.80 | 10.79 |
| **Average 1-5 (summer)** | | 1.05 | 0.14 | 1.68 | 2.40 | 7.25 | 4.22 |
| **Average 6-11 (winter)** | | 1.05 | 1.23 | 3.28 | 4.08 | 6.70 | 8.59 |

Table 3: Physico-chemical data from weekly sampling at the GGC spring

| Location | Sample | $HCO_3$ (mmol/L) | Ca (mmol/L) | Mg (mmol/L) | Sp. Cond. (µS/cm) | Temp. (°C) | $pP_{CO2}$ | Ca/Mg | Ca/$HCO_3$ | SI calcite | SI dolomite |
|---|---|---|---|---|---|---|---|---|---|---|---|
| Spring | GT032115A ENT | 2.83 | 0.88 | 0.25 | 319.10 | 13.8 | 2.08 | 3.56 | 0.31 | -0.78 | -2.13 |
| | GT051615 ENT | 3.12 | 1.09 | 0.58 | 346.00 | 14.0 | 2.04 | 1.89 | 0.35 | -0.66 | -1.62 |
| | GT052215 ENT | 2.63 | 0.89 | 0.37 | 297.50 | 13.7 | 2.11 | 2.41 | 0.34 | -0.81 | -2.03 |
| | GT053015ENT | 2.99 | 1.26 | 0.41 | 313.00 | 14.1 | 2.06 | 3.06 | 0.42 | -0.61 | -1.73 |
| | GT060515ENT | 3.12 | 0.95 | 0.51 | 348.50 | 14.2 | 2.04 | 1.86 | 0.30 | -0.71 | -1.70 |
| | GT061215 ENT | 3.04 | 1.12 | 0.66 | 359.00 | 14.2 | 2.05 | 1.70 | 0.37 | -0.66 | -1.57 |
| | GT062715 ENT | 3.05 | 0.93 | 0.37 | 352.00 | 14.2 | 2.05 | 2.50 | 0.30 | -0.73 | -1.87 |
| | GT070315 ENT | 3.36 | 0.89 | 0.45 | 325.00 | 14.2 | 2.01 | 1.95 | 0.26 | -0.70 | -1.72 |
| | GT070915 ENT | 3.32 | 0.92 | 0.33 | 318.30 | 14.5 | 2.01 | 2.79 | 0.28 | -0.73 | -1.92 |
| | GT071915 ENT | 3.58 | 1.17 | 0.52 | 360.80 | 14.4 | 1.98 | 2.26 | 0.33 | -0.57 | -1.51 |
| | GT072515 ENT | 3.66 | 1.25 | 0.49 | 384.90 | 14.4 | 1.97 | 2.52 | 0.34 | -0.55 | -1.52 |
| | GT080215 ENT | 3.61 | 1.31 | 0.46 | 401.40 | 14.3 | 1.97 | 2.83 | 0.36 | -0.55 | -1.57 |
| Northern branch | GT051615 H | 3.10 | 1.17 | 0.60 | 342.20 | 14.1 | 2.04 | 1.94 | 0.38 | -0.64 | -1.58 |
| | GT070315 H | 2.89 | 1.46 | 0.58 | 324.50 | 14.1 | 2.07 | 2.52 | 0.50 | -0.60 | -1.63 |
| | GT080215 H | 3.06 | 1.24 | 0.49 | 393.30 | 14.3 | 2.05 | 2.51 | 0.41 | -0.60 | -1.63 |
| Southern branch | GT051615 PLP | 2.94 | 0.88 | 0.35 | 340.50 | 14.4 | 2.06 | 2.48 | 0.30 | -0.77 | -1.95 |
| | GT070315 PLP | 2.57 | 1.05 | 0.56 | 320.50 | 14.3 | 2.12 | 1.87 | 0.41 | -0.75 | -1.80 |
| | GT080215 PLP | 3.47 | 1.29 | 0.59 | 387.60 | 14.6 | 1.99 | 2.17 | 0.37 | -0.54 | -1.43 |
| | GT090515B PLP | 2.99 | 1.90 | 0.64 | 349.53 | - | 2.06 | 2.95 | 0.63 | - | - |

Table 4: Volumetric contributions of the two conduit branches to the spring discharge using $Ca/HCO_3$ ratios mass-balance calculations (Equations 4 -16)

| **Date** | **$(Ca/HCO_3)_S$** | **$(Ca/HCO_3)_{SB}$** | **$(Ca/HCO_3)_{NB}$** | **$Q_S$ ($m^3/s$)** | **$Q_{SB}$ ($m^3/s$)** | **$Q_{NB}$ ($m^3/s$)** | **%SB** | **%NB** |
|---|---|---|---|---|---|---|---|---|
| 05/16/15 | 0.35 | 0.30 | 0.38 | 0.09 | 0.01 | 0.08 | 7.0 | 93.0 |
| 07/03/15 | 0.26 | 0.41 | 0.50 | 0.38 | 0.18 | 0.20 | 47.7 | 52.3 |
| 08/02/15 | 0.36 | 0.37 | 0.41 | 0.58 | 0.07 | 0.51 | 11.0 | 89.0 |

Table 5: Volumetric contributions and percentages of groundwater storage and recharge water discharging at the spring from 11 major storms ($Q > 0.5\ m^3/s$)

| | Average | % spring discharge |
|---|---|---|
| Conduit volume (L) | 5.84E+06 | 35.52 |
| Recharge volume (L) | 1.06E+07 | 64.48 |
| Total volume (L) | 1.64E+07 | 100.00 |

Table 6: Aquifer compartments response as inferred from cross-correlation analyses using *summer* 2015 and *winter* 2015 data. Values reflect the response of the fastest branch (NB)

| | **Summer (hours)** | **Winter (hours)** |
|---|---|---|
| Conduit water discharge (1) | 0.50 - 2.00 | 0.00 - 2.00 |
| Storm water infiltration (2) | 0.50 - 4.00 | 2.00 - 6.00 |
| Total storm duration (1+2) | 1.00 - 6.00 | 2.00 - 8.00 |

# CHAPTER 4:
# LAND-USE AND HYDROLOGIC CONTROLS ON NUTRIENT LOADS IN AQUIFERS DRAINING AGRICULTURAL AND MIXED-USE WATERSHEDS.

**Abstract**

Agricultural non-point-source pollution from the upper areas of the Upper Mississippi, Missouri, and Ohio River Basins account for the majority of the excess nitrogen that leads to the Gulf of Mexico's hypoxic zone. Mitigating long-term nutrient inputs at a large scale (Mississippi River Basin) requires understanding micro-scale changes at the small watershed level (less than 100 $km^2$). To assess land-use and hydrologic controls on nutrient fate and transport, temporal patterns in nutrient concentrations in a mixed land-use watershed, Grayson-Gunnar Cave (GGC), were analyzed. The cave is located in the Cumberland Plateau (Upper Ohio River Basin), a region where the proliferation of concentrated-animal feeding operations (CAFOs) is rapidly changing the predominantly rural landscape (forest and agriculture) into mixed-use covers. To assess the control of land-use on Total Inorganic Nitrogen (TIN) loads and the differences in nutrient loads between the recharge basins of the North Branch (NB) and South Branch (SB) of the GGC watershed, 4-months of weekly water sampling was performed at the GGC spring and at two underground conduit locations. The observed temporal variations in nutrients concentrations are primarily associated with seasonal changes in land-use associated with corn growth. Data show that land-use sources explain much of the temporal variability of TIN at the spring when weighted against the hydrological factor. End-member-mixing analysis of Dissolved Organic Carbon (DOC) shows a progressive depletion in DOC-depleted sources with the corn-growth season, a progressive increase in the contribution of DOC-enriched sources and a more labile form of carbon toward the harvest time. Overall, during high flow, non-point source infiltration from manure-fertilized croplands in the NB and point recharge from sewage in the SB dominates over inorganic fertilizers. However, poultry-manure sources exert more statistically significant control on TIN variability when compared to sewage inputs. Because conduit-dominated karstic aquifers such as the GGC are more susceptible to contamination from direct and fast (< 7 hours)

subsurface infiltration during late summer rainfall period (July to August), a slight advance in the timing of manure application could substantially reduce nutrient loads in the agricultural portion of the basin. These results suggest that evaluating hydrologic and land-use controls on nutrients at the scale of small watersheds (such as the GCC) is crucial to developing site-specific Nutrient Management Plans and managing the Gulf of Mexico's hypoxic zone.

Keywords: Contaminant Transport, Groundwater, Nutrient Pollution, Nonpoint Source, CAFO, Nutrient Management Plan.

## I. Introduction

A zone of hypoxia has developed in the Gulf of Mexico (GOM) due to excessive nutrient loadings (primarily nitrogen) from the Mississippi River Basin (MRB; Turner and Rabalais, 1994; Rabalais et al., 2002). This hypoxic zone varies annually in size from 40 $km^2$ to 20,000 $km^2$ with its peak area occurring in May (Turner et al., 2006). Primary sources of nutrient inputs in surface and groundwater in the MRB include non-point sources (precipitation/atmospheric deposition, fertilizer application on croplands, mineral dissolution) and point sources (sewage systems, domestic septic systems, concentrated-animal feeding operations). However, non-point source pollution from predominantly agricultural upper basins accounts for the majority of the spatio-temporal variability of the GOM hypoxic zone (Panagopoulos et al., 2014; Kladivko et al., 2014). More than 60% of the Dissolved Inorganic Nitrogen (DIN) export to the GOM is derived from the primarily agricultural Upper Mississippi, Missouri and Ohio River watersheds (Donner et al., 2002; Donner and Scavia, 2007; Randall and Mulla, 2001; Davis et al., 2014).

Despite efforts to reduce the extent of the hypoxia zone in the Gulf of Mexico, it is forecasted that the mid-summer 2018 hypoxic zone is approximately 14,790 $km^2$ (NOAA, 2018), about the

average value recorded for the last 33 years, and well below the target threshold (< 5,000 $km^2$) defined by the Mississippi River/GOM Hypoxia Task Force 2008 Action Plan. Loken et al. (2018) have observed that strategies to mitigate nitrogen export to the GOM have mainly relied on nutrient removal within the Mississippi River. They concluded that the lack of similar efforts in the upper part of the MRB (e.g., Ohio River) has caused no movement towards the target threshold to reduce nutrient export to the GOM. Moreover, implementing new strategies to target nutrient loads upstream of contributing watersheds such as the Ohio River Basin (ORB) will require extending the current monitoring network (USGS, 2018a, 2018b) to upper catchment basins where nutrient load data are unavailable. In the ORB, for instance, the only real-time data measurements are the ones currently recorded at the Olmsted Station (IL) at the confluence with the Upper Mississippi River, which leaves the entire upper part of the Ohio River Basin unmonitored.

As a major sub-basin of the MRB (Fig. 1), the Ohio River Basin (ORB) contributes 35 percent of the Mississippi River's total discharge and 30 percent of the average annual nutrient loads in the Gulf of Mexico (32% N and 29% P; USGS, 1995). Moreover, runoff from fertilized croplands is the dominant source of Total Nitrogen (TN; 58%) and Total Phosphorous (TP; 56%) within the ORB (White et al., 2014). Average daily loads from the ORB to the Mississippi River channel are estimated to $1.5 \times 10^6$ lb/day of TN and to $10^5$ lb/day of TP (Olszowka et al., 1994). Although the excessive loads of sediment and suspended material remain the primary concern for water quality at the ORB scale, dissolved nutrients (mainly nitrates) represent the fourth greatest cause of water quality impairment among its major tributaries (Olszowka et al., 1994).

Even though it covers less than 7% ($3.3 \times 10^4$ $km^2$) of the ORB, the Cumberland River (Fig. 1) is responsible for about 10% of the total nutrient daily loads (125,000 lb/day of TN +TP) to the Ohio River. The Cumberland River's headwaters are in the Upper Cumberland Plateau, a

mature and active cave-forming carbonate platform characterized by deep sinkholes and stream swallets (White, 1998; Ford and Williams, 2007). Because the majority of the water drainage occurs in subsurface caves and the regional groundwater flow gradient is from the Plateau to the Cumberland River, discharge from upstream springs likely plays a major role in nutrient export to the Cumberland and Ohio Rivers (Fig.1).

The surface landscape and land use of the Upper Cumberland region has undergone substantial changes over the last decade (2000-2009), mainly due to transition from open farming to CAFOs (concentrated animal feeding operations), as seen in other intensive farming regions across the United States (Brahana et al., 2014; Victor et al., 2014). Moreover, CAFOs' development on karstic terranes (e.g., Cumberland Plateau) is highly problematic considering the vulnerability of carbonate aquifers to surface contamination through surface sinkholes and sinking streams (Mull et al., 1988; Brahana et al., 2014). Nutrients in surface and groundwater in CAFO-dominated land covers (Fig. 2) primarily originate from point sources such as manure storage sites and effluent pipes and to a lesser extent from non-point sources (e.g., diffuse runoff over manure sprayfields). Nutrients loads usually increase in surface water and shallow groundwater following major rainfall events due to lagoon spill/overflow (Mallin et al., 1997) and lateral runoff over water-saturated arable or non-cultivated soils (Hooda et al., 2000). Groundwater contamination occurs primarily through direct leakage below manure storage lagoons (Hutchins et al., 2012), diffuse recharge from lagoon seeps (Burkholder et al., 2007; Hodne, 2005), and vertical leakage from drains underlying sprayfields (Brahana et al., 2014).

It is widely assumed that climate (interannual cycles, spatial and temporal distribution of precipitation and moisture) and hydrologic variables are the primary controlling factors of the spatial and temporal variability in nutrient flux within large predominantly agricultural landscapes such as the Cumberland Plateau (Donner et al., 2002; Donner and Scavia, 2007;

Howarth et al., 2012; Sinha and Michalak, 2016; Davis et al., 2014). At larger spatial scales, controllable factors such as land-use, crop types, drainage pathways and fertilizers application rates may play a secondary role in nutrient export (Davis et al., 2000; Jaynes et al., 2001; Randall et Mulla, 2001; Donner, 2003; Donner et al., 2004; Donner and Kucharik, 2008; Secchi et al., 2010). However, at the scale of small agricultural watersheds (less than 100 $km^2$) and karstic landscapes such as the smaller drainage basins within the Cumberland Plateau, where dominant subsurface flow and subsequently increased surface and subsurface connectivity are found, patterns of nutrient transport to groundwater may be driven by anthropogenic and surface land-use factors (Kastrinos and White, 1986; Currens, 1996; Taraba et al., 1997; Mahler et al., 2006; Stueber and Criss, 2005). Furthermore, the fate of nutrients in such small agriculturally-influenced basins are very dependent on surface end-member mixing sources, speciation, differential transport pathways, soil and the vadose zone characteristics (soil drainage, soil saturation), geomorphic factors (slope), in addition to hydrological factors such as precipitation, discharge (flow velocity), path length and stream orders (Dodds et al., 1996).

One of the biggest challenges for nutrient mitigation in small agricultural and mixed-use watersheds is the identification of contaminant sources (Panno et al., 2001). By assessing nutrient and select trace metal sources as well as land-use controls in a small scale watershed such as the Grayson-Gunnar Cave system in the Upper Cumberland Plateau, the impact of present and future land use changes (e.g., CAFO development) on groundwater quality may be predicted, and site-specific Nutrient Management Plans can be developed to minimize the effects of contaminants in streams and groundwater at the larger spatial scale, such as the Ohio River Basin and the Gulf of Mexico.

## II. Materials and Methods

### *II.1. Study Area*

The average landscape in the Cumberland Plateau includes 52.5% secondary-growth forests, 43.7% agricultural and mixed cover, 3.5% low-density pasture and grazing, and 0.3% semi-urban/ residential cover (Dale et al., 2009). Of the total agricultural and mixed land-use coverage, ~17.9% consists of cleared land and transitional covers (mainly from open and low-density grazing to intensive farming/ CAFO). Corn is the most common row-crop produced in the Upper Cumberland Plateau.

The present study focuses on the Grayson-Gunnar Cave, an 11-km-long mature epigenic cave system primarily developed in the Mississippian-age carbonates of the St. Louis and Ste. Genevieve Formations (Simpson and Florea, 2009). The recharge basin (12 $km^2$) is located in the Upper Cumberland Plateau physiographic province (Fig. 3) and its regional flow gradient is Northeast towards the Cumberland River. The system is classified as a branchwork network with curvilinear passages and vertical shafts connecting differential erosion levels within the cave (Palmer, 1991). Surveys at the GGC have identified two branches (North Branch, NB; South Branch, SB) of an underground stream (Fig. 3). The surface land cover in the SB recharge area of the cave includes low-density grazing and residential septic tanks. The NB recharge basin has primarily agriculture (corn) and CAFO (poultry). A previous study (Tagne and Dowling, 2018) describes how the two subsurface conduit branches respond differently to surface recharge. The NB has a faster response (30 minutes to 2 hours following the peak discharge) and contributes to about 80% of the total discharge at the spring during major storms. On the other hand, the SB exhibits a slower response to storm events and contributes a lesser proportion to the spring discharge (<20%). The Northern Branch is hydrologically connected to its recharge area through conduit-dominated recharge as evidenced from fast storm response (< 2 hours) and relatively low

groundwater residence time (< 7 days; Tagne and Dowling, 2018). Due to slower storm response in the Southern recharge area, it is likely that recharge occurs through a more diffuse pathway. The differences in contaminant behavior between the two portions of the watershed may be due to differential land cover, differential recharge pattern or a combination of both. Additionally, the presence of a single CAFO in the northern recharge basin allows for the examination and comparison of end-member nutrient sources in a CAFO-influenced landscape (NB recharge basin) and non-CAFO recharge area (SB).

*II.2. Data collection*

Discrete water samples were collected on a weekly basis from May to August 2015 at the GGC spring and at the upstream end of each contributing tributary (Fig. 3). All samples were filtered at 0.45 µm-cellulose to remove suspended fractions, transported to the field house within 24 hours and stored in a 4°C refrigerator until the time of analysis. Samples for nutrient speciation were collected in 250 mL HDPE bottles and analyzed within 48 hours at the field house to avoid microbially-derived conversions among nitrogen species. Speciation of nitrogen ($NH_4^+$, $NO_2^-$, $NO_3^-$) and orthophosphate ($PO_4^{3-}$) was performed using a colorimetric titration on a HACH DR 2800 portable spectrophotometer. Nitrate concentrations were analyzed using the cadmium reduction method high range mode (range = 4.84 – 484 µmol $NO_3^-$/L). Nitrite concentrations were below the instrument detection range (50 nmol/L to 7.1 µmol $NO_2^-$/L). Ammonia was analyzed using the salicylate method on the low range mode (0.5 − 48 µmol $NH_4^+$/L). Dissolved phosphate was analyzed using the molybdovanadate method on the lower (0.2 to 31.5 µmol $PO_4^{3-}$/L) and higher (3.1 to 473 µmol $PO_4^{3-}$/L) range modes. Water velocity measurements at the spring were performed on a weekly basis using a Type A current meter, and values were converted into discharge using standard USGS stream gauging protocols (Rantz, 1982). Samples

for metals analyses were collected in 250 mL HDPE bottles and analyzed using Inductively Coupled Plasma Mass Spectrometry (ICPMS) at the Muncie Water Quality Division Laboratory. Detection limits (in µmol/L) are reported as follows: 0.01 for Cr-III; 0.01 for Cu; 0.01 for Ni; 0.03 for Pb; 0.02 for Zn. Samples for Dissolved Organic Carbon (DOC) and DOC stable isotope ($\delta^{13}C_{DOC}$) were collected in 1 L Nalgene bottles and preserved with 1 mL of 12 N HCl. The DOC was extracted from samples in form of a resin using cryoconcentration (70% carbon yield) at the Ball State University Environmental and Aquatic Chemistry Lab, and the carbon isotopes were analyzed at the Ball State University Environmental Geology Lab using a Picarro cavity-ring-down spectroscopy (CRDS) on a low concentration mode (upper detection limit = 250 µmol C/L) and a method provided by Gandhi et al. (2004) for measuring $\delta^{13}C_{DOC}$ in stream water with low DOC concentrations (< 250 µmol of C per liter of water). As shown in equation 1, the carbon isotope ratio $\delta^{13}C_{DOC}$ is calculated using the Pee Dee Belemnite (PDB) standard ratio ($^{13}C/^{12}C = 0.0112372$):

$$\delta^{13}C\text{-}DOC = \left( \frac{^{13}C\ /^{12}C_{sample}}{^{13}C\ /^{12}C_{standard}} - 1 \right) \times 1000 \qquad \text{Eq. 1}$$

The measured organic carbon is the non-purgeable organic carbon (NPOC) resulting from persulfate oxidation of water samples at 100°C and further dissolution of the purged $CO_2$ into deionized water. The resulting DOC concentration is reported as mg of carbon per liter of water. Because the DOC concentration is not dependent on the molecular weight (M.W.) of the particular organic species ($C_xH_yO_z$) responsible for the purged $CO_2$, conversion from mg C/L to µmol C/L is made using equation 2, where M.W. (C) = 12 g/mol.

$$\mu M\ C/L = \frac{mg\ C/L}{M.W.} \times 10^3 \qquad \text{Eq. 2}$$

The Specific Ultra-Violet Absorbance of aromatic carbon fractions was obtained at a 254-nanometer wavelength ($SUVA_{254}$), as an indicator of the reactivity of the dissolved organic carbon using the methodology provided by Potter and Wimsatt (2005) in equation 3 where SUVA is the Specific Ultra-Violet Absorbance at a 254-nanometer (L/mg/m), UVA is the Ultra-Violet Absorbance coefficient at 254-nanometer ($cm^{-1}$), DOC is the Dissolved Organic Carbon concentration (in mg/L) and 100:1 is the centimeter to meter conversion factor.

$$SUVA_{254} = \frac{UVA_{254}}{DOC} \times \frac{100\ cm}{1\ m} \qquad \text{Eq. 3}$$

*II.3. Data analyses*

As in other heterogeneous land covers (CAFO, row crops, and residential land uses), it is difficult to distinguish the nutrient contribution of each land use within local waterways. Inferring land-use sources often requires that nutrients be analyzed in combination with other tracers of surface recharge such as dissolved organic carbon (Hood et al., 2005; Stepanauskas et al., 2005), stable isotopes (Cravotta, 2002; Burns and Kendall, 2002), optical properties (absorbance and fluorescence) of Dissolved Organic Matter (DOM) (Hansen et al., 2016), trace metals concentrations (Vesper and White, 2003), among others. Moreover, the use of multivariate statistical analyses such as discriminant analysis (Boyacioglu and Boyacioglu 2010; Garizi et al., 2011) and principal component and factor analysis (Belkhiri et al., 2011; Belkhiri and Narany, 2015) have proven successful in a variety of environmental settings for discriminating among various sources of nutrients based on significance ($p < 0.05$), and assessing spatial and temporal patterns in the variability of groundwater quality. Similar statistical methods were applied to karstic environments to identify factors responsible for the spatial variations in the groundwater quality (Boyer et al., 1997; Medina-Gomez and Herrera-Silveira, 2003).

Each portion of the GGC recharge basin (North and South) is characterized by distinct land use (fertilized corn crops and CAFO in the North; low-density pastures and residential in the South). To assess land use controls on nitrate concentrations at the spring and identify which land use exhibits the greatest influence on nutrient loads to groundwater, analysis of correlation and analysis of variance (ANOVA) were performed using selected dependent variables that most likely represent processes occurring within each land use. Analyses of correlation were performed between $NO_3^-$ concentrations and discharge to assess the extent of the hydrological control (climate conditions, recharge, and water volumes) on nutrient loads to the spring. Paired t-tests were calculated to contrast nutrient transfer between the two branches and identify differences in nutrient loads between the CAFO-affected recharge area (NB) and the residentially dominated basin (SB). $\delta^{13}C_{DOC}$, the dependent variable, can help determine recharge from fertilized cornfields (NB) and seasonal patterns of corn growth (Fig. 4). As primary components of residential sewage effluents (Spahr et al., 2010), $PO_4^{3-}$ and $NH_4^+$ are the variables that most likely indicate surface recharge from the residential part of the watershed. Since two tests were made simultaneously (one for each branch), a Bonferroni correction factor of 2 (alpha = 0.05/2 = 0.025) was used. To further assess the influence of land use on groundwater quality, correlation analyses were performed between $NO_3^-$ concentrations and trace metals used for poultry feed (Cu, Pb, Zn).

**III. Results and discussion**

Nitrate is the most labile form of nitrogen and is estimated to be 73 to 98% of Total Inorganic Nitrogen (TIN) being transported during major recharge events (Dorioz and Ferhi, 1994; Lowrance, 1992; Gangbazo et al., 1995). Because the GGC spring's TIN is dominated by nitrate (94%) with the remainder being ammonium (5%) and nitrite (1%), this investigation will

use nitrate concentrations as a proxy to examine spatio-temporal changes in TIN, similar to previous methods used by Kemp and Dodds (2001) and Dodds et al. (1996). Unlike nitrate ($NO_3^-$), ammonium ($NH_4^+$) ions tend to bond to negatively-charged soil particles. Phosphate ($PO_4^{3-}$) ions easily bond to organic matter through cation exchange mechanisms (Hooda et al., 2000) and are usually mobilized with the flux of sediments within hours following major storm events (Schofield et al., 1990; Stoner, 2008). Therefore, an emphasis will be given to temporal variations in nutrient ($NO_3^-$, $NH_4^+$ and $PO_4^{3-}$), DOC and trace metals concentrations occurring during high discharge conditions (Fig. 4).

*III.1. Influence of heterogeneous land use on temporal variations in nutrient and DOC concentration and loads.*

Table 1 lists the nutrients ($NO_3^-$, $NH_4^+$, and $PO_4^{3-}$), DOC, SUVA, trace metals, discharge, and $\delta^{13}C_{DOC}$ data measured values and calculated loads at the GCC Spring (Figures 4 and 5). The analysis of the discharge signal at the GGC spring (Fig. 4) enables us to distinguish between three major recharge phases. Although the majority of nutrient and DOC inputs occurs during peak discharge conditions, nutrient data show no significant correlation with discharge (Fig. 6), suggesting that nutrient export to the GGC aquifer is not solely controlled by the hydrology. There is likely a coupling with other factors such as land-uses and processes occurring within the epikarst (storage and gradual release of stored water from the epikarst; Tagne and Dowling, 2018). Thus, each one of the three recharge phases (Phases 1-3) is further associated to a differential response of the epikarst combined with surface land-use sources. A detailed analysis of nutrients, DOC, trace metal concentrations (Fig. 4) and corresponding loads (Fig. 5) in relation to those three (3) major recharge phases show that Phase 1 most likely corresponds to

the dominant recharge from the inorganically fertilized croplands in the NB, Phase 2 shows evidence of inputs dominated by the manure-fertilized croplands, and Phase 3 likely occurs in response to a diffuse recharge from residential sewage in the Southern portion..

The first responding phase (Phase 1: 05/16-6/20/2015) primarily occurs during base flow levels (discharge range: 63-94 L/s) and is characterized by relatively low nitrate concentrations (average = 39 ± 5 µmol/L), relatively low phosphate (4 ± 2 µmol/L), ammonium (6 ± 5 µmol/L) concentrations and low DOC content (40 ± 30 µmol/L). When combined with relatively low loads (< 5000 µmol/s for nitrate and < 2000 µmol/s for phosphate and ammonium) and isotopically-depleted $\delta^{13}C_{DOC}$ ($-40 < \delta^{13}C_{DOC} < -30$; average = -35‰), the aqueous geochemistry likely reflects diffuse recharge from inorganically fertilized corn fields (lower DOC and $\delta^{13}C_{DOC}$-depleted) in the Northern part of the GGC basin, with limited inputs from poultry-manure fertilizer or sewage that typically exhibit higher DOC and elevated $\delta^{13}C_{DOC}$. These observations are consistent with values of Fluorescent Dissolved Organic Matter (4 < fDOM < 6 RFU) and turbidity (< 50 NTU) varying within the expected range for nonpoint-source inputs from primarily agricultural lands during the similar period (Tagne and Dowling, 2018).

The second phase (Phase 2: 06/27-07/19/2015) corresponds to a period of higher discharge conditions characterized by varying nitrate (10-50 µmol/L), phosphate (2-12 µmol/L) and DOC (40-180 µmol/L) concentrations, peaks in trace metals, an overall enrichment in $\delta^{13}C_{DOC}$ values, and the occurrence of two major storm events on 07/03/2015 and 07/09/2015. During the first storm, the incoming volume of surface recharge caused a large decrease in nitrate, reaching values below background level (< 20 µmol/L). The initial dilution of nitrate concentration during this storm event reflects the influence of high antecedent moisture (relative wetness of soil and epikarst) on the aquifer's response. The following increase to a value of 40 µmol/L is consistent with the GGC system inertia and slow return to base flow conditions following high storm

conditions as previously recorded through discrete sampling by Tagne and Dowling (2018). However, although a dilution effect is not recorded in the nitrate signal during the following storm (07/09/2018), it is evident through instantaneous measurements of specific conductivity (SPC; Tagne and Dowling, 2018) that the water volume remains consistently high from July 03 to July 09, and that the two peaks could be attributed to a single long-term storm event. Moreover, when considering loads (µmol/s; Fig. 5) in lieu of concentrations (µmol/L; Fig. 4); it is apparent that the maximum inputs in nitrate (16900 µmol/s), ammonium (6260 µmol/s), and phosphate (4450 µmol/s) correlate to this extended high discharge period. Combined elevated loads in DOC (70700 µmol/s) and trace metals (Pb, Cu, Ni Cr), and enrichment in $\delta^{13}C_{DOC}$ (from -27 to -20‰) suggest that this high discharge period may be concomitant to a predominant recharge from manure-fertilized cornfields in the Northern recharge basin. Observations of physico-chemistry during that same period (Tagne and Dowling, 2018) reveal elevated peaks in turbidity (350 NTU), in FDOM (16 RFU) and Specific Conductivity (350 µS/cm) that could not be solely resulting from a diffuse recharge from inorganically fertilized areas in the NB, thus confirming the existence of a second end-member mixing source.

The third phase (Phase 3: 07/25-09/05/2015) also has high discharge with the occurrence of a storm peak on 08/02/2015 (max. discharge = 379 L/s), a measured increase in TIN (max = 50 µmol/L) and SUVA (average = 15.2 ± 7.0 L/mg/s; max = 23.12 L/mg/s), and still elevated DOC (average = 60 µmol/L; max = 130 µmol/L). Despite the much more elevated discharge peak in comparison to Phase 2, loads in nitrate, ammonium and phosphate remain within the same ranges as Phase 2. Although there is a clear enrichment in DOC isotopes during the third phase, the sourcing of organic carbon reveal highly labile (high SUVA) and isotopically enriched DOC (high $\delta^{13}C_{DOC}$: max= -5.44‰ on 08/02/2015), likely of a different origin compared to the DOC from Phase 2. Taking into the account the slow epikarst response in the Southern Branch basin

(Tagne and Dowling, 2018), the DOC and SUVA data suggest a prolonged decomposition of DOC in the SB epikarst and reveals the enhanced contribution of the Southern Branch basin (residential sewage systems) during larger storms (average discharge phase 3 = 379 L/s > phase 2 = 239 L/s; Table 1). During low to medium flow, the influence of the SB epikarst is muted, as suggested by the comparison of the highest SUVA peaks in the different phases (Phase 1: 18.85 L/mg/m 6/12/2015; Phase 2: 10.58 L/mg/m on 7/9/2015; Phase 3: 23.12 L/mg/m on 8/2/2015).

*III.1.1. Effect of corn growth on seasonal shift from inorganic to predominantly organic sources*

Seasonal patterns in nutrients, DOC, and trace metal concentrations (Fig. 4 and Fig. 5) show that surface land uses in the GGC watershed respond differently throughout the study period. Following fertilizer (inorganic and manure) application on fields in the spring, the subsequent uptake by growing corn (growth season) and runoff from rainfall, the pools of nitrogen and carbon change throughout the growth season. In Phase 1, the nitrogen load is mainly derived from inorganic fertilizers that are progressively depleted in the soils. Spring recharge from inorganically fertilized croplands is characterized by moderate $NO_3^-$ and $PO_4^{3-}$ levels and their corresponding loads. The DOC content is very low (very limited inputs from poultry manure or sewage) and $\delta^{13}C_{DOC}$ is relatively depleted ($\delta^{13}C_{DOC}$ varies from -40 to -30 ‰), thus reflecting the signature of inorganic fertilizers (Cravotta, 2002). In Phase 2, the nitrogen source is dominated by the slow mineralization (conversion of organic nitrogen into plant-available inorganic nitrogen) of organic N from poultry-manure fertilizers, as evident by the nitrogen loads. The DOC content increases to a maximum value of 3.1 mg/L along with an enrichment in $\delta^{13}C_{DOC}$ (~ -20 to -18 ‰), both of which are characteristic for poultry manures. The trace metals, micronutrients used in poultry feed (Barker and Zublena, 1995; Hancock et al., 2001), suggest that the inputs originate from CAFOs (Phase 2, Fig. 4 and Fig. 5). During Phase 3, the

combination of the peaks in discharge, SUVA (labile carbon), and overall enriched $\delta^{13}C_{DOC}$ (Fig. 4 and Fig. 5) indicate the domination of diffuse recharge from residential sewage wastes on GCC Spring's aqueous chemistry and corresponds to the row crop harvest in late July and early August.

Overall, the seasonal shift from inorganic to predominantly organic sources of nitrogen suggests that the pool of inorganic N added to the soil in the form of inorganic fertilizer prior to corn growth is readily depleted from its assimilation by the row crop (growing corn) and transported through runoff during early summer rainfall events. Moreover, the progressive enrichment in organic carbon content later throughout the summer reflects the combination of organic sources from manure (applied fertilizer and/or CAFO-derived waste storage) in the NB and the labile organic carbon sources from sewage in the SB.

*III.2. Differentiating among non-point sources of groundwater contamination.*

Although it is possible to distinguish the dominant recharge basins (NB and SB) of the GGC watershed based on nutrients and trace metal trends at the Spring (Fig. 4), it remains difficult to determine the contributions of each land use present in the watershed (inorganically fertilized croplands, CAFO-derived manure fertilizers, and sewage) using graphical means only. Statistical operations (correlations and ANOVA analysis) and end-member mixing equations using land-use dependent variables are used to provide supplementary methods to assess nutrients inputs from each land use.

*III.2.1. End-member mixing of DOC*

Due to the heterogeneous character of the land-use in the GGC recharge basin, it is essential to differentiate between contributions from non-point sources (NPS; natural sources, inorganic fertilizers applied over croplands in the NB, and CAFO-derived poultry manure applied as organic fertilizers to croplands in the NB) and point sources (mainly residential sewage in the SB). However, natural sources (atmospheric depositions, rainfall, snow melting, and deposition from native fauna in forested ecosystems) can be ignored in any loading equations because they are negligible compared to the contributions of land-uses (e.g., intensive farming practices), denitrification (release of volatile ammonia from livestock storage and fertilized lands) and fossil fuel combustion (Hallberg, 1989; West and Feagley, 1995). As there is no direct evidence that the CAFO-waste storage facilities leaked or spilled over during the sampling period, this term may also be considered negligible. The loads to the spring can be solely expressed as the sum of the loads from fertilizers (inorganic fertilizer; NPS-NB-1 and poultry-fertilizer; NPS-NB-2) and diffuse recharge from sewage (PS-SB).

Recorded values of $\delta^{13}C_{DOC}$ in the GCC Spring suggest a mixture of various surface land-use sources in the primarily agricultural Northern recharge basin because the data reflect the composition of inorganic fertilizers (average $\delta^{13}C_{DOC} \leq$ -30‰; Cravotta, 2002) and CAFO-derived poultry manure fertilizers (average $\delta^{13}C_{DOC}$ value of -18‰; Cravotta, 2002) applied to croplands. $\delta^{13}C_{DOC}$ values show that the changes in DOC contributions are primarily driven by recharge from inorganically and manure-fertilized lands in the Northern part of the GGC basin (Phases 1 and 2) and from sewage in the Southern part (Phase 3). Surface runoff over fertilized croplands creates an enrichment trend in DOC isotopic ratios from highly depleted sources in the Spring (Phase 1, diffuse recharge from inorganically fertilized croplands and soil litter

decomposition on forested covers) to less depleted sources (Phases 2 and 3; diffuse recharge from poultry-manure fertilizer and sewage) toward the end of the summer.

Moreover, because the majority of the dissolved organic carbon isotopic ratios data points vary across a wide range in composition (< 30‰ for inorganic fertilizers; ~ -20 to -18‰ for poultry manure (fertilizer or storage), and > -10 to -5‰ for sewage), $\delta^{13}C_{DOC}$ end-member mixing lines can be used to predict the contribution of NPS (inorganic fertilizers and poultry manure) in the Northern recharge basin (Table 2). This assumption is expressed in equation 4, where x, y, and (1 – x – y) are the respective proportions (%) of NPS and PS to the GCC Spring.

$$\delta^{13}C\text{-}DOC_{spring} = x\ \delta^{13}C\text{-}DOC_{(NPS\text{-}NB1)} + y\ \delta^{13}C\text{-}DOC_{(NPS\text{-}NB2)} + (1 - x - y)\ \delta^{13}C\text{-}DOC_{(PS\text{-}SB)} \quad \text{Eq. 4}$$

The previous equation can be resolved by replacing the constants ($\delta^{13}C_{(NPS\text{-}NB\text{-}1)}$ and $\delta^{13}C_{(NPS\text{-}NB\text{-}2)}$) with known isotopic ratios of applied fertilizers (inorganic and poultry-manure, respectively). Average values of -40‰ for inorganic fertilizers ($\delta^{13}C_{(NPS\text{-}NB\text{-}1)}$) and -18‰ for poultry wastes ($\delta^{13}C_{(NPS\text{-}NB\text{-}2)}$, assuming a predominant corn diet) were considered based on the range proposed by Cravotta (2002).

Table 2 represents the estimated contributions of the different contributions to DOC loads at the GGC using the mixing lines established in equation 4. As previously shown in Fig. 4, the SUVA signal from the SB recharge is muted during Phases 1 and 2, thus suggesting that the major land-use sources are derived from the NB recharge (inorganic fertilizers and poultry manure; Table 2). Therefore, for Phase 1 and Phase 2, equation 4 can be simplified:

$$\delta^{13}C\text{-}DOC_{spring} = x\ \delta^{13}C\text{-}DOC_{(NPS\text{-}NB1)} + (1 - x)\ \delta^{13}C\text{-}DOC_{(NPS\text{-}NB2)} \quad \text{Eq. 5}$$

Unlike Phases 1 and 2, there is an increased complexity of mixing proportions during Phase 3, as the overall increased discharge amplifies the recharge from the SB (Fig. 4). Moreover, the third phase clearly shows a dominance of inputs of labile organic carbon from the SB recharge

area (major load in SUVA during occurs during Phase 3; Fig. 5). A plausible mixing scenario during this phase (Table 2) assumes that in spite of a progressive depletion in NPS (inorganic and poultry-manure fertilizers) in the NB during the corn growth season, there is still a DOC reserve from NB sources by end of the summer, hence, equation 4 remains the same. However, the absence of peaks in trace metals and the elevated SUVA during the third phase (Fig. 4) rules out the possibility that the DOC is replenished by manure sources during that period, thus the DOC may originate primarily from a mixture of inorganic fertilizer (likely a small pool remaining) and sewage effluents with no contribution from manure fertilizers. Consequently, equation 4 is rearranged into equation 6:

$$\delta^{13}\text{C-DOC}_{spring} = x\ \delta^{13}\text{C-DOC}_{(NPS\text{-}NB1)} + (1 - x)\ \delta^{13}\text{C-DOC}_{(PS\text{-}SB)} \quad \text{Eq. 6}$$

The contributions of the different DOC sources evolve throughout the summer from higher percentages of inorganic fertilizers during late spring (fertilizer application on croplands) to a higher contribution of poultry-manure-fertilizers by the end of July to a greater proportion of sewage toward the beginning of September (Table 2). As the inorganic reservoir (inorganic fertilizers) is depleted in the soil, the organic content increases (poultry-manure fertilizer in Phase 2 and sewage in Phase 3) and becomes more labile (increased SUVA; Fig. 5) and isotopically enriched (high $\delta^{13}$C-DOC; Fig. 5) throughout the summer.

*III.2.2. Statistical analysis*

Data (Table 2) suggest that the contribution of inorganic fertilizer at the GGC spring is maximal during low discharge conditions (Phase 1, Fig. 4) while poultry manure and sewage overall exert a dominant control on nutrient response in high flow conditions (Phases 2 and 3, Fig. 4). However, it is still unknown as to which source accounts for the highest variability in TIN loads

at the Spring. Analysis of correlation and analysis of variance performed using dependent variables characteristics of each land-use source further allow to answer this concern.

*III.2.2.1. Choice of dependent variables*

Temporal variations in nutrient (mainly $NO_3^-$ and $NH_4^+$) loads (Fig. 5) suggest that maximum loads originate both from manure-applied fertilizer (Phase 2) and sewage (Phase 3), thus making it difficult to identify which one of the two exerts the highest control on TIN recharge during high discharge periods. However, distinguishing characteristics of poultry manure (Fig. 5, Phase 2) are high DOC and trace metal loads. In particular, the trace metals (Cu, Cr, Pb, and Ni) are used as additive micronutrients to poultry feeding in CAFOs (Barker and Zublena, 1995; Hancock et al., 2001). Two common groundwater contamination pathways for CAFO-derived wastes are from the diffuse runoff from manure-fertilized croplands (indirect recharge) or leakage/overflow from CAFO waste facilities (direct recharge). In this investigation, no leaking or overflow was observed at the poultry-CAFO waste storage facilities at the Grayson-Gunner site during Phases 2 and 3, and elevated trace metals at the GGC Spring were only observed in Phase 2 and not Phase 3, indicating the CAFO source is most likely the application of the poultry-waste as a crop fertilizer and mobilized during high flow conditions. Whether or not trace metal loads occur through diffuse or direct recharge, it is clear that they are associated with inputs from CAFO (Fig. 4 and Fig. 5, Phase 2) and are therefore used as dependent variables to characterize CAFO sources (Table 3).

Among the trace metals analyzed (Cu, Cr-III, Pb, Ni), copper is the most representative of poultry manure (CAFO), as it shows the highest ($R^2 = 0.52$) and most significant ($F = 0.05$) correlation with discharge (Table 4). In addition, copper concentrations are the most reflective of an anthropogenic origin as they occur constantly above the EPA chronic exposure level of 0.4

µmol/L (0.003 mg/L), with a maximum value of 0.1 µmol/L on the 7/3/2015 (Table 1). Unlike copper, however, Ni and Cr-III concentrations exhibit poor correlations with discharge ($R^2$ = 0.284 and $R^2$ = 0.298 respectively; Table 4) and occur primarily below chronic exposure levels of 0.14 µmol/L (0.074 mg/L) and 0.9 µmol/L (0.052 mg/L) respectively (Table 1). Despite showing a few values above the EPA chronic exposure level of 0.012 µmol/L (0.0025 mg/L; Table 1), lead (Pb) does not exhibit a significant correlation with discharge ($R^2$ = 0.08; Table 4) and therefore cannot be used as a predictor of CAFO inputs (Table 3).

While the majority of loads in DOC and trace metals derive from CAFO (Phase 2; Fig. 5), maximum inputs of labile DOC (high SUVA) are likely from sewage (Phase 3; Fig. 5), therefore SUVA is used as a dependent variable to trace inputs from sewage systems (Table 3). Overall, the interpretation of loads provides valuable information regarding specific dependent variables that are associated to each land-use source (Table 3) and can be further used in statistical analyses to assess dependency among the different land-use sources.

*III.2.2.2. Land-use controls on TIN variability*

For the samples at the GGC Spring, tests of correlations and ANOVA were performed between $NO_3^-$ concentrations (input variable and proxy for TIN) and four land-use and one hydrology dependent variables. The land-use dependent variables are $\delta^{13}C_{DOC}$ (indicator of diffuse recharge from inorganically and manure-fertilized croplands in the NB and sewage in the SB), DOC and Cu concentrations (primary indicators of recharge from poultry CAFO) and SUVA (primary indicator of recharge from sewage), while spring discharge (Q) represents the hydrology output variable. The significant results and correlation matrix between input variables are displayed in Tables 5 and Table 6 respectively. Analysis of variance performed between $NO_3^-$ (independent variable), Q, $\delta^{13}C_{DOC}$, Cu, DOC and SUVA (Table 5) reveal that among the

dependent variables (land-use and hydrology), the land-use variables ($\delta^{13}C_{DOC}$, Cu, DOC and SUVA) show better and generally more significant correlations to TIN variability when compared to the hydrological factor ($R^2$ = 0.130; F-significance ANOVA = 0.687), thus suggesting that land-use is more influential. Moreover, among all the land-use variables (Table 6), runoff from poultry-manure fertilizer shows the most significant effect ($R^2$ = 0.885; F-significance = $1.28 \times 10^{-4}$) on TIN variability at the GGC spring, while sewage has a lesser significance ($R^2$ = 0.374; F-significance = 0.231) on TIN variability, thus suggesting that TIN inputs from poultry manure (NPS) override those from sewage effluents (PS) at the scale of the GGC basin.

***IV. Conclusions and recommendations: Implications for land use management and nutrient mitigation***

Previous studies conducted in small conduit-flow-dominated karst aquifers have concluded that hydrology is the most important control in contaminant recharge (Kastrinos and White, 1986; Thomas et al., 1992; Currens, 1996; Boyer and Pasquarell, 1995; Taraba et al., 1997). However, this investigation shows that management strategies targeting hydrological variables, such as discharge, would not be effective because the land-use variables are statistically more important to the aqueous geochemistry of this small watershed. Additionally, any hydrologic controls would be difficult to implement in small epigenic karst basins due to 1) the difficulty of minimizing the high volume of water that transits through the cave during high flow conditions (~ $6x10^6$ Liters of groundwater per major storm, Tagne and Dowling, 2018), and 2) the relatively short residence time of groundwater in subsurface conduits (< 7 days; Tagne and Dowling, 2018) that may prevent any natural retention process (denitrification or water-sediments exchange) from occurring. Overall, it would be challenging to control the hydrology in conduit-flow-

dominated karst aquifers due to the complexity of recharge and infiltration mechanisms and the quasi-occurrence of flow in the subsurface (absence of surface flow). Strategies aiming to maximize nitrate retention through flow control (channel control or channel diversion) would not be useful to implement in such environments. Instead, in situations where the observed nutrient loads are primarily driven by land-use, the objectives for future mitigation plans in the GGC and potentially other Cumberland Plateau watersheds will need to be directed towards land-use practices.

Results for Phases 1 and 2 agree with TIN fluxes estimated in larger karst areas in the Upper MRB such as the Southern Illinois basin (37.7 $km^2$; Panno and Kelly, 2004; Stueber and Criss, 2005), in that non-point sources (fertilizers and soils) account for a higher proportion (> 70% in Southern Illinois and 52-77% in GCC) of terrestrial TIN inputs to groundwater in comparison to point sources (animal waste storage and septic effluents). The recharge patterns in the Southern Illinois basin are primarily diffuse—leaching and runoff from agricultural lands, which excludes the potential for higher loads from direct conduit infiltration from surface point sources (CAFOs and septic effluents) to the aquifer, and conversely enhances the possibilities for slow in-situ $NO_3$ retention in the epikarst. However, according to Phase 3, the GCC watershed and the Southern Illinois basin differ in that the point source (sewage) is the dominant source of TIN (>70%). In light of these results, it is crucial that future plans for reducing TIN concentrations below present-day background levels (1 - 2 mg $NO_3^-$/L) in conduit-dominated karstic basins under mixed agricultural land-use such as the GGC should specifically target PS inputs (e.g., CAFO and sewage) in addition to NPS (runoff from inorganically and organically fertilized croplands).

The challenges associated with implementing specific nutrient mitigation plans targeting CAFO-regions are multiple. Although potential groundwater contamination routes in CAFO-

affected land uses may occur through direct recharge from below animal waste storage sites, it remains difficult to show evidence of direct subsurface connectivity, even through dye tracing techniques (Brahana et al., 2014). In this study, it is probable that the poultry-CAFO waste signature observed in the aquifer resulted from the diffuse recharge from agricultural runoff and not direct recharge from storage facilities. In Phase 2, the dominant source of contaminants is the runoff from the poultry-manure fertilizers that were applied to corn fields towards the end of the spring. In this watershed, it would more beneficial to control indirect contamination paths (e.g., through diffuse runoff from manure-fertilized croplands) by modifying the timing and the rate of manure application on croplands (Randall and Mulla, 2001). A slight advance in the timing of the poultry-manure application to the fields (from late spring to early spring) could provide additional time for row crop assimilation and consequently help reduce the loads from CAFO sources during summer high discharge periods.

Overall, evaluating hydrologic and land-use controls on nutrients at the scale of small watersheds (such as the mature carbonate settings of the Cumberland Plateau) is critical to minimizing stream and groundwater contamination, developing site-specific Nutrient Management Plans to reduce nutrient exports to larger watersheds (e.g. Upper Cumberland, River, Ohio River Basin), and effectively managing the GOM Hypoxia Zone.

**Acknowledgements**

We are thankful to Harry Goepel for providing housing in Kentucky during sampling. We acknowledge the Greater Cincinnati Grotto of the National Speleological Society for the use of surveys data from the Grayson-Gunnar Cave. We expand our gratitude to Gary and Synda Heikkinen (and the wonderful dogs) for granting us access to the Grayson-Gunnar Cave property. Special appreciation goes to Bill Walden, for the valuable information and emotional

support he provided during our stay in Monticello, Kentucky. We acknowledge Dr Michael E. Perdue for graciously allowing us the use of the instrumentation at the Organic Chemistry Lab (Ball State University) and Shamus Driver for his tremendous help with the analyses. We thank the Delaware County Bureau of Water Quality for their help with the analyses of trace metals.

**Funding information**

We want to thank the following organizations for granting funding for this project: the National Speleological Society through the 2015 Ralph Stone Research Grant, the Cave Research Foundation through the 2015 Phillip M. Smith Graduate Research Grant, and the Geological Society of America through the 2015 Student Research Grant.

**References**

Barker, J.C., Zublena, J.P., 1995. Livestock manure nutrient assessment in North Carolina. Final Report. Raleigh, NC: North Carolina Agricultural Extension Service, North Carolina State University.

Belkhiri, L., Boudoukha, A., Mouni, L., 2011. A multivariate statistical analysis of groundwater chemistry data. Int. J. Environ. Res. 5, 537–544.

Belkhiri, L., Narany, T.S., 2015. Using multivariate statistical analysis, geostatistical techniques and structural equation modeling to identify spatial variability of groundwater quality. Water Resources Management 29(6), 2073-2089.

Boyacioglu, H., Boyacioglu, H., 2010. Detection of seasonal variations in surface water quality using discriminant analysis. Environ. Monit. Assess. 162, 15–20.

Boyer, D.G., Pasquarell, G.C., 1995. Nitrate concentrations in karst springs in an extensively grazed area. JAWRA Journal of the American Water Resources Association 31(4), 729-736.

Boyer, J.N., Fourqurean, J.W., Jones, R.D., 1997. Spatial characterization of water quality in Florida Bay and Whitewater Bay by multivariate analyses: zones of similar influence. Estuaries 20(4), 743–758.

Brahana V., Nix J., Bitting C., Bitting C., Quick R., Murdoch J., Roland V., West A., Sarah Robertson S., Scarsdale G., North V., 2014. CAFOs on Karst—Meaningful Data Collection to Adequately Define Environmental Risk, with a Specific Application from the Southern Ozarks of Northern Arkansas. In U.S. Geological Survey Karst Interest Group Proceedings, Carlsbad, New Mexico, April 29–May 2, 2014.

Burkholder, J., Libra, B., Weyer, P., Heathcote, S., Kolpin, D., Thome, P.S., Wichman, M., 2007. Impacts of waste from concentrated animal feeding operations on water quality. Environmental health perspectives, 308-312.

Burns, D.A. and Kendall, C., 2002. Analysis of δ15N and δ18O to differentiate NO3− sources in runoff at two watersheds in the Catskill Mountains of New York. Water Resources Research 38(5).

Cravotta, C.A., 2002. Use of stable isotopes of carbon, nitrogen, and sulfur to identify sources of nitrogen in surface waters in the Lower Susquehanna River Basin, Pennsylvania. Vol. 2497. USGPO.

Currens, J.C., 1996. Mass flux of agricultural nonpoint-source pollutants in a conduit-flow-dominated karst aquifer, Logan County, Kentucky. In International Journal of Rock Mechanics and Mining Sciences and Geomechanics Abstracts 2(33), 56A-57A.

Dale, V.H., Lannom, K.O., Tharp, M.L., Hodges, D.G., Fogel, J., 2009. Effects of climate change, land-use change, and invasive species on the ecology of the Cumberland forests. Canadian Journal of Forest Research 39(2), 467-480.

Davis, C.A., Ward, A.S., Burgin, A.J., Loecke, T.D., Riveros-Iregui, D.A., Schnoebelen, D.J., Just, C.L., Thomas, S.A., Weber, L.J., St Clair, M.A., 2014. Antecedent moisture controls on stream nitrate flux in an agricultural watershed. Journal of Environmental Quality 43(4), 1494-1503.

Davis, D.M., Gowda, P.H., Mulla, D.J., Randall, G.W., 2000. Modeling nitrate nitrogen leaching in response to nitrogen fertilizer rate and tile drain depth or spacing for southern Minnesota, USA. Journal of Environmental Quality 29(5), 1568-1581.

Dodds, W.K., Blair, J.M., Henebry, G.M., Koelliker, J.K., Ramundo, R., Tate, C.M.,1996. Nitrogen transport from tallgrass prairie watersheds. J. Environ. Qual. 25, 973–981,

Donner, S.D., Kucharik, C.J., 2008. Corn-based ethanol production compromises goal of reducing nitrogen export by the Mississippi River. Proceedings of the National Academy of Sciences 105(11), 4513-4518.

Donner, S.D., Scavia, D., 2007. How climate controls the flux of nitrogen by the Mississippi River and the development of hypoxia in the Gulf of Mexico. Limnology and Oceanography 52(2), 856-861.

Donner, S.D., 2003. The impact of cropland cover on river nutrient levels in the Mississippi River Basin. Global Ecology and Biogeography 12(4), 341-355.

Donner, S.D., Coe, M.T., Lenters, J.D., Twine, T.E., Foley, J.A., 2002. Modeling the impact of hydrological changes on nitrate transport in the Mississippi River Basin from 1955 to 1994. Global biogeochemical cycles 16(3).

Donner, S.D., Kucharik, C.J., Foley, J.A., 2004. Impact of changing land use practices on nitrate export by the Mississippi River. Global Biogeochemical Cycles 18(1).

Dorioz, J.M., Ferhi, A., 1994. Non-point pollution and management of agricultural areas: Phosphorus and nitrogen transfer in an agricultural watershed. Water Research 28(2), 95-410.

Ford, D., Williams, P., 2007. Introduction to Karst. Karst Hydrogeology and Geomorphology, 1-8.

Gandhi, H., Wiegner, T.N., Ostrom, P.H., Kaplan, L.A., Ostrom, N.E. (2004) Isotopic (13C) analysis of dissolved organic carbon in stream water using an elemental analyzer coupled to a stable isotope ratio mass spectrometer. Rapid Communications in Mass Spectrometry,18(8), 903-906.

Gangbazo, G., Pesant, A.R., Barnett, G.M., Charuest, J.P., Cluis, D., 1995. Water contamination by ammonium nitrogen following the spreading of hog manure and mineral fertilizers. Journal of Environmental Quality 24(3), 420-425.

Garizi Z.A., Sheikh V., Sadoddin A., 2011. Assessment of seasonal variations of chemical characteristics in surface water using multivariate statistical methods. Int. J. Environ. Sci. Technol. 8, 581–592

Hallberg, G.R., 1989. Nitrate in ground water in the United States. In Developments in Agricultural and Managed Forest Ecology 21, 35-74.

Hancock, T.C., Denver, J.M., Riedel, G.F., Miller, C.V., 2001. Reconnaissance for arsenic in a poultry dominated Chesapeake Bay watershed – Examination of source, transport, and fate (abstract), U.S. EPA Workshop Managing Arsenic Risks to the Environment: Characterization of Waste, Chemistry, and Treatment and Disposal, May 1-3, 2001, Denver, Colorado.

Hansen, A.M., Kraus, T.E., Pellerin, B.A., Fleck, J.A., Downing, B.D. and Bergamaschi, B.A., 2016. Optical properties of dissolved organic matter (DOM): Effects of biological and photolytic degradation. Limnology and Oceanography 61(3), 1015-1032.

Hodne, C.J., 2005. Concentrating on Clean Water: The Challenge of Concentrated Animal Feeding Operations. Iowa Policy Project Report. www.iowapolicyproject.org

Hood, E., M. W. Williams, D. M. Mcknight, 2005. Sources of dissolved organic matter (DOM) in a Rocky Mountain stream using chemical fractionation and stable isotopes. Biogeochemistry 74, 231–255. https://doi:10.1007/ s10533-004-4322-5.

Hooda, P.S., Edwards, A.C., Anderson, H.A., Miller, A., 2000. A review of water quality concerns in livestock farming areas. Science of the Total Environment 250(1-3), 143-167.

Hooda, P.S., Moynagh, M., Svoboda, I.F., Anderson, H.A., 1998. A comparative study of nitrate leaching from intensively managed monoculture grass and grass–clover pastures. The Journal of Agricultural Science 131(3), 267-275.

Howarth, R., Swaney, D., Billen, G., Garnier, J., Hong, B., Humborg, C., Johnes, P., Mörth, C.M., Marino, R., 2012. Nitrogen fluxes from the landscape are controlled by net anthropogenic nitrogen inputs and by climate. Frontiers in Ecology and the Environment 10(1), 37-43.

Hutchins S.R., White M.V., Mravik S.C., 2012, Case Studies on the Impact of Concentrated Animal Feeding Operations (CAFOs) on Ground Water Quality, In U.S. EPA 600/R-12/052, September 2012, Office of Research and Development, National Risk Management Research Laboratory, Ground Water and Ecosystems Restoration Division, Ada, OK.

Jaynes, D.B., Colvin, T.S., Karlen, D.L., Cambardella, C.A., Meek, D.W., 2001. Nitrate loss in subsurface drainage as affected by nitrogen fertilizer rate. Journal of Environmental Quality 30(4), 1305-1314.

Kastrinos, J.R., White, W.B., 1986. Seasonal, Hydrogeologic, and Land-use Controls on the Nitrate Contamination of Carbonate Ground Waters. In Proc. Environmental Problems in Karst Terranes and Their Solutions Conference. National Water Well Association, Dublin OH, 88-112.

Kemp, M.J., Dodds, W.K., 2001. Spatial and temporal patterns of nitrogen concentrations in pristine and agriculturally-influenced prairie streams. Biogeochemistry 53(2), 125-141.

Kladivko, E.J., Kaspar, T.C., Jaynes, D.B., Malone, R.W., Singer, J., Morin, X.K., Searchinger, T., 2014. Cover crops in the upper midwestern United States: Potential adoption and reduction of nitrate leaching in the Mississippi River Basin. Journal of Soil and Water Conservation 69(4), 279-291.

Loken, L.C., Crawford, J.T., Dornblaser, M.M., Striegl, R.G., Houser, J.N., Turner, P.A. and Stanley, E.H., 2018. Limited nitrate retention capacity in the Upper Mississippi River. Environmental Research Letters 13(7), 074030.

Lowrance, R., 1992. Nitrogen outputs from a field-size agricultural watershed. Journal of Environmental Quality, 21(4), 602-607.

Mahler, B.J., Garner, B.D., Musgrove, M., Guilfoyle, A., Rao, M.V., 2006. Recent (2003-05) water quality of Barton Springs, Austin, Texas, with emphasis on factors affecting variability. USGS Scientific Investigations Report 2006-5299. Reston, Virginia: USGS.

Mallin, M.A., Burkholder, J.M., McIver, M.R., Shank, G.C., Glasgow, H.B., Touchette, B.W., Springer, J., 1997. Comparative effects of poultry and swine waste lagoon spills on the quality of receiving streamwaters. Journal of Environmental Quality 26(6), 1622-1631.

Medina-Gomez, I. and Herrera-Silveira, J.A., 2003. Spatial characterization of water quality in a karstic coastal lagoon without anthropogenic disturbance: a multivariate approach. Estuarine, Coastal and Shelf Science 58(3), 455-465.

National Oceanic and Atmospheric Administration, 2018. Average sized dead zone forecast for Gulf of Mexico: NOAA's annual prediction based on USGS data. http://www.noaa.gov. (accessed on 8/1/2018).

Olszowka, D.M., Heath, J.P., Tennant, P.A., 1994. Evaluation of nutrient loads and sources in the Ohio River Basin. Ohio River Valley Water Sanitation Commission (ORSANCO).

Palmer, A.N., 1991. Origin and morphology of limestone caves. Geological Society of America Bulletin 103(1), 1-21.

Panagopoulos, Y., Gassman, P.W., Arritt, R.W., Herzmann, D.E., Campbell, T.D., Jha, M.K., Kling, C.L., Srinivasan, R., White, M., Arnold, J.G., 2014. Surface water quality and cropping systems sustainability under a changing climate in the Upper Mississippi River Basin. Journal of Soil and Water Conservation 69(6), 483-494.

Panno, S.V., Hackley, K.C., Hwang, H.H. and Kelly, W.R., 2001. Determination of the sources of nitrate contamination in karst springs using isotopic and chemical indicators. Chemical Geology 179(1-4), 113-128.

Panno, S.V. and Kelly, W.R., 2004. Nitrate and herbicide loading in two groundwater basins of Illinois' sinkhole plain. Journal of Hydrology 290(3-4), 229-242.

Potter, B.B. and Wimsatt, J.C., 2005. Measurement of total organic carbon, dissolved organic carbon and specific UV absorbance at 254 nm in source water and drinking water: US Washington. DC: Environmental Protection Agency.

Rabalais, N.N., Turner, R.E., Wiseman Jr, W.J., 2002. Gulf of Mexico hypoxia, aka “The dead zone”. Annual Review of ecology and Systematics 33(1), 235-263.

Randall, G.W., Mulla, D.J., 2001. Nitrate nitrogen in surface waters as influenced by climatic conditions and agricultural practices. Journal of Environmental Quality 30(2), 337-344.

Rantz S.E., 1982. Indirect Determination of Peak Discharge. In: Measurement and computation of streamflow, Volume 1, Measurement of stage and discharge. United States Geological Survey Water Supply Paper 2175. p 284

Schofield, K., Seager, J., Merrlman, R.P., 1990. The impact of intensive dairy farming activities on river quality: the Eastern Cleddau catchment study. Water and Environment Journal 4(2), 176-186.

Secchi, S., Gassman, P.W., Jha, M., Kurkalova, L., Kling, C.L., 2011. Potential water quality changes due to corn expansion in the Upper Mississippi River Basin. Ecological Applications 21(4), 1068-1084.

Simpson, L.C., Florea, L.J., 2009. The Cumberland Plateau of Eastern Kentucky. Caves and Karst of America, 2009, p 70.

Sinha, E., Michalak, A.M., 2016. Precipitation dominates interannual variability of riverine nitrogen loading across the continental United States. Environmental Science & Technology 50(23), 12874-12884.

Spahr, N.E., Dubrovsky, N.M., Gronberg, J.M., Franke, O.L., Wolock, D.M., 2010. Nitrate loads and concentrations in surface-water base flow and shallow groundwater for selected basins in the United States, water years 1990-2006 (No. 2010-5098). US Geological Survey.

Stepanauskas, R., Moran, M.A., Bergamaschi, B.A., Hollibaugh, J.T., 2005. Sources, bioavailability, and photoreactivity of dissolved organic carbon in the Sacramento-San Joaquin River Delta. Biogeochemistry 74, 131–149. https://doi: 10.1007/s10533-004-3361-2.

Stoner, R., 2008. Phosphorus Dynamics in the Columbia Hollow Catchment in Northwest Arkansas (Thesis). University of Arkansas

Stueber, A.M., Criss, R.E., 2005. Origin and transport of dissolved chemicals in a karst watershed, southwestern Illinois. JAWRA Journal of the American Water Resources Association 41(2), 267-290.

Tagne, G.V., Dowling, C.B., 2018. Inferring groundwater flow and recharge from time series analysis of storm responses in a karst aquifer of southeastern Kentucky (USA). Hydrogeology Journal. https://doi.org/10.1007/s10040-018-1837-

Taraba, J.L., Dinger, J.S., Sendlein, L.V.A, Felton, G.K., 1997, October. Land use impacts on water quality in small karst agricultural watersheds. In Karst-Water Environment Symposium, p 127.

Thomas, G.W., Haszler, G.R., Crutchfield, J.D., 1992. Nitrate-nitrogen and phosphate-phosphorus in seven Kentucky streams draining small agricultural watersheds: Eighteen years later. Journal of Environmental Quality 21(1), 147-150.

Turner, R.E., Rabalais, N.N., 1994. Coastal eutrophication near the Mississippi river delta. Nature 368(6472), p 619.

Turner, R.E., Rabalais, N.N., Justic, D., 2006. Predicting summer hypoxia in the northern Gulf of Mexico: Riverine N, P, and Si loading. Marine pollution bulletin 52(2), 139-148.

United States Geological Survey, 1995. Contaminants in the Mississippi River, 1987-92 (Vol. 1133). Meade, R.H. ed. US Government Printing Office. Reston, Virginia.

United States Geological Survey, 2018. Nutrient Loading for the Mississippi River and Subbasins. https://nrtwq.usgs.gov/mississippi_loads/#/ (accessed on 8/1/2018).

United States Geological Survey, 2018. Water-quality loading to the Gulf of Mexico from October 2017 to May 2018 (Preliminary). https://nrtwq.usgs.gov/mississippi_loads/#/GULF_PRELIM (accessed on 8/1/2018).

Vesper, D.J., White, W.B., 2003. Metal transport to karst springs during storm flow: an example from Fort Campbell, Kentucky/Tennessee, USA. Journal of Hydrology 276, 20–36.

Victor L.R., Wright T., Brahana J.V., Hays, P.D., 2014. An Initial Investigation of Hydrogeology and Water Quality of Big Creek in the Buffalo River Watershed near a Major Concentrated

Animal Feeding Operation. In,. U.S. Geological Survey Karst Interest Group Proceedings, Carlsbad, New Mexico, April 29–May 2, 2014.

West, L.M., Feagley, S.E., 1995. The chemical composition of atmospheric deposition collected from six Louisiana sites from 1983 to 1992. Atmospheric Environment 29(11), 1211-1217.

White, W.B., 1988. Geomorphology and Hydrology of Karst Terrains. New York: Oxford University Press, 464 p.

White, M.J., Santhi, C., Kannan, N., Arnold, J.G., Harmel, D., Norfleet, L., Allen, P., DiLuzio, M., Wang, X., Atwood, J., Haney, E., 2014. Nutrient delivery from the Mississippi River to the Gulf of Mexico and effects of cropland conservation. Journal of Soil and Water Conservation 69(1), 26-40.

**Figures**

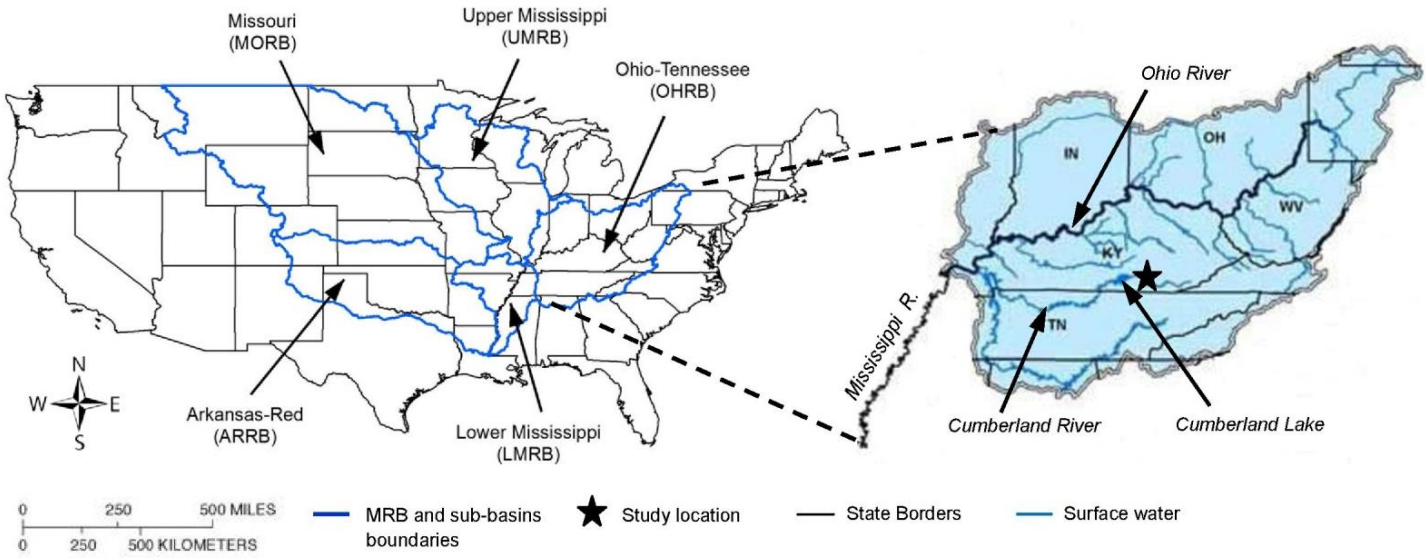


Figure 1: Mississippi River Basin Boundaries and location of the study area (Grayson-Gunnar Cave watershed, Cumberland Plateau, Southeastern Kentucky) within the Ohio River Basin

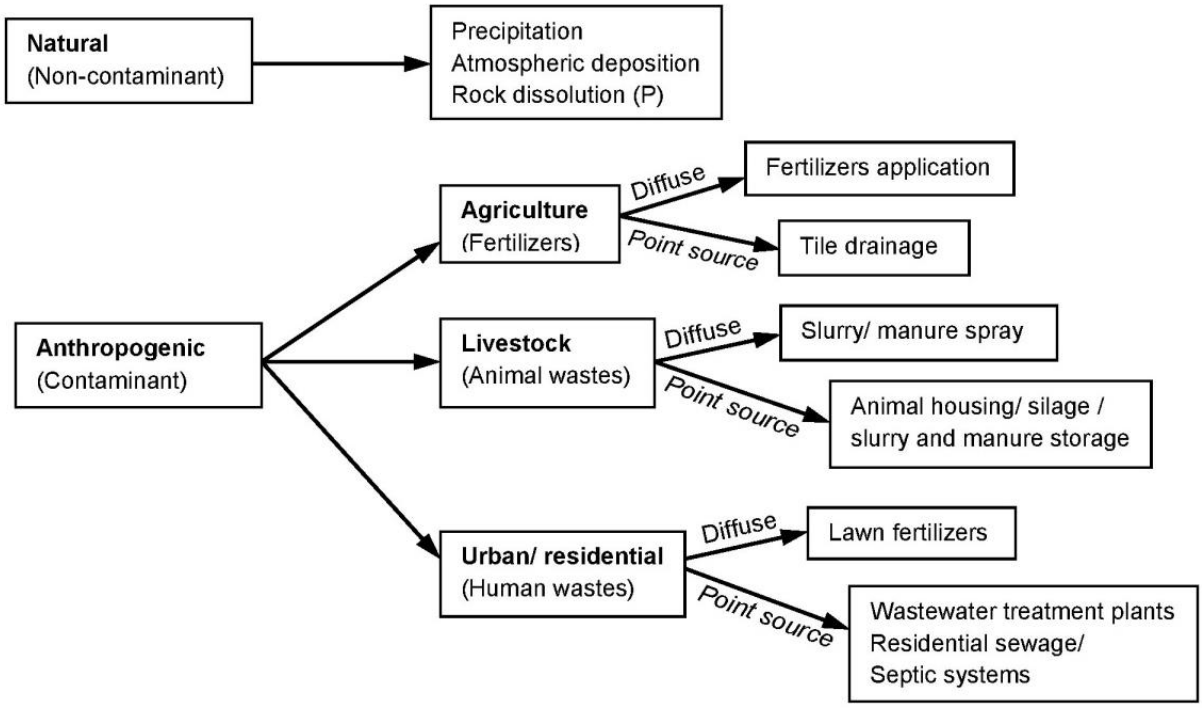


Figure 2: Sources of nutrients in natural waters differentiated by land-use and contamination pathways (diffuse and point sources)

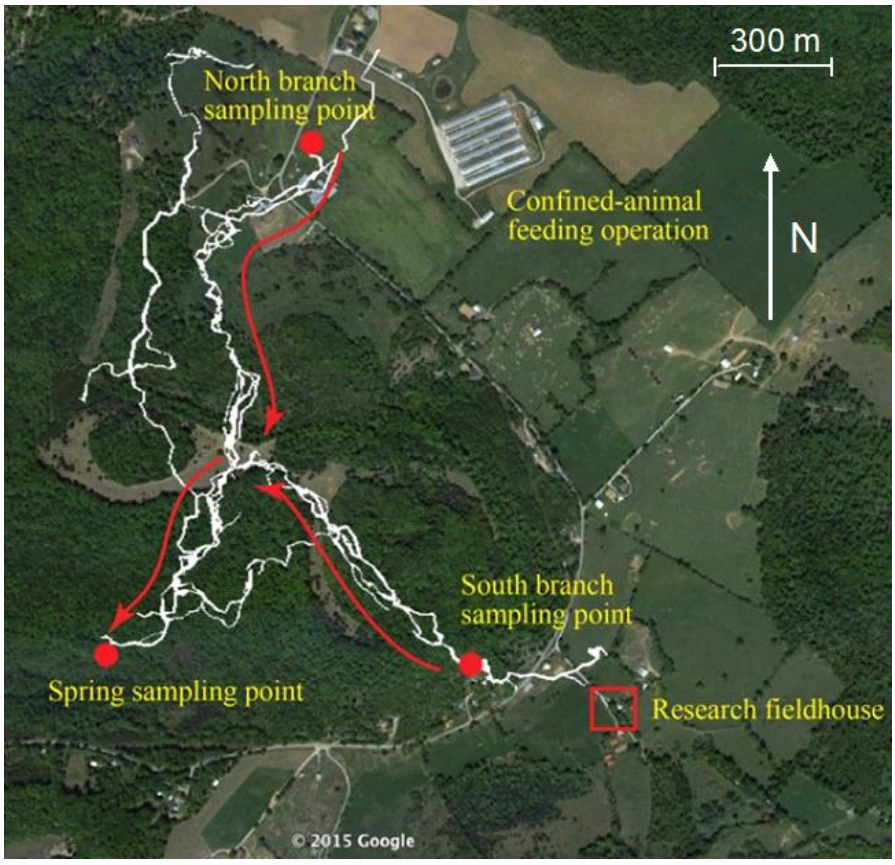


Figure 3: Surveyed passages of Grayson-Gunnar Cave are shown in white (courtesy of members of the Greater Cincinnati Grotto of the National Speleological Society). Red arrows illustrate primary groundwater flow paths. Red dots are the selected sites for data collection from each conduit (North and South Branches) of the cave and from the combined flow at the spring. The research field house that served as a base of operations is shown in the red square. Source: Satellite imagery from Google Earth (2015)

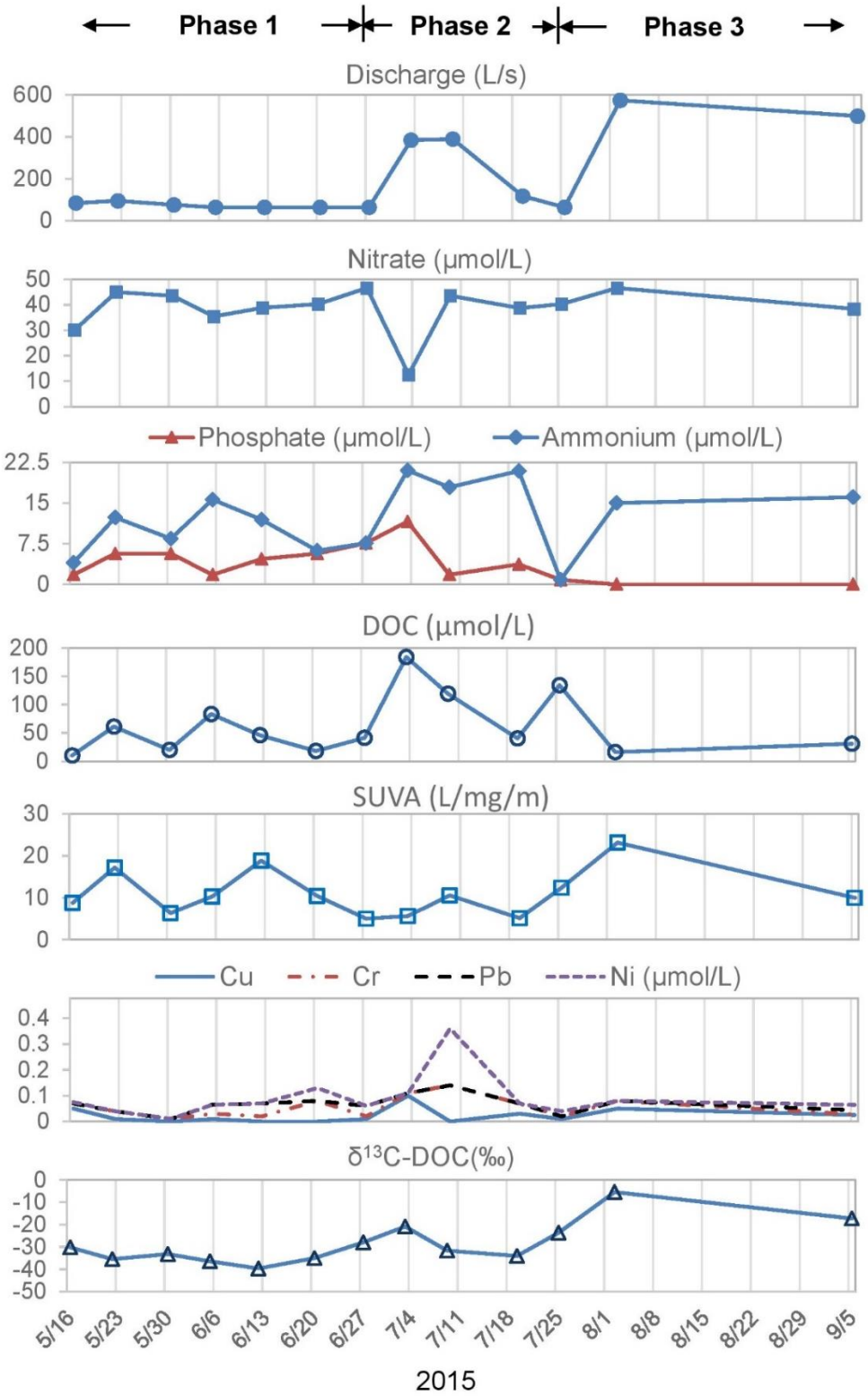


Figure 4: Nutrient, dissolved organic carbon (DOC), and trace metals concentrations, Specific Ultra-Violet Absorbance (SUVA), and dissolved organic carbon isotopes ($\delta^{13}$C-DOC) plotted against measured discharge at the GGC spring. Samples were collected weekly from late spring 2015 to early fall 2015

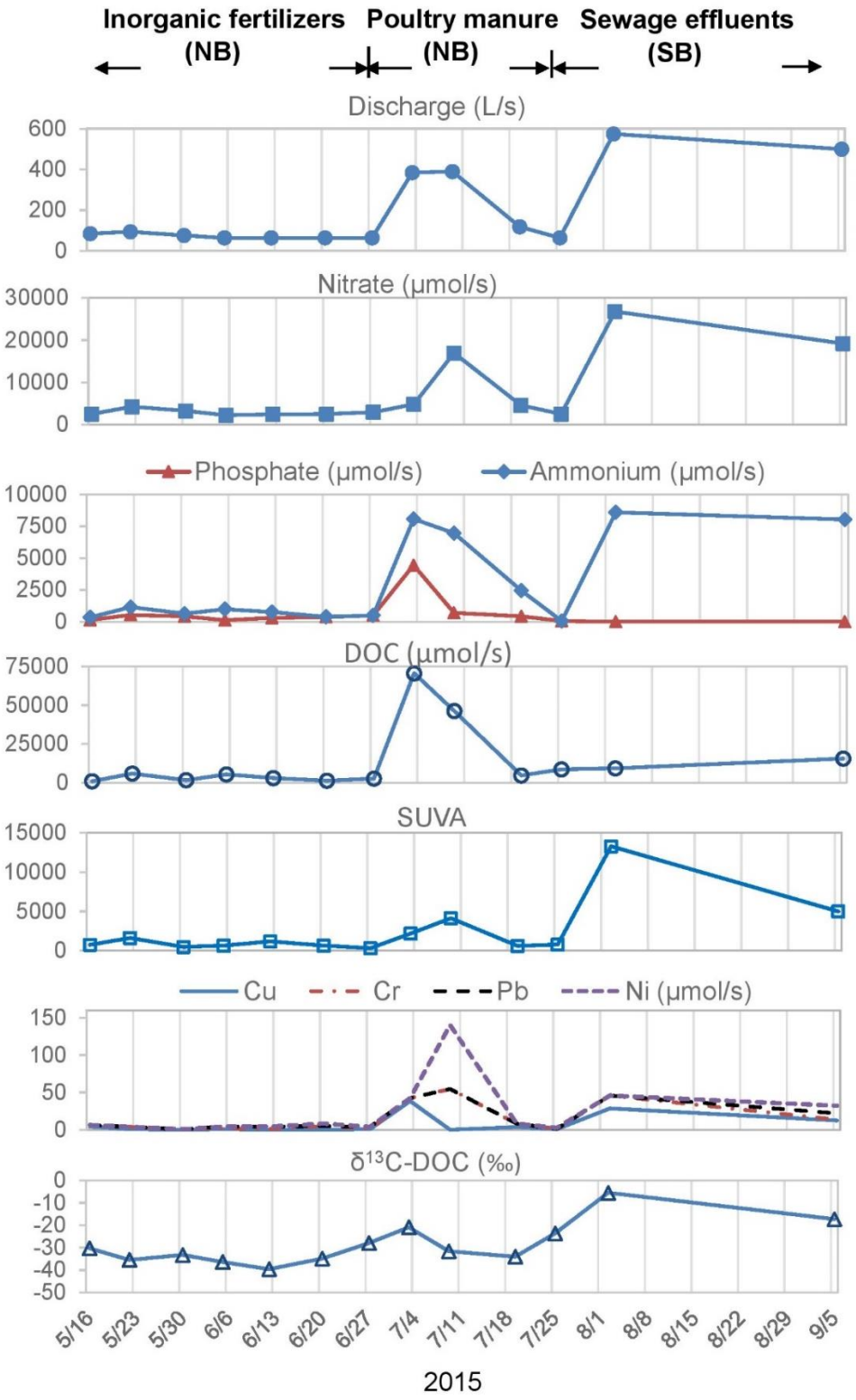


Figure 5: Nutrients, dissolved organic carbon (DOC), trace metals, Specific Ultra-Violet Absorbance (SUVA), and dissolved organic carbon isotopes ($\delta^{13}$C-DOC) loads plotted against collection date. Loads are calculated by multiplying concentrations (µmol/L) from the discharge factor

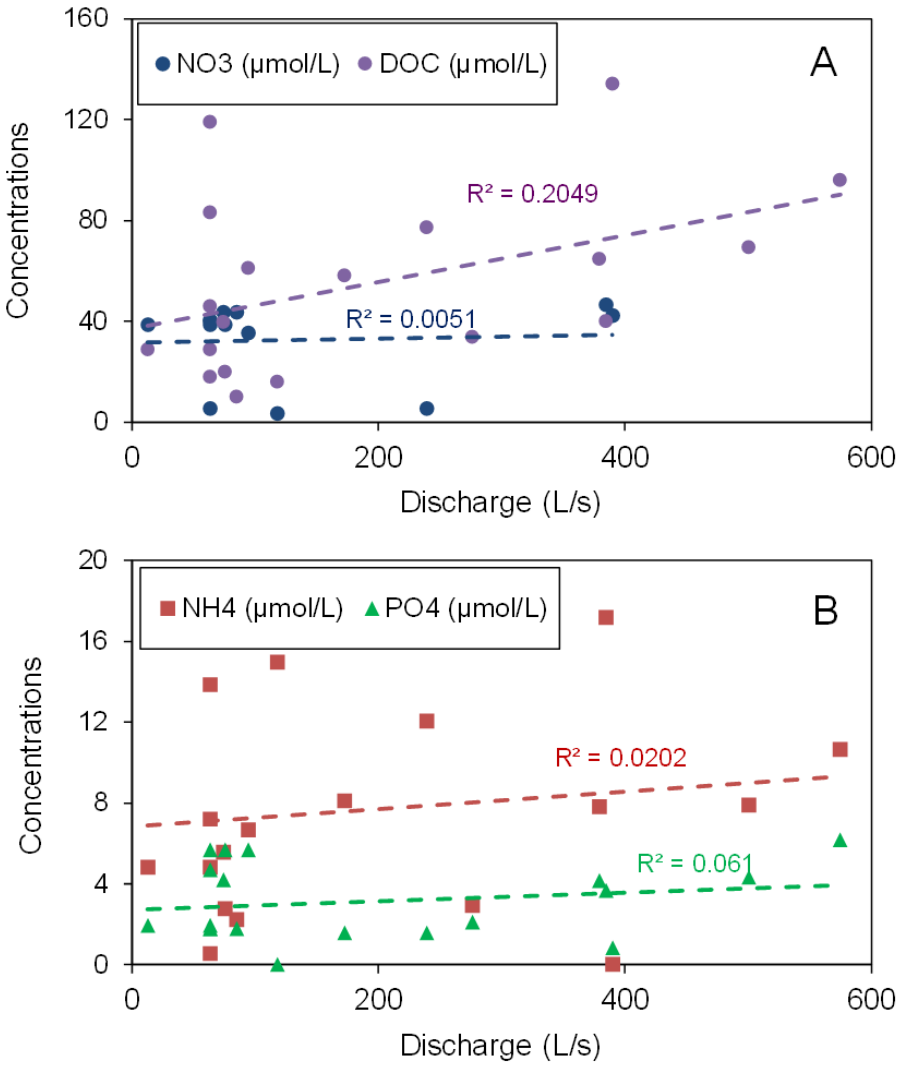


Figure 6: Concentrations of nitrate and dissolved organic carbon (A) and ammonium and phosphate (B) plotted in relation to discharge

## Tables

Table 1: Discharge, nutrients ($NO_3^-$, $NH_4^+$ and $PO_4^{3-}$), trace metals (Cu, $Cr^{3+}$, Pb, Ni) and organic carbon (DOC, SUVA, $\delta^{13}C_{DOC}$) concentrations from weekly measurements at the GGC spring during spring and summer 2015. Discharge values are expressed in L/s. Concentrations are in µmol/L

| | Sampling date | $Q_S$ (L/s) | TIN (µmol/L) | $NO_3$ (µmol/L) | $NH_4$ (µmol/L) | $PO_4$ (µmol/L) | DOC (µmol/L) | SUVA (L/mg/m) | $\delta^{13}C$-DOC (‰) | Cu (µmol/L) | Cr-III (µmol/L) | Pb (µmol/L) | Ni (µmol/L) |
|---|---|---|---|---|---|---|---|---|---|---|---|---|---|
| **Phase 1** | 5/16/2015 | 85.0 | 32.35 | 30.09 | 2.22 | 1.77 | 10.00 | 8.76 | -30.24 | 0.05 | 0.02 | 0.00 | 0.01 |
| | 5/22/2015 | 94.4 | 51.80 | 45.06 | 6.65 | 5.68 | 61.00 | 17.15 | -35.49 | 0.01 | 0.03 | 0.00 | 0.00 |
| | 5/30/2015 | 75.8 | 46.32 | 43.53 | 2.77 | 5.68 | 20.00 | 6.38 | -33.22 | 0.00 | 0.01 | 0.00 | 0.00 |
| | 6/5/2015 | 63.7 | 49.27 | 35.41 | 13.86 | 1.77 | 83.00 | 10.27 | -36.42 | 0.01 | 0.02 | 0.04 | 0.00 |
| | 6/12/2015 | 63.7 | 45.96 | 38.75 | 7.21 | 4.70 | 46.00 | 18.82 | -39.61 | 0.00 | 0.02 | 0.05 | 0.00 |
| | 6/20/2015 | 63.7 | 40.87 | 40.32 | 0.55 | 5.69 | 18.00 | 10.41 | -34.92 | 0.00 | 0.08 | 0.00 | 0.05 |
| **Average phase 1** | | 74.4 | 44.43 | 38.86 | 5.54 | 4.22 | 39.67 | 11.97 | -34.98 | 0.01 | 0.03 | 0.01 | 0.01 |
| **Std. Dev. phase 1** | | 13.1 | 6.96 | 5.50 | 4.83 | 1.93 | 28.67 | 4.91 | 3.14 | 0.02 | 0.03 | 0.02 | 0.02 |
| **Phase 2** | 6/27/2015 | 63.7 | 46.65 | 46.61 | 0.00 | 7.58 | 41.00 | 5.02 | -27.90 | 0.01 | 0.01 | 0.00 | 0.00 |
| | 7/3/2015 | 384.3 | 22.00 | 12.58 | 9.42 | 11.58 | 184.00 | 5.66 | -20.87 | 0.10 | 0.01 | 0.00 | 0.00 |
| | 7/9/2015 | 389.7 | 66.14 | 43.55 | 16.08 | 1.79 | 119.00 | 10.58 | -31.64 | 0.00 | 0.14 | 0.04 | 0.22 |
| | 7/19/2015 | 118.0 | 55.89 | 38.71 | 17.18 | 3.69 | 40.00 | 5.16 | -34.06 | 0.03 | 0.04 | 0.00 | 0.00 |
| **Average phase 2** | | 238.9 | 47.67 | 35.36 | 10.67 | 6.16 | 96.00 | 6.61 | -28.62 | 0.04 | 0.05 | 0.01 | 0.06 |
| **Std. Dev. phase 2** | | 172.4 | 18.87 | 15.53 | 7.90 | 4.35 | 69.36 | 2.66 | 5.75 | 0.05 | 0.06 | 0.02 | 0.11 |
| **Phase 3** | 7/25/2015 | 63.7 | 40.39 | 40.32 | 0.00 | 0.84 | 134.00 | 12.41 | -23.60 | 0.01 | 0.01 | 0.00 | 0.02 |
| | 8/2/2015 | 574.6 | 61.64 | 46.61 | 14.97 | 0.00 | 16.00 | 23.12 | -5.44 | 0.05 | 0.03 | 0.00 | 0.00 |
| | 9/5/2015 | 500.0 | 40.64 | 38.38 | 16.08 | 0.00 | 31.00 | 10.00 | -17.30 | 0.03 | 0.00 | 0.02 | 0.02 |
| **Average phase 3** | | 379.4 | 47.56 | 41.77 | 10.35 | 0.28 | 60.33 | 15.18 | -15.45 | 0.03 | 0.01 | 0.01 | 0.01 |
| **Std. Dev. phase 3** | | 275.9 | 12.20 | 4.30 | 8.98 | 0.49 | 64.24 | 6.98 | 9.22 | 0.02 | 0.01 | 0.01 | 0.01 |

Table 2: Temporal variations of land-use sources contributing to aquifer recharge. Calculations are based on end-member mixing sources of DOC ($\delta^{13}$C-DOC). Inorganic fertilizers ($\delta^{13}$C-DOC = -40‰), manure fertilizers ($\delta^{13}$C-DOC = -18‰), and sewage ($\delta^{13}$C-DOC = -10‰) are used as end-member mixing values respectively

| | **Sampling date** | **$Q_S$ (L/s)** | **$\delta^{13}$C-DOC (‰)** | **Dominant source (%)** | **Secondary source (%)** | **Source description** |
|---|---|---|---|---|---|---|
| **Phase 1** | 5/16/2015 | 85.0 | -30.2 | **55.5** | 44.5 | • Dominant: inorganic fertilizers<br>• Secondary: poultry manure fertilizers<br>• Sewage muted |
| | 5/22/2015 | 94.4 | -35.5 | **79.5** | 20.5 | |
| | 5/30/2015 | 75.8 | -33.2 | **69.0** | 31.0 | |
| | 6/5/2015 | 63.7 | -36.4 | **83.6** | 16.4 | |
| | 6/12/2015 | 63.7 | -39.6 | **98.2** | 1.8 | |
| | 6/20/2015 | 63.7 | -34.9 | **76.8** | 23.2 | |
| ***Average Ph.1*** | – | 74.4 | -35.0 | **77.1** | 22.9 | |
| **Phase 2** | 6/27/2015 | 63.7 | -27.9 | **55.0** | 45.0 | • Dominant: poultry manure fertilizers<br>• Secondary: inorganic fertilizers<br>• Sewage muted |
| | 7/3/2015 | 384.3 | -20.9 | **86.8** | 13.2 | |
| | 7/9/2015 | 389.7 | -31.6 | **38.2** | 61.8 | |
| | 7/19/2015 | 118.0 | -34.1 | **26.8** | 73.2 | |
| ***Average Ph.2*** | – | 238.9 | -28.6 | **51.7** | 48.3 | |
| **Phase 3** | 7/25/2015 | 63.7 | -23.6 | **54.7** | 45.3 | • Dominant: sewage<br>• Secondary: inorganic fertilizers<br>• Manure muted |
| | 8/2/2015 | 574.6 | -5.4 | **100.0** | 0.0 | |
| | 9/5/2015 | 500.0 | -17.3 | **75.0** | 24.0 | |
| ***Average Ph.3*** | – | 379.4 | -15.4 | **76.6** | 23.1 | |

Table 3: Summary of controls, dominant loads and sources of nutrients and DOC based on the interpretation of temporal changes in loads at the GGC

| Controls | Input variables | Dominant load | Primary source(s) |
|---|---|---|---|
| Land-use | Nutrients | Phases 2 and 3 | Manure fertilizers + sewage |
| | $\delta^{13}$C-DOC | Phases 2 and 3 | Manure fertilizers + sewage |
| | DOC | Phase 2 | Manure fertilizers |
| | Trace metals (Cu, Zn, Pb) | Phase 2 | Manure fertilizers |
| | SUVA | Phase 3 | Sewage effluents |
| Hydrology | Spring discharge (Q) | Phase 2 and 3 | Rainfall infiltration + groundwater storage (Tagne and Dowling, 2018) |

Table 4: Correlation statistics between discharge (independent variable) and metal concentrations. Boldface values are significant at $p \leq 0.05$

| Metal | Correlation coef. | Standard Error | Significance (ANOVA) | Sample size |
|---|---|---|---|---|
| Cr-III | 0.284 | 0.161 | 0.325 | 13 |
| Cu | **0.521** | 0.144 | **0.056** | 13 |
| Pb | 0.286 | 0.161 | 0.322 | 13 |
| Ni | 0.298 | 0.161 | 0.302 | 13 |

Table 5: Results of analysis of variance performed between TIN (input variable) and the hydrologic variable (Q) and land-use variables ($\delta^{13}$C-DOC, Cu, DOC, SUVA). Boldface values are significant at $p \leq 0.05$

| Controls | Hydrology | Land-use | | |
|---|---|---|---|---|
| Source(s) | Rain + storage | CAFO + sewage | CAFO | Sewage |
| Dependent variable | Q | $\delta^{13}$C-DOC | Cu | DOC | SUVA |
| Correlation coefficient | 0.130 | 0.707 | **0.885** | 0.562 | 0.374 |
| Standard Error | 0.010 | 0.434 | 0.285 | 0.008 | 0.009 |
| F-significance (ANOVA) | 0.687 | 0.010 | **1.28E-04** | 0.057 | 0.231 |
| Observations | 13 | 13 | 13 | 13 | 13 |

Table 6: Correlation matrix obtained using TIN, Q, $\delta^{13}$C-DOC, Cu, DOC, SUVA as input variables. Boldface values are the most significant correlations at $p \leq 0.05$

| | **$NO_3$** | **Q** | **$\delta^{13}$C-DOC** | **Cu** | **DOC** | **SUVA** |
|---|---|---|---|---|---|---|
| **$NO_3$** | 1.000 | | | | | |
| **Q** | 0.130 | 1.000 | | | | |
| **$\delta^{13}$C-DOC** | 0.707 | 0.771 | 1.000 | | | |
| **Cu** | **0.885** | 0.530 | 0.561 | 1.000 | | |
| **DOC** | 0.562 | 0.861 | 0.137 | 0.368 | 1.000 | |
| **SUVA** | 0.374 | 0.349 | 0.308 | 0.128 | 0.196 | 1.000 |

# CHAPTER 5:

# EFFECTS OF PRESENT AND PAST LAND USE ON CHEMICAL EVOLUTION OF SHALLOW GROUNDWATER IN THE CUMBERLAND SINKHOLE ESCARPMENT OF SOUTHEASTERN KENTUCKY.

**Abstract**

Sulfuric acid speleogenesis has been widely addressed as a common dissolution pattern in epigenic karst systems around the world. However, it remains unclear whether this non-traditional speleogenetic process has affected cave formation in the Cumberland Escarpement and to what extent it occurs. A combination of recent geochemical data collected at Grayson-Gunnar cave and Mill Springs was used. The two small karstic watersheds (12 $km^2$ and 18 $km^2$ respectively) are located in the lower part of the Plateau to complement the pre-existing data from cave streams in the Upper Cumberland Escarpment (Florea 2013; 2017). This study is the first one to provide a regional picture of the water quality in the SE Kentucky in relation with the implication of sulfur brines on the genesis of sulfuric acid associated with carbonate dissolution. Although ionic data reveals the existence of two end-member mixing components corresponding to carbonate bedrock dissolution on one-hand and shallow sulfur brine on the other both at GGC and MS, results suggest that non-traditional sulfuric acid speleogenesis has a secondary role in defining the chemistry of spring waters across the whole physiographic region when compared to the traditional carbonic acid dissolution pattern. However, the results of this investigation have enabled us to 1) define more clearly a conceptual scheme for carbonate dissolution across the SE Kentucky carbonate platform which takes into account the understanding of the regional geology, the historical (shallow petroleum exploration) and present land-uses, and differences in epikarst-groundwater connectivity, and 2) confirm the origin of sulfates involved in sulfuric acid speleogenesis from the assessment of the various anthropogenic sources of salts.

Keywords: Carbonate dissolution, Sulfuric-acid-speleogenesis, Geochemical modelling, Oil exploration, Sulfur brines.

## I. Introduction

Based on general literature of water quality studies in the area, the understanding of present and past land use changes in the Cumberland physiographic area, and the understanding of regional subsurface recharge (Tagne and Dowling, 2018a), it is likely that three primary processes are influencing groundwater evolution at Mill Springs (MS) and other small karstic watersheds in the Cumberland Plateau. In addition to atmospheric deposition and carbonate bedrock dissolution, Tagne and Dowling (2018b) concluded that diffuse subsurface infiltration from agricultural land-use (inorganic and organic fertilizers) has a strong control on nutrient variability at the Grayson-Gunnar Cave (GGC) spring (Fig. 1). Moreover, Florea (2013, 2017) presented preliminary data suggesting non-traditional carbonate dissolution may be occurring from the entrainment of sulfide minerals and dissolved salts from shallow subsurface brines in the Otter Creek and the Beaver Creek. These two surface creeks are produced from the discharging waters from mature cave systems in the piedmont of the Cumberland Plateau and constitute two of the main headwaters of the Cumberland River. The location of the MS watershed in the valley at the convergence of the regional flow line and the Cumberland River suggests that the spring water likely reflects all the geochemical processes that happened within the MS as well as the upstream Otter Creek, Beaver Creek and GGC watersheds. Because Beaver Creek and Otter Creek watersheds drain primarily forested land-uses which strongly contrasts with the mixed land-uses at GGC (forest + fertilized croplands + CAFO + residential) and MS (fertilized croplands + residential + semi-urban), a complete model of groundwater chemical evolution in the region needs to take into account end-member mixing geochemical processes (Fig. 2) and the differences in spring response in relation to varying land-uses and epikarst-groundwater connectivity. In addition, other end-member sources that may be more

specific to the MS watershed and could include: 1) diffuse infiltration of surface salts from allogenic recharge underneath nearby highways (Kentucky State Road 90), and 2) carbonate water degassing at the contact of $CO_2$-rich groundwater with the atmosphere as evidenced by the travertine deposited around the Mill Springs. A conceptual model of how these geochemical processes may affect carbonate water evolution in this shallow groundwater system of the Cumberland karst is presented in Figure 2. This investigation will assess how these processes affect the chemical evolution of shallow groundwater in the Cumberland Sinkhole Escarpment of southeastern Kentucky. Although no evidence of seeping of oil and/or sulfur brine was found in the MS cave system nor discussed for GGC in the previous chapter (chapter 4), the potential for non-traditional speleogenesis is being considered in the following for both systems.

***I.1. Effect of mixed agricultural land-uses on chemical balance of natural waters***

Background levels are expected concentrations in natural waters in the absence of significant human influence. Nutrients background concentrations in surface water and groundwater are usually reflective of natural sources such as atmospheric deposition, rainfall, snow melting, and deposition from native fauna in forested ecosystems (Nolan and Hitt, 2002). However, nutrient levels in surface water and groundwater across the U.S. Midwest have varied over the last decades due to increased contamination from intensive farming practices in predominantly agricultural watersheds (Arnold et al., 2016; De Cicco et al., 2017; Kalkhoff et al., 2016; Kelly et al., 2015; Mills et al., 2017; Nolan et al., 2002; Oelsner et al., 2017). Present-day nitrate background concentrations are now exceeding the natural background threshold of 1 mg $NO_3^-$/L, which specifically corresponds to maximum nitrate levels in groundwater discharging from pristine areas, such as primarily forested and unfertilized regions (Hallberg, 1989; Nolan and

Hitt, 2002). Many studies have also recorded similar trends at the farm to watershed levels (Brakebill and Gronberg, 2017; Miller et al., 2016; Panno et al., 2006; Owen and Pavlowsky, 2011). Panno et al. (2006) describes an increase of > 1.6 mg $NO_3^-$/L in nitrate background concentrations in groundwater discharging from springs in the predominantly agricultural basin of Southern Illinois (Upper Mississippi) from measurements made over less than a decade.

Nitrate concentrations in groundwater draining intensive agricultural areas generally exceed natural background levels and may occasionally exceed U.S.E.P.A Maximum Contaminant Levels (10 mg $NO_3^-$/L; Tab.1). In the Upper Mississippian basin – Illinois sub-basin (Panno et al., 2006), groundwater directly affected by runoff from fertilized croplands exhibit concentrations higher than 2.1 mg/L, with a maximum value of 2.5 mg $NO_3^-$/L. In the Konza Prairie Basin in Kansas, Kemp and Dodds (2001) found that $NO_3^-$ concentrations in groundwater affected by recharge from fertilized croplands (max 1.4 mg $NO_3^-$/L) ranged up to a hundred folds higher than $NO_3^-$ concentrations in groundwater draining pristine land-use (unfertilized grasslands) in the same basin.

Changes in land-use in karstic and non-karstic basins associated with the transition from natural conditions to intensive concentrated agriculture have caused a progressive degradation of groundwater quality across the U.S. Midwest. Studies conducted at the national, regional and farm scales have indicated a correlation between increasing use of manure on row croplands and high nitrate and DOC loads (Gronberg and Arnold, 2017; Tagne and Dowling, 2018b). Nutrients in concentrated-farming land-use often originate from point-sources leakage such as manure storage sites, effluents pipes and septic tanks leakages (Hooda et al., 2000, Brahana et al., 2014). However, study at the scale of Cumberland Plateau aquifers and adjacent systems in the South-Central Kentucky carbonate platform (Crawford and Groves, 1996; Coulter et al., 2004; Currens,

1999; Hampson et al., 1994; Tagne and Dowling, 2018b; Taraba et al., 1997) have shown that nutrients and DOC loads in groundwater mainly increase following major rainfall events due to diffuse infiltration from non-point sources (inorganically and organically fertilized croplands). Moreover, data have shown a clear time-correlation between increase in DOC and peaks in trace metals incorporated in animal diets (Vesper and White, 2003).

In watersheds characterized by a dense concentration of CAFOs, surface water and groundwater nitrate levels are consistently greater than present-day background levels (1-2 mg $NO_3^-$/L), with values greatly exceeding nitrogen MCL for drinking water (10 mg $NO_3^-$/L) in some cases (Tab.1). Becher et al. (2001) reported median concentrations of 5.1 mg $NO_3^-$/L in streams draining an eastern Iowa watershed, one of the most concentrated CAFO's spatial distributions in the United States. Westerman et al. (1995) found 3 to 6 mg $NO_3^-$/L in surface runoff from sprayfields that received CAFO effluents at recommended rates. Stone et al. (1998) measured 6 to 8 mg/L of total nitrogen in a stream adjacent to CAFO effluents' sprayfields in Duplin County (North Carolina). An average range of 3 to 10 mg $NO_3^-$/L was reported in subsurface drains underlying pastures fertilized with cattle and sheep slurry/ manure (Hooda et al., 1998; Scholefield et al., 1993). Record concentrations exceeding MCL (50 to 100 mg $NO_3^-$/L) were reported in shallow wells affected by direct leaking from animal waste lagoons in Oklahoma (Hutchins et al., 2012). Brahana et al. (2014) found that elevated $NO_3^-$ concentrations (2 to >10 mg/L) at the Big Creek Cave springs (Ozark Plateau of Northern Arkansas) were associated to conduit-surface connectivity with a swine CAFO located 10 km north of the cave recharge area.

These data support an existing trend for basins with a higher density of livestock operations and manure-fertilized lands to exhibit higher TIN levels in groundwater and subsurface water

than equally-sized basins with a higher percentage of inorganically fertilized lands and less or no CAFO distribution. However, there is still a lack of information regarding the particular processes controlling fate and transport of nitrogen in cave streams influenced by CAFO production. Several factors such as the size and the morphology of the watershed, the characteristics of the soil and vadose zone (Tagne and Dowling, 2018a; Brahana et al., 2014), climate and hydrologic factors (Davis et al., 2014; Kemp and Dodds, 2001; McCrackin et al., 2017; Mueller and Spahr, 2006; Randall and Mulla, 2001), the type of animal facility (swine, cattle, poultry; Hutchins et al., 2012), the amount of animals per facility, the amount and composition of wastes, and timing and rates of manure application on croplands (Randall and Mulla, 2001) may account for the variability of TIN loads in CAFO-influenced aquifers.

### *I.2. Potential for sulfuric-acid-driven carbonate dissolution in the karst of the Cumberland Plateau.*

#### *I.2.1. Evidence from major ions chemistry*

Traditional carbonate dissolution pathways in karsts include carbonic acid produced primarily by the reaction between water and dissolved carbon dioxide originating from the atmosphere and soils (Eq.1), and the dissolution of carbonate enhanced by carbonic acid (carbonic acid speleogenesis; Eq.2). However, in anthropogenic settings such as acid mine drainage (Haubrich and Tichomirowa, 2002) or in areas affected by loads from surface or deep brines (Panno et al., 2006), sulfide minerals (e.g., pyrite) and sulfate-enriched salts can be oxidized to generate $H_2SO_4$ that is subsequently used to dissolve carbonates and produce DIC. Conceptual models for non-traditional mechanisms of carbonate dissolution involving sulfuric acid (sulfuric acid speleogenesis; Eq.3) or a combination of sulfuric and carbonic acids (Eq.4), and the formation of

gypsum as a secondary mineral deriving from reprecipitation of calcium and sulfate ions (Eq.5) are presented below:

$$CO_2 + H_2O \rightarrow H_2CO_3 \quad \text{(Eq.1)}$$

$$[(1\text{-}x)\ Ca, x\ Mg]\ CO_3 + H_2CO_3 \rightarrow (1\text{-}x)\ Ca^{2+} + x\ Mg^{2+} + 2\ HCO_{3\ (aq)} \quad \text{(Eq.2)}$$

$$2\ [(1\text{-}x)\ Ca, x\ Mg]\ CO_3 + H_2SO_4 \rightarrow 2\ (1\text{-}x)\ Ca^{2+} + 2x\ Mg^{2+} + SO_4^{2-} + 2\ HCO_{3\ (aq)} \quad \text{(Eq.3)}$$

$$3\ [(1\text{-}x)\ Ca, x\ Mg]\ CaCO_3 + H_2CO_3 + H_2SO_4 \rightarrow 3\ (1\text{-}x)\ Ca^{2+} + 3x\ Mg^{2+} + 3\ HCO_3^- + SO_4^{2-} \quad \text{(Eq.4)}$$

$$Ca^{2+} + SO_4^{2-} \leftrightarrow CaSO_4 \quad \text{(Eq.5)}$$

In a system where carbonate dissolution is solely driven by carbonic acid (Eq.2) from the dissolution of atmospheric $CO_2$ into water (Eq.1), the total molar ratio of dissolved cations over dissolved anions $(Ca+Mg)/(HCO_3)$ yields a value of 0.5 (1:2), and Dissolved Inorganic Carbon (DIC) at equilibrium (2 moles of $HCO_{3(aq)}$) is equivalent to an equal contribution of bedrock carbon (1 mole from $CaCO_3$) and atmospheric/soil carbon (1 mole from $H_2CO_3$). This mechanism is referred to as carbonic acid-driven dissolution or Carbonic Acid Speleogenesis (CAS) given that calcium and carbonate ions can precipitate into limestone.

If the carbonate dissolution is primarily derived from the oxidation of sulfide minerals that produces sulfuric acid (Eq.3), the total molar ratio of dissolved cations over dissolved anions $(Ca+Mg)/(HCO_3+SO_4)$ has a value of 1 (1:1 or x = y), and DIC is entirely derived from the bedrock. This mechanism is referred to as sulfuric acid-driven dissolution or Sulfuric Acid Speleogenesis (SAS) given that calcium and sulfate ions in solution can precipitate into gypsum (Eq.5).

Therefore, if both dissolution mechanisms within the same proportions (i.e. dissolution of carbonates by both carbonic and sulfuric acids; Eq.4) are present, they would yield a $(Ca+Mg)/(HCO_3+SO_4)$ ratio of 0.75 (3:4). Water samples collected along petroleum-related

sulfur seeps in the Otter Creek watershed (Florea, 2017) align with the molar ratio expected for primary sulfuric-acid-driven (SAS) carbonate dissolution. However, in the same study, groundwater collected at various springs in the headwaters of Otter Creek and Beaver Creek watersheds (Fig. 1) revealed a primary contribution of carbonic-acid-driven dissolution (CAS; average $(Ca+Mg)/(HCO_3+SO_4)$ ratio ~ 0.51). Despite such evidence that SAS occurs in the upper parts of the Cumberland Escarpment Region (e.g., seeps in Otter Creek), it remains unclear whether or not similar non-traditional dissolution processes exist further downstream at Grayson-Gunnar Spring and Mill Springs (Fig. 1). Moreover, assuming sulfuric-acid-driven dissolution occur in these lower land watersheds, potential sources of sulfate ions could include pyrite oxidation in upper-Pennsylvanian caprock sediments, diffusion from oil-related shallow brines and input from road salts (Fig. 2). So far, the occurrence of concentrations of Volatile Organic Compounds (VOCs) above Maximum Contaminants Levels (> 0.5 mg/L for benzene, toluene and ethylbenzene) in groundwater at Mill Springs constitutes one line of evidence that subsurface diffusion of petroleum brines is driving SAS (Blair et al., 2012) . Quantifying the molar compositions of end-member sources (e.g., pyrite oxidation, sulfur brines) is critical to identify their potential roles as drivers of CAS and SAS in these cave systems (GGC and MS).

### *I.2.2. Evidence from isotope chemistry.*

In previous sulfur speleogenetic models, sulfuric acid originates from the hydrolysis of sulfides entrained from underlying brines in anaerobic conditions in the vadose zone (hypogene speleogenesis; Engel et al., 2004, Wynn et al., 2010, Onac et al., 2011, Florea, 2013). Various "hypogenic" features have been identified in the caves of South-Central Kentucky, such as the existence of active petroleum seeps in surface streams (Otter Creek karstic watershed; Florea,

2013), visible petroleum related brines seeping into cave passages (e.g. Stream Cave), gypsum deposits in subaerial parts of the caves (e.g. Triple-S cave), inverted-V-shaped features from fibrous deposition of gypsum along cave wall and floor sediments (e.g, Spelunger cave in the Otter Creek watershed; Florea, 2013). All the above features are very characteristic of non-traditional carbonates dissolution and sulfuric acid generation in partially anoxic conditions in cave environments (Ford and Williams, 1989).

Palmer (2009) and Metzger et al. (2015) used $\delta^{34}S$ isotopes to illustrate that secondary gypsum deposits along cave walls and pyrite minerals at Mammoth Cave have a similar composition, suggesting that sulfuric acid generation could originate from the oxidation of pyrite-bearing caprock sediments in aerobic conditions as described by Haubrich and Tichomirowa (2002) in the context of acid mine drainage (Eq.6). This reaction occurs under fairly acidic conditions ($3 < pH < 5$) which is in the lower range of pH values observed in the majority of groundwater in equilibrium with carbonate minerals ($4.5 < pH < 8.5$; Langmuir, 1971; Plummer et al., 1978).

$$FeS_{2(s)} + 3/2\ O_2 + H_2O \rightarrow Fe^{2+} + 2\ SO_4^{2-} + 2H^+ \quad \text{(Eq.6)}$$

Following their work, the analysis of gypsum samples collected from three caves in South-Central Kentucky (Spelunger and Bowman's caves in the Otter Creek watershed, and Grayson-Gunnar Cave, Fig. 3) revealed that a combination of subsurface oxidation of pyrite in shallow Pennsylvanian caprock sediments and oxidation of sulfide-rich petroleum brines explain the origin of sulfuric acid involved in SAS at the regional level. The distribution of gypsum samples Grayson-Gunnar Cave (Fig. 3) suggests a dominant sourcing of sulfate from pyrite oxidation ($+6.9 < \delta^{34}S < +10.6‰$; $0 < \delta^{18}O < +13.8‰$), which is consistent but slightly below the range of values described by Onac et al. (2011) for gypsum minerals that are formed through the

oxidation of pyrite in carbonate caprock sediments in the hypogenic caves of the Cerna Valley, Romania ($+5.8 < \delta^{34}S < +6.5$ ‰; $+11.9 < \delta^{18}O < +13.9$ ‰; Fig. 3). On the other hand, the isotope composition of three gypsum samples collected at Spelunger cave in the same watershed (Otter Creek) show mixed sources both from pyrite oxidation and sulfide with a dominant contribution of sulfide hydrolysis from petroleum brines similar to the composition described by Balci et al. (2012) in coal mine drainage areas ($\delta^{18}O$ values range: $-2.3 < \delta^{34}S < +3$‰ ; $\delta^{18}O$ average ~ +9.5‰; Fig. 3). Samples at Bowman's cave also reveal mixed sources but with more enriched $\delta^{34}S$ values consistent with dominant pyrite oxidation.

The oxidation of pyrite generally occurs in the zone of fluctuations of the water table and the incorporation of atmospheric $O_2$ or meteoric $O_2$ depends on whether the reactions occur above or below the water table (redox conditions). Because the atmospheric $O_2$ is considerably more enriched in $^{18}O$ ($\delta^{18}O = +24$‰) in comparison to meteoric water ($\delta^{18}O = -11$‰), gypsum samples deriving primarily from the oxidation of pyrite above the water table (e.g., Otter Creek at Bowman's cave and Grayson Gunnar Cave) will tend to have a higher $\delta\,^{18}O$ content compared to samples in which sulfate originates primarily from sulfide hydrolysis close to or under the water table (Otter Creek at Spelunger cave).

Because of the non-linear behavior of recharge in epigenic karst aquifers and fast changes in water levels in subsurface conduits (Tagne and Dowling, 2018a), it is expected that water levels in the vadose zone may be the primary control for this reaction. Therefore, the reactional scenario presented in Eq.6 is more likely to occur when pyrite-bearing non-carbonate caprock is exposed to atmospheric $O_2$ during soil and epikarst desaturation following major storms in a manner similar to what is described in acid mine drainage (Haubrich and Tichomirowa, 2002). However, under highly saturated (reductive and anaerobic) conditions during high discharge

periods, when the soil and pyrite-bearing caprock sediments are completely submerged by water, it is hypothesized that ferric ions are more likely to replace oxygen as pyrite oxidizing agents in a manner described by equations 7 and 8 (Haubrich and Tichomirowa, 2002). Because this reaction occur under the water table, 100% of the oxygen incorporated into sulfate minerals (gypsum) is derived from meteoric water (low $\delta^{18}O$). Therefore, this reactional mechanism may explain the location of some gypsum samples at GGC and Bowman's cave closer to the meteoric water line (Fig. 3).

$Fe_2O_3$ (hematite) + $6H^+ \rightarrow 2\ Fe^{3+} + 3\ H_2O$ (Eq.7)

$FeS_{2(s)} + 14\ Fe^{3+} + 8H_20 \rightarrow 15\ Fe^{2+} + 2\ SO_4^{2-} + 16H^+$ (Eq.8)

Although no direct evidence of sulfur seeping or oil leakage along the waterways was found in the Mill Springs recharge area or near the spring, the similarity in geological settings between Mill Springs and other brines-affected watersheds in the Cumberland escarpment (Otter Creek, Redmond Creek and Grayson-Gunnar cave), combined with the occurrence of high concentrations of volatile organic compounds at the spring (Blair et al., 2012) are highly suggestive of the possibility that SAS from the entrainment of oil-related brines may occur at MS as well.

### *I.3. Research goals and objectives*

This research aims to 1) study the end-member mixing of the expected geochemical sources (surface and subsurface brines, carbonate weathering and agriculture) and 2) assess whether or not sulfur-rich brines influence on carbonate dissolution patterns. To achieve these goals, quarterly water quality data collected from 2005 to 2013 (KGS, 2019a) within the Mill Spring watershed were used. The Mill Spring karst aquifer is located along the Cumberland River near

Monticello, KY in the lower part of the Cumberland Plateau physiographic region. We have conducted regressions analyses in AquaChem version 1 (2014) using local precipitation chemistry (National Atmospheric Deposition data), the average regional composition of brines, and dissolved ions concentrations at Mill Springs as input variables. However, because of the lack of isotope measurements ($\delta^{18}O$ and $\delta^{34}S$) from bedrock samples at Mill Springs, the present hypothesis for CAS/SAS at Mill Springs can only be tested using major ion chemistry ratios ($(Ca+Mg)/(HCO_3+SO_4)$) from spring samples.

This investigation will further define the processes of carbonate dissolution in the SE Kentucky platform and will take into account the geology (Simpson and Florea 2009), the historical and present land-use (Dugan et al. 2012; Florea 2013; Tagne and Dowling 2018b) and the flow dynamics (Tagne and Dowling, 2018a). However, because of the absence of sulfur isotope data, it is not possible, beyond the observation of geochemical trends, to fully differentiate among the potential sources of anthropogenic salts (road salts and subsurface brines) that are involved in sulfuric-acid speleogenesis. Results from this study can serve to constrain any upcoming detailed hydrogeological models of SE Kentucky karsts.

## II. Site description

### *II.1. Hydrogeological settings*

The study area is located within the Cumberland Escarpment of southeast Kentucky (Simpson and Florea, 2009), a part of the Interior Lowland Plateaus Physiographic Province. A mature karst landscape has developed in Mississippian-age carbonates of the Slade Formation (Ettensohn et al., 1984) that have deeply incised valleys that drain the non-carbonate uplands of the Cumberland Plateau and underlying an adjoining sinkhole plain on a broad Miocene-age

geomorphic surface—the Highland Rim (Anthony and Granger, 2007). Waters conveyed through these karst aquifers undergo significant geochemical changes from recharge points along the plateau margin to springs at the base of the carbonate sequence (Florea, 2013). Springs emerging from these karst aquifers form tributaries of the Cumberland River, the regional base level (Anthony and Granger, 2007).

A generalized stratigraphic cross-section from the Southwest to the Northeast along the Cumberland Escarpment in eastern Kentucky is presented in Chapter 3, Fig.1. Surface geomorphology in the SE Kentucky carbonate platform is dominated by streams swallets and sinking streams. The Pennsylvanian epikarst-forming clastic sediments have a high porosity, which likely causes the majority of water to flow through underlying fractures and local interbeddings as inferred from dye tracing studies (Blair et al., 2012; Fig. 2A) performed within the Mill Springs watershed

The Mill Springs watershed, as delineated west by the Kentucky State Road 1275 and east by the State Road 90 (Fig. 1), is a 7.1-square miles (18.3 $km^2$) drainage basin (not including the upper watersheds' areas; Blair et al., 2012). The karst system occurs within the fine to medium-grained thick Reelsville Limestones. Although no cave passage has been mapped in the area, dye trace studies revealed potential flowpaths from surface recharge (sinkholes located up to 2 miles south of the major spring) to the springs and a regional flow gradient converging towards the Cumberland River (Fig. 1). The average discharge at the springs is estimated to 3 $ft^3/s$ (85 L/s), and TIN concentrations at the springs vary between 2 and 4 mg/L (Blair et al., 2012). Waters discharging at the springs are nearly saturated to supersaturated with respect to calcite, as shown by the travertine deposits around the springs (Fig. 2B). Water discharging from Mill Springs will

flow through a sharp escarpment of about 250 m before joining the Cumberland River, the regional base level.

### *II.2. Historical land-use legacy and the potential for non-traditional carbonate dissolution:*

The Wayne County experienced an oil boom in shallow Mississippian-age reservoirs beginning in the 1880s near the communities of Slickford along Otter Creek and Oilton along Beaver Creek. Production peaked in 1920 from permeable limestone units in the Fort Payne Formation (McFarlan, 1943), the focus of early operations because of its relatively shallow depth (dozens of natural seeps of brine and oil rise through stress release fractures and discharge into streambeds). Initial production was, in some cases intense but short-lived. Commonly, sustainable rates of production remained within the order of a few barrels per day. Vestiges of the pipeline and pumping stations associated with that oil boom remain. For example, improperly cased wells from that era continue to leak oil into caves and streams (Florea, 2013). To this date, hydrogen sulfide gas and microbial mats persist near these leaking well casings (Fig. 4).

In the Mill Springs watershed, the contribution of allochtonous sources of salts likely affects the sulfur cycle and its SAS patterns. Although underlying oil-related brines composition may account for substantial loads of Na, Cl and $SO_4$ (Table 1), two main state roads identified in the recharge area of the MS watershed (SR 90 and SR 1275; Fig. 4) are likely to provide additional loads of salts (Na, Cl, $SO_4$) to the spring from winter road de-icing (Panno et al., 2006). Other sources of naturally-derived ions are: 1) carbonate bedrock dissolution within the cave aquifer (likely the major sources of Ca, Mg, Na, K, and $HCO_3$), and 2) atmospheric depositions likely accounting for non-negligible concentrations of Ca, Na, Mg, K, Cl and $SO_4$ (cf. Table 2).

### *II.3. Present land-use*

The Mill Springs watershed is a forested, agricultural (corn and soybean), and residential basin (79.1, 18.5, and 2.5% of total basin area respectively; Blair et al., 2012). While the majority of the Mississippi River basin has experienced an increase in corn coverage relative to soy bean production over the last decade (corn-based ethanol production, Donner and Kucharik, 2008; Secchi et al., 2011), the Mill Spring basin has undergone a reverse trend with an increase in soy bean production in the late 2000s (unpublished data, personal communication) and a progressive transition from corn row-crop to corn-soybean rotation. A Concentrated Animal Feeding Operation (CAFO) has been identified in the Southwestern part of the recharge area (Hannah Hills), but no connection to the regional flowpaths has been found. The forested part of the basin is unfertilized and thus relatively pristine with regards to nutrient inputs (expected nutrient levels below background levels; Table 1). Therefore, cropland fertilization and mineralization of soil organic matter from agricultural practices (David et al., 1997) are likely the primary sources of nitrogen contamination in groundwater.

### *II.3. Climate*

A detailed description of regional climate patterns and implications for recharge and subsurface infiltration mechanisms is provided by Tagne and Dowling (2018a). Cross-correlation analyses between precipitation and discharge for the adjacent Grayson-Gunnar epikarst suggest that regional aquifer discharge is primarily driven by rainfall infiltration, and to a smaller extent the contribution of groundwater storage during summer high rainfall period (July and August).

As suggested from the yearly record of rainfall at the Beaver Creek USGS Gauging Station (KY-WY-1; Fig. 5), daily precipitation increases with the occurrence with summer extreme

storms towards the end of the summer. A maximum rainfall range is identified during a multiday period extending from July 11 to July 19, 2015 (Fig. 5B), which also corresponds to the maximum discharge and the maximum loads of surface contaminants at the Grayson-Gunnar cave (Tagne and Dowling, 2018a; 2019b). This specific precipitation window is critical in understanding subsurface flowpaths at the regional scale of the Cumberland Plateau. For the 2015 water year, cumulative monthly precipitation data (Fig. 5C) peak at a value of 58 inches, 7 inches above the 30-year average of 51 inches, suggesting a general trend toward increased precipitation on the area.

Average spring water temperatures vary for a 13-year record (2000-2013) from 13°C to 16°C (average of 14°C; Blair et al., 2012) at Mill Springs. As the average ambient temperature in the region is 12.8°C (55°F, average 1990-2001, www.usclimatedata.com at Monticello, KY), it is assumed that the temperature rainwater in equilibrium with the atmosphere will be close to 13°C (default temperature).

## III. Methods

### *III.1. Data collection*

Annual Precipitation chemistry data (Table 2) from 2000 to 2013 were obtained from the National Atmospheric Deposition Program (http://waterdata.usgs.gov/NADP; accessed on 11/11/2014, 2:53:25 PM) at the Mackville Station (KY03) located 70 miles North of Mill Springs (http://nadp.sws.uiuc.edu/data/sites/map/). NADP data include major ions chemistry (Ca, Mg, K, Na, $NH_4$, $NO_3$, Cl, $SO_4$) and physico-chemistry (pH, electrical conductivity). Because bicarbonate concentrations are not included in the data, they were calculated from pH using a theoretical relationship provided by Kulshrestha et al. (2003):

$$[HCO_3^-] = 10^{(pH-5.05)} \quad \text{(Eq.9)}$$

Quarterly spring flow data at Mill Springs (Table 2) were extracted from the Kentucky Geological Survey Division of Water Groundwater Database (https://kgs.uky.edu/kgsweb/datasearching/Water/WaterWellSearch.asp) for a total of 33 samples from between November 2000 and September 2013. Part of the data available for the Mill Springs system was also obtained from the Integrated Surface Water and Groundwater Assessment Report for the Green River Basin (Blair et al., 2012). Data include pH, temperature and Total Dissolved Solids, trace metals, nutrients, and Dissolved Organic Carbon (DOC). Nutrient speciation includes nitrate ($NO_3$), nitrite ($NO_2$), ammonia ($NH_3$) and total dissolved phosphorous ($PO_4$). No isotope measurement is available on the Kentucky Water Division database.

## IV. Results

### *IV.1. Major ions chemistry: precipitation and carbonate dissolution background concentrations.*

The Piper Diagrams presented in Fig. 6A and Fig. 6B highlight the contribution of two end-member sources to the major ion chemistry at Mill Spring and GGC. For Mill Spring, ionic balance for rainwater samples vary within a wider range (+3.5% and +8.7%) in comparison to spring water (+0.8% to +1.1%; Table 2). The rainwater is relatively enriched in sulfate (0.6 – 1.9 mg/L) and nitrate (0.6 – 1.9 mg/L) but exhibit very low concentrations on Ca, Mg and $HCO_3$, suggesting no water interaction with carbonate bedrock prior to entrance in the cave system. Mill Spring samples show an enrichment in calcium, carbonate and bicarbonate ions, comparable to the work done by Dugan et al. (2012) in the headwaters of the Otter Creek (Fig. 6B) for near-equilibrium between groundwater and carbonate bedrock.

Because the groundwater average residence time estimated by Tagne and Dowling (2018a) for the St Louis limestone ranges from two to seven days, it is expected that the groundwater evolution is driven by mixing between rainwater and groundwater storage or a dilution of concentrated storage by fairly dilute rain water (Fig. 2). Because of the low complexity and relatively shorter length of the subsurface conduit network at Mill Springs (Fig. 2A) in comparison to the Grayson Gunnar cave system, it is hypothesized that major ion chemistry (Ca, Mg, $HCO_3$) will reflect a shorter interaction between rainfall and carbonate bedrock compared to what is observed at GGC (Tagne and Dowling, 2018a). Moreover, because there is no major difference in temperature between rainfall (input) and spring water (output), it is very unlikely that major $CO_2$ degassing or $CaCO_3$ reprecipitation occur along the subsurface flowpath from rain infiltration to the spring.

Fig. 7 presents long-term (2005 to 2013) variations of in physical (pH and SpC) and ion chemistry (Ca, Na, Mg, K, $SO_4$, $HCO_3$, Cl) from quarterly measurements at Mill Springs. With the exception of calcium, average concentrations of major cations (Na, K, Ca, and Mg) at Mill Springs (0.25 ± 0.11, 0.03 ± 0.01, 1.80 ± 0.22, and 0.26 ± 0.09 mmol/L) are lower than average values at the Grayson-Gunnar spring (1.58 ± 2.09, 0.10 ± 0.10, 1.15 ± 0.28, and 0.49 ± 0.11 mmol/L; Tagne and Dowling, 2018a). Average concentrations of major anions ($HCO_3$, Cl and $SO_4$) at Mill Springs (3.38 ± 0.30, 0.30 ± 0.12 and 0.15 ± 0.04 mmol/L) are comparable but slightly higher than the values at Grayson-Gunnar (3.13 ± 0.31, 0.12 ± 0.00 and 0.07 ± 0.02 mmol/L). Because Ca, Mg and $HCO_3$ account for 84 to 94% (average = 90%) of the total ionic content at Mill Springs, long-term trends in Ca, Mg and $HCO_3$ concentrations reveal significant correlation with changes in Specific Conductivity (Fig. 7). Ca, Mg and $HCO_3$ concentrations explain 82% of the temporal variability in Specific Conductivity at the spring. Long-term

changes in discharge at Mill Spring (average 0.12 ± 0.19 $m^3/s$) are not as important to its aqueous geochemistry as the short-term fluctuations observed at Grayson Gunnar spring during the course of summer 2015 (0.06 to 0.45 $m^3/s$).

Specific Conductivity values range from 300 to 500 µS/cm which is consistent with water flowing through carbonate bedrock or mixing with carbonate groundwater reserve (Desmarais and Rojstaczer, 2002) and with values observed at the Grayson Gunnar spring (Tagne and Dowling, 2018a). However, SpC ranges slightly above values expected for spring water recharging from primarily agricultural watersheds (Ryan and Meiman, 1996; 200 < SPC < 300 µS/cm), which may suggest the existence of other sources of major ions such as brines and road salts (Fig. 2). The average value and the range of variation of pH (7.15 ± 0.39) at Mill Springs are not significantly different compared to Grayson-Gunnar (7.77 ± 0.37).

Fig. 8 illustrates the carbonate-water interactions along flow lines between Mill Springs and GGC. Spring samples show near saturation with respect to calcite (-0.39 < calcite SI < -0.13) and dolomite (-3.53 < dolomite SI < -0.91; Table 2). However, Mill Springs water is more saturated in comparison to GGC spring samples (-0.78 < calcite SI < -0.54; -1.57 < dolomite SI < -2.13; Tagne and Dowling, 2018a). The distribution of spring samples at Mill Springs (Fig. 8A), combined with the relative enrichment in Ca (and low Mg content) from rainwater to spring (Fig. 6) and a closer saturation with calcite than with dolomite (SI calcite > SI dolomite; Table 2) reflects a mixture of calcite and dolomite dissolution similar to GGC. However, unlike GGC samples, MS samples exhibit a predominant calcite dissolution pattern (ideally: $Ca+Mg)/(HCO_3) = 0.5$) and limited dolomite dissolution (ideally: $Ca+Mg)/(HCO_3) = 0.25$) as shown by the distribution of the $(Ca+Mg)/HCO_3$ ratios (calculated average = 0.41, close to the ideal calcite dissolution line of 0.5; Fig. 8A), thus suggesting that the groundwater has shorter

contact time with calcite-bearing bedrocks compared to GGC where spring samples mimic dominant dolomite dissolution (calculated average = 0.28, close to ideal dolomite dissolution line of 0.25) because of a greater residence time ( > 7 days average; Tagne and Dowling, 2018a). This observation is consistent with results from dye trace studies conducted at Mill Springs suggesting a much faster dye recovery rate (2 to 3 days) from injection in surface wells compared to GGC (personal communications with staff at the Kentucky Water Division).

Values of SI calcite and SI dolomite (Table 2) also reveal that rain water is 6 to 14 times less saturated in calcite and dolomite, suggesting that a process of desaturation by $CO_2$ degassing occurs at the contact of groundwater with the atmosphere at the spring. Travertine deposits at the spring (Fig. 1B) constitutes additional evidence that calcite supersaturation and high $CO_2$ partial pressure in groundwater may cause immediate calcite precipitation at the spring at the contact with the atmosphere. Therefore, major chemistry data suggests faster flow dynamics and relatively shorter equilibrium with carbonate bedrock at MS in comparison to GGC.

### *IV.2. Nutrients and DOC*

Long-term trends in nutrients (nitrogen, ammonium, phosphate) and DOC concentrations (Fig. 9) at Mill springs show a predominant surface recharge from inorganically fertilized croplands. The average range of nitrate concentrations (49 ± 8 µmol/L) at Mill Springs is comparable to the average range observed at Grayson Gunnar during low discharge periods (< 0.8 $m^3/s$) whose nitrate concentrations (44 ± 7 mg/L) originate from inorganically fertilized croplands (Tagne and Dowling, 2018b). However, due to the short-term fluctuations in discharge and the subsequent dilution of nitrogen during high discharge periods, nitrate concentrations at Grayson-Gunnar (12.5 – 46.6 µmol/L) vary across a wider range than nitrate concentrations at Mill Springs (30.0

– 60.9 mmol/L) where discharge seems to be more evenly distributed during the sampling period ($0.12 \pm 0.019$ $m^3/s$). Moreover, it is likely that because the timing of quarterly sampling at Mill Spring did not specifically target periods of discharge peaks, the background-to-noise ratio in the discharge is very low. Although nitrate concentrations at Mill Springs are more representative of base flow conditions, they largely exceed (even the minimum value of 30 µmol/L recorded on the 11/27/12) the nitrate background average of 16 µmol/L (1 mg/L) for natural waters discharging from pristine and unfertilized land-uses (Nolan and Hitt, 2002), thus suggesting the influence of agricultural land-use in the recharge area of the springs (Fig. 2A). During discharge increases recorded in February 2009, March 2010 and March 2013 (marked 1, 2 and 3 respectively, Fig. 9), nitrate concentrations exhibit a dilution comparable to the Grayson Gunnar karstic system (Tagne and Dowling, 2018b).

Ammonia and phosphate average values at Mill Springs ($2.11 \pm 0.75$ µmol/L; $0.24 \pm 0.09$ µmol/L) are 7 and 20 times more diluted than concentrations at Grayson-Gunnar ($15.5 \pm 20.7$ µmol/L; $4.7 \pm 3.3$ µmol/L). Moreover, DOC concentrations average range ($54 \pm 30$ µmol/L) lies well below the average of $96 \pm 69$ µmol/L recorded during primarily recharge from manure fertilizers at Grayson-Gunnar (phase 2, Tagne and Dowling, 2018b). Because maximum loads in ammonia, phosphate and DOC were associated with the response of the manure-fertilized land-use at Grayson-Gunnar during high discharge conditions (Tagne and Dowling, 2018b), the previous values likely suggest no major influence of CAFO on nutrient concentrations at Mill Springs, and combined with evidence from dye trace studies (Blair et al., 2012), suggest that there is no direct subsurface connectivity between CAFO and Mill Springs.

A scatter plot diagram between $NO_3$ and DOC concentrations (Fig. 10) with known background values for primarily fertilized-agricultural field crops (Table 1) further reveals that

the aqeuous geochemistry of the spring samples are dominated by the inorganic-fertilizer end member and not manure-fertilizer. Combined with evidence from long-term sampling showing ammonia concentrations below trace levels (< 0.1 mg/L) and a dominance of nitrate ($N\text{-}NO_3$) species on TIN concentrations (98.9%), this suggests very low inputs of nitrogen from organic sources and reinforces the hypothesis that runoff from inorganically fertilized croplands is the principal source of TIN at Mill Springs. However, in the absence of isotope measurements of DOC ($\delta^{13}C$-DOC) or $\delta^{15}N$ and SUVA (Specific Ultra-Violet Absorbance of DOM), the above evidence is not sufficent to quantify the specific contributions of mixing sources of Total Inorganic Nitrogen in a way that is described by Tagne and Dowling (2018b).

### *IV.3. Trace metals*

Fig. 11 presents the concentrations of selected dissolved trace metals (ppb) from quarterly measurements from 2005 to 2013 at Mill Springs samples. The average concentrations of all trace metals (As = 0.87 ppb, Cu = 1.19 ppb; Zn = 6.38 ppb; Pb = 1.19 ppb; Ni = 0.97 ppb; Cr = 0.94 ppb) and their respective maximum concentrations (As = 10 ppb, Cu = 9 ppb; Zn = 42 ppb; Pb = 20 ppb; Ni = 5 ppb; Cr = 9 ppb) are well below the EPA Maximum Exposure Levels for drinking water (As = 10 ppb, Cu = 3 ppb, Zn = 5 ppb, Pb = 2.5 ppb, Ni = 52 ppb, Cr = 74 ppb). Regarding the hydrologic control, general trend over the 8-year period for all the trace metal data show an inverse correlation with increasing discharge that could correspond to the effect of dilution of background concentrations by increasing volume of water at the spring during extreme recharge events. This lack of hydrological control, combined with very low concentrations in trace metals, suggests that unlike the GGC system where trace metals concentrations reflect primarily mobilization of concentrated farming land-use contaminants

during periods of significant recharge (positive correlations with DOC and discharge, Tagne and Dowling, 2018b), trace metal concentrations at MS likely do not reflect any anthropogenic source.

## V. Discussion

### *V.1. Assessing the potential role of brine chemistry in sulfuric acid-driven dissolution*

Figure 12 is a graphical representation of the possible carbonate dissolution scenarios occurring within the karstic system of the Cumberland Escarpment Region based on the respective stoichiometry of equations 2, 3 and 4. Carbonate dissolution driven by carbonic acid ($H_2CO_3$ + $CO_{2(aq)}$) originating from natural sources (atmospheric depositions and/or solubilization of atmospheric $CO_{2(g)}$) would yield a (Ca+Mg)/($HCO_3$+$SO_4$) ratio of 0.5 (1:2), which is consistent with water composition at various spring locations in the headwaters of Otter Creek (Sandy Springs, Stream Cave and Tufa Springs; Dugan et al., 2012). Moreover, water samples collected in the close vicinity of petroleum sulfur seeps along Otter Creek and Beaver Creek (Upper Cumberland; Fig. 1) reflect the $SO_4$−driven dissolution end-member, as they plot along a line of equal molarity between cations (Ca+Mg) and anions ($HCO_3$+$SO_4$). In the case of Mill Springs and Grayson-Gunnar spring, groundwater chemistry reflects the contribution of two end-members carbonate dissolution processes: CAS and SAS. While Grayson-Gunnar springs samples reveal a dominance of traditional carbonic-acid driven dissolution (calculated average = 0.51), differences in dissolution kinetics between the Northern and the Southern conduit branches (Tagne and Dowling, 2018a) may account for the distribution of spring water samples toward the $SO_4$−driven dissolution end-member. On the other hand, Mill Springs samples follow a regression line (calculated average = 0.66) that is more reflective of equal proportions of

sulfuric-acid and carbonic-acid driven dissolution (ideally: equal proportions of CAS and SAS: $(Ca+Mg)/(HCO_3+SO_4)$ ratio = 0.75). Combined with evidence of $SO_4$ enrichment during groundwater evolution as shown on the Piper diagram (Fig. 6), this strongly supports $SO_4$ entrainment from allochtonous sources (sulfur brines, pyrite oxidation and/or road salts). Furthermore, regression analysis (Fig. 13 and Fig. 14) are used to identify which one of the aforementioned end-member mixing sources is likely to account for the majority of the sulfate content in Mills Spring water.

### *V.2. End-member mixing sources: brines and bedrock composition*

Table 3 presents the average composition of brines in Lower Pennsylvanian-age limestones in South-Central Appalachian region in Western Pennsylvania (Krieger et al., 1957; Dresel and Rose, 2010), in the Cumberland Plateau escarpment (Florea, 2013), and in stream water near a shallow oil production well (KGS, 2019b) in the Newman Limestone (Slade Formation) along the Pottsville Escarpment in eastern Kentucky (Ettensohn et al., 1984). Average concentrations are obtained using the composition of 40 samples collected near shallow oil seeps during well-drilling operations in Pennsylvania (Krieger et al., 1957) and in Upper Devonian carbonate formations in Western Pennsylvania (Dresel and Rose, 2010). The composition of brines in the Upper-Cumberland escarpment is defined using average bimonthly concentrations for water samples collected near three sulfur seep sites at Beaver Creek and Otter Creek, respectively (Florea, 2013). In addition, the Ca, Mg, $HCO_3$, and $SO_4$ values at Sandy Springs and Stream Cave in the headwaters of Otter Creek above the locations of major oil seeps (Fig. 12) reveal that water in these two locations is likely to reflect the original composition of the carbonate bedrock

(no influence of brines). Therefore, these two locations (Sandy Springs and Stream Cave) are used as end-members for carbonate bedrock composition (Table 2; Fig. 12).

The brine end-member is characterized by elevated Total Dissolved Solutes (TDS) concentration (2100 < TDS < 4300 mmol/L) and elevated specific conductivity (> 158,000 µS/cm) consistent with expected concentrations for saline water (25 <TDS< 1,000 mmol/L) and brine water (TDS > 1,000 mmol/L). However the TDS range for Beaver Creek and Otter Creek is significantly lower (16 < TDS < 26 mmol/L), likely due to a dilution effect by high volume of fresh water discharging in the Otter Creek basin (30 < discharge < 70 L/s; Florea, 2013). The ionic composition of brines for stream water near oil seeps in the Slade Formation (KGS, 2019b) varies between dominant Na-Cl type (800 < Na < 1200 mmol/L; 1200 < Na < 2600 mmol/L; Na and Cl ions account for 88 to 93% of the total ionic balance) (Krieger et al., 1957; Dresel and Rose, 2010) to a dominant Na−$SO_4$ composition for water samples near sulfur seeps in the Otter Creek and Beaver Creek watersheds (Na and $SO_4$ values are 35% and 29% of the total ionic balance at both locations respectively), thus suggesting that shallow petroleum brines are likely the major contributor to Cl and $SO_4$ ions in water flowing or discharging near major seeps in the Cumberland escarpment region. Ca/(Ca+$SO_4$) molar ratio vary across brines end-member locations from 0.49 at Otter Creek to 0.92 and 0.99 at Lower Pennsylvanian limestone locations (Krieger et al., 1957; Dresel and Rose, 2010), and a median range of 0.62 − 0.69 (Newman's limestones and Beaver Creek locations) which is consistent with the stoichiometry expected for limestone dissolution solely driven by sulfuric acid (Eq. 3, Ca/(Ca+$SO_4$) = 2/3 = 0.66) and the distribution of Beaver Creek samples in Fig.12. Ca/Na ratios for brines locations varies from 0.11 to 2.49 with a median range of 0.37 – 0.39 (0.38 average) for Lower Pennsylvanian limestone locations. Because brines are significantly more enriched in Cl in comparison to $SO_4$,

$SO_4$/Cl ratios are relatively low at all locations (< 0.02). However, Beaver Creek represents an upper outlier ($SO_4$/Cl = 3.12). Similarly, Na/Cl ratio varies within a median range of 0.4 – 0.53 with Beaver Creek (Na/Cl = 2.05) again as an outlier.

Carbonate bedrock composition as reflected by samples at Sandy Springs and Stream Cave (Table 3) is characterized by lower TDS and specific conductivity values (SpC = 32 µS/cm at Stream Cave; 0.64 < TDS < 3.2 mmol/L) in comparison to what is observed near brines. The ionic balances reflect a dominant composition of calcium and bicarbonate ions (Ca and $HCO_3$ concentrations are 81% and 75% of the ionic balance at Sandy Springs and Stream Cave, respectively), which is consistent with carbonic acid dissolution (CAS; no contribution of sulfuric acid; Fig. 12) and an enrichment in calcium and bicarbonate ions (Dugan et al., 2012) at both locations (Fig. 6B). Molar ratios (Ca/(Ca+$SO_4$), Ca/Na, $SO_4$/Cl and Na/Cl) are significantly different from range values aforementioned for brine chemistry (4.87 < Ca/Na < 5.17; 0.58 < $SO_4$/Cl < 1.57; 1.08 < Na/Cl < 0.94), with the exception of Ca/(Ca+$SO_4$) ratio (0.76 < Ca/(Ca+$SO_4$) < 0.96). While the Ca/(Ca+$SO_4$) ratio at Sandy Springs (0.9) is consistent with limestone dissolution solely driven by carbonic acid (Eq.2, Ca/(Ca+$SO_4$) = 1:1), the ratio at the Stream Cave spring (0.76) is consistent with a combined carbonic-acid and sulfuric-acid-driven dissolution (Eq.3, Ca/(Ca+$SO_4$) = 3:4 = 0.75).

Figure 13 shows results of regression analyses performed between Ca and (Ca+$SO_4$) molarity (Fig. 13A), Ca and Na molarity (Fig. 13B), $SO_4$ and Cl concentrations (Fig. 13D), and Na and Cl molarity (Fig. 13D). The Ca/(Ca+$SO_4$) molar ratios at both GGC and Mill Springs locations (Fig. 13A) reflect the dominance of bedrock dissolution solely driven by carbonic acid as regression line describes a slope (Ca/(Ca+$SO_4$) ratio) of 0.9 consistent with the composition of a sulfuric acid-free location (Sandy Springs). Na and Ca molar compositions (Fig. 13B) reveal that while

samples at Grayson-Gunnar Spring occur along or above the composition range expected for bedrock dissolution driven by carbonic acid only (Ca/Na = 4.86 at Sandy Springs), Mill Springs samples describes an intermediate distribution between two end-member dissolution kinetics (carbonic-acid and sulfuric-acid dissolution), thus suggesting an enrichment in calcium in groundwater from the dissolution of sulfides entrained from oil seeps.

Similarly, regression analysis between sulfate and chlorine concentrations (Fig. 13C) reveals that Mill Springs and Grayson-Gunnar springs reflects a mixed-composition between carbonic-acid driven carbonate dissolution as shown at Sandy Springs ($SO_4$/Cl = 0.58) and a combined carbonic-acid and sulfuric-acid driven dissolution ($SO_4$/Cl) = 1.57 at Stream Cave.

Regression between sodium and chloride (Fig. 13D) also confirms the existence of two-end member mixing sources at Na/Cl = 1.08 corresponding to the calculated composition at Sandy Springs (close to the hypothetical ratio 1:1 for carbonate bedrock composition with no influence of sulfuric-acid driven dissolution) and at Na/Cl = 0.5, the expected median composition of regional brines (Table 3). Mill Springs samples reflect no influence of sulfuric acid while samples at Grayson-Gunnar spring describe a mixed composition between sulfur-free end-member (Sandy Springs) and brines, thus suggesting an enrichment in chlorine from primarily Na-Cl brines (Table 3). However, because the Na/Cl = 1 regression line is the same molar range expected for halite dissolution (Eq.10) and sulfur isotope data are not available, it remains uncertain whether or not the observed regression may signify additional inputs from road salts or this potential end-member source may be prevailing over mixing with overlying brines.

$$NaCl \leftrightarrow Na^{+} + Cl^{-} \quad \text{(Eq.10)}$$

Figure 13E represents a regression scatter plot between specific conductivity (SpC) and chlorine concentrations for samples collected at Mill Springs, Grayson-Gunnar cave spring, the

Otter Creek watershed headwaters (Sandy Springs and Stream Cave) and around sulfur seeps. Spring samples for all 4 locations (MS, GGC, SS and SC) align along a positively sloped end-member mixing line between carbonate bedrock (Ca-$HCO_3$) represented by Stream Cave samples (SPC average = 32 µS/cm; $Cl^-$ average = 0.027 mmol/L; Table 3) and brine composition (Na−Cl end-member) represented by water samples near sulfur seeps (SPC average > 600 µS/cm and 1.05 < $Cl^-$ < 3.94 mmol/L). Because a peak specific conductivity value of 450 µS/cm is measured at Grayson-Gunnar Cave spring (Tagne and Dowling, 2018a) where extended groundwater residence time (2 to 7 days) was found, a threshold of 450 µS/cm is defined as a limit between carbonate-water equilibrium (Ca−HCO3 end-member) and brine water (Na−Cl; Fig. 13E). Moreover, Panno et al. (2006a) found that a chlorine threshold of 0.8 mmol/L (15 mg $Cl^-$/L) differentiates groundwater discharging at a spring affected by road salt intrusion in the Northern Illinois basin (McHenry County) and springs discharging from pristine land-use with regards to road salts in the Mammoth Cave Region; hence, a value of 0.8 mmol $Cl^-$/L is defined in the Cumberland escarpment as a threshold between groundwater contaminated by brines (Na−Cl end-member) and groundwater deriving from prolonged interaction with carbonate (Ca−$HCO_3$ end-member, see Fig. 13E). Data also show that Mill Springs are slightly more enriched towards the Na−Cl end-member (average $Cl^-$ = 0.30 ± 0.12 mmol/L; SPC = 411 ± 50 µS/cm; max SPC = 500 µS/cm) in comparison to Grayson-Gunnar spring samples ($Cl^-$ = 0.12 ± 0.02 mmol/ L; SPC = 348 ± 30 µS/cm; max SPC = 450 µS/cm). This suggests that if road salt intrusion is to be considered as a brine end-member in addition to oil-related sulfur brines in the region, the Mill Springs watershed is likely the most affected watershed due to the presence of two major highways (State Roads 1275 and 90) in the vicinity of its recharge area.

### *V.3. Temporal variations in nutrients concentrations: contrasting hydrology and land-use controls on spring response at Mill Springs and GGC.*

Understanding hydrological and land-use effects on nutrient loading at springs discharging from small agricultural watersheds is essential for the design of nutrient management plans for small watersheds (Tagne and Dowling, 2018b). Although the increasing discharge trend toward the end of the sampling period for Mill Springs (2011-2013) exhibits apparent control on nitrate dilution, the majority of quarterly changes in nutrients ($N\text{-}NO_3$, $NH_4$ and $PO_4$) and DOC concentrations (Fig. 9) did not show a significant relation with fluctuations in discharge. The goal is to determine whether or not long-term changes in land-use at the local scale of the Mill Springs watershed (transition from continuous corn row crop before 2009 to corn-soybean crop rotation after 2009) may better explain the long-term variability in TIN at Mill Springs. Moreover, as it was determined that short-term changes in land-use associated with corn-growth and manure application had a quick effect on nutrient load response at the spring (less than 3 months), it will be important to test whether a similar tendency occurs in the Mill Springs watershed.

In order to assess if decadal changes in crop rotation system exert an influence in TIN loads within the Mill Springs watershed, long-term quarterly record in nitrate concentrations data was considered separately first between 2005 and 2009 (prior to change) and after 2009 following the implementation of the changes, and t-tested for significant similarity/difference among the two data subsets. Results reveal that nitrate concentrations are relatively constant from 2005 to 2013 and show no significant difference between the first half (average $N\text{-}NO_3 = 3.15 \pm 0.32$ mg/L) and the significant second half following crop rotation changes (average $N\text{-}NO_3 = 3.04 \pm 0.67$ mg/L; P-value = 0.55 > 0.05; Tab. 4). Therefore any change in the variance of $N\text{-}NO_3$ fluctuations before and after 2009 (Fig. 9) may instead result from changes in instrumental

precision. In addition, phosphate concentrations show no significant difference before and after 2009 ($P = 0.12 > 0.05$). Assuming that the Upper-Cumberland agricultural region is undergoing a trend toward increasing manure-derived fertilization as shown by Tagne and Dowling (2018b), any change in ammonia concentration in relation to agricultural land-use should reflect an increase as organic nitrogen sources readily convert into ammonia. Thus the apparent decrease in average ammonia concentrations before and after 2009 (Table 4) is likely not indicative of any change in fertilizers composition or fertilizers application rates on row-crop fields.

Also at stake at Mill Springs, is the assessing the potential connectivity between a CAFO facility located in the Northwestern part of the recharge area of the watershed into nutrient chemistry at the spring, especially TIN variability. In a manner similar to what is described by Tagne and Dowling (2018b) for the Grayson-Gunnar cave system, statistical correlations were performed between TIN concentrations measured at Mill Springs and trace metals concentrations measured within the same time interval ($n = 32$). Results (Table 5) show that unlike observations at the Grayson-Gunnar spring, there is no significant correlation between NO3 concentrations and trace metals concentrations at MS ($F > 0.05$), therefore revealing no apparent control of CAFOs storage leaking underground into subsurface conduits and/or no dominant diffuse inputs from manure-fertilized inputs comparable to what is described at Grayson-Gunnar watershed. Combined with dye tracing observations (Blair et al., 2012), the absence of correlation between trace metals concentrations and discharge (Fig. 10), and lower DOC, phosphate and ammonia concentrations at Mill Springs comparatively to Grayson-Gunnar, this clearly suggests differential spring response between a pristine system with respect to CAFO inputs (MS) and a system contaminated by manure deriving from concentrated farming (GGC; Tagne and Dowling, 2018b).

In the CAFO-affected landscape (GGC), data reveal: 1) a combined effect of hydrological and land-use factors on temporal variations in TIN at the spring; 2) a seasonal effect of corn growth that significantly affect nitrogen load to the spring; 3) a dominance of TIN loads from manure-derived fertilizers compared to inorganic fertilizers, thus suggesting that CAFO-wastes control on nitrogen at the spring largely override the control of other portions of the land-use. In CAFO-unaffected (MS) in the other hand, 1) long-term changes (in crop rotation) have no significant impact on nutrient variability at the spring, and 2) long-term TIN and DOC concentrations trends reveal a dominance of inorganic fertilizers over organically-derived fertilizers, thus supporting evidence of no direct or diffuse CAFO connectivity with the spring.

Because short-term changes in land-use (seasonal corn growth) in CAFO-affected systems (GGC) have more effect on TIN export than long-term disturbances (change in crop rotation) in the CAFO-unaffected system (MS), the key control to spring response between the two systems likely lies on the nature of the subsurface connectivity between the epikarst and the conduit system. The relatively flashy hydraulic response to rainfall and surface recharge, the shorter groundwater transit time during peak discharge events (2-4 hours) and the rare intricacy of the conduit subsurface network (2 main subsurface conduit branches) in the Grayson-Gunnar system may explain the differences in the springs' responses to land-use changes between the two watersheds.

## VI. Conclusion

### *VI.1. Effect of past land-use: legacy of regional oil-related brines*

Overall, regression analyses suggest that the variability of the ionic composition of spring samples at Mill springs and Grayson-Gunnar Cave can be both explained by carbonate-water interactions (calcite dissolution with no contribution of sulfuric acid) and sulfuric-acid driven dissolution from the entrainment of sulfate ions from shallow sulfur brines. Therefore, both spring systems show significant potential for petroleum-related brines to account for major ion chemistry. Although no evidence of oil seeping around cave streams or in subsurface conduits have been identified either within the GGC and the MS basins, sulfuric acid-driven dissolution is likely driven by the hydrolysis of sulfur brines near oil seeping zones in a manner similar to what is described in the Otter Creek and Beaver Creek basins (Dugan et al., 2012; Florea, 2017). Results of regression analyses for all 4 locations (GGC, MS, Otter Creek above sulfur seeps, Otter Creek near sulfur seeps) show that while traditional dissolution model (carbonic acid dissolution) may still be the dominant process of carbonate dissolution mechanisms occurring within the Cumberland Escarpment Region, sulfuric-acid may play a secondary role in DIC fluxes at the regional level. Further model approaches to attempt to quantify the contributions of allochtonous sources of salts (differentiate between road salts and brines end-members) may involve the use of isotopes of oxygen and chlorine.

### *VI.2. Effect of recent land-use change on spring response*

Overall, long-term data collected at MS before and after 2009 does not suggest an explicit control of crop rotation change on TIN loads at Mill springs. Results from t-tests before and after 2009 suggests that biogeochemical processes associated to crop rotation changes (differential in N-fertilizers application rates and composition, differences in N assimilation by corn and

soybean) have little effect on TIN export at the scale of the MS basin, or that the effect of changes are too slow to be noticeable on a timescale of a few years to a decade. In addition, due to the mixed-character of the land-use in the recharge area of Mill Springs (forested, residential and fertilized croplands), changes in crop rotation system are likely not homogeneously distributed across the whole surface of the watershed.

Similarly, long-term changes in trace-metal concentrations do not suggest either a hydrological control or subsurface connectivity between manure-fertilized croplands and the spring as suggested by Tagne and Dowling (2018b) at the Grayson-Gunnar cave location. The comparative approach in the study of the two karstic systems is very critical in understanding the behavior of the two adjacent spring systems. Although two karstic systems (GGC and MS) are both located in the same physiography ensemble (Cumberland Plateau), exhibit similar geology (both occur within the Ste-Genevieve Mississippian limestones), and drain similar surface land-use (primarily agricultural and residential), their differential spring response is more likely to be dictated by the characteristics of the subsurface zones and the general connectivity between the epikarst and conduit compartments as suggested by Tagne and Dowling (2018a). Grayson-Gunnar system is definitely the fastest and most responsive to change in water volume caused by rainfall and the displacement of conduit storage (2 to 4 hours). Unlike Mill Springs where the memory of recent changes (change in crop rotation) is relatively low and the spring response seems to be very slow to occur, changes in surface contaminants concentrations at the Grayson-Gunnar cave spring are very reflective of a fast flow dynamics as the aquifer exhibit a large memory effect to short-term changes in precipitation and surface recharge. Therefore, comparing the effects of short-term (seasonal) changes in land-use at Grayson-Gunnar with long-term (decadal) changes in crop rotation on nutrient export to groundwater at the scale the two karstic

watersheds could only make sense if done in light of the understanding of differential subsurface processes.

**Acknowledgements**

We want to thank the Water Division at the Kentucky Geological Survey for giving us access to the quarterly data from Mill Springs, and specifically Rob Blair for providing the results of dye tracing studies.

**References**

Anthony, D.M. and Granger, D.E., 2007. A new chronology for the age of Appalachian erosional surfaces determined by cosmogenic nuclides in cave sediments. Earth Surface Processes and Landforms: The Journal of the British Geomorphological Research Group, 32(6), pp.874-887.

Arnold, T.L., DeSimone, L.A., Bexfield, L.M., Lindsey, B.D., Barlow, J.R., Kulongoski, J.T., Musgrove, MaryLynn, Kingsbury, J.A., and Belitz, K., 2016. Groundwater quality data from the National Water-Quality Assessment Project, May 2012 through December 2013: U.S. Geological Survey Data Series 997, 56 p. DOI: 10.3133/ds997

Balci, N., Mayer, B., Shanks III, W.C. and Mandernack, K.W., 2012. Oxygen and sulfur isotope systematics of sulfate produced during abiotic and bacterial oxidation of sphalerite and elemental sulfur. Geochimica et Cosmochimica Acta, 77, pp.335-351.

Becher, K.D., Schnoebelen, D.J. and Akers, K.K.B., 2000. Nutrients Discharged To The Mississippi River From Eastern Iowa Watersheds. JAWRA Journal of the American Water Resources Association, 36(1), pp.161-173.

Blair, R.J., Ray, J.A. and O'dell, P.W., 2012. Integrated surface water and groundwater assessment of large springs in the Green River Basin (BMU4, round 2). Kentucky Division of Water. Available online: http://water. ky. gov/groundwater/Documents/NPS0503-IntegratedSWGWAssessmentGreenRiver. pdf.

Brahana, J.V., Nix, J., Bitting, C., Bitting, C., Quick, R., Murdoch, J., Roland, V,, Wets, A,, Robertson, S,, Scardale, G,, North, V., 2014. CAFOs on karst—meaningful data collection to adequately define environmental risk, with a specific application from the Southern Ozarks of Northern Arkansas. U.S. Geological Survey Scientific Investigations Report 2014–5035, pp 97–102

Brakebill, J.W. and Gronberg, J.M., 2017. County-Level Estimates of Nitrogen and Phosphorus from Commercial Fertilizer for the Conterminous United States, 1987-2012: U.S. Geological Survey data release, 10.5066/F7H41PKX

Coulter, C.B., Kolka, R.K. and Thompson, J.A., 2004. Water quality in agricultural, urban, and mixed land use watersheds 1. JAWRA Journal of the American Water Resources Association, 40(6), pp.1593-1601.

Crawford, N.C. and Groves, C.G., 1996. Sinkhole collapse and ground water contamination problems resulting from storm water drainage wells on karst terrain. In International Journal of Rock Mechanics and Mining Sciences and Geomechanics Abstracts 2(33), p. 56A.

Currens, J.C., 1999. Mass flux of agricultural nonpoint-source pollutants in a conduit-flow-dominated karst aquifer, Logan County, Kentucky. Kentucky Geological Survey Report of Investigation 1, Series XII, 1999. https://uknowledge.uky.edu/cgi/. Accessed on 1/29/2019

David, M.B., Gentry, L.E., Kovacic, D.A. and Smith, K.M., 1997. Nitrogen balance in and export from an agricultural watershed. Journal of Environmental Quality, 26(4), pp.1038-1048.

Davis, C.A., Ward, A.S., Burgin, A.J., Loecke, T.D., Riveros-Iregui, D.A., Schnoebelen, D.J., Just, C.L., Thomas, S.A., Weber, L.J., St Clair, M.A., 2014. Antecedent moisture controls on stream nitrate flux in an agricultural watershed. Journal of Environmental Quality 43(4), 1494-1503.

De Cicco, L.A., Sprague, L.A., Murphy, J.C., Riskin, M.L., Falcone, J.A., Stets, E.G., Oelsner, G.P., and Johnson, H.M., 2017. Water-quality and streamflow datasets used in the Weighted Regressions on Time, Discharge, and Season (WRTDS) models to determine trends in the Nation's rivers and streams, 1972-2012: U.S. Geological Survey data release.

Desmarais, K. and Rojstaczer, S., 2002. Inferring source waters from measurements of carbonate spring response to storms. Journal of hydrology 260(1-4): 118-134.

Donner, S. D., and Kucharik, C. J., 2008. Corn-based ethanol production compromises goal of reducing nitrogen export by the Mississippi River. Proceedings of the National Academy of Sciences 105(11): 4513-4518.

Dresel, P.E. and Rose, A.W., 2010. Chemistry and origin of oil and gas well brines in western pennsylvania. Pennsylvania Geological Survey, 4th ser.: 48 p.

Dugan, C.R., Florea, L.J. and Walden, W.D., 2012. A geochemical investigation of springs within the Otter Creek watershed: Wayne County, southeastern Kentucky. In Geological Society of America Abstracts with Programs 44(4): 26.

Engel, A. S., Stern, L.A. and Bennett, P.C., 2004. Microbial contributions to cave formation: New insights into sulfuric acid speleogenesis. Geology 32(5): 369.

Ettensohn F.R., Rice C.R., Dever G.R., Chesnut D.R., 1984. Slade and Paragon formations: new stratigraphic nomenclature for Mississippian rocks along the Cumberland Escarpment in Kentucky. US Geol Surv Bull 1605-B:37

Florea, L.J., 2013. Investigations into the potential for hypogene speleogenesis in the Cumberland Plateau of southeast Kentucky, USA.

Florea, L.J., 2017. Sulfur-Based Speleogenesis in the Cumberland Plateau, USA. In Hypogene Karst Regions and Caves of the World (pp. 683-690). Springer, Cham.

Ford, D.C. and Williams, P.W., 1989. Karst geomorphology and hydrology, 601. London: Unwin Hyman.

Gronberg, J.M., and Arnold, T.L., 2017. County-level estimates of nitrogen and phosphorus from animal manure for the conterminous United States, 2007 and 2012: U.S. Geological Survey Open-File Report 2017-1021, 6 p. 10.3133/ofr 20171021

Hallberg, G.R., 1989. Nitrate in ground water in the United States. In Developments in Agricultural and Managed Forest Ecology, 21, pp. 35-74.

Hampson, S.K., Sendlein, L. V. A., Keagy, D. M., and Dinger, J. S., 1994. Impact of Agricultural Practices on a Karst Ground Water System in the Inner Blue Grass Region, Kentucky. Open File Report OF-93-05, KY Geological Survey, Univ. of Kentucky.

Haubrich, F., and Tichomirowa, M., 2002. "Sulfur and oxygen isotope geochemistry of acid mine drainage—the polymetallic sulfide deposit “Himmelfahrt Fundgrube” in Freiberg (Germany)." Isotopes in environmental and health studies 38(2): 121-138.

Hooda, P.S., Edwards, A.C., Anderson, H.A., Miller, A., 2000. A review of water quality concerns in livestock farming areas. Science of the Total Environment 250(1-3): 143-167.

Hooda, P.S., Moynagh, M., Svoboda, I.F., Anderson, H.A., 1998. A comparative study of nitrate leaching from intensively managed monoculture grass and grass–clover pastures. The Journal of Agricultural Science 131(3), pp. 267-275.

Hutchins, S.R., White, M.V., Mravik, S.C., 2012. Case Studies on the Impact of Concentrated Animal Feeding Operations (CAFOs) on Ground Water Quality, In U.S. EPA 600/R-12/052, September 2012, Office of Research and Development, National Risk Management Research Laboratory, Ground Water and Ecosystems Restoration Division, Ada, OK.

Kalkhoff, S.J., Hubbard, L.E., Tomer, M.D., and James, D.E., 2016. Effect of variable annual precipitation and nutrient input on nitrogen and phosphorus transport from two Midwestern agricultural watersheds: Science of The Total Environment, 559, p. 53-62. doi:10.1016/j.scitotenv.2016.03.127

Kelly, V., Stets, E.G., Crawford, C., 2015. Long-term changes in nitrate conditions over the 20th century in two Midwestern Corn Belt streams: Journal of Hydrology, 525(0), pp. 559-571. doi:10.1016/j.jhydrol.2015.03.062

Kemp, M.J. and Dodds, W.K., 2001. Spatial and temporal patterns of nitrogen concentrations in pristine and agriculturally-influenced prairie streams. Biogeochemistry, 53(2), pp.125-141.

Kentucky Geological Survey, 2019a. Kentucky Oil and Gas Repository. Oil and Gas Well Database Search. https://kgs.uky.edu/kygeode/services/oilgas/. Last Accessed 2/9/2019

Kentucky Geological Survey, 2019b. Water Well & Spring Records Database. KY Groundwater Data Repository. https://kgs.uky.edu/kgsweb/datasearching/Water/ WaterWellSearch.asp. Last Accessed 2/10/2019

Krieger, R.A., Hatchett, J.L. and Poole, J.L., 1957. Preliminary survey of the saline-water resources of the United States (p. 174). Washington: US Government Printing Office.

Langmuir, D., 1971. The geochemistry of some carbonate ground waters in central Pennsylvania. Geochimica et Cosmochimica Acta, 35(10), pp.1023-1045.

McCrackin, M.L., Cooter, E.J., Dennis, R.L., Harrison, J.A. and Compton, J.E., 2017. Alternative futures of dissolved inorganic nitrogen export from the Mississippi River Basin: influence of crop management, atmospheric deposition, and population growth. Biogeochemistry, 133(3), pp.263-277.

McFarlan, A.C., 1943. Geology of Kentucky: Lexington. University of Kentucky, 531.

Metzger, J.G., Fike, D.A., Osburn, G.R., Guo, C.J., Aadison, A.N., 2015. The source of gypsum in Mammoth Cave, Kentucky. GSA Bull 43(2):187–190. doi:10.1130/G3613 1.1

Miller, M.P., Tesoriero, A.J., Capel, P.D., Pellerin, B.A., Hyer, K.E., and Burns, D.A., 2016. Quantifying watershed-scale groundwater loading and in-stream fate of nitrate using high-frequency water quality data: Water Resources Research, 52, doi:10.100 2/2015WR017753

Mills, T.J., Sprague, L.A., Murphy, J.C., Riskin, M.L., Falcone, J.A., Stets, E.G., Oelsner, G.P, and Johnson, H.M., 2017. Water-quality and streamflow datasets used in Seasonal Kendall trend tests for the Nation's rivers and streams, 1972-2012: U.S. Geological Survey data release

Mueller, D.K. and Spahr, N.E., 2006. Nutrients in streams and Rivers across the nation-1992-2001. US Department of the Interior, US Geological Survey.

Nolan, B.T., Hitt, K.J., 2002. Nutrients in shallow ground waters beneath relatively undeveloped areas in the conterminous United States. U.S. Geological Survey water resources investigation report 02-4289, 21 p.

Oelsner, G.P., Sprague, L.A., Murphy, J.C., Zuellig, R.E., Johnson, H.M., Ryberg, K.R., Falcone, J.A., Stets, E.G., Vecchia, A.V., Riskin, M.L., De Cicco, L.A., Mills, T.J., and

Farmer, W.H., 2017, Water-quality trends in the nation's rivers and streams, 1972-2012-Data preparation, statistical methods, and trend results: U.S. Geological Survey Scientific Investigations Report 2017-5006, 136 p. doi:10.3133/sir20175006

Onac, B. P., Wynn, J.G. and Sumrall, J.B., 2011. "Tracing the sources of cave sulfates: a unique case from Cerna Valley, Romania." Chemical Geology 288(3-4): 105-114.

Owen, M.R. and Pavlowsky, R.T., 2011. Base flow hydrology and water quality of an Ozarks spring and associated recharge area, southern Missouri, USA. Environmental Earth Sciences, 64(1), pp.169-183.

Palmer, A.N., 2009. The Mammoth Cave Region, Kentucky. In: Palmer AN, Palmer MV (eds) Caves and karst of America. National Speleological Society, Huntsville, AL, pp 108–113.

Panno, S.V., Kelly, W.R., Martinsek, A.T. and Hackley, K.C., 2006. Estimating background and threshold nitrate concentrations using probability graphs. Groundwater, 44(5), pp.697-709.

Plummer, L.N., Wigley, T.M.L. and Parkhurst, D.L., 1978. The kinetics of calcite dissolution in CO2-water systems at 5$^{o}$ to 60$^{o}$ C and 0.0 to 10.0 atm CO2. Am. J. Sci. 278: 179-216.

Randall, G.W., Mulla, D.J., 2001. Nitrate nitrogen in surface waters as influenced by climatic conditions and agricultural practices. Journal of Environmental Quality 30(2), 337-344.

Ryan, M., Meiman, J., 1996. An examination of short-term variations in water quality at a karst spring in Kentucky. Groundwater 34(1):23–30

Schofield, K., Seager, J., Merrlman, R.P., 1990. The impact of intensive dairy farming activities on river quality: the Eastern Cleddau catchment study. Water and Environment Journal 4(2): 176-186.

Secchi, S., Gassman, P.W., Jha, M., Kurkalova, L., Kling, C.L., 2011. Potential water quality changes due to corn expansion in the Upper Mississippi River Basin. Ecological Applications 21(4): 1068-1084.

Simpson, L. C. and Florea, L. J., 2009. The Cumberland Plateau of Eastern Kentucky. Caves and Karst of America, National Speleological Society: 70-79.

Stone, K.C., Hunt, P.G., Humenik, F.J. and Johnson, M.H., 1998. Impact of swinewaste application on ground and stream water quality in an eastern coastal plain watershed. Transactions of the ASAE, 41(6), p.1665.

Tagne, G.V. and Dowling, C., 2018a. Inferring groundwater flow and recharge from time series analysis of storm responses in a karst aquifer of southeastern Kentucky (USA). Hydrogeology Journal, 26(8), pp.2649-2668.

Tagne, G.V. and Dowling, C., 2018b. Land-use control on Total Inorganic Nitrogen in karst aquifers in the Cumberland Plateau (Southeastern Kentucky) in the Upper Ohio River Basin. Geological Society of America Abstracts with Programs 50 (4).

Taraba, J.L., Dinger, J.S., Sendlein, L.V.A. and Felton, G.K., 1997. Land use impacts on water quality in small karst agricultural watersheds. In Karst-Water Environment Symposium, p. 127.

Vesper, D.J. and White, W.B., 2003. Metal transport to karst springs during storm flow: an example from Fort Campbell, Kentucky/Tennessee, USA. Journal of Hydrology, 276: 20–36.

Westerman, P.W., Huffman, R.L. and Feng, J.S., 1995. Swine-lagoon seepage in sandy soil. Transactions of the ASAE, 38(6), pp.1749-1760.

Wynn, J. G., Sumrall, J.B. and Onac, B.P., 2010. Sulfur isotopic composition and the source of dissolved sulfur species in thermo-mineral springs of the Cerna Valley, Romania. Chemical Geology 271(1-2): 31-43.

**Figures**

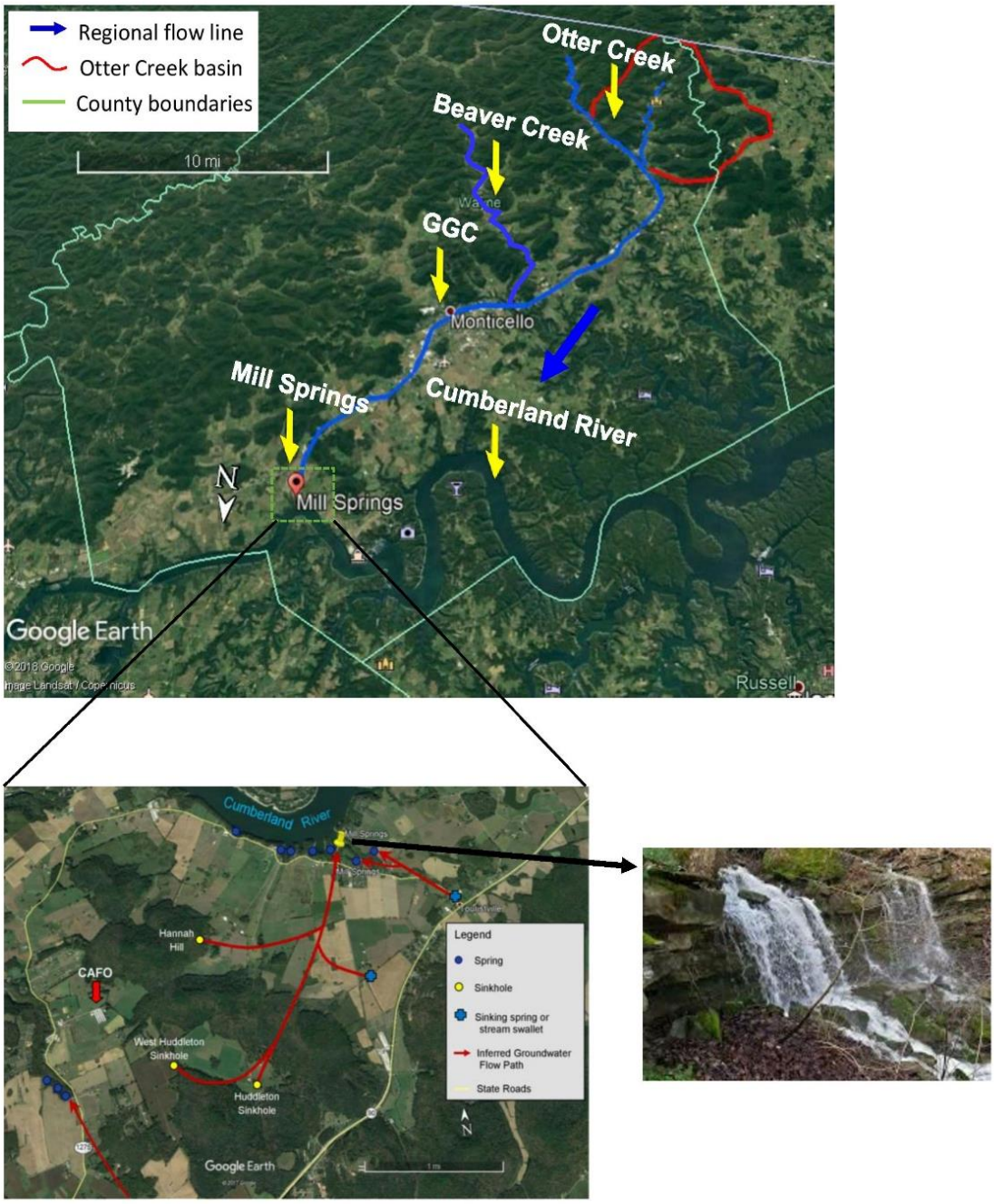


Figure 1: General location of the Mill Springs, Grayson Gunnar Cave (GGC) and Otter Creek basins in the Cumberland Plateau physiographic region and regional flow direction (blue arrow) along a decreasing altitude gradient from the headwaters (Otter Creek) to the edge of the escarpment and convergence with the Cumberland River to Mill Springs. A. Inferred groundwater flowpath (red arrows) from dye tracer injections in sinkholes and dye recovery at Mill Springs (data source: Kentucky Division of Water). B. Cascade on Meadow Creek at Mill Springs near Lake Cumberland (Source: Mill Spring Park).

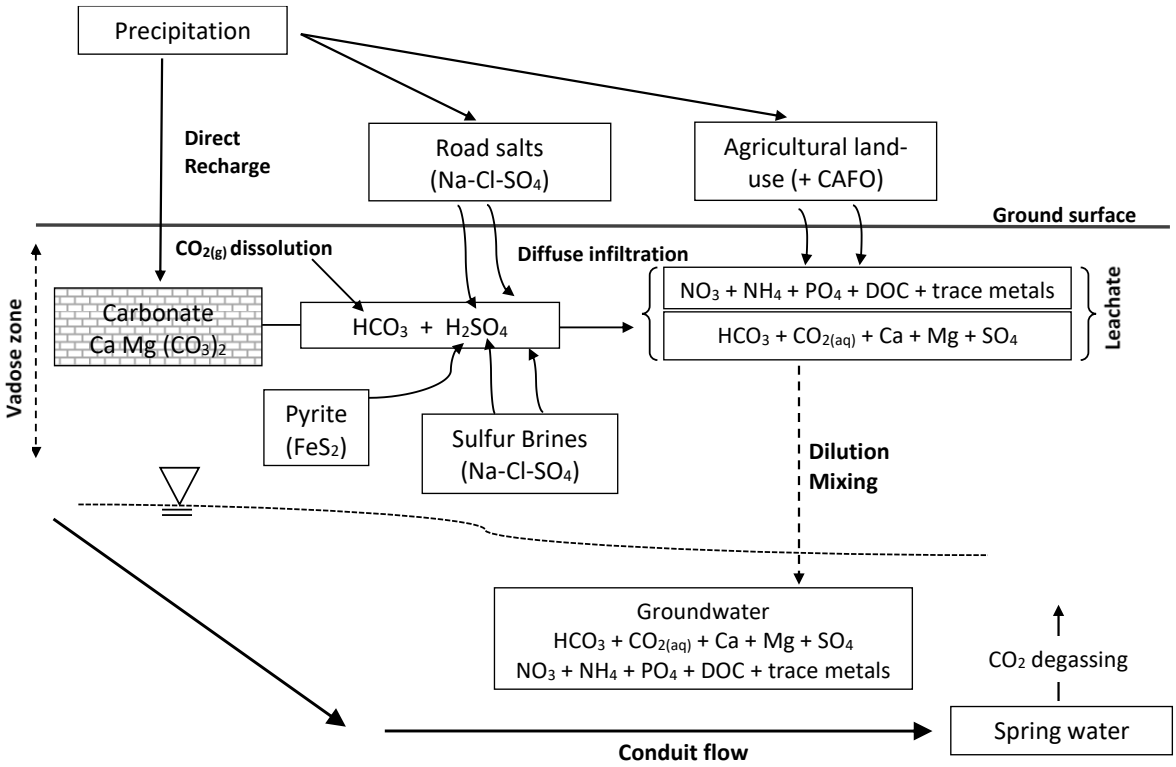


Figure 2: Conceptual model of end-member sources of groundwater chemistry in the Cumberland Escarpment. Mixing model defined based on general geochemical understanding of Cumberland Plateau karst aquifers. The spring water is a mixed proportion of reactions between 4 primary end-members (precipitation, surface and subsurface brines, carbonate weathering and agricultural land-use) that define groundwater evolution.

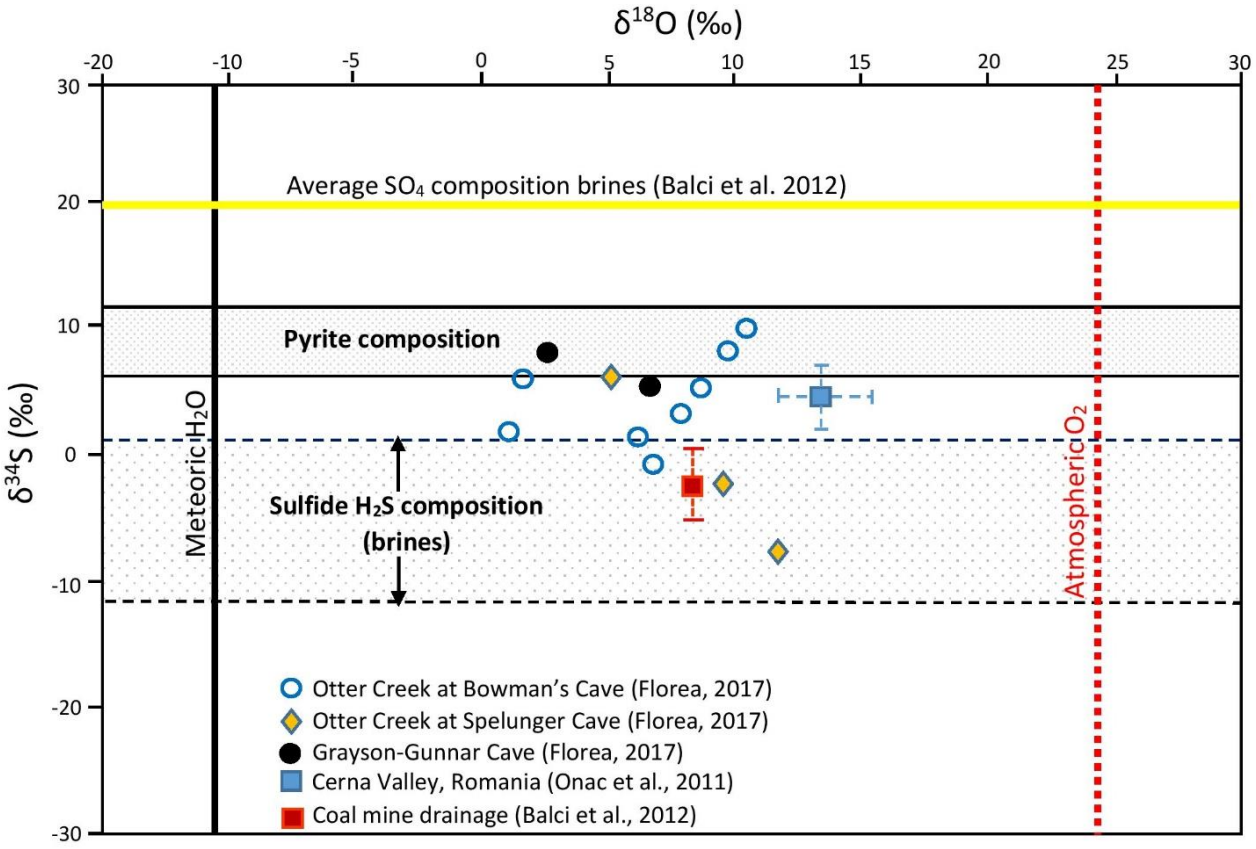


Figure 3: End-member sources of sulfur involved in sulfuric-acid speleogenesis in carbonate and acid mine drainage settings. Isotope composition of gypsum samples at Bowman's cave, Spelunger cave and Grayson-Gunnar Cave describes a combination of two primary end-member processes in the Cumberland platform of Southeastern Kentucky: pyrite oxidation and sulfide hydrolysis/oxidation of deep brines.

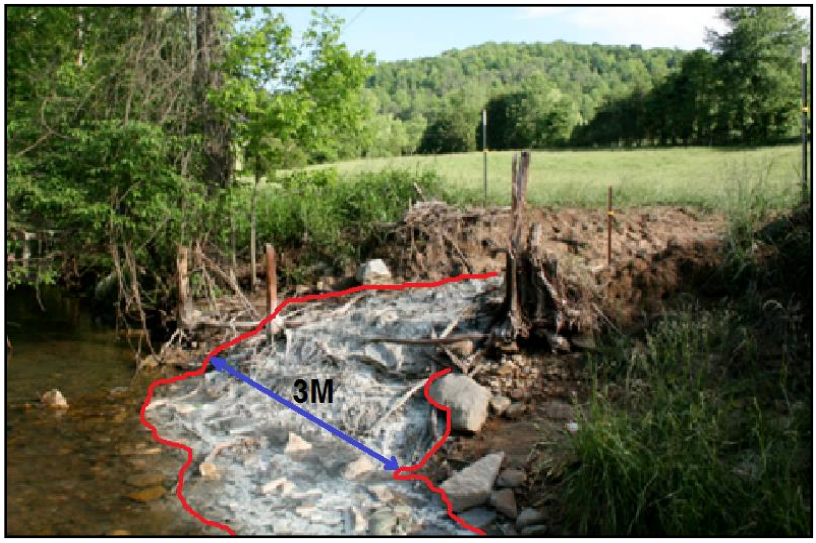


Figure 4: A view of microbial mat (in white) developed on a sulfur seepage around an abandoned petroleum well along Beaver Creek and Oilton (Kentucky), 20 miles South of the Mill Springs area toward Otter Creek (see Fig. 1)

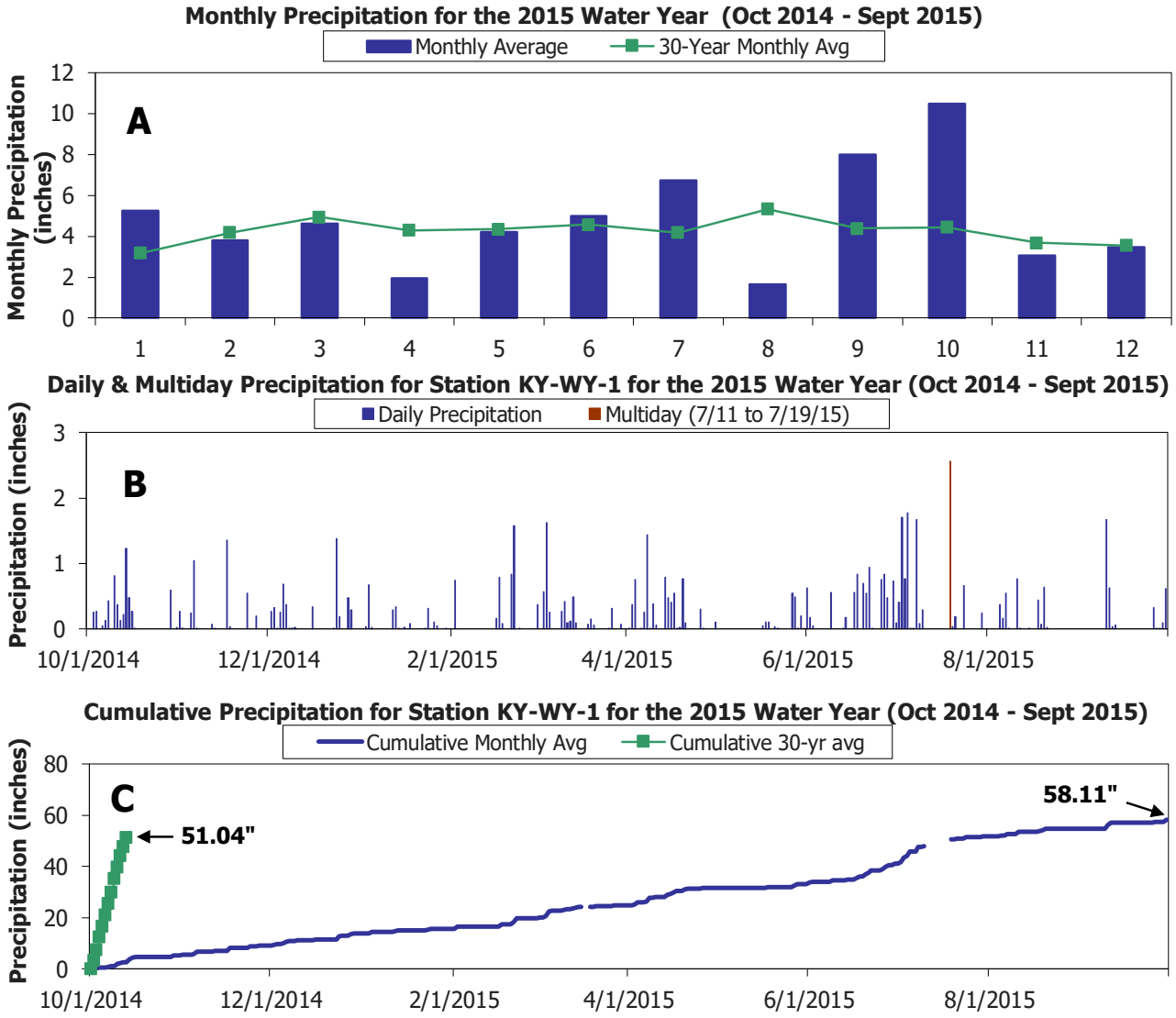


Figure 5: Precipitation data for the hydrological year 2015 from the Beaver Creek Gauging Station (USGS #KY-WY-1).

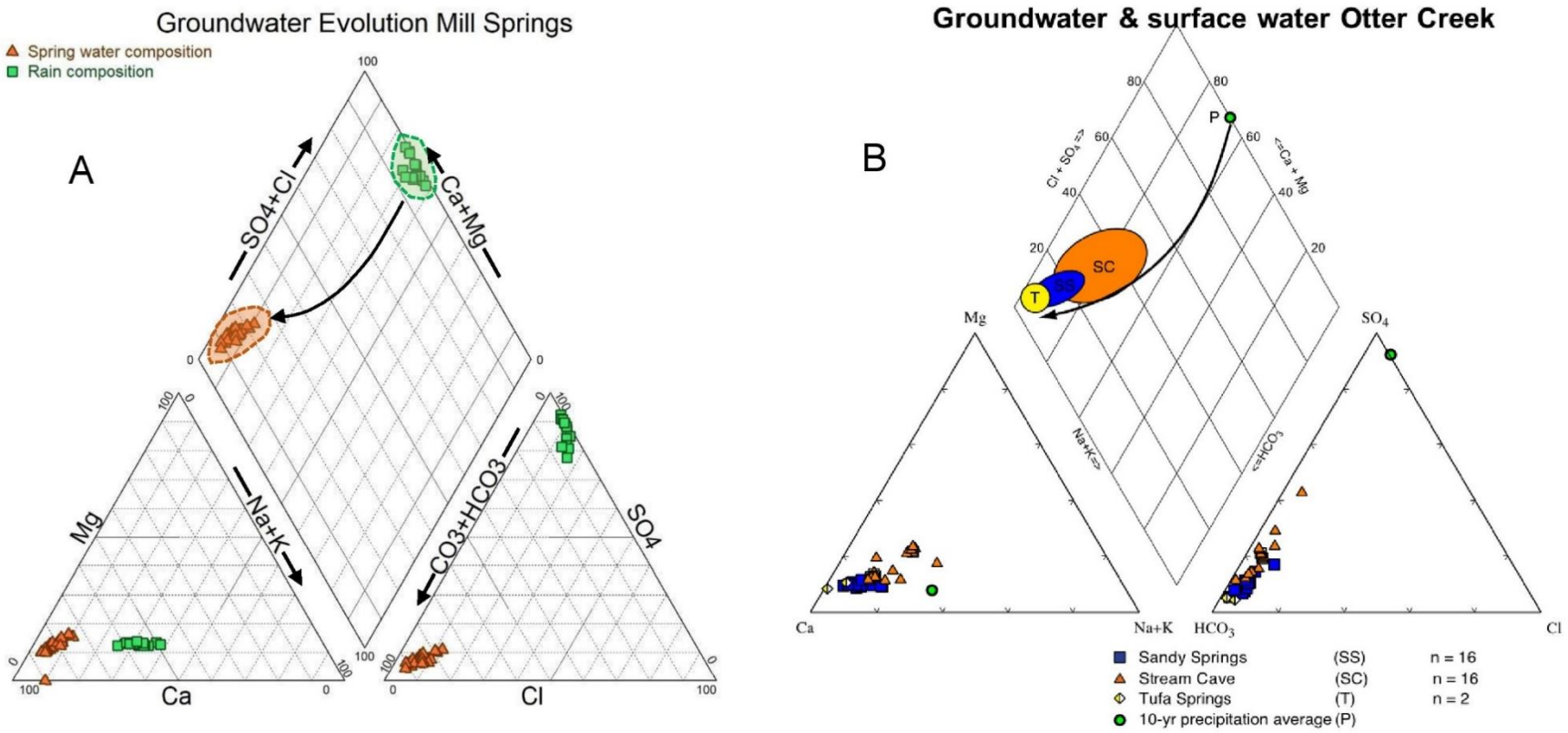


Figure 6: Piper diagram showing carbonate groundwater evolution from rainfall infiltration to the spring at A. Mill Springs and B various locations within the Otter Creek watersheds (Dugan et al., 2012).

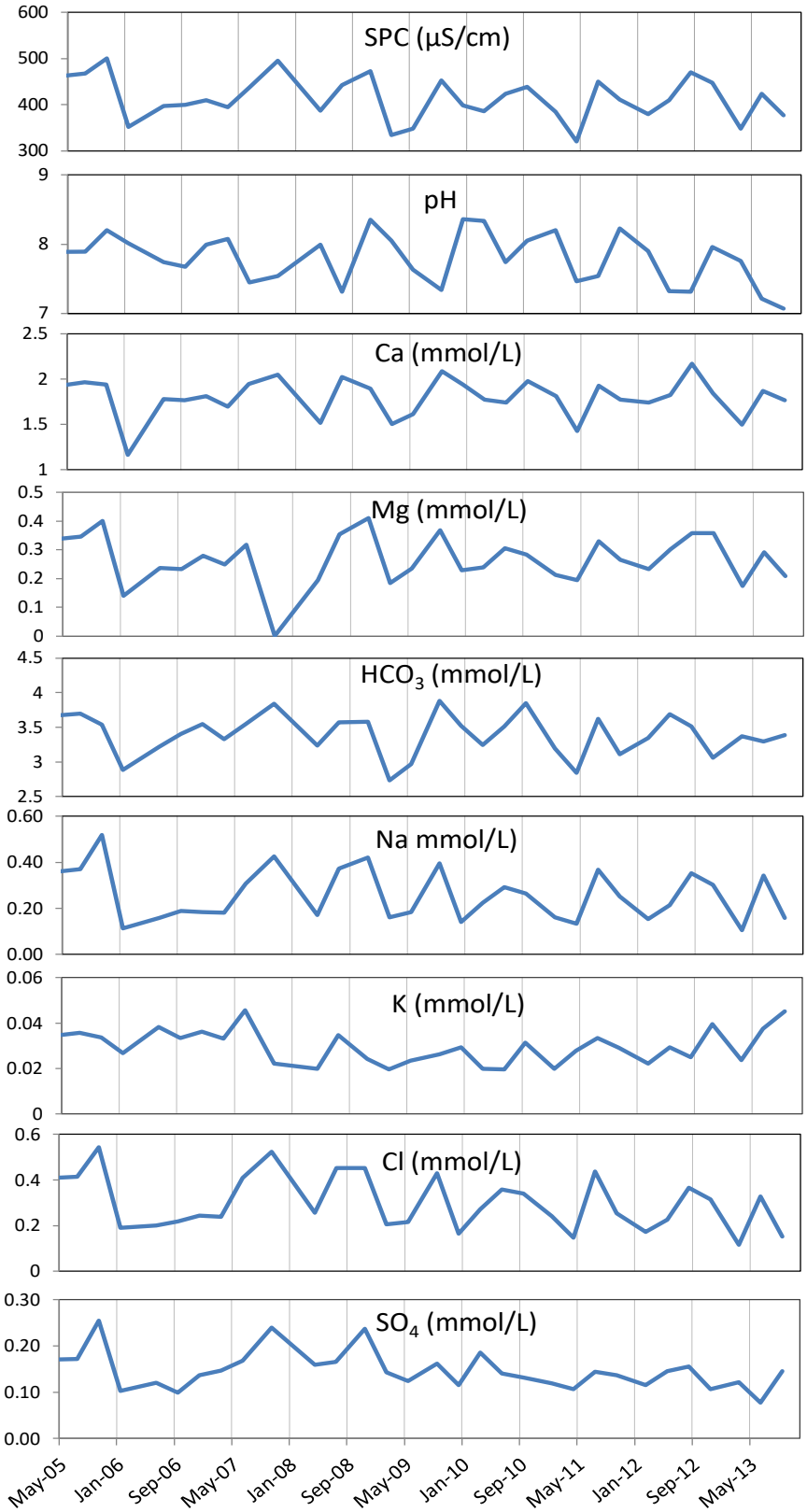


Figure 7: Long-term trends in pH, specific conductivity and major ion chemistry (2005-2013) from quarterly measurements at Mill Springs.

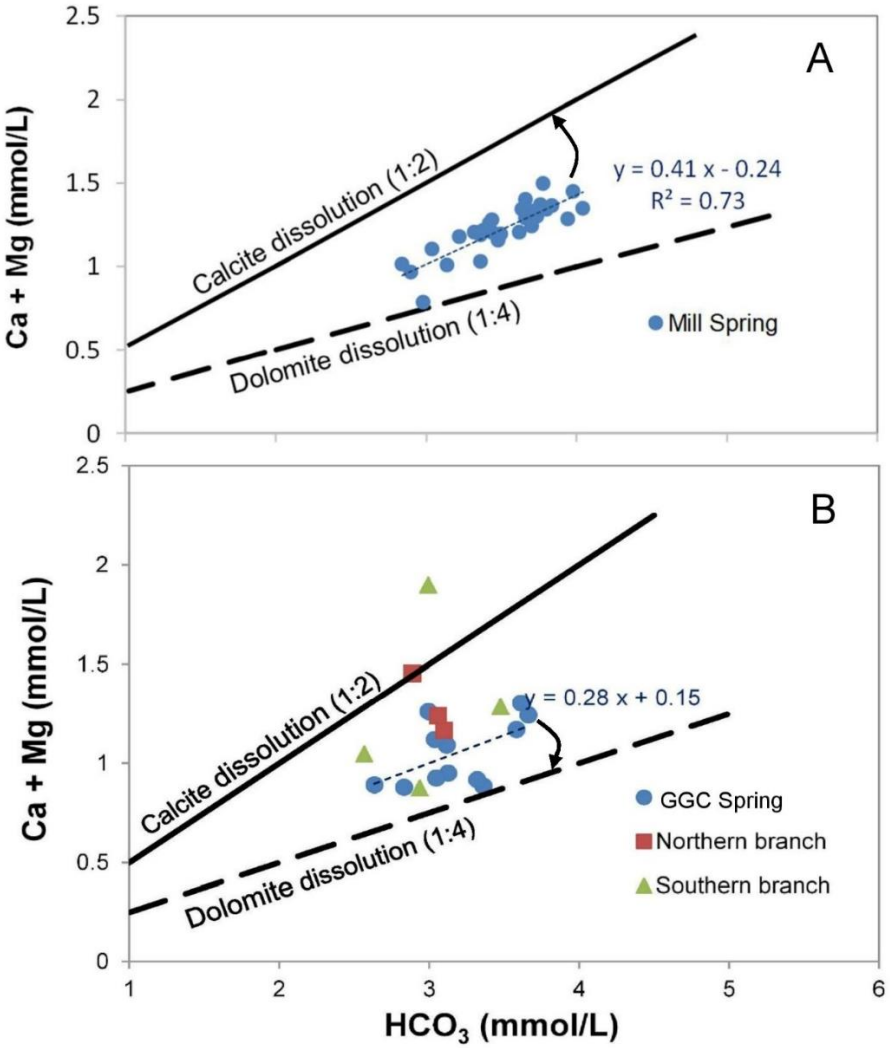


Figure 8: Comparison of carbonate dissolution kinetics between Mill Springs (A) and Grayson Gunnar (B) using Ca+Mg and HCO3 scatter plots, and Ca+Mg/HCO3 ratios.

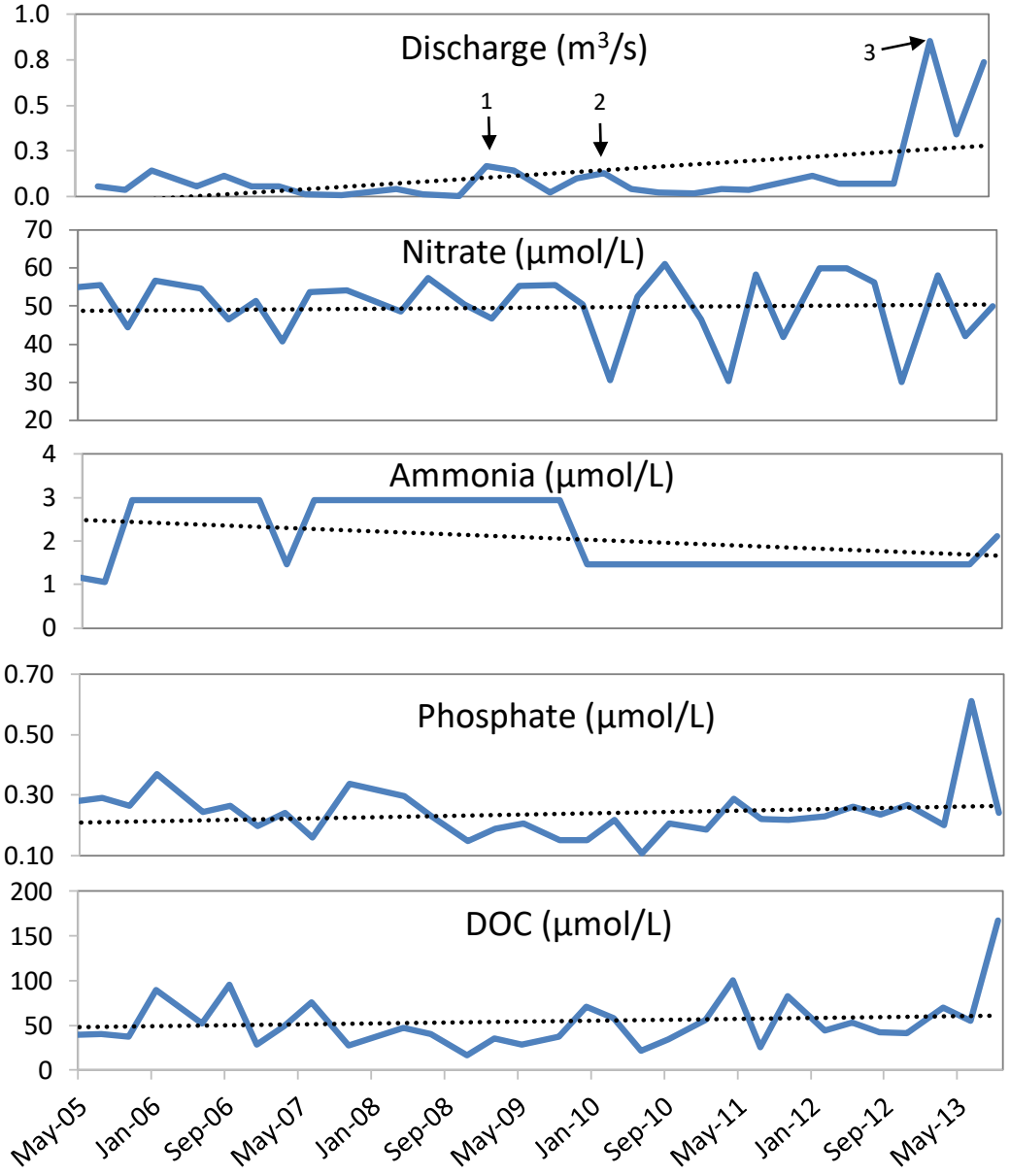


Figure 9: Long-term trends in nutrients and DOC concentrations (2005-2013) from quarterly measurements at Mill Springs.

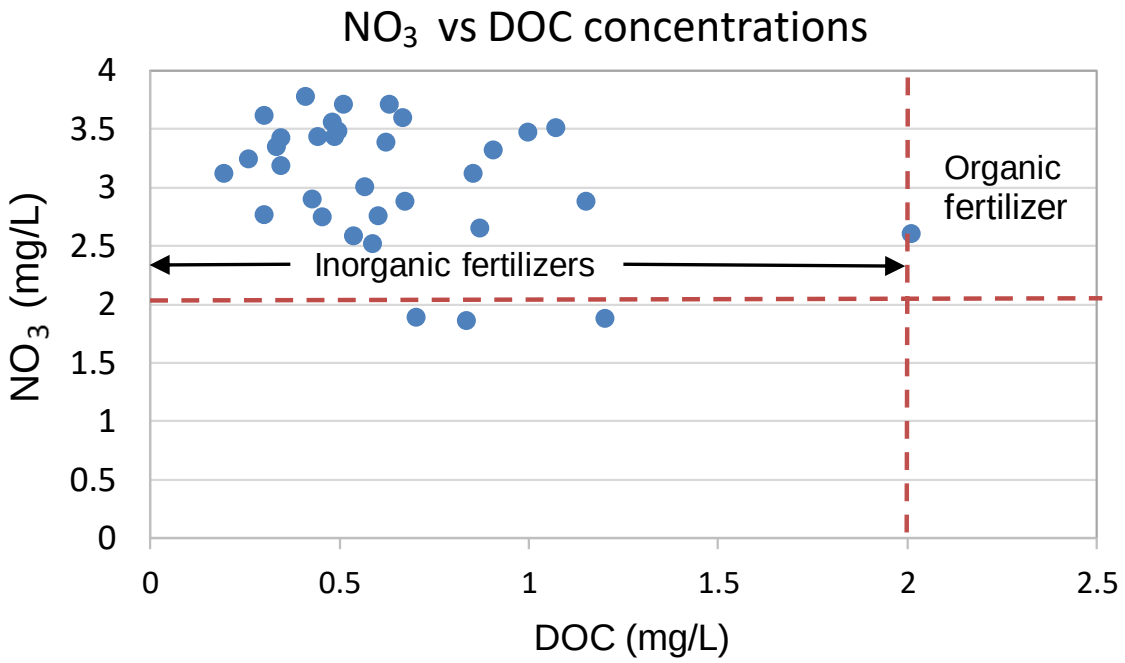


Figure 10: Nitrate and DOC regression for quarterly water samples collected at Mill Springs from 2000 to 2013. Red lines represent present-day background concentrations of $NO_3$ and DOC for primarily agricultural land-uses (fertilized croplands).

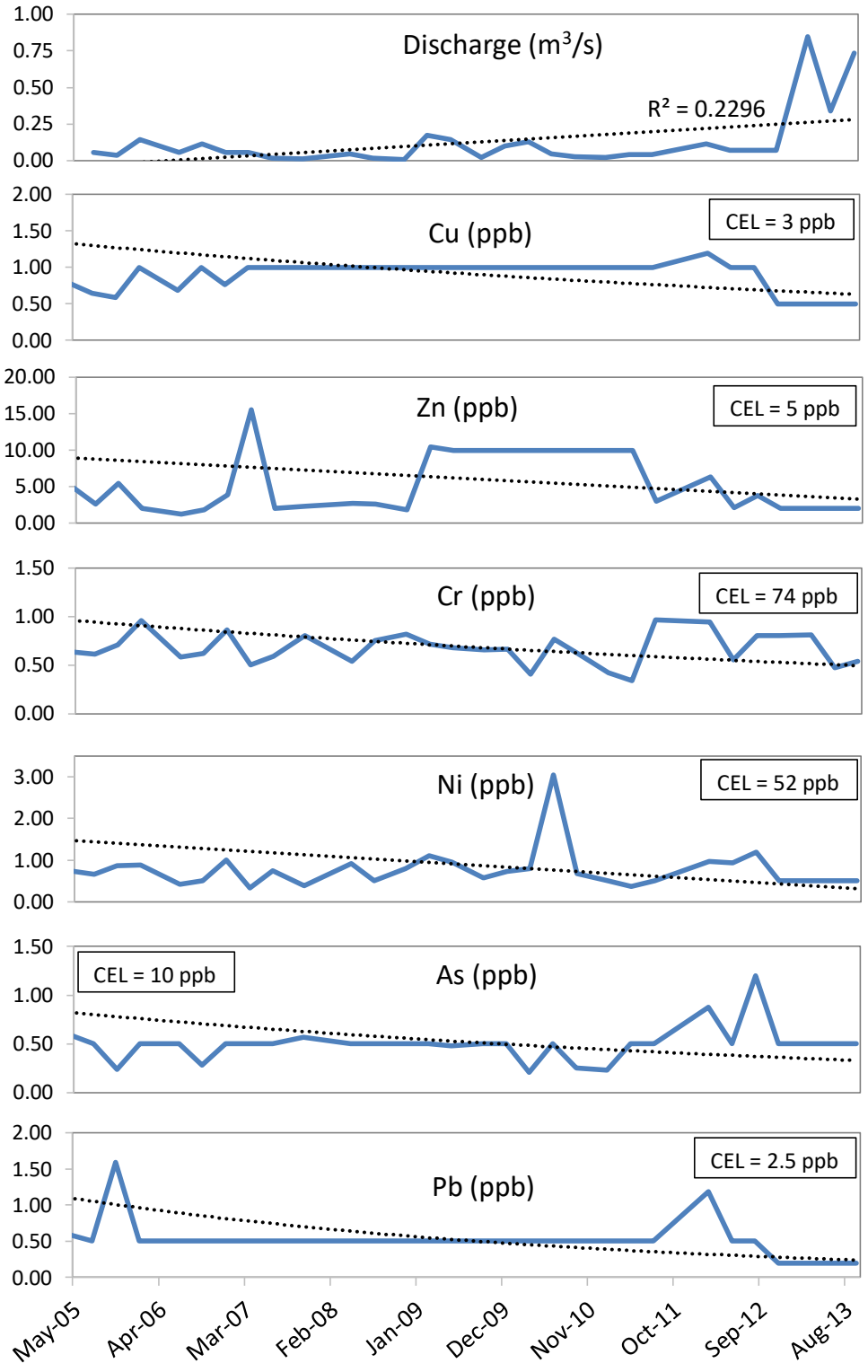


Figure 11: Long-term trends in trace metal concentrations (2005-2013) from quarterly measurements at Mill Springs.

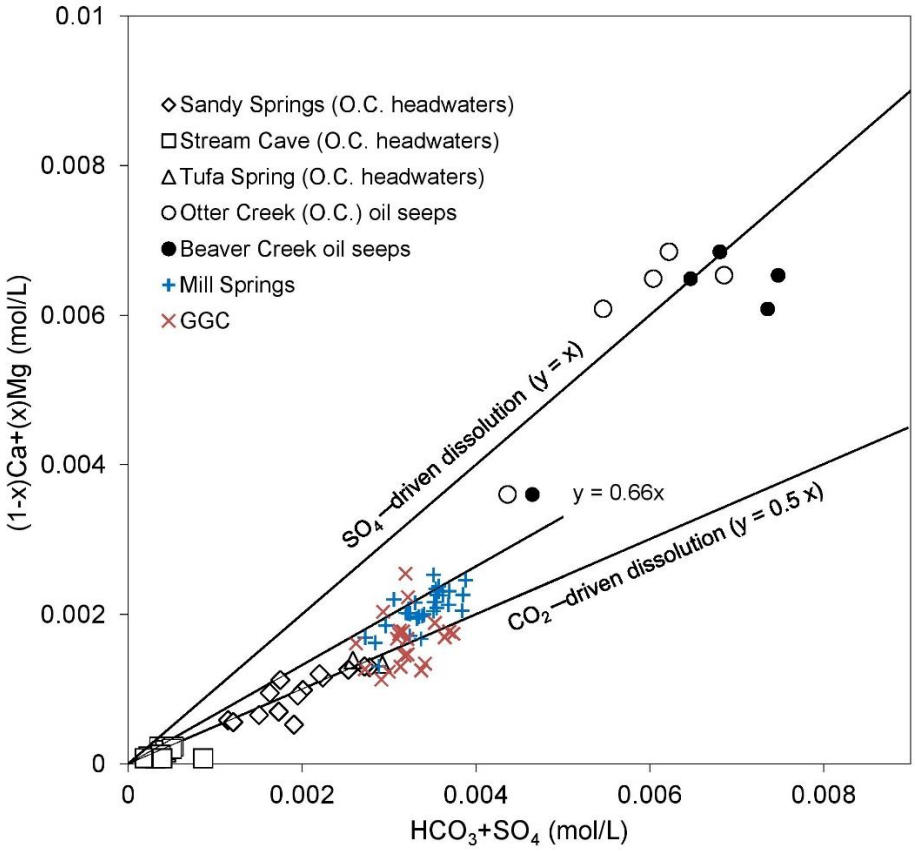


Figure 12: Diagram showing concentrations of Ca, Mg, $HCO_3$ and $SO_4$ from quarterly samples collected at Mill Springs from 2005-2013. Data fall between ranges for both traditional ($CO_2$-driven) and non-traditional ($SO_4$-driven) carbonate dissolution pathways suggesting the potential existence of two mechanisms.

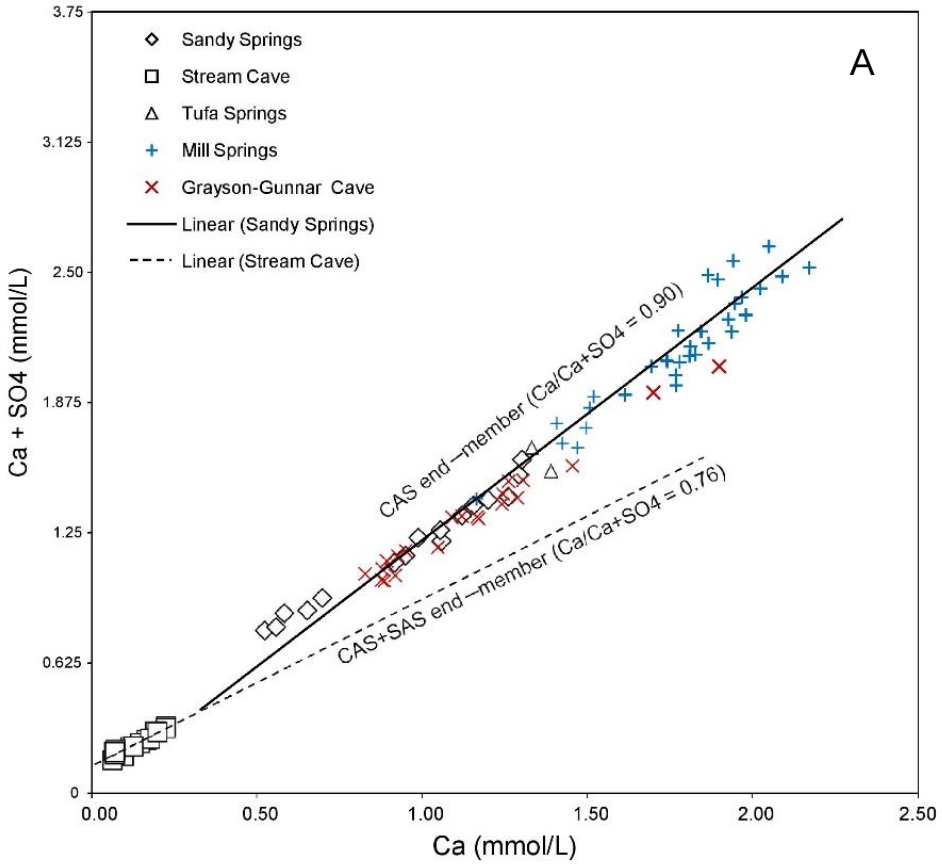
A
Sandy Springs
Stream Cave
Tufa Springs
Mill Springs
Grayson-Gunnar Cave
Linear (Sandy Springs)
Linear (Stream Cave)
CAS end–member (Ca/Ca+SO4 = 0.90)
CAS+SAS end–member (Ca/Ca+SO4 = 0.76)
Ca + SO4 (mmol/L)
Ca (mmol/L)
3.75
3.125
2.50
1.875
1.25
0.625
0
0.00
0.50
1.00
1.50
2.00
2.50

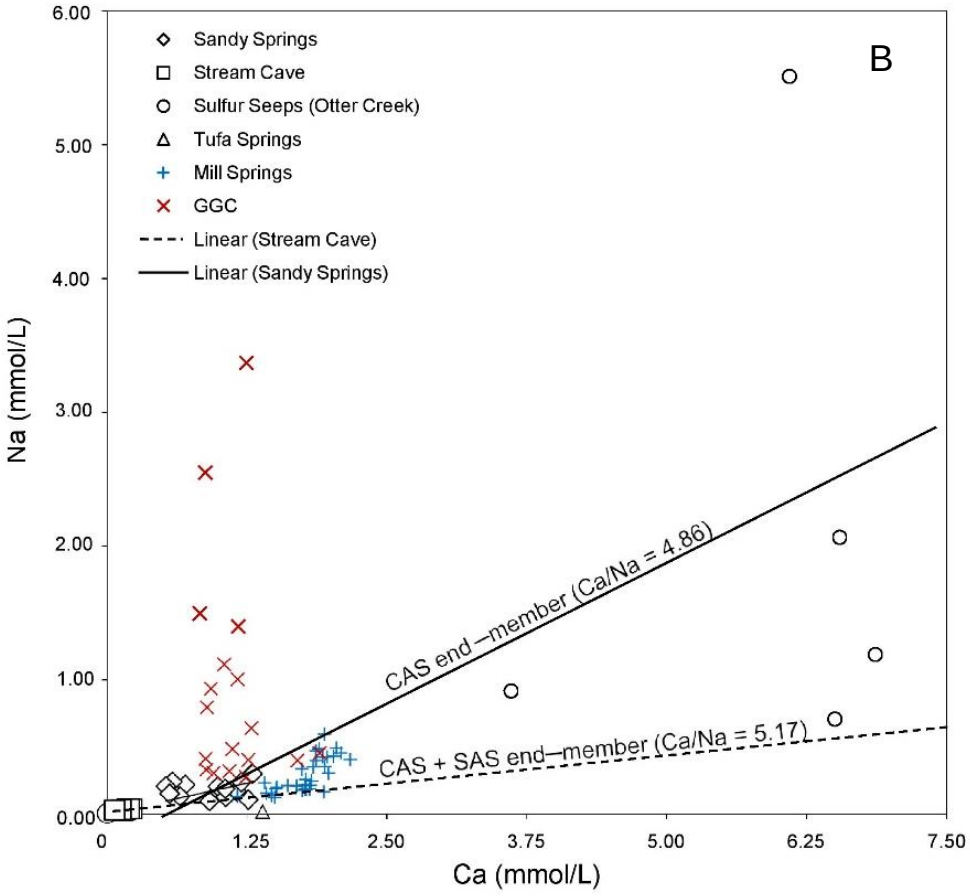
B
Sandy Springs
Stream Cave
Sulfur Seeps (Otter Creek)
Tufa Springs
Mill Springs
GGC
Linear (Stream Cave)
Linear (Sandy Springs)
CAS end –member (Ca/Na = 4.86)
CAS + SAS end–member (Ca/Na = 5.17)
Na (mmol/L)
Ca (mmol/L)
6.00
5.00
4.00
3.00
2.00
1.00
0.00
0
1.25
2.50
3.75
5.00
6.25
7.50

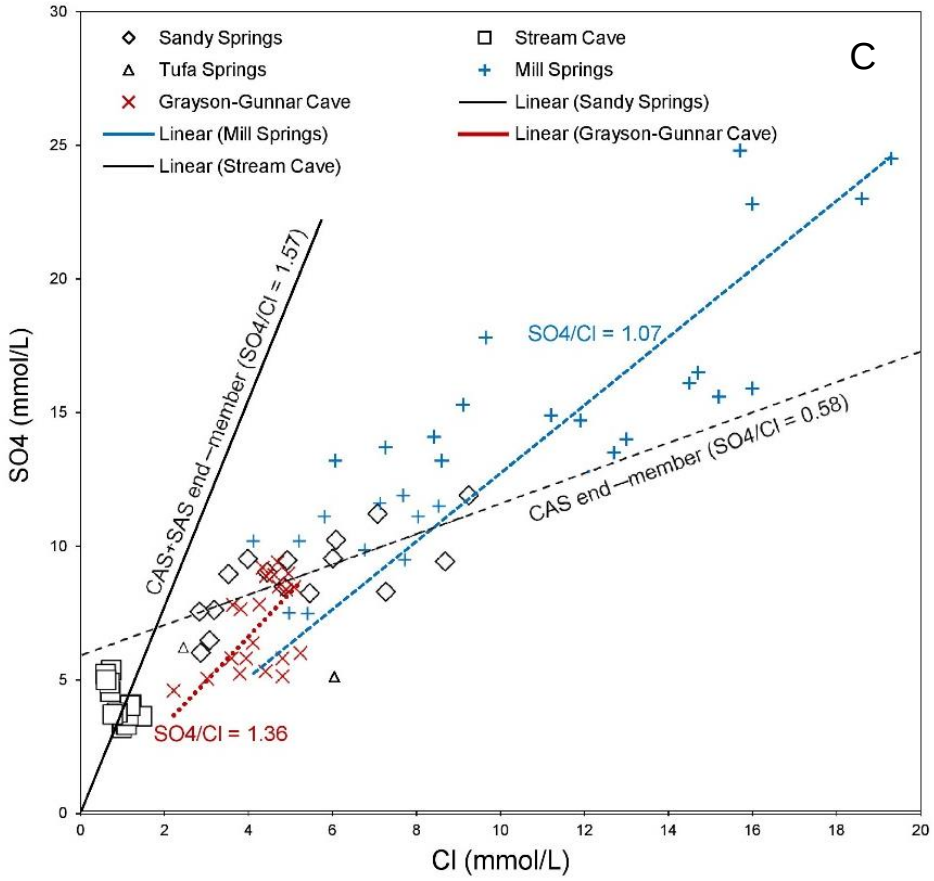
Sandy Springs
Tufa Springs
Grayson-Gunnar Cave
Linear (Mill Springs)
Linear (Stream Cave)
Stream Cave
Mill Springs
Linear (Sandy Springs)
Linear (Grayson-Gunnar Cave)
C
CAS+SAS end –member (SO4/Cl = 1.57)
SO4/Cl = 1.07
CAS end –member (SO4/Cl = 0.58)
SO4/Cl = 1.36
SO4 (mmol/L)
Cl (mmol/L)
0
5
10
15
20
25
30
0
2
4
6
8
10
12
14
16
18
20

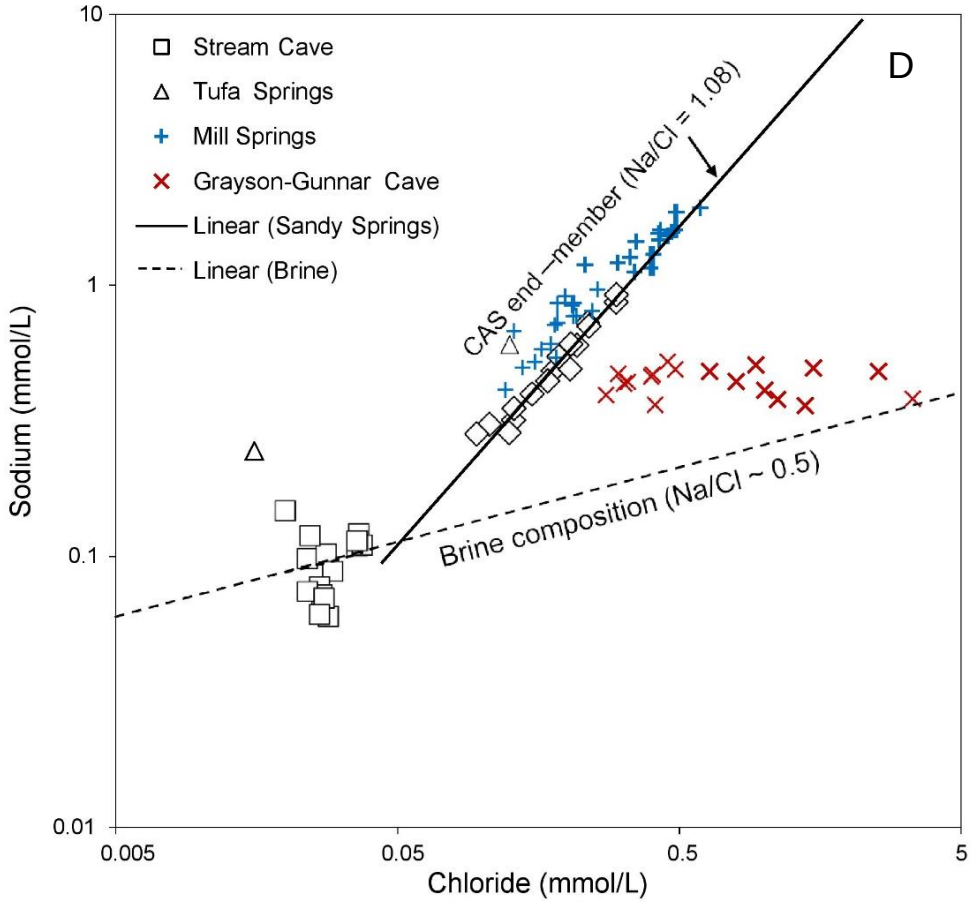
10
1
0.1
0.01
0.005
0.05
0.5
5
Sodium (mmol/L)
Chloride (mmol/L)
Stream Cave
Tufa Springs
Mill Springs
Grayson-Gunnar Cave
Linear (Sandy Springs)
Linear (Brine)
D
CAS end –member (Na/Cl = 1.08)
Brine composition (Na/Cl ~ 0.5)

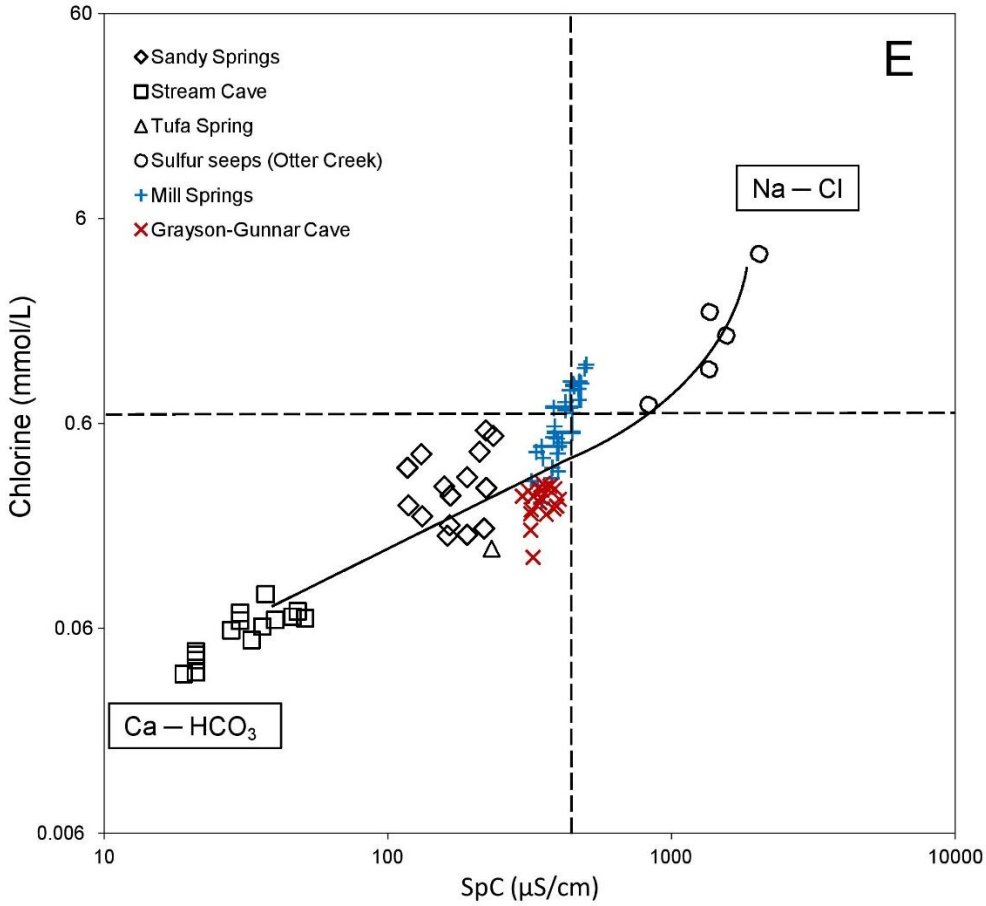


Figure 13: Scatter plots using molar concentrations (mmol/L) from quarterly water chemistry at Mill Springs (2005-2013), bimonthly measurements at Grayson-Gunnar Spring (2015-2016), and known concentrations at various locations in the Otter Creek watershed (Sandy Springs, Stream Cave and Tufa Springs). **A.** Ca and $Ca+SO_4$; **B.** Ca and Na; **C.** Cl and $SO_4$; **D.** Na and Cl; **E.** Cl and SPC. Dark plain and dark dotted lines represent the composition of end-member for a carbonic-acid driven dissolution (CAS; Eq.2) and mixed carbonic and sulfuric-acid driven dissolution (CAS +SAS; Eq.4). Molar ratios for each end-member is derived from median values shown in Table 3.

## Tables

Table 1: Synopsis of total Inorganic Nitrogen levels in agricultural and mixed-use watersheds

| Land-use | Total Nitrogen levels in groundwater (mg $NO_3$ / L) | Standards | Qualitative assessment | References |
|---|---|---|---|---|
| Forested | < 1 | Present-day background: 1-2 mg $NO_3$ / L | Below background | Hallberg (1989) |
| Unfertilized grasslands | < 0.1 | | Below background | Kemps and Dodds (2001) |
| **Primarily agricultural** | | | | |
| Fertilized croplands | 1.4 - 2.5 | | Above background | Panno et al. (2006); Kemps and Dodds (2001) |
| **Mixed CAFO-influenced** | | | | |
| Diffuse recharge/runoff from swine effluents sprayfields | 3.0 - 8.0 | EPA Maximum Contaminant Levels for drinking water: 10 mg / L | Above background | Westerman et al. (1995); Stone et al. (1995); MacDonald et al. (1995) |
| Direct leakage from swine wastes lagoons | 50 -100 | | Above MCL | Hutchins et al. (2012) |
| Cattle/sheep manure fertilized pastures | 3.0 - 10 | | Above background | Hooda et al. (1998a); Scholefield et al. (1993) |
| CAFO-affected cave aquifers | 2.0 -10 | | Above background | Brahana et al. (2014) |

*MCL= maximum level of a contaminant in drinking water without adverse effects on human health

*Background level= concentration of a contaminant in an area that is no longer affected by a contamination.

Table 2: Groundwater evolution from rain composition (average annual rain composition from 2000 to 2013, National Atmospheric Deposition Program) to the Spring (quarterly measurements from 2000 to 2013). Ionic balance and saturation indexes for calcite and dolomite are calculated using PHREEQ-C (version 2). A. Sample Location, Sample Date, Field Data, Cations, Anions, Charge Balance, Saturation Indexes (SI calcite and SI dolomite). B. Nutrients and metals.

A

| Sample Location | Sample Date | Discharge ($m^3/s$) | Field data | | Cations | | | | Anions | | | Charge Bal (%) | SI calcite | SI dolomite |
|---|---|---|---|---|---|---|---|---|---|---|---|---|---|---|
| | | | pH | Cond (µS/cm) | $Na^+$ (mmol/L) | $K^+$ (mmol/L) | $Mg^+$ (mmol/L) | $Ca^{2+}$ (mmol/L) | $Cl^-$ (mmol/L) | $SO_4^{2-}$ (mmol/L) | $HCO_3^-$ (mmol/L) | | | |
| Rain | 2000 | – | 4.59 | 16.12 | 0.003 | 0.001 | 0.001 | 0.003 | 0.003 | 0.016 | 0.021 | 7.6 | -6.83 | -14.18 |
| Rain | 2001 | – | 4.49 | 19.49 | 0.002 | 0.000 | 0.001 | 0.003 | 0.003 | 0.019 | 0.017 | – | -6.98 | -14.48 |
| Rain | 2002 | – | 4.72 | 14.05 | 0.004 | 0.001 | 0.001 | 0.003 | 0.004 | 0.015 | 0.029 | 7.4 | -6.73 | -13.9 |
| Rain | 2003 | – | 4.61 | 15.29 | 0.002 | 0.001 | 0.001 | 0.003 | 0.003 | 0.015 | 0.022 | 7.4 | -6.82 | -14.2 |
| Rain | 2004 | – | 4.69 | 12.71 | 0.003 | 0.001 | 0.001 | 0.002 | 0.003 | 0.012 | 0.027 | 8.7 | -6.91 | -14.27 |
| Rain | 2005 | – | 4.59 | 16.39 | 0.002 | 0.001 | 0.001 | 0.003 | 0.003 | 0.016 | 0.021 | 8.3 | -6.86 | -14.24 |
| Rain | 2006 | – | 4.63 | 14.89 | 0.003 | 0.001 | 0.001 | 0.003 | 0.004 | 0.016 | 0.023 | 6.7 | -6.75 | -14.02 |
| Rain | 2007 | – | 4.65 | 13.95 | 0.003 | 0.001 | 0.001 | 0.003 | 0.003 | 0.015 | 0.024 | 7.5 | -6.79 | -14.08 |
| Rain | 2008 | – | 4.74 | 12.05 | 0.004 | 0.001 | 0.001 | 0.003 | 0.004 | 0.013 | 0.030 | 6 | -6.67 | -13.84 |
| Rain | 2009 | – | 4.87 | 9.13 | 0.002 | 0.001 | 0.001 | 0.002 | 0.003 | 0.009 | 0.040 | 5.5 | -6.65 | -13.8 |
| Rain | 2010 | – | 4.96 | 8.21 | 0.002 | 0.000 | 0.001 | 0.002 | 0.003 | 0.008 | 0.050 | 5.5 | -6.58 | -13.67 |
| Rain | 2011 | – | 5.01 | 8.14 | 0.003 | 0.001 | 0.001 | 0.003 | 0.003 | 0.009 | 0.056 | 4.2 | -6.4 | -13.28 |
| Rain | 2012 | – | 5.09 | 7.5 | 0.002 | 0.001 | 0.001 | 0.003 | 0.002 | 0.008 | 0.067 | 4.9 | -6.38 | -13.28 |
| Rain | 2013 | – | 5.11 | 7.02 | 0.003 | 0.001 | 0.001 | 0.003 | 0.003 | 0.007 | 0.070 | 3.5 | -6.28 | -13.04 |
| Spring | 11/14/00 | – | 8.31 | 479 | 0.41 | 0.03 | 0.41 | 1.87 | 0.44 | 0.26 | 4.07 | – | – | – |
| Spring | 02/19/01 | – | 7.79 | 337 | 0.12 | 0.02 | 0.18 | 1.47 | 0.14 | 0.08 | 2.70 | – | – | – |
| Spring | 05/08/01 | – | 7.85 | 384 | 0.20 | 0.02 | 0.22 | 1.41 | 0.34 | 0.15 | 3.29 | – | – | – |
| Spring | 07/27/05 | 0.06 | 7.89 | 468 | 0.37 | 0.04 | 0.35 | 1.97 | 0.41 | 0.17 | 3.69 | 0.9 | -0.17 | -0.96 |
| Spring | 10/26/05 | 0.04 | 8.2 | 500 | 0.52 | 0.03 | 0.40 | 1.94 | 0.54 | 0.26 | 3.54 | 0.8 | -0.2 | -0.95 |
| Spring | 01/25/06 | 0.14 | 8.02 | 352 | 0.11 | 0.03 | 0.14 | 1.17 | 0.19 | 0.10 | 2.88 | 1.3 | -0.47 | -1.73 |
| Spring | 06/07/06 | 0.06 | 7.74 | 397 | 0.16 | 0.04 | 0.24 | 1.78 | 0.20 | 0.12 | 3.22 | 0.9 | -0.26 | -1.26 |
| Spring | 09/27/06 | 0.11 | 7.67 | 400 | 0.19 | 0.03 | 0.23 | 1.77 | 0.22 | 0.10 | 3.40 | 0.9 | -0.24 | -1.23 |
| Spring | 12/13/06 | 0.06 | 7.99 | – | 0.18 | 0.04 | 0.28 | 1.81 | 0.24 | 0.14 | 3.55 | 0.9 | -0.22 | -1.11 |
| Spring | 03/27/07 | 0.06 | 8.08 | 394 | 0.18 | 0.03 | 0.25 | 1.70 | 0.24 | 0.15 | 3.33 | 0.9 | -0.27 | -1.24 |
| Spring | 06/26/07 | 0.01 | 7.45 | 438 | 0.31 | 0.05 | 0.32 | 1.95 | 0.41 | 0.17 | 3.55 | 0.9 | -0.19 | -1.04 |
| Spring | 10/23/07 | 0.01 | 7.54 | 495 | 0.43 | 0.02 | 0.00 | 2.05 | 0.52 | 0.24 | 3.84 | 1.1 | -0.13 | -3.53 |
| Spring | 04/29/08 | 0.04 | 7.99 | 387 | 0.17 | 0.02 | 0.19 | 1.52 | 0.26 | 0.16 | 3.24 | 1.1 | -0.32 | -1.4 |
| Spring | 07/29/08 | 0.01 | 7.31 | 442 | 0.37 | 0.03 | 0.35 | 2.03 | 0.45 | 0.17 | 3.57 | 0.8 | -0.17 | -0.97 |
| Spring | 11/05/08 | 0.01 | 8.35 | 473 | 0.42 | 0.02 | 0.41 | 1.90 | 0.45 | 0.24 | 3.58 | 0.9 | -0.2 | -0.94 |
| Spring | 02/23/09 | 0.17 | 8.05 | 334 | 0.16 | 0.02 | 0.18 | 1.51 | 0.20 | 0.14 | 2.73 | 0.9 | -0.39 | -1.57 |
| Spring | 05/26/09 | 0.14 | 7.63 | 348 | 0.18 | 0.02 | 0.23 | 1.62 | 0.22 | 0.12 | 2.96 | 0.9 | -0.33 | -1.37 |
| Spring | 09/08/09 | 0.02 | 7.34 | 453 | 0.40 | 0.03 | 0.37 | 2.09 | 0.43 | 0.16 | 3.88 | 0.8 | -0.13 | -0.87 |
| Spring | 12/08/09 | 0.10 | 8.36 | 398 | 0.14 | 0.03 | 0.23 | 1.94 | 0.16 | 0.12 | 3.52 | 0.9 | -0.19 | -1.17 |
| Spring | 03/23/10 | 0.13 | 8.34 | 386 | 0.22 | 0.02 | 0.24 | 1.78 | 0.27 | 0.19 | 3.24 | 0.9 | -0.26 | -1.26 |
| Spring | 06/29/10 | 0.04 | 7.74 | 423 | 0.29 | 0.02 | 0.31 | 1.74 | 0.36 | 0.14 | 3.51 | 0.9 | -0.24 | -1.1 |
| Spring | 09/28/10 | 0.02 | 8.05 | 439 | 0.26 | 0.03 | 0.28 | 1.98 | 0.34 | 0.13 | 3.85 | 0.9 | -0.15 | -1.01 |
| Spring | 01/25/11 | 0.02 | 8.2 | 384 | 0.16 | 0.02 | 0.21 | 1.81 | 0.24 | 0.12 | 3.19 | 0.9 | -0.26 | -1.31 |
| Spring | 04/25/11 | 0.04 | 7.46 | 320 | 0.13 | 0.03 | 0.20 | 1.43 | 0.15 | 0.11 | 2.84 | 0.9 | -0.4 | -1.53 |
| Spring | 07/26/11 | 0.04 | 7.54 | 450 | 0.37 | 0.03 | 0.33 | 1.93 | 0.44 | 0.14 | 3.62 | 0.9 | -0.19 | -1.01 |
| Spring | 02/28/12 | 0.11 | 7.9 | 379 | 0.15 | 0.02 | 0.23 | 1.74 | 0.17 | 0.14 | 3.34 | 0.8 | -0.28 | -1.31 |
| Spring | 05/30/12 | 0.07 | 7.32 | 410 | 0.21 | 0.03 | 0.30 | 1.83 | 0.23 | 0.12 | 3.69 | 0.8 | -0.24 | -1.12 |
| Spring | 08/28/12 | 0.07 | 7.31 | 470 | 0.35 | 0.02 | 0.36 | 2.17 | 0.37 | 0.15 | 3.51 | 0.8 | -0.13 | -0.91 |
| Spring | 11/27/12 | 0.07 | 7.96 | 447 | 0.30 | 0.04 | 0.36 | 1.85 | 0.32 | 0.16 | 3.06 | 0.9 | -0.22 | -1.01 |
| Spring | 03/27/13 | 0.85 | 7.76 | 348 | 0.11 | 0.02 | 0.17 | 1.50 | 0.12 | 0.11 | 3.37 | 1 | -0.35 | -1.49 |
| Spring | 06/25/13 | 0.34 | 7.21 | 423 | 0.34 | 0.04 | 0.29 | 1.87 | 0.33 | 0.12 | 3.30 | 0.8 | -0.23 | -1.13 |
| Spring | 09/03/13 | 0.74 | 7.07 | 377 | 0.16 | 0.05 | 0.21 | 1.77 | 0.15 | 0.08 | 3.38 | 0.9 | -0.25 | -1.3 |

B

| Sample Location | Sample Date | Nutrients | | | | Metals | | | |
|---|---|---|---|---|---|---|---|---|---|
| | | $NO_3^-$ (µmol/L) | $NH_4^+$ (µmol/L) | $PO_4^{3-}$ (mmol/L) | DOC (µmol/L) | $As^{5+}$ (ppb) | $Cu^{2+}$ (ppb) | $Zn^{2+}$ (ppb) | $Pb^{2+}$ (mg/L) |
| Rain | 2000 | 0.018 | 0.26 | – | – | – | – | – | – |
| Rain | 2001 | 0.020 | 0.31 | – | – | – | – | – | – |
| Rain | 2002 | 0.016 | 0.28 | – | – | – | – | – | – |
| Rain | 2003 | 0.017 | 0.27 | – | – | – | – | – | – |
| Rain | 2004 | 0.013 | 0.21 | – | – | – | – | – | – |
| Rain | 2005 | 0.016 | 0.30 | – | – | – | – | – | – |
| Rain | 2006 | 0.016 | 0.30 | – | – | – | – | – | – |
| Rain | 2007 | 0.015 | 0.32 | – | – | – | – | – | – |
| Rain | 2008 | 0.014 | 0.26 | – | – | – | – | – | – |
| Rain | 2009 | 0.010 | 0.20 | – | – | – | – | – | – |
| Rain | 2010 | 0.010 | 0.21 | – | – | – | – | – | – |
| Rain | 2011 | 0.011 | 0.25 | – | – | – | – | – | – |
| Rain | 2012 | 0.012 | 0.31 | – | – | – | – | – | – |
| Rain | 2013 | 0.010 | 0.24 | – | – | – | – | – | – |
| Spring | 11/14/00 | 44.51 | 1.17 | 0.21 | 49.96 | 10.00 | 9.00 | 2.00 | 20.00 |
| Spring | 02/19/01 | 42.74 | 2.93 | 0.14 | 72.44 | 2.00 | 1.00 | 7.00 | 2.00 |
| Spring | 05/08/01 | 44.67 | 2.93 | 0.09 | 24.98 | 2.00 | 3.00 | 42.00 | 2.00 |
| Spring | 07/27/05 | 55.48 | 1.06 | 0.29 | 40.38 | 0.50 | 0.64 | 2.56 | 0.50 |
| Spring | 10/26/05 | 44.35 | 2.93 | 0.26 | 37.80 | 0.23 | 0.59 | 5.42 | 1.59 |
| Spring | 01/25/06 | 56.61 | 2.93 | 0.37 | 89.09 | 0.50 | 1.00 | 2.00 | 0.50 |
| Spring | 06/07/06 | 54.67 | 2.93 | 0.24 | 51.79 | 0.50 | 0.69 | 1.25 | 0.50 |
| Spring | 09/27/06 | 46.45 | 2.93 | 0.26 | 95.75 | 0.28 | 1.00 | 1.82 | 0.50 |
| Spring | 12/13/06 | 51.45 | 2.93 | 0.20 | 28.56 | 0.50 | 0.76 | 3.84 | 0.50 |
| Spring | 03/27/07 | 40.64 | 1.47 | 0.24 | 48.88 | 0.50 | 1.00 | 15.50 | 0.50 |
| Spring | 06/26/07 | 53.54 | 2.93 | 0.16 | 75.35 | 0.50 | 1.00 | 2.00 | 0.50 |
| Spring | 10/23/07 | 54.03 | 2.93 | 0.34 | 27.64 | 0.57 | 1.00 | 2.28 | 0.50 |
| Spring | 04/29/08 | 48.55 | 2.93 | 0.29 | 47.13 | 0.50 | 1.00 | 2.67 | 0.50 |
| Spring | 07/29/08 | 57.42 | 2.93 | 0.23 | 39.88 | 0.50 | 1.00 | 2.57 | 0.50 |
| Spring | 11/05/08 | 50.32 | 2.93 | 0.15 | 16.07 | 0.50 | 1.00 | 1.82 | 0.50 |
| Spring | 02/23/09 | 46.77 | 2.93 | 0.19 | 35.47 | 0.50 | 1.00 | 10.40 | 0.50 |
| Spring | 05/26/09 | 55.32 | 2.93 | 0.20 | 28.64 | 0.48 | 1.00 | 10.00 | 0.50 |
| Spring | 09/08/09 | 55.48 | 2.93 | 0.15 | 36.89 | 0.50 | 1.00 | 10.00 | 0.50 |
| Spring | 12/08/09 | 50.32 | 1.47 | 0.15 | 70.94 | 0.50 | 1.00 | 10.00 | 0.50 |
| Spring | 03/23/10 | 30.48 | 1.47 | 0.22 | 58.37 | 0.21 | 1.00 | 10.00 | 0.50 |
| Spring | 06/29/10 | 52.42 | 1.47 | 0.11 | 21.65 | 0.50 | 1.00 | 10.00 | 0.50 |
| Spring | 09/28/10 | 60.96 | 1.47 | 0.21 | 33.97 | 0.25 | 1.00 | 10.00 | 0.50 |
| Spring | 01/25/11 | 46.45 | 1.47 | 0.19 | 55.87 | 0.23 | 1.00 | 10.00 | 0.50 |
| Spring | 04/25/11 | 30.32 | 1.47 | 0.29 | 99.92 | 0.50 | 1.00 | 10.00 | 0.50 |
| Spring | 07/26/11 | 58.38 | 1.47 | 0.22 | 25.06 | 0.50 | 1.00 | 3.00 | 0.50 |
| Spring | 02/28/12 | 59.83 | 1.47 | 0.23 | 44.55 | 0.50 | 1.00 | 2.08 | 0.50 |
| Spring | 05/30/12 | 59.83 | 1.47 | 0.26 | 52.62 | 1.20 | 1.00 | 3.81 | 0.50 |
| Spring | 08/28/12 | 56.13 | 1.47 | 0.23 | 42.55 | 0.50 | 0.50 | 2.00 | 0.20 |
| Spring | 11/27/12 | 30.00 | 1.47 | 0.27 | 41.22 | 0.50 | 0.50 | 2.00 | 0.20 |
| Spring | 03/27/13 | 58.06 | 1.47 | 0.20 | 69.44 | 0.50 | 0.50 | 2.00 | 0.20 |
| Spring | 06/25/13 | 42.09 | 1.47 | 0.61 | 55.54 | 0.50 | 0.50 | 2.00 | 0.20 |
| Spring | 09/03/13 | 49.94 | 2.11 | 0.24 | 167.36 | 0.50 | 0.50 | 2.00 | 0.20 |

Table 3: Physical and ionic composition of end-member mixing sources (brines and carbonate bedrock) in Wayne County (Kentucky). Brine composition is estimated using historical and recent oil and gas well production data in Mississipian and Pennsylvanian carbonates (Krieger et al., 1957; Dresel and Rose, 2010; KGS, 2019) and average concentrations of bimonthly water samples collected between 2010 and 2012 near sulfur seeps in the Beaver and Otter Creek watersheds (Florea, 2013). Carbonate bedrock composition is reflected from the analysis of gypsum samples collected near Sandy Springs and Stream Cave in the headwaters of Otter Creek above sulfur seeps.

| | | Regional Brine Composition | | | | | Bedrock composition | |
|---|---|---|---|---|---|---|---|---|
| | Parameters | Dresel and Rose (2010) | Krieger et al. (1957) | Newman's Ls. KGS (2019) | Beaver Creek (Florea, 2013) | Otter Creek (Florea, 2013) | Sandy Springs (Otter Creek) | Stream Cave (Otter Creek) |
| Physical data | Temperature(°C) | 16 | – | – | 14 | 11 | 13 | 12 |
| | Conductivity (µS/cm) | 158608 | – | – | – | – | – | 32 |
| | TDS (mmol/L) | 4275 | 3444 | 2102 | 16.11 | 26.65 | 3.234 | 0.643 |
| | pH | 6 | – | 7 | 6.89 | 7.32 | 7.71 | 7.26 |
| Cations | Ca (mmol/L) | 441 | 318 | 71 | 5.51 | 7.37 | **0.857** | **0.131** |
| | Mg (mmol/L) | 52 | 85 | 37 | 0.91 | 0.60 | 0.165 | 0.048 |
| | Na (mmol/L) | **1139** | **853** | **675** | 2.21 | – | 0.176 | 0.025 |
| | K (mmol/L) | 21 | 24 | 4 | 0.06 | – | 0.021 | 0.015 |
| Anions | $HCO_3$ (mmol/L) | 4 | 4 | 8 | 2.97 | 3.73 | **1.755** | **0.350** |
| | $SO_4$ (mmol/L) | 4 | 27 | 32 | **3.36** | **7.63** | 0.094 | 0.042 |
| | Fl (mmol/L) | 0.16 | – | 0.28 | 0.02 | – | 0.005 | 0.004 |
| | Cl (mmol/L) | **2614** | **2136** | **1275** | 1.08 | – | 0.163 | 0.027 |
| | Br (mmol/L) | – | – | – | – | – | – | – |
| | I (mmol/L) | – | – | – | – | – | – | – |
| End-member composition and molar ratios | Dominant cation-anion | Na-Cl | Na-Cl | Na-Cl | Na-$SO_4$ | $SO_4$ | Ca-$HCO_3$ | Ca-$HCO_3$ |
| | % of ionic balance dominant cation-anion | 88 | 87 | 93 | 35 | 29 | 81 | 75 |
| | Ca/Ca+$SO_4$ | 0.99 | 0.92 | 0.69 | 0.62 | 0.49 | 0.90 | 0.76 |
| | Ca/Na | 0.39 | 0.37 | 0.11 | 2.49 | – | 4.87 | 5.17 |
| | $SO_4$/Cl | 0.00 | 0.01 | 0.02 | 3.12 | – | 0.58 | 1.57 |
| | Na/Cl | 0.44 | 0.40 | 0.53 | 2.05 | – | 1.08 | 0.94 |

Table 4: Results of t-test before and after change corn-soybean reveal no major influence of crop changes on nutrient variability at the spring.

| | Before 2009 | After 2009 |
|---|---|---|
| **$NO_3$** | | |
| Mean | 3.195 | 3.046 |
| Variance | 0.105 | 0.600 |
| Observations | 12 | 12 |
| P-value | 0.544 | |
| | | |
| **$NH_4$** | | |
| Mean | 0.045 | 0.025 |
| Variance | 0.000 | 0.000 |
| Observations | 12 | 12 |
| P-value | **$6.11 \times 10^{-5}$** | |
| | | |
| **$PO_4$** | | |
| Mean | 0.024 | 0.021 |
| Variance | 0.000 | 0.000 |
| Observations | 12 | 12 |
| P-value | 0.166 | |

Table 5: Results of correlation analyses and ANOVA between TIN and trace metal concentrations reveal no apparent control of CAFO wastes in the spring water chemistry.

| Statistics | **Cu** | **Zn** | **Pb** |
|---|---|---|---|
| Correlation coefficient | 0.134 | 0.219 | 0.135 |
| Standard Error | 0.537 | 0.529 | 0.537 |
| F-significance (ANOVA) | 0.465 | 0.229 | 0.462 |
| Observations | 32 | 32 | 32 |

# CHAPTER 6.

# GENERAL CONCLUSIONS AND FUTURE WORK

The general purpose of this work was to generate sound evidence for use by water and land-use managers at the farm and regional watershed scales and help predict nutrient export toward the bigger Ohio River Basin by improving the understanding of contaminant transport and fate in conduit-dominated karstic aquifers in the Cumberland Escarpment of Southeastern Kentucky. Results highlight: 1) the necessity of using time-series analyses (chapter 3) and multi-criteria approaches (chapter 4) to identify the origins of surface contaminants in mixed-use small-scale watersheds; and 2) the need to take into account coupling effects between changes in land-use practices and differences in surface-groundwater connectivity (chapters 4 and 5) when defining nutrient management strategies (nitrate and DOC) at the farm scale.

Firstly, through the assessment of surface-groundwater interactions in the vadose zone and the understanding of subsurface conduit flow routes, timing of recharge, groundwater residence time following major storms (discharge > 0.5 $m^3/s$) in the Grayson-Gunnar aquifer, potential contaminant pathways from heterogeneous surface land-use were predicted at the farm scale. Through contrasting these results to studies conducted within similar cave systems across the South-Central Kentucky carbonate platforms (Maynardville limestones and Mammoth cave formations), it became evident based on the average volume of groundwater displaced following major storms (order of millions of liters), the general response time (2 to 7 hours), and the relatively complex subsurface conduit network (existence of two separate conduit branches) that the Grayson-Gunnar system is overly responsive to short-term changes in recharge in comparison to similar epikarst systems within the same physiographic ensemble.

Secondly, the effect of enhanced surface-groundwater connectivity in the transfer of nutrients (more specifically N, P and DOC) is discerned by understanding the pathways and timing of recharge. End-member mixing analyses were used to differentiate subsurface recharge signals from agricultural non-point sources (inorganically and manure-fertilized lands) and point-sources (residential septic systems). It was then established that short-term changes in agricultural land-use (seasonal corn growth) are more predictive of temporal variations in nutrients and DOC loads when balanced against the hydrological factor at the scale of small karstic aquifers.

Finally, a comparative analysis of regional karstic watersheds (Otter Creek basin, Beaver Creek basin, Grayson-Gunnar and Mill Springs) from the headwaters to the regional flow baseline (Cumberland River) of the Cumberland Escarpment has enabled the understanding of how changing land-use gradient, past land-use legacy (shallow oil exploration) and differences in surface-groundwater connectivity have affected groundwater evolution across the Cumberland physiographic region. Despite similarities in surface land-use between GGC and MS, the variations in surface-conduit connectivity influence the respective springs' behavior to short and long-term changes, thus suggesting that the characteristics of the vadose zone constitute a more predictive control of groundwater evolution than land-use factor at the regional level. Despite various response in present surface land-use changes, the legacy of past land-use changes (shallow oil exploration in the early 1900's) has remained consistent across the Bluegrass region, thus confirming the extreme vulnerability of epigenic karst aquifers to contaminants from human-induced changes.

At a larger scale, evidence gathered from this work definitely challenge the broader understanding that nitrogen and carbon export at the scale of the Mississippi River Basin is

primarily dominated by inputs from non-point sources associated with agricultural land-uses. Because maximal fluxes of nitrogen ($NO_3^-$ and $NH_4^+$) and DOC were recorded during primary recharge from CAFO, it is inferred that the recent proliferation of intensive animal farming facilities in the upper part of the Mississippi River Basin may have a significant impact of nutrient transport. A major large-scale implication for this investigation is that a careful assessment of these sources and their respective contributions is needed to support long-term mitigation strategies in the Gulf of Mexico and the management of its hypoxia zone.

Last but not least, an important large-scale implication of this work is the importance of carbonate dissolution kinetics on landscape evolution and global carbon cycle. Because modern karst processes such as carbonate rock dissolution and weathering play an active role as a global atmospheric $CO_2$ sink (Eq. 1-8, p. 34), it is anticipated that the progressive addition of sulfuric acid from regional brines and the subsequent occurrence of a non-traditional dissolution (sulfuric-acid-based) pathway within the Cumberland Plateau region may substantially enhance DIC fluxes at the output of these karst aquifers beyond current average concentrations (DIC $\leq$ 3 mmol/L). Thus the understanding of the contribution of sulfuric-acid dissolution on DIC export at the scale of the Cumberland region is a vital component of a larger-scale investigation of carbon flux from US continental karst to the Mississippi River Basin, the Gulf of Mexico and the global ocean.

Despite the amount of work done, this dissertation work did not answer all the potential inquiries remaining with regards to the original research goals. For this reason, future research plans may include:

1) Stable isotopes of O and H may help complement the information regarding recharge patterns, groundwater residence times, and regional evaporation processes occurring

during rain water infiltration in the vadose zone. For example, they may be helpful to differentiate between rainfall end-member and the portion of rainfall that interacted with the surface land-use prior to infiltration.

2) A combination of multiple isotope tracers ($\delta^{13}C$ and $\delta^{15}N$) could enable us to better differentiate the contribution of surface end-member sources of C and N from agricultural non-point sources (synthetic versus organic fertilizers/manure) and to investigate the potential for direct leaking under CAFOs storage areas to subsurface groundwater conduits. In addition, the monitoring of fertilizers and pesticides concentrations in springs draining primarily agricultural watersheds is a potential avenue of research.

3) Concerning the impact of shallow oil exploration and entrainment of hydrocarbon-rich compounds into regional groundwater, the use of Volatile Organic Compounds (VOCs) concentrations in addition to sulfur and oxygen isotopes may further reinforce this investigation's inferences about CAS and SAS.